
Dissertation
submitted to the
Combined Faculty of Natural Sciences and Mathematics
of the Ruperto Carola University Heidelberg, Germany
for the degree of
Doctor of Natural Sciences

Presented by
M.Sc. Lasse Neukirch
Born in Flensburg

Oral examination: 17.06.2021

**Evaluation of antigen-displaying adeno-associated
virus-like particles (AAVLPs) as future candidates for
personalized cancer vaccination**

Referees: apl. Prof. Dr. Martin Müller

Prof. Dr. Dirk Jäger

For my parents

Natura artis magistra - Nature is the teacher of the arts

Abstract

Despite extensive research and significant advances in the past decades, cancer is still the second leading cause of deaths worldwide. Within cancer research, a promising and growing field is the immuno-oncology, which takes advantage of a patient's immune system to elicit a protective response against malignant cells. Personalized vaccination against neoantigens is an encouraging approach to target different types of cancer. Neoantigens result from point mutations in the cancer cell genome and transform originally non-immunogenic sequences into immunogenic epitopes that overcome central immune tolerance. Despite different vaccine designs, which are primarily based on dendritic cells, DNA, RNA or synthetic peptides, additional strategies are required to reach sufficient immune responses.

In this study, a novel approach was tested by displaying (neo-)antigens on adeno-associated virus-like particles (AAVLPs) to effectively prime CD8⁺ T cell responses. AAV was chosen as an antigen-presentation-scaffold owing to its excellent safety profile in humans and tolerance towards genetic engineering of the capsid, allowing presentation of 60 antigen copies per particle.

The general vaccination strategy was tested in mice with AAVLPs displaying the ovalbumin-derived model antigen SIINFEKL. Initial experiments showed induction of long-lasting CD8⁺ T cell responses, sufficient to protect mice completely from B16F10-OVA tumor growth. Based on the SIINFEKL vaccine, the strategy was optimized by defining the most suitable injection routes, adjuvants and capsid insertion sites. Highest CD8⁺ T cell responses were achieved when the vaccine was I) injected s.c. into the hock, II) adjuvanted with Montanide ISA 51, III) injected at a high local concentration and IV) was composed of vector DNA-containing particles that V) display the antigen in the VR-IV loop of the capsid proteins.

While tested prime-boost strategies and coupling of anti-CD40 to the capsid had no benefit for the vaccination, co-display of the immune stimulatory peptide J-ICBL improved T cell responses significantly.

Interestingly, the presence of B cells was disadvantageous for the induction of antigen-specific CD8⁺ T cells and tumor protection, while the presence of CD4⁺ T cells was essential. Accordingly, T helper epitopes were identified within the AAVLP capsid sequence.

In addition to SIINFEKL-presenting AAVLPs, particles were designed to present a set of different B16F10-derived neoantigens. While a head-to-head comparison showed no effect of a peptide vaccine against B16F10 tumor growth, injection of neoantigen-displaying AAVLPs significantly reduced the tumor growth rate.

Although the general strategy requires further refinement and mechanistic analyses, neoantigen-AAVLPs represent an alternative for current therapy approaches and could be a promising candidate for future clinical applications.

Zusammenfassung

Trotz umfangreicher Forschung und signifikanter Fortschritte, ist Krebs weiterhin die zweithäufigste Todesursache weltweit. Ein vielversprechendes und wachsendes Feld im Bereich der Krebsforschung ist die Immunonkologie, welche das Immunsystem von Krebspatienten nutzt, um eine schützende Antwort gegen maligne Zellen hervorzurufen. Personalisierte Vakzinierung gegen Neoantigene ist ein aussichtsreicher Ansatz um verschiedene Arten von Krebs zu therapieren. Neoantigene entstehen durch Punktmutationen im Genom der Krebszellen und transformieren nicht-immunogene Sequenzen in immunogene Epitope, welche die zentrale Immuntoleranz überwinden können. Trotz verschiedener Vakzin-Entwürfe, welche hauptsächlich auf dendritischen Zellen, DNA, RNA oder synthetischen Peptiden beruhen, werden weitere Strategien benötigt um ausreichende Immunantworten zu erreichen.

In dieser Studie wurde ein neuer Ansatz getestet, in dem (Neo-)Antigene auf Adeno-assoziierten Virus-ähnlichen Partikeln (AAVLPs) präsentiert werden, um effektiv CD8+ T-Zell Antworten hervorzurufen. AAV wurde als Antigen-Träger-Partikel ausgewählt, da es ein hervorragendes Sicherheitsprofil im Menschen aufweist und das Kapsid gentechnisch verändert werden kann, so dass 60 Kopien eines Antigens pro Partikel präsentiert werden.

Die generelle Vakzinierungsstrategie wurde in Mäusen getestet, indem AAVLPs injiziert wurden, die das Ovalbumin-Modellantigen SIINFEKL präsentieren. Erste Experimente zeigten langlebige CD8+ T-Zell Antworten, die ausreichten, um Mäuse vor B16F10-OVA Tumorwachstum zu schützen. Basierend auf dem SIINFEKL-Vakzin wurde die Strategie optimiert, indem am besten geeignete Injektionsrouten, Adjuvantien und Kapsid-Insertionsstellen definiert wurden. Die stärksten CD8+ T-Zell Antworten wurden erreicht, wenn das Vakzin I) subkutan in die Hacke injiziert, II) mit Montanide ISA 51 adjuvantiert, sowie III) mit einer lokal hohen Konzentration verabreicht wurde und IV) aus DNA-enthaltenden Partikeln bestand, die V) das Antigen im VR-IV Loop präsentierten. Während getestete Prime-Boost-Strategien und Bindung von anti-CD40 an das Kapsid keinen Vorteil erzielten, war es möglich die T-Zell Antworten durch zusätzliche Präsentation des immunstimulierenden Peptides J-ICBL signifikant zu verstärken.

Interessanterweise war die Präsenz von B-Zellen nachteilig für die Generierung von antigenspezifischen CD8+ T-Zellen, während CD4+ T-Zellen essenziell waren. Dementsprechend wurden T-Helferepitope in der AAVLP Kapsidsequenzen identifiziert.

Zusätzlich zu den SIINFEKL-präsentierenden AAVLPs wurden Partikel hergestellt, die verschiedene B16F10-Neoantigene präsentieren. In einem direkten Vergleich hatte eine Peptid-Vakzinierung keinen Effekt auf das B16F10 Tumorwachstum, während Neoantigen-präsentierende AAVLPs die Wachstumsrate signifikant verringerten.

Obgleich die generelle Strategie weiterer Verbesserungen und mechanistischer Analysen bedarf, sind Neoantigen-AAVLPs eine Alternative zu geläufigen Therapieansätzen und könnten ein vielversprechender Kandidat für zukünftige klinische Anwendungen sein.

Table of contents

Abstract	1
Zusammenfassung.....	2
Table of contents.....	3
1 Background.....	7
1.1 Virus-like particles (VLPs) as vaccines	7
1.2 Adeno-associated virus (AAV).....	8
1.2.1 <i>A small virus with a big impact</i>	8
1.2.2 <i>The structure and biology of AAVs</i>	8
1.2.3 <i>Recombinant AAVs – from natural viruses to vectors</i>	10
1.2.4 <i>AAVs and the immune system</i>	11
1.2.5 <i>AAVs as vaccines – a failed gene therapy makes a good vaccine</i>	13
1.3 Cancer vaccines – getting personal.....	15
1.4 Aim of the study.....	18
2 Material.....	19
2.1 Equipment.....	19
2.2 Consumables.....	20
2.3 Standard Kits	20
2.4 Chemicals, mediums, additives.....	21
2.5 Antibodies and Tetramers	22
2.6 Enzymes	23
2.7 Peptides	24
2.8 Plasmids	24
2.9 Single-stranded oligonucleotides.....	27
2.10 PCR-Primers	31
2.11 Cell lines	32
3 Methods.....	33

Table of contents

3.1	Peptides.....	33
3.2	Cell culture	33
3.3	Molecular biology	34
3.3.1	<i>Agarose gel electrophoresis</i>	34
3.3.2	<i>Bacterial cultures</i>	35
3.3.3	<i>Transformation and Miniprep</i>	35
3.3.4	<i>Maxiprep</i>	35
3.3.5	<i>Oligo annealing and ligation</i>	36
3.3.6	<i>Site-directed mutagenesis (SDM)</i>	38
3.3.7	<i>Cloning of BirA expression plasmid</i>	39
3.3.8	<i>Cloning of CD40 expression plasmid</i>	41
3.3.9	<i>Confirm mutations in B16F10</i>	41
3.4	Production of AAVLPs	43
3.4.1	<i>Small-scale production of AAVLPs in crude lysates</i>	44
3.4.2	<i>Particle titration of AAVLP small-scale productions by sandwich ELISA</i>	44
3.4.3	<i>Large-scale production of purified AAVLPs</i>	45
3.4.4	<i>Particle titration of AAVLP large-scale productions by ELISA</i>	47
3.4.5	<i>Genomic titration of AAVLP large-scale productions by qPCR</i>	48
3.5	Production of AAVLPs with bound anti-CD40.....	49
3.5.1	<i>Production of biotinylated AAVLPs</i>	49
3.5.2	<i>Confirmation of AAVLP-biotinylation by ELISA</i>	50
3.5.3	<i>Conjugation of streptavidin to anti-CD40</i>	50
3.5.4	<i>Confirmation of streptavidin/anti-CD40 conjugation by western blot</i>	50
3.5.5	<i>Binding of streptavidin-conjugated anti-CD40 to biotinylated AAVLPs</i>	52
3.5.6	<i>Confirmation of anti-CD40 coupling to AAVLPs by ELISA</i>	52
3.6	<i>In silico</i> prediction of antigens	52
3.7	<i>In vitro</i> experiments.....	53
3.7.1	<i>AAVLP uptake into DC2.4</i>	53
3.7.2	<i>AAVLP-anti-CD40 binding assay</i>	53
3.8	Animal experiments.....	54
3.8.1	<i>Vaccination</i>	54
3.8.2	<i>Tumor challenge</i>	55
3.8.3	<i>Immune cell depletion</i>	55
3.8.4	<i>Intracellular staining (ICS)</i>	55
3.8.5	<i>Tetramer staining</i>	56
3.8.6	<i>Collecting blood serum samples</i>	57
3.8.7	<i>Determine GFP copy numbers in murine tissues by qPCR</i>	57
3.8.8	<i>Peptide ELISA of blood serum samples</i>	57
3.8.9	<i>Tumor infiltration of immune cells</i>	58

3.9	Statistical analyses	58
4	Results.....	60
4.1	Design and production of AAVLPs	60
4.2	General tests of the vaccination strategy (AAVLP-SIINFEKL).....	62
4.2.1	<i>AAVLP-SIINFEKL vaccination induces antigen-specific CD8+ T cells in spleen and blood.....</i>	62
4.2.2	<i>AAVLP-SIINFEKL induces long lasting CD8+ T cell responses with a peak after 3 weeks</i>	65
4.2.3	<i>AAVLP-SIINFEKL vaccination via s.c. but not i.m. injection route induces CD8+ T cell responses.....</i>	66
4.2.4	<i>High local concentration of AAVLP-SIINFEKL promotes generation of CD8+ T cell responses</i>	67
4.2.5	<i>Adjuvants Montanide ISA 51 but not CpG ODNs or c-di-AMP promote induction of CD8+ T cells by AAVLP-SIINFEKL</i>	68
4.2.6	<i>DNA packaged in AAVLP-SIINFEKL particles increases CD8+ T cell responses.....</i>	69
4.2.7	<i>Insertion of SIINFEKL in the VR-IV loop (aa453) of AAVLPs yields higher CD8+ T cell responses than VR-VIII loop (aa588) insertion</i>	70
4.2.8	<i>Neither homologous nor heterologous prime-boost strategies improve AAVLP-SIINFEKL vaccination.....</i>	73
4.2.9	<i>CD8+ T cells induced by AAVLP-SIINFEKL are able to prevent B16F10-OVA tumor growth in mice</i>	75
4.3	Improvement strategies (AAVLP-SIINFEKL)	77
4.3.1	<i>Generation of anti-CD40-coupled AAVLPs.....</i>	77
4.3.2	<i>Anti-CD40-coupled AAVLPs bind to CD40-expressing cells.....</i>	80
4.3.3	<i>Coupling anti-CD40 to AAVLP-SIINFEKL does not improve CD8+ T cell responses.....</i>	81
4.3.4	<i>Co-display of ICBL on AAVLP-SIINFEKL increases CD8+ T cell responses.....</i>	83
4.4	The role of B cells (AAVLP-SIINFEKL).....	84
4.4.1	<i>Absence of B cells increases CD8+ T cell responses induced by AAVLP-SIINFEKL</i>	84
4.5	The role of CD4+ T cells (AAVLP-SIINFEKL).....	85
4.5.1	<i>Presence of CD4+ T cells is required for CD8+ T cell responses induced by AAVLP-SIINFEKL</i>	85
4.5.2	<i>Identification of potential helper epitopes in the AAVLP capsid.....</i>	87
4.6	Targeted induction of antibody and CD4+ T cell responses (AAVLP-OVAII).....	89
4.6.1	<i>Vaccination with AAVLP-OVAII induces strong antibody responses against the target antigen.....</i>	90
4.6.2	<i>Vaccination with AAVLP-OVAII does not induce CD4+ T cell responses against the target antigen.....</i>	91
4.7	Testing alternative CD8+ T cell epitopes (AAVLP-LCMV and AAVLP-HPV)	93
4.7.1	<i>Vaccination with AAVLPs displaying an LCMV but not HPV antigen induces antigen-specific CD8+ T cell responses</i>	93

4.8	Targeting neoantigens (AAVLP-Neo).....	94
4.8.1	<i>Selection of neoantigens for the AAVLP-Neo vaccine.....</i>	94
4.8.2	<i>Vaccination with AAVLP-Neo does not induce detectable CD8+ T cell responses</i>	97
4.8.3	<i>Vaccination with AAVLP-Neo induces antibody responses against the mutated and wild type peptide</i>	99
4.8.4	<i>Vaccination with AAVLP-Neo reduces B16F10 tumor growth in mice.....</i>	100
4.8.5	<i>Vaccination with AAVLP-Neo increases immune cell infiltration into tumor tissue .</i>	102
5	Discussion	104
5.1	AAVLPs as a vaccine platform	104
5.2	Optimizing AAVLP vaccination	108
5.2.1	<i>The effect of injection route and local concentration.....</i>	108
5.2.2	<i>Effects of external and internal adjuvants.....</i>	111
5.2.3	<i>The role of AAVLP tropism and endosomal escape.....</i>	113
5.2.4	<i>Prime-boost strategies and pre-existing immune responses.....</i>	114
5.2.5	<i>Improvement strategies of AAVLP vaccines.....</i>	116
5.3	Role of helper T cells and B cells in AAVLP-induced CD8+ T cell responses	119
5.4	Targeting neoantigens with AAVLP-based vaccines	123
5.5	Evaluation of AAVLPs as future (cancer) vaccine candidates	126
5.6	Outlook.....	128
6	Conclusion	129
7	References	130
8	Appendices	144
8.1	Additional data.....	144
8.2	List of figures	149
8.3	List of tables	150
8.4	Abbreviations	152
	Acknowledgements	157

1 Background

1.1 Virus-like particles (VLPs) as vaccines

The history of vaccines began in 1796, when the English doctor Edward Jenner injected humans with live cowpox viruses for protection against smallpox infection [2]. While the mechanistic effect was far from being uncovered, the efficacy of this first vaccine spoke for itself and led to the worldwide eradication of smallpox, several decades later.

Today, a common vaccine design is the attenuation of whole viruses and bacteria by physical or chemical treatment [3-5]. Vaccines against rabies, polio or measles are based on this strategy and examples for successful applications [3]. Yet, a risk of incomplete attenuation remains and functional, replicating pathogens might be administered [3, 5].

As an alternative, single pathogen-derived proteins or peptides can be used for vaccination. While being safer than attenuated viruses, these subunit vaccines are often less immunogenic [5].

A compromise between safety and immunogenicity is the administration of virus-like particles (VLPs) [4, 5]. These multi-protein structures resemble real viruses but do not contain viral genomes and are therefore replication-deficient [4, 6]. VLPs of diverse viruses can be produced comparably easy in a broad spectrum of expression host systems, such as mammalian-, insect-, plant- or bacterial cells. A number of VLP-based vaccines have been licensed already, and particles derived from pathogenic viruses, such as *hepatitis B virus* (HBV) or *human papillomavirus* (HPV) [4, 5], are administered to induce protective responses. While in these examples immune responses are directed against the original virus, the immunogenic capacity of VLPs can also be exploited to induce immunity against unrelated antigens. In this case, target proteins or peptides, derived from alternative pathogens or cancer cells, are displayed on the surface of VLPs and take advantage of their immune-stimulating properties.

The great immunogenic potential of VLPs is attributed to their viral resemblance, promoting both humoral [7] and cellular immune responses [8, 9]. The dense and ordered structure of antigens on the virus-like surface helps to cross-link B cell receptors for an activation, proliferation and migration of B cells, combined with an upregulation of co-stimulatory molecules [10-12]. Next to antibody responses, cytotoxic T lymphocytes (CTL) can be induced efficiently by VLP administration [8, 9]. In this respect, particle sizes

between 20 and 200 nm are of advantage, by promoting both transport in the lymphatic system [4, 6, 13, 14] as well as active internalization and processing by antigen-presenting cells (APCs) [15-18].

1.2 Adeno-associated virus (AAV)

1.2.1 A small virus with a big impact

When AAVs were discovered almost 60 years ago, the 25 nm small particles [19, 20] were initially seen as contaminants of adenovirus productions [21, 22]. Today, with over 12 000 publications around AAVs (search result for “adeno-associated virus” at Pubmed.gov, 12.03.2021) and 15-20 new publications each week, this virus has a major impact on the natural and health sciences. The non-pathogenic character and ability to transduce a broad spectrum of target cells [19] made AAVs safe and efficient vectors in gene therapy approaches against various diseases [19, 20, 23]. A particular safety advantage of this non-enveloped, single-stranded DNA (ssDNA) virus is the inability to propagate independently, as AAV replication requires co-infection with helper viruses (e.g. adenovirus or herpesvirus) [19, 20]. Extensive pre-clinical research on AAVs finally led to registration in currently 250 clinical trials (search results for “AAV” at clinicaltrials.gov, 12.03.2021) and two licensed AAV-based gene therapies approved by the U.S. Food and Drug Administration (FDA) [20, 24].

1.2.2 The structure and biology of AAVs

The AAV genome consist of two genes, flanked by inverted terminal repeats (ITRs) [25] (*Figure 1.1A*).

The *rep* gene encodes four Rep proteins (Rep78, Rep68, Rep52, Rep40) [26], which are expressed via alternative splicing from two promoters (p5, p19) [27]. These functional proteins are important for regulating AAV gene expression and DNA replication [27], as well as the accumulation and packaging of the viral genome [28].

The *cap* gene encodes three structural capsid proteins (VP1, VP2, VP3) [25], which build up the viral particle [29]. The capsid proteins are expressed under the p40 promoter [30] via alternative splicing [31]. Consequently, VP2 and VP3 are homologous to the C-terminal sequence of VP1 with different degrees of N-terminal truncation (*Figure 1.1A*). In presence

of the assembly-activating protein (AAP), which is expressed from an alternative open reading frame in the *cap* gene [32], VP1, VP2 and VP3 are assembled in an approximate ratio of 1:1:8 [29] to form an icosahedral particle of 60 VP subunits [33] (**Figure 1.1B**).

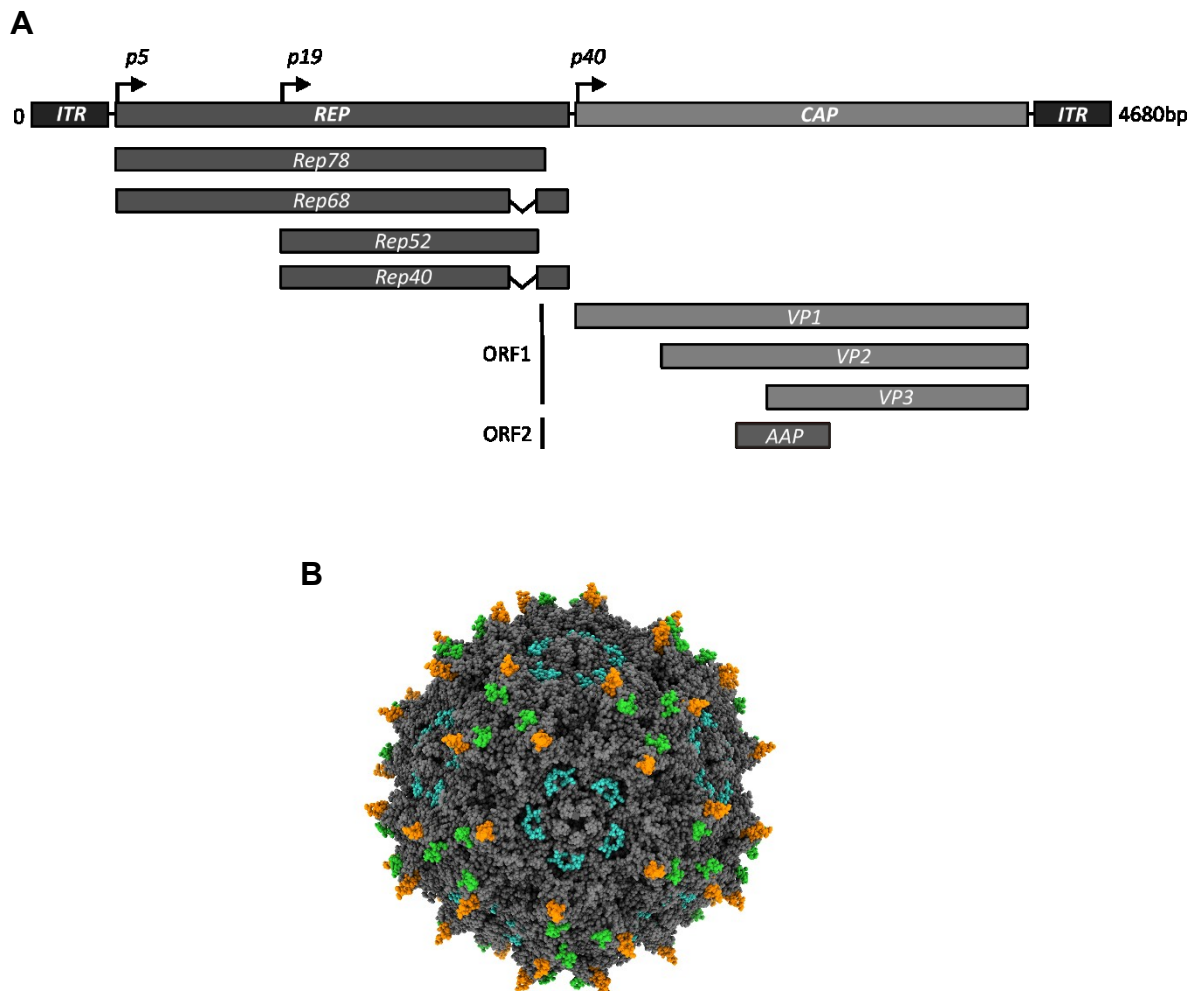


Figure 1.1: Structure of the AAV genome and capsid.

A) The AAV genome consists of two genes, *rep* and *cap*, which are flanked by inverted terminal repeats (ITRs). The *rep* gene encodes four proteins from two promoters via alternative splicing. The *cap* gene encodes three capsid proteins (VP1, VP2, VP3) via alternative splicing and an assembly activating protein (AAP) from a second open reading frame (ORF). Figure modified from [1].

B) Capsid structure of AAV. The three capsid proteins VP1, VP2 and VP3 assemble into an icosahedral particle of 60 subunits. The colored structures mark the variable region (VR)-IV loop (orange), the VR-VIII loop (green) and the HI loop (blue), which tolerate peptide insertions. (Figure modified from PDB entry 6CBE using ChimeraX 1.1)

The capsid does not only define the serotype of AAVs but also biological properties. Numerous serotypes and variants from humans and nonhuman primates have been characterized [34, 35] with differences in tropism and immunogenicity. In general, the AAV tropism is defined by binding to proteoglycan conjugates as primary receptors and

proteinaceous co-receptors. For example, the most studied AAV serotype 2 (AAV2) binds to heparan sulfate proteoglycan (HSPG) on cell surfaces [36], while different co-receptors facilitate internalization into the cell [37-43]. In accordance, different pathways of cell entry have been described for AAV2, including clathrin-mediated endocytosis [44-46], micropinocytosis [47] or the CLIC/GEEC endocytic pathway [48]. Once inside the cell, AAVs are transported from early endosomes via late endosomes [49] to the trans-Golgi network [50]. From here, the particles transit into the cytosol and enter the nucleus, where viral replication takes place [19]. The AAV capsid proteins play an active role in the endosomal escape into the cytosol, as a phospholipase A2 (PLA2) domain in the N-terminal regions of VP1 leads to lipolytic pore formation and particle release from vesicles [51].

1.2.3 Recombinant AAVs – from natural viruses to vectors

Next to the already mentioned advantages of a good safety profile and transduction capacity, AAVs are also comparably easy to produce and offer the possibility of capsid modifications.

First advancements in the production of recombinant AAVs were made in 1982 by cloning the viral genome into bacterial replication plasmids, enabling a simple propagation and handling [52]. Around 20 years after the AAV discovery, first recombinant viruses were finally produced, marking the start of numerous AAV-based therapy developments. By flanking foreign genes with ITRs, target sequences were packaged into assembling AAVs, which were subsequently used as gene vectors for the transduction of mammalian cells [23, 53]. Over the years, further improvements were made and the recombinant AAV production was optimized. The identification of required helper genes (E1, VA, E2A, E4), which could be delivered on DNA plasmids [54], made the inclusion of live helper adenoviruses redundant for the production process. Thus, a current standard procedure is triple-transfection of producer cell lines, such as Human embryonic kidney (HEK) 293 cells, with one plasmid encoding AAV Rep, Cap and AAP proteins, a second plasmid with the ITR-flanked transgene, and a third plasmid containing adenoviral helper genes (*Figure 1.2*).

Despite genome modifications, the capsid proteins of AAVs can be genetically altered in several ways to generate viral particles that display foreign amino acid sequences. Next to attaching peptides or whole proteins to the N-terminal end of VPs [55, 56], peptide sequences can be inserted into distinct sites of the capsid [57] (*Figure 1.2*). Common

insertion sites for peptides of up to 30 amino acids include the variable region IV (VR-IV) loop around amino acid 453 (aa453) [58], the VR-VIII loop around aa588 [58-60] or the HI loop around aa660 [61, 62] of the AAV2 VP1 protein. Next to generating an alternative AAV tropism by the display of receptor-binding peptides [46, 57-59, 63, 64], capsid insertion of antigens can be utilized to induce immune responses.

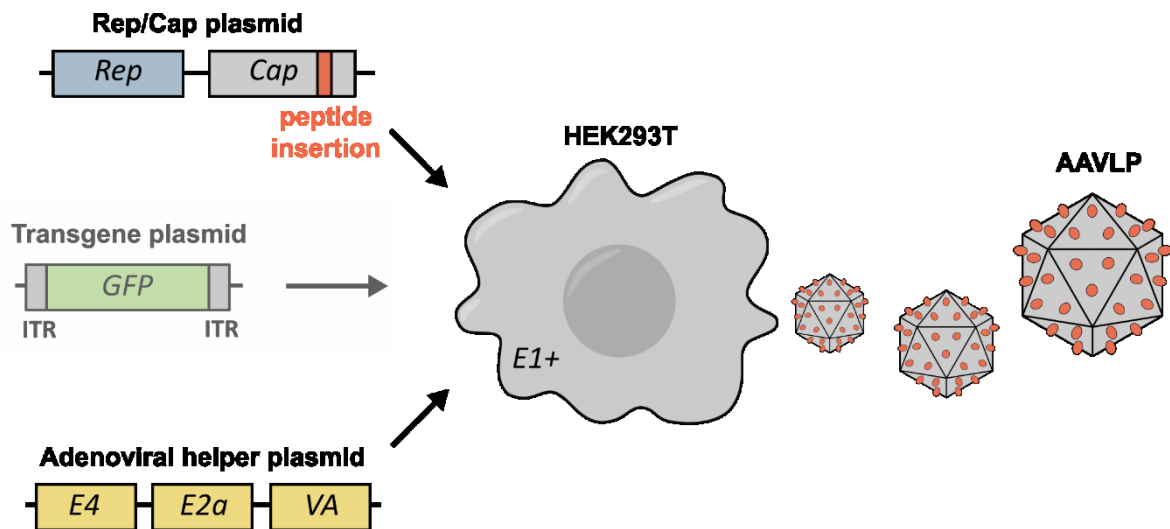


Figure 1.2: Production of recombinant AAVs/AAVLPs.

A producer cell line, in this case HEK293T, is transfected with three plasmids. The **Rep/Cap plasmid** corresponds to the natural AAV genome (**Figure 1.1**) but lacks the inverted terminal repeats (ITRs) that facilitate packaging of the genome. The *rep* and *cap* genes encode functional and structural proteins, respectively. Peptides (red) can be cloned into the capsid sequence and are later displayed on assembled particles. The **Adenoviral helper plasmid** contains the adenoviral genes *E4*, *E2a* and *VA*, which are required for the replication and assembly of AAVLPs. A fourth adenoviral gene, *E1*, is already encoded in the produced cell line, as a remnant of the HEK293T cell genesis. The **Transgene plasmid** is optional for the generation of AAVLPs, as empty particles assemble even in the absence of a transgene. To generate particles containing a transgene, the gene of interest and a respective promoter are flanked by ITRs, which deliver the packaging signal.

Upon assembly, AAVLPs accumulate in the nucleus. As the virus itself is not lytic, AAVLPs need to be released by mechanical or chemical disruption of producer cells. Particles can be purified from the cell lysate by ultracentrifugation in a discontinuous iodixanol gradient.

1.2.4 AAVs and the immune system

AAVs are frequently described as non-immunogenic, especially in comparison to other vectors like the adenovirus [65]. Yet, several studies showed clear signs of both innate and adaptive immune responses against AAVs.

Usually, innate responses are induced by pattern recognition receptors (PRRs) on immune cells, detecting pathogen-associated molecular patterns (PAMPs) of invading pathogens

[66]. Most PRRs are Toll-like receptors (TLRs) that recognize different kinds of PAMPs, such as nucleic acids or membrane glycoproteins [66]. A typical signal transduction of activated TLRs occurs via myeloid differentiation factor 88 (MyD88) and nuclear factor kappa-light-chain-enhancer of activated B cells (NF- κ B) causing release of pro-inflammatory cytokines like tumor necrosis factor alpha (TNF α), interleukin 6 (IL6) or type I interferons (IFNs) [66]. Innate immune responses against AAVs are induced by two TLRs. TLR2, known to detect glyco- and lipoproteins, is activated by the AAV capsid proteins [67]. TLR9 recognizes ssDNA or self-complementary DNA (scDNA) packaged within the AAV capsid [68-70]. Especially the TLR9-mediated signaling via MyD88 and type I interferons has a critical role in the induction of adaptive immune responses to AAVs [68]. In addition to TLRs, the complement system plays a role in the innate immunity to AAVs. Thus, binding of iC3b to capsid proteins is important for ingestions of particles by macrophages and production of pro-inflammatory cytokines [71].

Both humoral and cellular immune responses to AAVs are induced in the adaptive immunity. The detection of capsid-specific antibodies in a great fraction of the human population is already evidence for a distinct humoral response to AAVs. Even early in life, many humans develop antibody responses to several AAV serotypes after natural infections [72-74]. This was further confirmed in pre-clinical [75] and clinical trials [76, 77] under defined conditions, by showing the generation of neutralizing antibodies.

In addition, the AAV capsid contains immunogenic T cell epitopes [78, 79] that induce CTLs in mice [75, 79, 80]. Also in humans, acute and memory CD8⁺ T cell responses against the AAV capsid are induced [76, 77, 81, 82]. While capsid-specific CTLs do not eradicate AAV-transduced cells in mice [75, 79, 80], cytotoxicity against capsid-presenting cells has been shown in humans [81-83].

The scope of immune responses is partly influenced by the AAV serotype and their different tropisms. Thus, AAV1, which efficiently transduces dendritic cells (DCs), is more immunogenic than AAV8 [84]. In general, serotypes with intact HSPG binding, such as AAV2, induce higher immune responses [79, 85].

1.2.5 AAVs as vaccines – a failed gene therapy makes a good vaccine

Describing AAVs as failed gene therapy vectors does not represent their value in this field. Yet, in several clinical studies, AAVs induced substantial immune responses against the vector and encoded transgenes, which led to eradication of transduced cells [81, 82]. Consequently, AAVs were tested as vaccine vectors. Two different approaches can be applied to AAVs for induction of immune responses, which is packaging of antigens as a transgene or the display of antigenic peptides on the viral surface (**Figure 1.3A**). In the former case, AAVs transduce target cells, which subsequently express the antigen. Antigenic epitopes are presented on major histocompatibility complex (MHC) class I for cellular immune responses, or the whole antigen is released into circulation, where antibody responses are induced. The strategy of AAV-encoded antigens has been tested in numerous pre-clinical mouse studies to induce immune responses against ovalbumin (Ova) [86-89], viruses [90-101], parasites [102] and cancer antigens [103]. In addition, efficacy of this vaccination strategy has been tested against *simian immunodeficiency virus* (SIV) in macaques [104] and *human immunodeficiency virus* (HIV) in two clinical trials [105, 106]. In both, pre-clinical and clinical studies, explicit antibody as well as cellular immune responses were observed.

Vaccines based on capsid-presented antigens were primarily designed to activate B cells for the induction of antibody responses (**Figure 1.3B**). In pre-clinical trials, AAV-displayed B cell epitopes induced antibodies against ovalbumin [107], HPV [91, 108, 109], *Mycobacterium tuberculosis* [110] and the cancer antigen human epidermal growth factor receptor 2 (HER-2) [111].

Only few studies tested the induction of CD8+ T cell responses after antigen-display on AAV particles [62, 112, 113]. These experiments were primarily initiated because effective vector-directed cytotoxic T cell responses were observed in human clinical trials but not in pre-clinical mouse studies [62]. To increase immunogenicity of AAV capsids in mice and test antigen presentation *in vitro* and *in vivo*, the ovalbumin antigen SIINFEKL was displayed on the surface of AAVs [112-116]. However, the final aim of these studies was the prevention of immune responses in gene therapy trials rather than capitalizing them for vaccination approaches.

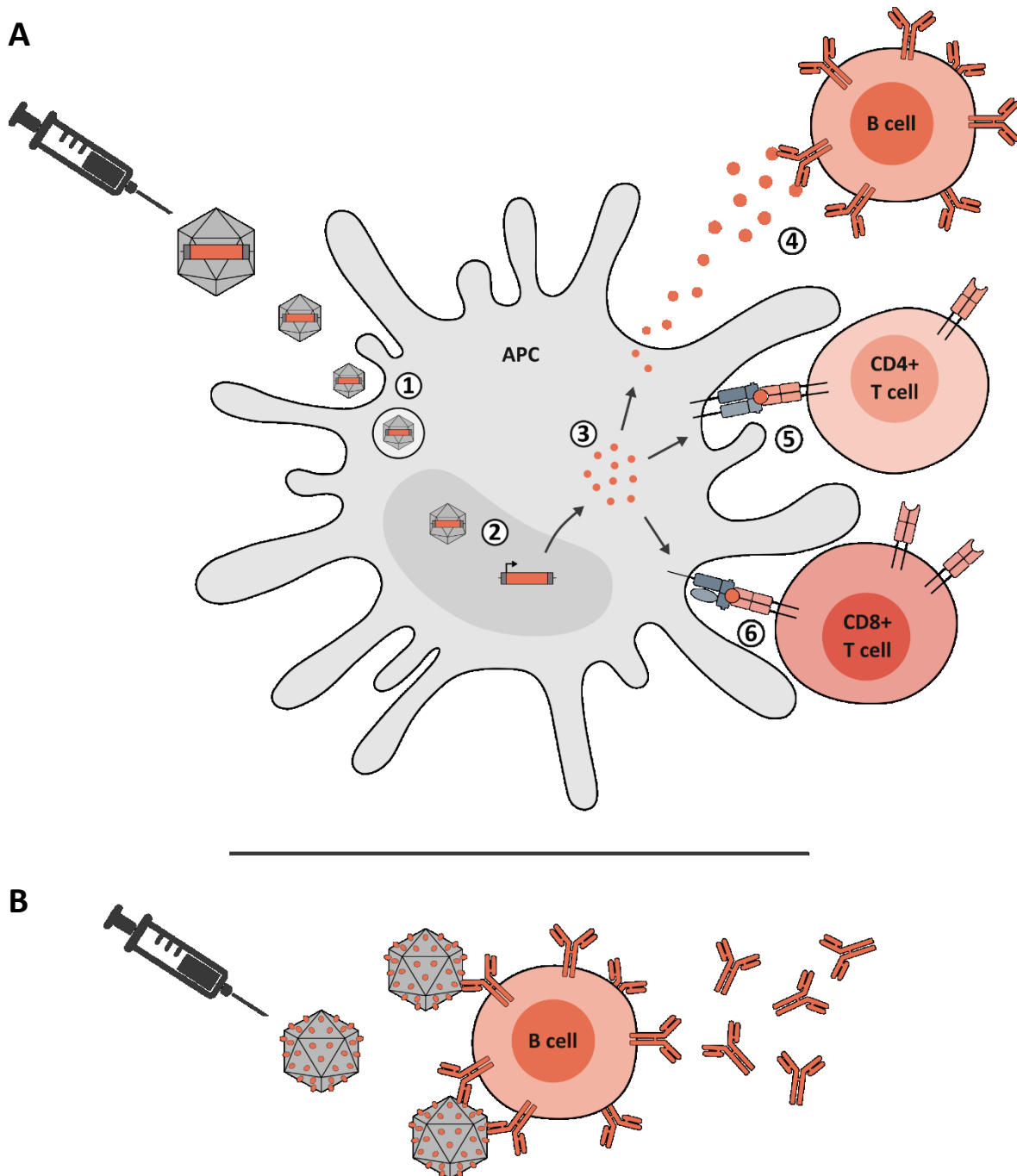


Figure 1.3: Current vaccination strategies using AAVs.

A) AAV vectors containing a target antigen as a transgene. AAVs enter antigen presenting cells (1) and transduce the cells with the packaged antigen (2). Antigenic proteins are expressed within the cells (3). Released antigens encounter B cells and induce antibody responses (4). In addition, processed antigens are presented on MHC class II (5) and MHC class I (6) for the priming of CD4+ T cells and CD8+ T cells, respectively.

B) AAVs presenting antigenic peptides on the capsid surface. AAV particles encounter B cells and induce antibody responses against the displayed antigen.

1.3 Cancer vaccines – getting personal

While the immune system is able to eradicate abnormal cells in healthy humans, the propagation of tumors in cancer patients is driven by a dysfunctional interaction between the immune system and tumor. The growing field of immuno-oncology set a focus on shifting the balance towards the immune system, in order to facilitate cancer immune surveillance. The first immunotherapy of malignant tumors can be traced back to the year 1891, in which William B. Coley treated bone and soft-tissue sarcomas by injecting bacteria or bacterial products into the tumor site [117]. Due to general immune activation and local inflammatory responses, even established tumors were eradicated [117]. This treatment modality called “Coley’s toxins” was later replaced by more defined immune stimulators, such as IFN or IL2, to boost immune responses against malignant cells [118, 119]. However, the general activation of immune responses is a rather unspecific treatment modality and can act on several signaling pathways in the human body, potentially leading to severe side effects and cellular toxicity [119].

A major advancement in cancer immunotherapy was the development of the Nobel Prize-honored immune checkpoint inhibitors. Immune checkpoint proteins, such as cytotoxic T-lymphocyte-associated protein 4 (CTLA4) and programmed cell death protein 1 (PD1), are expressed on activated T cells and are part of a natural regulation mechanism to prevent over-reactive T cells and autoimmunity [120]. Tumor cells frequently express checkpoint proteins, such as programmed death-ligand 1 (PDL1), to induce an immunosuppressive state and escape immune surveillance [120]. The administration of monoclonal antibodies against CTLA4, PD1 or PDL1 as checkpoint inhibitors alleviates the T cells from their suppression and enables a strengthened immune response against malignant cells [120, 121]. Since a first therapy approval in 2011, checkpoint inhibitors proved their worth in the treatment of solid tumors [121]. Yet, not all patients are cured by this treatment strategy and additional tumor-selective immunotherapies are required for administration as a single therapy or in combination with checkpoint inhibitors.

For a selective targeting, cancer cells can be treated by monoclonal antibody administration, adoptive cell therapy or vaccination.

Monoclonal antibodies mark tumors for recognition by innate and adaptive immune cells, which subsequently attack the malignant cells [122, 123]. In addition, certain antibodies

are able to neutralize functional proteins on tumor cells and block tumor-favorable receptor signaling [122].

Adoptive cell therapy describes the isolation and *in vitro* expansion of tumor-specific T cells, which are subsequently reinfused into the patient [118, 124]. Two common examples in this respect are the expansion of tumor infiltrating lymphocytes (TILs) or the genetic engineering of autologous T cells with a tumor-directed T cell receptor (TCR) or chimeric antigen receptor (CAR T cells).

Vaccination is a rather old approach in the field of immuno-oncology, but still under development. First vaccination studies were performed in the early 20th century by Paul Ehrlich, who injected mice with attenuated cancer cells and observed reduced tumor progression upon challenge with the same tumor cell line [125]. Such autologous tumor vaccines are currently in clinical trials, but still seek approval as licensed therapies [124]. The spectrum of approved cancer vaccine is sparse with only few preventive vaccines against virus-induced cancers and few therapeutic vaccines [126].

One of the major obstacles in developing cancer vaccines is the identification of suited target proteins. The first report of a tumor T cell antigen was in 1991, with identification of the melanoma antigen-encoded gene (MAGE) [127]. Tumor antigens can be divided into two classes, which are tumor-associated antigens (TAAs) and tumor-specific antigens (TSA). TAAs are overexpressed in tumor cells due to differentially regulated transcription, but can also be found in non-malignant tissue [128]. As these self-antigens are also presented on MHC molecules of healthy cells, they are likely part of the immunological tolerance and immune responses are difficult to induce [124, 128]. TSAs, on the other hand, are exclusively expressed in tumor cells [124, 128] and are able to induce a more robust immune response with less autoimmune-related toxicity [124, 128]. TSAs are usually novel antigens generated by single-nucleotide mutations, insertions, deletions or frameshifts [128] and occur frequently in tumors, which might have hundreds to thousands of coding mutations [129]. As the mutated sequences differ from the wild type sequence and are not part of central tolerance, some of the mutations are able to generate new antigens. Due to their novel character they are commonly called neoantigens, and respective immunogenic peptides that contain the mutation are called neoepitopes [130]. In recent years, efforts have been made to induced neoantigen-directed immune responses by vaccination [130]. A first step in this process is the identification of mutations by next-generation sequencing

of cancer exomes and comparison to a healthy tissue reference genome [124, 130]. To narrow the selection, a current strategy is to validate mRNA expression of mutated genes and *in silico* prediction of MHC molecule binding [130]. In addition, direct identification of neoantigens can be achieved by tandem mass spectrometry (MS/MS) of MHC-eluted ligands [128]. A final confirmation, which is comparably laborious, is characterization of the existing T cell repertoire in the blood or tumor tissue [128].

Vaccination approaches against neoantigens have shown promising results in pre-clinical mouse experiments [131, 132] but also in human clinical trials [133-138]. Common strategies include vaccination with neoepitope-loaded autologous DCs [133, 134], peptides [135, 136], or RNA [137, 138] against different types of cancer.

The endless heterogeneity within but also between different types of cancer makes a universally applicable vaccine almost impossible. A promising solution is the personalized vaccination against individual neoantigens. However, this requires sufficient induction of immune responses by a well-designed vaccination approach.

1.4 Aim of the study

Current vaccine candidates against tumor antigens are elaborate to produce or might show deficiencies in the induction of immune responses. Therefore, new vaccination approaches are constantly required to induce strong anti-tumor effects. The aim of this project was to develop, test and improve a novel vaccination platform for the induction of CD8⁺ T cell responses by displaying antigens on the surface of AAVLPs. As a final aim, the AAVLP-based strategy was to be designed for targeting murine neoantigens and tested as a personalized tumor vaccine in mice (*Figure 1.4*).

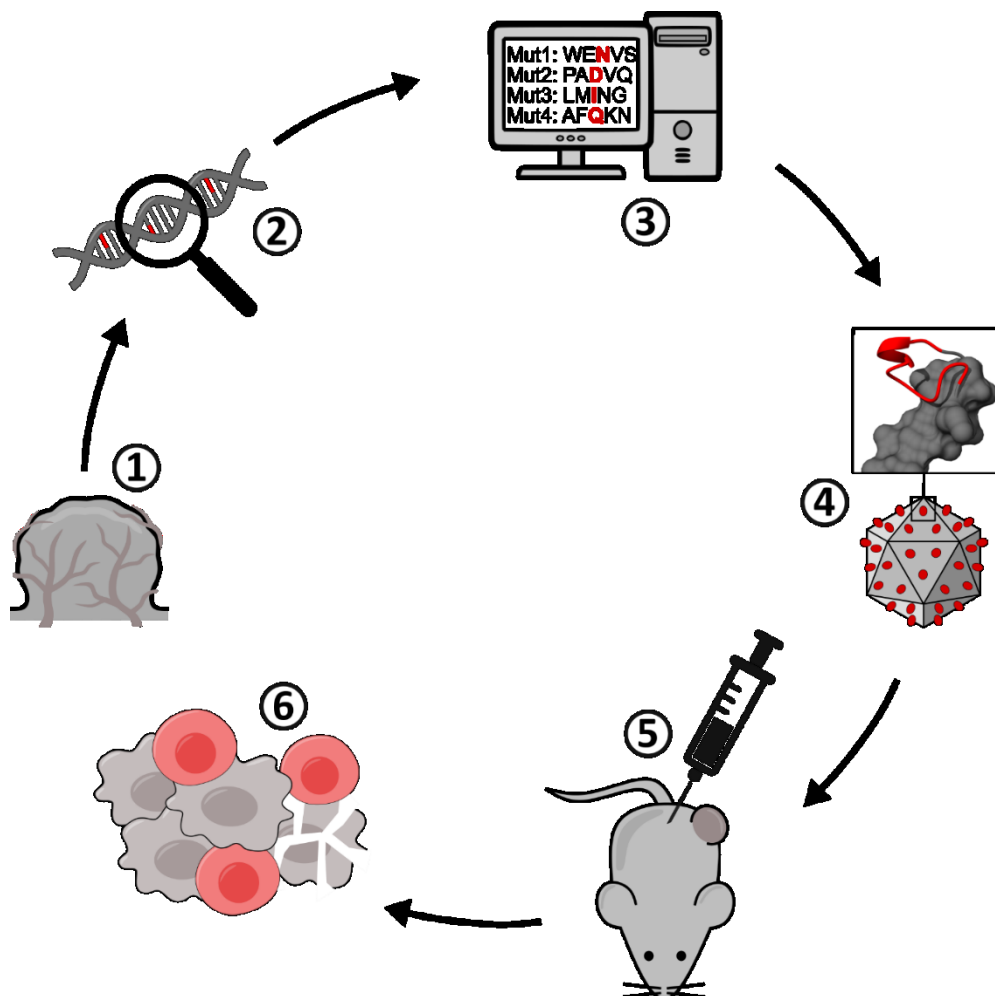


Figure 1.4: Vaccination strategy.

Tumor cells are isolated (1) and analyzed for mutations by whole exome sequencing (2). Potential neoantigens are predicted in silico (3) and neoepitopes are inserted into the capsid of AAVLPs (4). Mice are vaccinated with the antigen-displaying AAVLPs (5) causing a priming of T cell responses. Tumors are infiltrated and killed by the generated T cells (6). As neoantigens in the murine model system were already known from the literature, this project focused on the steps 4 to 6, with the aim to validate and improve anti-cancer immune responses induced by the AAVLP vaccine.

2 Material

2.1 Equipment

Equipment	Manufacturer
2-Gel Tetra and Blotting Module	Bio-Rad
CellDrop Cell Counter	DeNovix
CKX31 Microscope	Olympus
CKX41 Microscope	Olympus
EG Präzisionswaage	Kern
Epoch Photometer	BioTek
FACSCanto™ II	BD Biosciences
Fusion-SL	Vilber Lourmat
Heracell 150 CO2 Incubator	Thermo Scientific
Heraeus Fresco 21 Centrifuge	Thermo Scientific
Heraeus Megafuge 40R Centrifuge	Thermo Scientific
Heraeus Multifuge X1R Centrifuge	Thermo Scientific
Innova® 44 Incubator Shaker	New Brunswick
J2-MC High Speed Centrifuge	Beckman
L8-70M Ultracentrifuge	Beckman
Light Cycler® Instrument 480 II	Roche
Matrx VIP3000 Isoflurane Vaporizer	Midmark
Mini Vortex Mixer	Fisher Scientific
Mini-PROTEAN Tetra Cell	Bio-Rad
MR Hei-Standard	Heidolph
pipetus®	Hirschmann Laborgeräte
Power Pac 300	Bio-Rad
Quantum-ST4	Vilber Lourmat
Safe 2020 Class II Biological Safety Cabinet	Thermo Scientific
SevenEasy pH Meter	Mettler Toledo
Sonorex	Bandelin
Sub Cell GT	Bio-Rad
T3000 Thermocycler	Biometra
Tube Sealer	Beckman
Type 70 Ti Rotor	Beckman
U-RFL-T Power Supply	Olympus

2.2 Consumables

Product	Catalog number	Manufacturer
0.45 µm membrane filter	SLGS033SS	Millipore
14 mL Round Bottom Polypropylene Tube	187262	Greiner Bio-One
15 mL Conical Polypropylene Tube	188271	Greiner Bio-One
5 mL Round Bottom Polystyrene Tube	352052	Falcon
50 mL Conical Polypropylene Tube	227261	Greiner Bio-One
96 well ELISA plate	3690	Greiner Bio-One
96-well LC480 PCR plate	I2249.0050	Genaxxon
Amicon Ultra-15, Centrifugal Filter, 50 kDa	UFC905024	Merck
Cell Culture dishes (15 cm)	353025	Falcon
Cell Culture Flask (T25; T75; T175)	690175; 658175; 660175	Greiner Bio-One
Cell Culture Microplates (96 well, U-bottom)	650185	Greiner Bio-One
Cell Culture Multiwell Plates (6 well; 24 well)	657160; 662160	Greiner Bio-One
CryoTube™ Vials	377267	Thermo Scientific
EASYstrainer Cell Strainer	542000	Greiner Bio-One
Nalgene™ 250 mL conical PPCO tube	3143-0175	Thermo Scientific
Needle (20G x 0.90X40 mm)	CH20112	Medoject
Needle (27G x 0.40X20 mm)	CH27034	Medoject
Pasteur pipette	E327.1	Carl Roth
PVDF Membrane	IPVH00010	Millipore
Quick-Seal® Round-Top Polypropylene Tube	342414	Beckman Coulter
Solofix® Lancet	6185002	B. Braun
Sterican® blunt end needle (18G; 1.20X40 mm)	613-2948	VWR International
Syringe 1 mL	309628	BD
Syringe 10 mL	301604	BD
Whatman™ paper	3030-917	GE Healthcare

2.3 Standard Kits

Kit	Catalog number	Manufacturer
AAV5 Titration ELISA	PRAAV5	PROGEN
Cytofix/Cytoperm™ Fixation/Permeablization Kit	554714	BD Biosciences
DNeasy Blood and Tissue Kit	69504	QIAGEN
Maxima H Minus First Strand cDNA Synthesis Kit	K1651	Thermo Scientific
NucleoBond Xtra Maxi Kit	740414	Macherey-Nagel
PfuPlus! DNA Polymerase Kit	EK1118-02	Roboklon
qPCRBIO SyGreen Mix Hi-ROX	PB20.12	PCR Biosystems
Streptavidin Conjugation Kit	ab102921	Abcam
QIAprep Spin Miniprep Kit	27104	QIAGEN
QIAquick Gel Extraction Kit	28704	QIAGEN
QIAquick PCR Purification Kit	28104	QIAGEN
Zombie Aqua™ Fixable Viability Kit	423102	BioLegend

2.4 Chemicals, mediums, additives

Product	Catalog number	Manufacturer
2-Mercaptoethanol	31350010	Thermo Scientific
Acetic acid (CH ₃ COOH)	3738	Carl Roth
Acrylamide/bisacrylamide 30% (37,5:1)	3029	Carl Roth
Agar-Agar	1347.2	Carl Roth
Agarose	16500500	Thermo Scientific
Albumin Fraktion V (BSA)	T844.4	Carl Roth
Ammonium chloride (NH ₄ Cl)	P726	Carl Roth
Ammoniumperoxodisulfat (APS)	9592	Carl Roth
BD OptEIA (TMB)	555214	BD Biosciences
Bicine	10100525	MP Biomedicals
Biotin	B4501	Sigma-Aldrich
Bis-Tris	10103825	MP Biomedicals
Brefeldin A	420601	BioLegend
Bromophenol blue	T8154	Sigma-Aldrich
c-di-AMP	HY-12326	MedChemExpress
Carbenicillin disodium salt	6344.2	Carl Roth
Cell Activation Cocktail	423301	BioLegend
CpG ODN 2395	IAX-200-007-M001	Biomol
CutSmart Buffer	B7204	New England Biolabs
Dasatinib	1586	BioVision
Dimethyl Sulfoxide (DMSO)	20385	Serva
DMEM + GlutaMAX TM -I	61965-026	Thermo Scientific
Ethanol	32221	Sigma-Aldrich
Ethidium Bromide	2218.1	Carl Roth
Ethylenediaminetetraacetic acid (EDTA)	E5134	Sigma-Aldrich
FCS	P40-47500	PAN-Biotech
Gel Loading Dye, Purple (6X)	B7024	New England Biolabs
Geneticindisulfat (G418)	CP11.2	Carl Roth
Glycerol	A0970	AppliChem
HEPES Buffer Solution	15630056	Thermo Scientific
Hydrogen chloride (HCl)	4625	Carl Roth
Isoflurane	1182097	HenrySchein
Isopropanol	33539	Sigma-Aldrich
Kanamycin	T832.1	Carl Roth
Magnesium chloride (MgCl ₂)	2189	Carl Roth
MEM Non-Essential Amino Acids	11140050	Thermo Scientific
Methanol	32213	Sigma-Aldrich
Milk powder	T145.2	Carl Roth
Monensin	420701	BioLegend
Montanide ISA 51 VG	36362ZFL2R3	SEPPIC
NEBuffer 2	B7002	New England Biolabs
OptiMEM + GlutaMAX TM -I	51985-026	Thermo Scientific

Material

OptiPrep (Ioidixanol)	7820	Stemcell
PBS	14190-094	Thermo Scientific
PEG 8000	41600048-3	Biotrend
Pen/Strep	15070-063	Thermo Scientific
Phenol red	P0290	Sigma-Aldrich
Polyethylenimine (PEI)	23966-2	Sigma-Aldrich
Potassium bicarbonate (KHCO ₃)	P748	Carl Roth
Potassium chloride (KCl)	6781	Carl Roth
RPMI 1640 + GlutaMAX™-I	61870-010	Thermo Scientific
Sodium azide (NaN ₃)	K305	Carl Roth
Sodium bicarbonate (NaHCO ₃)	6885.2	Carl Roth
Sodium carbonate (Na ₂ CO ₃)	A135.1	Carl Roth
Sodium citrate	A2403	AppliChem
Sodium chloride (NaCl)	3957	Carl Roth
Sodium dodecyl sulfate (SDS)	A7249	AppliChem
Strep-AF488	S11223	Thermo Scientific
Strep-HRP	N100	Thermo Scientific
Sucrose	A4734	AppliChem
Sulfuric acid (H ₂ SO ₄)	4623	Carl Roth
T4 DNA Ligase Reaction Buffer	B0202	New England Biolabs
TEMED	2367	Carl Roth
Tricine	6977	Carl Roth
Tris	4855	Carl Roth
Trypsin-EDTA	25300-054	Thermo Scientific
Tryptone	6681	Carl Roth
Tween20	P2287	Sigma-Aldrich
UltraComp eBeads Compensation Beads	01-2222-41	Thermo Scientific
Western-Lightning Plus	NEL105001EA	PerkinElmer
Yeast extract	2363.3	Carl Roth

2.5 Antibodies and Tetramers

Antibody	Clone	Host	Catalog number	Manufacturer
PacificBlue anti-mouse B220	RA3-6B2	rat	103227	BioLegend
anti-mouse CD20	SA271G2	rat	152104	BioLegend
APC-CD3	17A2	rat	565643	BD Biosciences
PE anti-mouse CD3	145-2C11	armenian hamster	100307	BioLegend
anti-mouse CD4	GK1.5	rat	BE0003-1	BioXCell
FITC anti-mouse CD4	GK1.5	rat	100406	BioLegend
PE anti-mouse CD4	RM4-4	rat	116005	BioLegend
anti-mouse CD40	FGK45	rat	BE0016-2	BioXCell
PE anti-mouse CD40	3/23	rat	124609	BioLegend
BV510 anti-mouse CD8	53-6.7	rat	100751	BioLegend

Material

FITC anti-mouse CD8	KT15	rat	D271.4	MBL
PerCP/Cy5.5 anti-mouse CD8	53-6.7	rat	100734	BioLegend
APC anti-mouse IFN- γ	XMG1.2	rat	505810	BioLegend
PE/Cy7 anti-mouse TNF- α	MP6-XT22	rat	506324	BioLegend
anti-AAV2 (intact particle)	A20	mouse	61055	PROGEN
anti-AAV2 (intact particle), biotin conjugate	A20	mouse	61555	PROGEN
anti-AAV2 (intact particle), hybridoma supernatant	A20	mouse	/	kindly provided by Martin Müller (DKFZ, Heidelberg)
HRP anti-mouse IgG	polyclonal	goat	115-035-003	Dianova
PE anti-mouse IgG	polyclonal	goat	115-116-072	Jackson ImmunoResearch
HRP anti-rat IgG	polyclonal	goat	405405	BioLegend
Rat IgG2b isotype control	LTF-2	rat	BE0090	BioXCell
anti-mouse CD16/CD32 (BD Fc Block TM)	2.4G2	rat	553141	BD Biosciences
Tetramer			Catalog number	Manufacturer
APC H-2Kb/SIINFEKL MHC Tetramer			MKb-001	Tetramer Shop

2.6 Enzymes

Enzyme	Catalog number	Manufacturer
Ascl	R0558	New England Biolabs
Benzonase Nuclease	70746-3	Merck Millipore
Calf Intestinal Phosphatase (CIP)	M0290S	New England Biolabs
HindIII	R0104	New England Biolabs
MluI-HF	R3198	New England Biolabs
NheI	R0131	New England Biolabs
SpeI	R0133	New England Biolabs
T4 DNA Ligase	M0202	New England Biolabs
T4 Polynukleotidkinase	M0201S	New England Biolabs
XbaI	R0145	New England Biolabs

2.7 Peptides

Peptide	Sequence	Catalog number	Manufacturer
Chicken Ovalbumin(257-264)	SIINFEKL	S7951	Sigma-Aldrich
Chicken Ovalbumin(323-339) (OVAII)	ISQAVHAAHAEINEAGR	RP10610-1	GenScript
PADRE	AKFVAAWTLKAAA	P2284.9505	Genaxxon Bioscience
AAV_p0	PPPKPAERHKDDSRGLV		DKFZ
AAV_p1	NPYLKYNHADAQEFQERL		DKFZ
AAV_p2	VFTDSEYQLPYVLGSAHQGC		DKFZ
AAV_p3	TFEDVPFHSSYAHSQSLDR		DKFZ
AAV_p4	QYLYLSRTNTPSGTT		DKFZ
AAV_p5	TTQSRLQFSQAGASDIRDQ		DKFZ
AAV_p6	NGRDSLVPNGPAMASHKDD		DKFZ
AAV_p7	TDEEEIRTTNPVATEQYG		DKFZ
AAV_p8	VATEQYGSVSTNASASIINF		DKFZ
AAV_p9	ILIKNTPVPANPSTTFSAAKFASFITQ		DKFZ
AAV_p10	FITQYSTGQVSVEIEW		DKFZ
AAV_p11	VDTNGVYSEPRPIGTRYLT		DKFZ
Kif18b(21)mut	PSFQEFVDWENVSPELNSTDQ		DKFZ
Kif18b(21)wt	PSFQEFVDWEKVSPELNSTDQ		DKFZ
Ddb1(21)mut	SFVGQTRVLMINGEEVEEEL		DKFZ
Ddb1(21)wt	SFVGQTRVLMINGEEVEEEL		DKFZ
Golgb1(21)mut	AAPSAASSPADVQSLKKAMSS		DKFZ
Golgb1(21)wt	AAPSAASSPAEVQSLKKAMSS		DKFZ
Snx5(21)mut	NFKRKRVAAFQKNLIEMSELE		DKFZ
Snx5(21)wt	NFKRKRVAAFRKNLIEMSELE		DKFZ
FLAGTag	DYKDDDDK		DKFZ
LCMV_NP ₃₉₆₋₄₀₄	FQPQNGQFI		DKFZ
HPV_E6 ₄₈₋₅₇	EVYDFAFRDL		DKFZ

2.8 Plasmids

Expression plasmids

pDB2_CMV_xxx	Expression plasmid. Target protein (xxx) is flanked by CMV promoter and SV40 poly(A) signal. Kanamycin resistance.
pDB2_CMV_BirA	<i>BirA expression plasmid. Cloned into pDB2_CMV_xxx via HindIII and XbaI.</i>
pDB2_CMV_CD40	<i>Murine CD40 expression plasmid. Cloned into pDB2_CMV_xxx via NotI and XbaI.</i>

Plasmids for AAVLP production

pds-CMV-eGFP	AAV packaging plasmid. eGFP cDNA controlled by CMV promoter is flanked by AAV2 ITRs. Ampicillin resistance. Kindly provided by Oliver Müller (DKFZ, Heidelberg).
pDGΔVP	Adenoviral helper plasmid. Encoding VA, E2A and E4. Ampicillin resistance. Kindly provided by Oliver Müller (DKFZ, Heidelberg).

Capsid plasmids with wt sequence

pMT-AAV2wtRC	AAV <i>rep/cap</i> plasmid. Encodes AAV2 Rep and Cap proteins with wt sequence. Ampicillin resistance.
--------------	--

Capsid plasmids with peptide insertion at aa588

pMT-187-XX2_(588)mut	AAV <i>rep/cap</i> plasmid. Encodes AAV2 Rep and Cap proteins. Insertion site in <i>cap</i> for the integration of peptides (mut) via MluI and AscI at aa588. Ampicillin resistance.
pMT-187-XX2_(588)SIINFEKL	Cap with SIINFEKL antigen inserted at aa588: SIINFEKL
pMT-187-XX2_(588)OVAII-L	Cap with OVAII antigen inserted at aa588, including linker sequences: GGGGS ISQAVHAAHAEINEAGR GGGGA
pMT-187-XX2_(588)OVAII-L_PLA2mut	Cap with mutated PLA2 site and OVAII antigen inserted at aa588: GGGGS ISQAVHAAHAEINEAGR GGGGA
pMT-187-XX2_(588)Kif18b(21)	Cap with neoantigen Kif18b (21 aa long) inserted at aa588: QQLDITYILKNVVAFSRTDKYR
pMT-187-XX2_(588)Pbk(21)	Cap with neoantigen Pbk (21 aa long) inserted at aa588: SPFPAAVILRDLHMARGLKY
pMT-187-XX2_(588)Ddb1(21)	Cap with neoantigen Ddb1 (21 aa long) inserted at aa588: SFVGQTRVLMINGEEVEETEL
pMT-187-XX2_(588)Dpf2(21)	Cap with neoantigen Dpf2 (21 aa long) inserted at aa588: GLALPNNYCDVCLGDSKINKK
pMT-187-XX2_(588)Rpl13a(21)	Cap with neoantigen Rpl13a (21 aa long) inserted at aa588: HLLGRLAAIVGKQVLLGRKVV
pMT-187-XX2_(588)Fat1(21)	Cap with neoantigen Fat1 (21 aa long) inserted at aa588: SMDHKTGTIAMQNTTQLRSRY
pMT-187-XX2_(588)Fzd7(21)	Cap with neoantigen Fzd7 (21 aa long) inserted at aa588: YFMVAVAHVAAFLEDRVCV
pMT-187-XX2_(588)Golgb1(21)	Cap with neoantigen Golgb1 (21 aa long) inserted at aa588: AAPSAASSPADVQSLKKAMSS
pMT-187-XX2_(588)Plod2(21)	Cap with neoantigen Plod2 (21 aa long) inserted at aa588: NYNTSHLNNDVWQIFENPVDW
pMT-187-XX2_(588)Orc2(21)	Cap with neoantigen Orc2 (21 aa long) inserted at aa588: QKTLHNLLRKVVPSFAEIER
pMT-187-XX2_(588)Klh12(21)	Cap with neoantigen Klh12 (21 aa long) inserted at aa588: QQLDITYILKNVVAFSRTDKYR

Material

<i>pMT-187-XX2_(588)Tm9sf3(21)</i>	Cap with neoantigen <i>Tm9sf3</i> (21 aa long) inserted at aa588: AFFINFIAIY H HASRAIPFGT
<i>pMT-187-XX2_(588)Snx5(21)</i>	Cap with neoantigen <i>Snx5</i> (21 aa long) inserted at aa588: NFKRKRVA A F Q KNLIEMSELE
<i>pMT-187-XX2_(588)Armc1(21)</i>	Cap with neoantigen <i>Armc1</i> (21 aa long) inserted at aa588: KMKGELGMMLILQNV I QKTTT
<i>pMT-187-XX2_(588)LCMV_NP₃₉₆₋₄₀₄</i>	Cap with LCMV antigen <i>NP₃₉₆₋₄₀₄</i> inserted at aa588: FQPQNGQFI
<i>pMT-187-XX2_(588)HPV_E₆₄₈₋₅₇</i>	Cap with HPV antigen <i>E₆₄₈₋₅₇</i> inserted at aa588: EYDFAFRDL

*Bold letter indicates mutated amino acid

Capsid plasmids with peptide insertion at aa453

<i>pMT-187-XX2_(453)mut</i>	AAV <i>rep/cap</i> plasmid. Encodes AAV2 Rep and Cap proteins. Insertion site in <i>cap</i> for the integration of peptides (mut) via NheI and SpeI at aa453. Ampicillin resistance.
<i>pMT-187-XX2_(453)SIINFEKL</i>	Cap with <i>SIINFEKL</i> antigen inserted at aa453: SIINFEKL
<i>pMT-187-XX2_(453)OVAII</i>	Cap with <i>OVAII</i> antigen inserted at aa453: ISQAVHAAHAEINEAGR
<i>pMT-187-XX2_(453)OVAII_PLA2mut</i>	Cap with mutated <i>PLA2</i> site and <i>OVAII</i> antigen inserted at aa453: ISQAVHAAHAEINEAGR
<i>pMT-187-XX2_(453)Kif18b(21)</i>	Cap with neoantigen <i>Kif18b</i> (21 aa long) inserted at aa453: QQLD T YILKN V VAFSRTDKYR
<i>pMT-187-XX2_(453)Pbk(21)</i>	Cap with neoantigen <i>Pbk</i> (21 aa long) inserted at aa453: SPFPAAVIL R DALHMARGLKY
<i>pMT-187-XX2_(453)Ddb1(21)</i>	Cap with neoantigen <i>Ddb1</i> (21 aa long) inserted at aa453: SFV G QTRVLMINGEEVEE T EL
<i>pMT-187-XX2_(453)Dpf2(21)</i>	Cap with neoantigen <i>Dpf2</i> (21 aa long) inserted at aa453: GLALPN N YCDVCLGDSKIN K K
<i>pMT-187-XX2_(453)Rpl13a(21)</i>	Cap with neoantigen <i>Rpl13a</i> (21 aa long) inserted at aa453: HLLGRLAA I V G KQVLLGRK V V
<i>pMT-187-XX2_(453)Fat1(21)</i>	Cap with neoantigen <i>Fat1</i> (21 aa long) inserted at aa453: SMDHKTGTIAMQNTTQLRSRY
<i>pMT-187-XX2_(453)Fzd7(21)</i>	Cap with neoantigen <i>Fzd7</i> (21 aa long) inserted at aa453: YFMVAVAHV A AFLLEDRAVC V
<i>pMT-187-XX2_(453)Golgb1(21)</i>	Cap with neoantigen <i>Golgb1</i> (21 aa long) inserted at aa453: AAPSAASS P AD V QSLKKAMSS
<i>pMT-187-XX2_(453)Plod2(21)</i>	Cap with neoantigen <i>Plod2</i> (21 aa long) inserted at aa453: NYNTSHLN N D V WQIFENPVD W
<i>pMT-187-XX2_(453)Orc2(21)</i>	Cap with neoantigen <i>Orc2</i> (21 aa long) inserted at aa453: QKTLHN L L R K V VPFS A EIER
<i>pMT-187-XX2_(453)Klh122(21)</i>	Cap with neoantigen <i>Klh122</i> (21 aa long) inserted at aa453: QQLD T YILKN V VAFSRTDKYR

Material

<i>pMT-187-XX2_(453)Tm9sf3(21)</i>	<i>Cap with neoantigen Tm9sf3 (21 aa long) inserted at aa453: AFFINFIAYHHASRAIPFGT</i>
<i>pMT-187-XX2_(453)Snx5(21)</i>	<i>Cap with neoantigen Snx5 (21 aa long) inserted at aa453: NFKRKRVAAFQKNLIEMSELE</i>
<i>pMT-187-XX2_(453)Armc1(21)</i>	<i>Cap with neoantigen Armc1 (21 aa long) inserted at aa453: KMKGELGMMLILQNVIQKTTT</i>

Capsid plasmids with double peptide insertion at aa453 and aa588

<i>pMT-187-XX2_(453)mut_(588)mut</i>	AAV <i>rep/cap</i> plasmid. Encodes AAV2 Rep and Cap proteins. Insertion site in <i>cap</i> for the integration of peptides (mut) via NheI and SpeI at aa453, and MluI and AclI at aa588. Ampicillin resistance.
<i>pMT-187-XX2_(453)BAP-L_(588)SIINFEKL-L</i>	<i>Cap with BAP inserted at aa453 and SIINFEKL antigen inserted at aa588, including linker sequences: GGGGS GLNDIFEAQKIEWHE GGGGA (453) + GGGGS SIINFEKL GGGGA (588)</i>
<i>pMT-187-XX2_(453)ICBL_(588)SIINFEKL</i>	<i>Cap with J-ICBL peptide inserted at aa453 and SIINFEKL antigen inserted at aa588: DLLKNGERIEKVE (453) + SIINFEKL (588)</i>

Capsid plasmid of AAV serotype 5 with peptide insertion at aa578

<i>pMT-rep2cap5-SfiI578</i>	AAV <i>rep/cap</i> plasmid. Encodes AAV2 Rep and AAV5 Cap proteins. Insertion site in <i>cap</i> for the integration of peptides (SfiI578) via SfiI at aa578. Ampicillin resistance. Kindly provided by Oliver Müller (DKZF, Heidelberg).
<i>pMT_rep2cap5_SIINFEKL</i>	<i>AAV5 Cap with SIINFEKL antigen inserted at aa578: SIINFEKL</i>

2.9 Single-stranded oligonucleotides

Oligonucleotides for capsid insertion at aa588

O345	SIINFEKL588_fwd	5'-cgcgTCCGCGAGCATCATCAACTTCGAGAAGCTTGCGG-3'
O346	SIINFEKL588_rev	5'-cgcgCCGCAAGCTTCTCGAAGTTGATGATGCTCGCGGA-3'
O699	Kif18b(21)588_fwd	5'-cgcgTCCGCGCCAAGCTTTCAGGAATTTGTGGATTGGGAAAACGTGAGC CCGG AACTGAACAGCACCGATCAGGCGG-3'
O700	Kif18b(21)588_rev	5'-cgcgCCGCTGATCGGTGCTGTTTTCAGTTCCGGGCTCACGTTTTCCCAATC CACAAATTCCTGAAAGCTTGGCGCGGA-3'
O701	Pbk(21)588_fwd	5'-cgcgTCCGCGAGCCGTTTCCGGCGGCGGTGATTCTGCGGATGCGCTG CATAT GGCTCGAGGCTGAAATATGCGG-3'
O702	Pbk(21)588_rev	5'-cgcgCCGCATATTTTCAGGCTCGAGCCATATGCAGCGCATCGCGCAGAA TCACCGCCCGGAAACGGGCTCGCGGA-3'
O703	Ddb1(21)588_fwd	5'-cgcgTCCGCGAGCTTGTGGGCCAGACCCGGGTGCTGATGATTAACGGC GAAGA AGTGGAAGAAACCGAACTGGCGG-3'

Material

0704	Ddb1(21)588_rev	5'-cgcgCCGCCAGTTCGGTTTCTTCCACTTCTTCGCCGTTAATCATCAGCACC CGGGTCTGGCCCAAAGCTCGCGGA-3'
0705	Dpf2(21)588_fwd	5'-cgcgTCCGCGGGGCTAGCGCTGCCGAACAACTATTGCGATGTGTGCCTG GGCGA TAGCAAAATTAACAAAAAAGCGG-3'
0706	Dpf2(21)588_rev	5'-cgcgCCGCTTTTTTGTAAATTTTGCTATCGCCCAGGCACACATCGCAATA GTTGTTTCGGCAGCGCTAGCCCCGCGGA-3'
0707	Rpl13a(21)588_fwd	5'-cgcgTCCGCGCATCTGCTGGGCCGGCTAGCGGCGATTGTGGGCAAACA GGTGCTGCTGGGCCGAAAGTGGTGGCGG-3'
0708	Rpl13a(21)588_rev	5'-cgcgCCGCCACCACTTTGCGGCCAGCAGCACCTGTTTGCCACAATCGC CGTAGCCGGCCCAGCAGATGCGCGGA-3'
0709	Fat1(21)588_fwd	5'-cgcgTCCGCGTCCATGGATCATAAAACCGGCACCATTGCGATGCAGAAC ACCACCCAGCTGCGCAGCCGCTATGCGG-3'
0710	Fat1(21)588_rev	5'-cgcgCCGCATAGCGGCTGCGCAGCTGGGTGGTGTCTGCATCGCAATGG TGCCGGTTTTATGATCCATGACGCGGA-3'
0721	Fzd7(21)588_fwd	5'-cgcgTCCGCGTATTTTATGGTGGCGGTGGCGCATGTGGCGGCGTTTCTT CTAGAAGATCGCGCGGTGTGCGTGGCGG-3'
0722	Fzd7(21)588_rev	5'-cgcgCCGCCACGCACACC CGCGATCTTCTAGAAGAAACGCCCCACAT GCGCCACCGCCACCATAAAATACGCGGA-3'
0723	Golgb1(21)588_fwd	5'-cgcgTCCGCGGGCGCGCCGAGCGCGGCGAGCAGCCCGGCGGATGTGCA AAGCTTGAAAAAAGCGATGAGCAGCGCGG-3'
0724	Golgb1(21)588_rev	5'-cgcgCCGCGCTGCTCATCGCTTTTTTCAAGCTTTCACATCCGCCGGGCT GCTCGCCGCGCTCGGCGCCGCCGCGGA-3'
0725	Plod2(21)588_fwd	5'-cgcgTCCGCGAACTATAACACCAGCCATCTGAACAACGATGTGTGGCAG ATTTTTGAAAACCCGGTCTGACTGGGCGG-3'
0726	Plod2(21)588_rev	5'-cgcgCCGCCAGTCGACCGGGTTTTCAAAAATCTGCCACACATCGTTGTT CAGATGGCTGGTGTATAGTTCGCGGA-3'
0727	Orc2(21)588_fwd	5'-cgcgTCCGCGCAGAAAACCTGCATAACCTGCTGCGCAAAGTGGTGCCA AGCTTTAGCGCGGAAATTGAACGCGCGG-3'
0728	Orc2(21)588_rev	5'-cgcgCCGCGCGTTCAATTTCCGCGCTAAAGCTTGGCACCCTTTGCGCAG CAGGTTATGCAGGGTTTTCTGCGCGGA-3'
0729	Klhl22(21)588_fwd	5'-cgcgTCCGCGCAGCAGCTGGATACCTATATTCTTAAGAACGTGGTGGCG TTAGCCGCACCGATAAAATATCGCGCGG-3'
0730	Klhl22(21)588_rev	5'-cgcgCCGCGCGATATTTATCGGTGCGGCTAAACGCCACCACGTTCTTAAG AATATAGGTATCCAGCTGCTGCGCGGA-3'
0731	Tm9sf3(21)588_fwd	5'-cgcgTCCGCGGCGTTTTTTATAAACTTTATTGCGATTTATCATCATGCGAG CCGCGCGATTCCGTTTGGCACCCGCGG-3'
0732	Tm9sf3(21)588_rev	5'-cgcgCCGCGGTGCCAAACGGAATCGCGCGGCTCGCATGATGATAAATCG CAATAAAGTTTATAAAAAACGCCGCGGA-3'
0733	Snx5(21)588_fwd	5'-cgcgTCCGCGAACTTTAAACGCAAACGCGTGGCGGCGTTTCAGAAAAAC CTGATTGAAATGAGCGAACTCGAGGCGG-3'
0734	Snx5(21)588_rev	5'-cgcgCCGCTCGAGTTCGCTCATTTCAATCAGTTTTTCTGAAACGCCGC CACGCGTTTGCGTTTAAAGTTCGCGGA-3'
0735	Armc1(21)588_fwd	5'-cgcgTCCGCGAAAATGAAAGGCGAACTGGGCATGATGCTGATTCTGCAG AACGTGATTGAGAAAACCACCACCGCGG-3'
0736	Armc1(21)588_rev	5'-cgcgCCGCGGTGGTGGTTTTCTGAATCACGTTCTGCAGAATCAGCATCAT GCCAGTTCGCTTTCAATTTTCGCGGA-3'

Material

0784	LCMV_NP_588_fwd	5'-cgcgTCCGCGTTTCAGCCGCAGAACGGCCAGTTTATTGCGG-3'
0785	LCMV_NP_588_rev	5'-cgcgCCGCAATAAACTGGCCGTTCTGCGGCTGAAACGCGGA-3'
0790	HPV_E6_588_fwd	5'-cgcgTCCGCGGAAGTGTATGATTTTTCGTTTCGCGATCTGGCGG-3'
0791	HPV_E6_588_rev	5'-cgcgCCGCCAGATCGCGAAACGCAAATCATACACTTCCGCGGA-3'

*lowercase letters indicate DNA overhangs

Oligonucleotides for capsid insertion at aa453

0651	Kif18b(21)453_fwd	5'-ctagCAGCGGACCAAGCTTTCAGGAATTTGTGGATTGGGAAAACGTGAG CCCGAACTGAACAGCACCGATCAGA-3'
0652	Kif18b(21)453_rev	5'-ctagTCTGATCGGTGCTGTTTCAGTTCGGGCTCACGTTTTCCCAATCCAC AAATTCCTGAAAGCTTGGTCCGCTG-3'
0653	Pbk(21)453_fwd	5'-ctagCAGCGGAAGCCCGTTTCCGGCGGCGGTGATTCTGCGCGATGCGCT GCATATGGCTCGAGGCTGAAATATA-3'
0654	Pbk(21)453_rev	5'-ctagTATATTTTCAGGCCTCGAGCCATATGCAGCGCATCGCGCAGAATCAC CGCCCGGAAACGGGCTTCCGCTG-3'
0655	Ddb1(21)453_fwd	5'-ctagCAGCGGAAGCTTGTGGGCCAGACCCGGGTGCTGATGATTAACG GCGAAGAAGTGAAGAAACCGAACTGA-3'
0656	Ddb1(21)453_rev	5'-ctagTCAGTTCGGTTTCTTCCACTTCTTCGCCGTTAATCATCAGCACCCGG GTCTGGCCACAAAGCTTCCGCTG-3'
0657	Dpf2(21)453_fwd	5'-ctagCAGCGGAGGGCTAGCGCTGCCGAACAATTTGCGATGTGTGCCT GGGCGATAGCAAAATTAACAAAAAAA-3'
0658	Dpf2(21)453_rev	5'-ctagTTTTTTGTAAATTTTGCTATCGCCAGGCACACATCGCAATAGTTG TTCGGCAGCGCTAGCCCTCCGCTG-3'
0659	Rpl13a(21)453_fwd	5'-ctagCAGCGGACATCTGCTGGGCGGCTAGCGGCGATTGTGGGCAAAC AGGTGCTGCTGGGCCGCAAAGTGGTGA-3'
0660	Rpl13a(21)453_rev	5'-ctagTCACCACTTTGCGGCCAGCAGCACCTGTTGCCACAATCGCCGC TAGCCGGCCAGCAGATGTCCGCTG-3'
0661	Fat1(21)453_fwd	5'-ctagCAGCGGATCCATGGATCATAAAACCGGCACCATTGCGATGCAGAA CACCACCAGCTGCGCAGCCGCTATA-3'
0662	Fat1(21)453_rev	5'-ctagTATAGCGGCTGCGCAGCTGGGTGGTGTCTGCATCGCAATGGTGC CGTTTTATGATCCATGGATCCGCTG-3'
0667	Fzd7(21)453_fwd	5'-ctagCAGCGGATATTTTATGGTGGCGGTGGCGCATGTGGCGGCGTTTCT TCTAGAAGATCGCGCGGTGTGCGTGA-3'
0668	Fzd7(21)453_rev	5'-ctagtCACGCACACCGCGCATCTTCTAGAAGAAACGCCGCCACATGCGC CACCGCCACCATAAAATATCCGCTG-3'
0669	Golgb1(21)453_fwd	5'-ctagCAGCGGAGCGGCCGAGCGCGGCGAGCAGCCCGGCGGATGTG CAAAGCTTGAAAAAGCGATGAGCAGCA-3'
0670	Golgb1(21)453_rev	5'-ctagTGCTGCTCATCGCTTTTTCAAGCTTTCACATCCGCCGGGCTGCTC GCCGCGCTCGGCGCCGCTCCGCTG-3'
0671	Plod2(21)453_fwd	5'-ctagCAGCGGAACTATAACACCAGCCATCTGAACAACGATGTGTGGCA GATTTTTGAAAACCCGGTCTGACTGGA-3'
0672	Plod2(21)453_rev	5'-ctagTCCAGTCGACCGGTTTTCAAAAATCTGCCACACATCGTTGTTTCCAG ATGGCTGGTGTATAGTTTCCGCTG-3'

Material

O673	Orc2(21)453_fwd	5'-ctagCAGCGGACAGAAAACCTGCATAACCTGCTGCGCAAAGTGGTGCC AAGCTTTAGCGCGGAAATTGAACGCA-3'
O674	Orc2(21)453_rev	5'-ctagTGC GTTCAATTTCCGCGCTAAAGCTTGGCACC ACTTTGCGCAGCAG GTTATGCAGGGTTTTCTGTCCGCTG-3'
O675	Klhl22(21)453_fwd	5'-ctagCAGCGGACAGCAGCTGGATACCTATATTCTTAAGAACGTGGTGCC GTTTAGCCGCACCGATAAAATATCGCA-3'
O676	Klhl22(21)453_rev	5'-ctagTGC GATTTTATCGGTGCGGCTAAACGCCACCACGTTCTTAAGAAT ATAGGTATCCAGCTGCTGTCCGCTG-3'
O677	Tm9sf3(21)453_fwd	5'-ctagCAGCGGAGCGTTTTTTATAAACTTTATTGCGATTTATCATCATGCG AGCCGCGCGATTCCGTTTGGCACCA-3'
O678	Tm9sf3(21)453_rev	5'-ctagTGGTGCCAAACGGAATCGCGCGGCTCGCATGATGATAAATCGCAA TAAAGTTTATAAAAAACGCTCCGCTG-3'
O679	Snx5(21)453_fwd	5'-ctagCAGCGGAAACTTTAAACGCAAACGCGTGGCGGCGTTTCAGAAAAA CCTGATTGAAATGAGCGAACTCGAGA-3'
O680	Snx5(21)453_rev	5'-ctagTCTCGAGTTCGCTCATTTCAATCAGGTTTTTCTGAAACGCCGCCAC GCGTTTGC GTTTAAAGTTTCCGCTG-3'
O681	Armc1(21)453_fwd	5'-ctagCAGCGGAAAAATGAAAGGCGAACTGGGCATGATGCTGATTCTGC AGAACGTGATTGAGAAAACCACCACCA-3'
O682	Armc1(21)453_rev	5'-ctagTGGTGGTGGTTTTCTGAATCACGTTCTGCAGAATCAGCATCATGCC CAGTTCGCCTTTTCATTTTTCCGCTG-3'
O66	ICBL_453_fwd	5'-ctagCAGCGGAGATCTGCTTAAGAACGGCGAACGCATTGAAAAAGTGG AAA-3'
O67	ICBL_453_rev	5'-ctagTTTCCACTTTTTCAATGCGTTCGCCGTTCTTAAGCAGATCTCCG CTG-3'

Oligonucleotides for capsid insertion at aa453 and aa588 with linkers

O515	Linker453_fwd1	5'-ctagCGGCGGTGGCGGTagc-3'
O517	Linker453_rev1	5'-ACCGCCACCGCCG-3'
O516	Linker453_fwd2	5'-GGTGGCGGTGCCA-3'
O518	Linker453_rev2	5'-ctagTGGCACC GCCACCgcc-3'
O519	Linker588_fwd1	5'-cgcgGGCGGTGGCGGTagc-3'
O521	Linker588_rev1	5'-ACCGCCACCGCC-3'
O520	Linker588_fwd2	5'-GGTGGCGGTGCCG-3'
O522	Linker588_rev2	5'-cgcgCGGCACC GCCACCgcc-3'
O345	SIINFEKL-Linker_fwd	5'AGCATCATCAACTTCGAGAAGCTTggc-3'
O346	SIINFEKL-Linker_rev	5'AAGCTTCTCGAAGTTGATGATGCTgct-3'
O503	OVAII-Linker_fwd	5'-ATCAGCCAGGCCGTGCACGCTGCACACGCCGAGATCAACGAGGCCGG CAGAggc-3'
O505	OVAII-Linker_rev	5'-TCTGCCGGCCTCGTTGATCTCGGCGTGTGCAGCGTGCACGGCCTGGCT GATgct-3'
O443	BAP-Linker_fwd	5'-GGTTTAAACGACATCTTCGAGGCCAGAAGATCGAGTGGCACG AGggc-3'
O445	BAP-Linker_rev	5'-CTCGTGCCACTCGATCTTCTGGG CCTCGAAGATGTCGTTAAACCgct-3'

Oligonucleotides for AAV5 capsid insertion at aa578

O593	SIINFEKL_AAV5_fwd	5'-TGGCGCGAGCATCATCAACTTCGAGAAGCTTGCCGccc-3'
O594	SIINFEKL_AAV5_rev	5'-CGGCAAGCTTCTCGAAGTTGATGATGCTCGCGCCAgtg-3'

2.10 PCR-Primers**Primers for subcloning**

P558	CD40_fwd	5'-tatgcgccgcATGGTGTCTTTCCTCGGCT-3'
P559	CD40_rev	5'-gtatctagaTCAGACCAGGGGCTCAAGG-3'
P483	BirA_fwd	5'-cagaagcttATGAAGGATAACACCGTGCCACT-3'
P484	BirA_rev	5'-gtatctagaTTATTTTCTGCACTACGCAGGG-3'

Primers for site-directed mutagenesis

P581	PLA2-mut_fwd	5'-CCGCGGCCCTCGAGGCCAACAAAGCCTACGAC-3'
P582	PLA2-mut_rev	5'-GTCGTAGGCTTTGTTGGCCTCGAGGGCCGCGG-3'

Sequencing primers

	CMV_fwd	5'-CGCAAATGGGCGGTAGGCGTG-3'
P50	AAV2-cap_fwd	5'-AGAGTCATCACCACCAGCAC-3'
P65	AAV2-cap_rev	5'-TTACAGATTACGAGTCAGGT-3'

qPCR primers

P61	GFP_qPCR_fwd	5'-ACGTAAACGGCCACAAGTTC-3'
P62	GFP_qPCR_rev	5'-AAGTCGTGCTGCTTCATGTG-3'

Primers to confirm neoantigen mutations in B16F10 cells

P306	Kif18b_seq_fwd	5'-GGACCATGGCAAAGCAACTG-3'
P307	Kif18b_seq_rev	5'-TTGTCTGCGGGACACAAACT-3'
P633	Pbk_seq_fwd	5'-TGTTTTGGTGTGCTGGTCCTGT-3'
P634	Pbk_seq_rev	5'-CATGTGGTAAGGAGGCCCAA-3'
P637	Ddb1_seq_fwd	5'-GTGCTGGCTCATGGTACACT-3'
P638	Ddb1_seq_rev	5'-CCCATGTCAAGCAAGGACCA-3'
P639	Dpf2_seq_fwd	5'-CAATCTTCTCCCGCCAGT-3'
P640	Dpf2_seq_rev	5'-AGGGAGTTAGGGAGGAGCAG-3'
P461	Rpl13a_seq_fwd	5'-GGTAGTAGGCATCCTGACGG-3'
P462	Rpl13a_seq_rev	5'-AAGTATGTGAGGCACCTTGG-3'

Material

P645	Fat1_seq_fwd	5'-ATCGCTGTCACTGTTGCTGA-3'
P646	Fat1_seq_rev	5'-CAGCTCATAGCGGCTTCGTA-3'
P619	Fzd7_seq_fwd	5'-ATGCTCTATGTACGCACCCG-3'
P620	Fzd7_seq_rev	5'-GGTAGCCATCGTCCGAGAAG-3'
P623	Golgb1_seq_fwd	5'-AAACAGCCGAAGAGAGGGTG-3'
P624	Golgb1_seq_rev	5'-TCCATGTGAAGAATGGCCCC-3'
P629	Plod2_seq_fwd	5'-GCCACTTGCTGATGTGTGTG-3'
P630	Plod2_seq_rev	5'-AAGGTCTTTCTCCACCCCCT-3'
P631	Orc2_seq_fwd	5'-TGGTTCTAGGCAAACCTTAGCAA-3'
P632	Orc2_seq_rev	5'-AGGTGTTACCCTTGGACCCT-3'
P635	Klhl22_seq_fwd	5'-GTGGCATCTCCTGCTTCCTT-3'
P636	Klhl22_seq_rev	5'-AAGCCCACAACACACTGGAA-3'
P481	Tm9sf3_seq_fwd	5'-GTCAGGATGGTTCAATGGCAAAA-3'
P482	Tm9sf3_seq_rev	5'-GTAGCCGATAGTTTTTGGAGCC-3'
P641	Snx5_seq_fwd	5'-GGGTGGGCATGAAACAAAGC-3'
P642	Snx5_seq_rev	5'-TCACCACTAAGCATGCACCA-3'
P643	Armc1_seq_fwd	5'-GCCTCGTTTTGACCTTGCAG-3'
P644	Armc1_seq_rev	5'-CTAGGTACGGTGGCACACAC-3'
P621	Eef2_seq_fwd	5'-CATGCTGATGCCATTACCG-3'
P622	Eef2_seq_rev	5'-GGTGTCTTCTGATGGGTGGG-3'
P310	Tnp03_seq_fwd	5'-TAGGGCCACCTGACACTACA-3'
P311	Tnp03_seq_rev	5'-GATCGCGACAAACGGAACAA-3'
P625	Atp11a_seq_fwd	5'-AGCCTCTTAGCCTCTGCTCT-3'
P626	Atp11a_seq_rev	5'-TCCCCGATCTGAAACTGTGC-3'
P627	Wdr82_seq_fwd	5'-GTGACTCACCTCTGCTGTC-3'
P628	Wdr82_seq_rev	5'-GCTGCTCCCACACAAAACAC-3'
P308	Cpsf3l_seq_fwd	5'-TGGGTACACGCTAAAAGGT-3'
P309	Cpsf3l_seq_rev	5'-ATTCCTGCCCACTTTCGGA-3'

2.11 Cell lines

Cell line	Provider
HEK293T	ACC 635; DSMZ
DC2.4	kindly provided by Kenneth Rock (UMass Medical School, Worcester)
B16F10	kindly provided by Stefan Eichmüller (DKFZ, Heidelberg)
B16F10-OVA	Kindly provided by Stefan Eichmüller (DKFZ, Heidelberg)

3 Methods

3.1 Peptides

Lyophilized peptides were dissolved in dimethyl sulfoxide (DMSO) and diluted to 10 mg/mL in H₂O with 10 % DMSO. If precipitation occurred upon dilution, peptides were dissolved in repeated cycles of vortexing and sonication.

3.2 Cell culture

All cell lines were maintained at 37 °C and 5 % CO₂ in a humidified atmosphere.

For subculturing of cells, culture medium was removed and cells were covered in trypsin-EDTA solution (0.05 %). Detached cells were resuspended in complete culture medium, counted using a CellDrop (DeNovix) and re-seeded at desired densities.

For long-term storage, cells were resuspended in fetal calf serum (FCS) containing 10 % DMSO and stored at -150 °C. Frozen cells were brought into culture by resuspension in warm culture medium, followed by centrifugation, resuspension and seeding into culture flasks.

HEK293T

Human embryonic kidney (HEK) 293T cells have been generated by transformation with sheared adenovirus type 5 DNA [139] and stable transfection with the simian virus 40 (SV40) large T antigen [140, 141]. As a remnant, they express the adenoviral gene E1, which is required for recombinant production of AAVs [54]. HEK293T cells were maintained in Dulbecco's Modified Eagle's Medium (DMEM) with GlutaMax™ supplemented with 10 % heat-inactivated FCS and 50 U/mL penicillin + 50 µg/mL streptavidin (Pen/Strep).

DC2.4

DC2.4 is a cell line derived from C57BL/6 mice, generated and immortalized by transduction of bone marrow cultures with granulocyte-macrophage colony-stimulating factor (GM-CSF) and oncogenes *myc* and *raf* [142]. DC2.4 cells were maintained in Gibco Roswell Park Memorial Institute (RPMI) 1640 Medium with GlutaMax™ supplemented with 10 % heat-

inactivated FCS, Pen/Strep, 1 % non-essential amino acids (NEAA), 10 mM HEPES and 50 μ M 2-mercaptoethanol.

B16F10

B16 is a melanoma cell line derived from C57BL/6 mice. B16F10 is a more proliferative variant of B16 and frequently used to study tumor growth and metastasis in C57BL/6 mice [143]. The cell line has been generated by ten successive rounds of intravenous (i.v.) injection into mice and excision of lung metastases [143]. B16F10 cells were maintained in RPMI 1640 Medium with GlutaMax™ supplemented with 10 % heat-inactivated FCS and Pen/Strep.

B16F10-OVA

B16F10-OVA is a variant of the B16F10 cell line that was transduced with chicken egg ovalbumin (Ova). The cells were maintained in RPMI 1640 Medium with GlutaMax™ supplemented with 10 % heat-inactivated FCS and Pen/Strep. In order to select for Ova expressing cells, 1 mg/mL G418 (Geneticin) was added to the culture medium.

3.3 Molecular biology

3.3.1 Agarose gel electrophoresis

Separation of DNA samples by size was performed using agarose gel electrophoresis. DNA was mixed with Gel Loading Dye and loaded on gels of 1 % agarose in Tris-acetate EDTA (TAE) buffer (w/v) (**Table 3.1**) containing 0.0001 % ethidium bromide. Electrophoresis was performed at 100 V in TAE buffer.

Table 3.1: TAE buffer

Component	Concentration
Tris	40 mM
EDTA	1 mM
Acetic acid	20 mM
H ₂ O	

3.3.2 Bacterial cultures

Bacteria were grown at 37 °C in lysogeny broth (LB) medium (**Table 3.2**) containing antibiotics Carbenicillin (100 µg/mL) or Kanamycin (100 µg/mL). For single cloning, bacteria were streaked and grown on plates of 15 g/L agar-agar in LB medium. Liquid bacterial cultures of 4 mL (small-scale; Miniprep) or 400 mL (large-scale; Maxiprep) LB medium were inoculated with single-cloned bacteria and grown shaking at 37 °C.

For long-term storage of cultures at -80 °C, glycerol was added to bacterial suspensions for a final concentration of 30 %.

Table 3.2: LB medium

Component	Concentration
Tryptone	10 g/L
Sodium chloride	10 g/L
Yeast extract	5 g/L
H ₂ O	

3.3.3 Transformation and Miniprep

Heat-competent *Escherichia coli* (*E. coli*) bacteria of the XL1 strain were thawed on ice, mixed with 25 ng plasmid DNA and pre-chilled for 15 min. To induce DNA internalization into XL1, bacteria were heated to 42 °C for 45 sec, cooled down on ice for 2 min, supplemented with 200 µL LB medium, and incubated shaking at 37 °C for 1 h. Transformed bacteria were grown overnight at 37 °C on antibiotic-containing LB agar plates. Single clones were selected and grown in small-scale liquid bacterial cultures, followed by plasmid purification using the Monarch Plasmid Miniprep Kit (NEB) according to manufacturer's instructions. Correct plasmid sequences were confirmed by control digest and sequencing (GENEWIZ, Leipzig, Germany).

3.3.4 Maxiprep

To expand plasmid DNA, LB medium containing the respective antibiotic was inoculated with transformed bacteria from small-scale liquid bacterial cultures or from frozen glycerol stocks. The culture was incubated overnight at 37 °C, before harvesting the bacteria by centrifugation at 5000 x g for 15 min. The plasmid DNA was isolated using the NucleoBond

Xtra Maxi kit (MACHEY-NAGEL) according to manufacturer's instructions and stored in H₂O at -20 °C.

3.3.5 Oligo annealing and ligation

To generate serotype 2 AAVLP capsid sequences with an inserted antigen, the target peptide sequence was translated into a DNA sequence using the "Reverse Translate" tool at bioinformatics.org and inserted into the AAV capsid DNA sequence via ligation, as follows:

Three capsid backbones encoding serotype 2 *rep* and *cap* genes with insertion sites were kindly provided by Silke Uhrig-Schmidt (DKFZ, Heidelberg). pMT-187-XX2_(588)mut for insertion in the VR-VIII loop ("aa588 peak") contains MluI and AclI restriction sites spanning amino acids 583 to 589 of the wt VP sequence. pMT-187-XX2_(453)mut for insertion in the VR-IV loop ("aa453 peak") contains NheI and SpeI restriction sites spanning amino acids 451 to 458. pMT-187-XX2_(453)mut_(588)mut contains both insertion sites (**Figure 3.1**). For each insertion, two complementary DNA oligonucleotides were designed (**2.9**) to build double-stranded DNA (dsDNA) sequences with single-stranded overhangs matching the restriction sites. Prior to annealing of oligonucleotides, ssDNA was phosphorylated by T4 Polynucleotide Kinase (T4 PNK) according to **Table 3.3**. To anneal ssDNA, phosphorylated forward (fwd) and reverse (rev) oligonucleotides were mixed according to **Table 3.4**, heated to 95 °C for 3 min and cooled down steadily to RT. The vector DNA containing the capsid backbone was linearized by restriction enzyme digest according to **Table 3.5**. Restriction sites were dephosphorylated by addition of 1 µL Calf Intestinal Alkaline Phosphatase (CIP), followed by incubation at 37 °C for 1 h. Phosphorylated dsDNA oligonucleotides were inserted into the linearized capsid vector using T4 DNA Ligase as shown in **Table 3.6**.

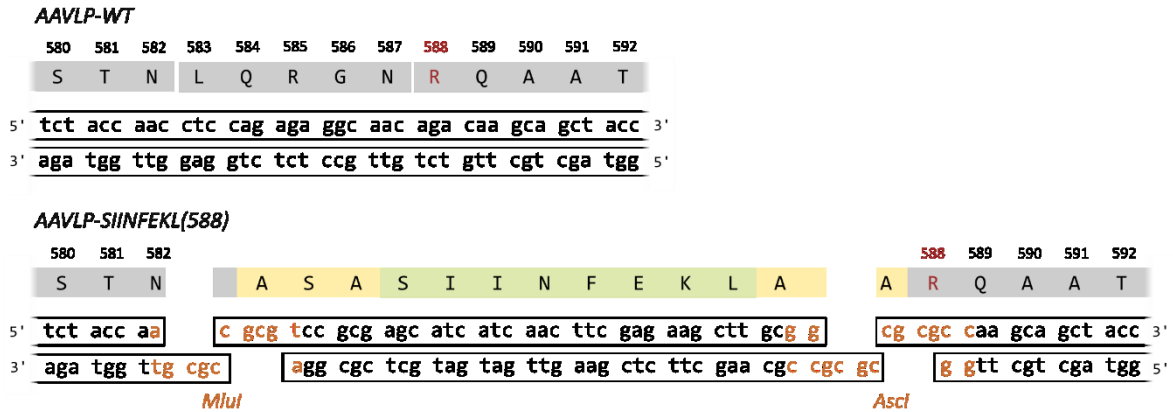
In some constructs, inserts contained additional linker sequences and the inserted oligonucleotides consisted of three fragments with matching overhangs. Annealed fragments were fused by ligation, and the full insert was purified by agarose gel electrophoresis. Purified inserts were integrated into the vector backbone by ligation as described for single-fragment inserts.

To generate serotype 5 AAVLP capsid sequences, annealed DNA oligonucleotides were inserted into the capsid backbone pMT-rep2cap5-SfiI578. The plasmid encodes AAV serotype 2 *rep* and AAV serotype 5 *cap* with two *SfiI* restriction sites spanning amino acids

576 to 579 of the wt VP sequence. Oligonucleotides were inserted as described previously, without the requirement for oligonucleotide phosphorylation and vector dephosphorylation.

Ligation products were transformed into XL1 bacteria and correct clones were selected as described in 3.3.3.

VR-VIII loop insertion (aa588)



VR-IV loop insertion (aa453)

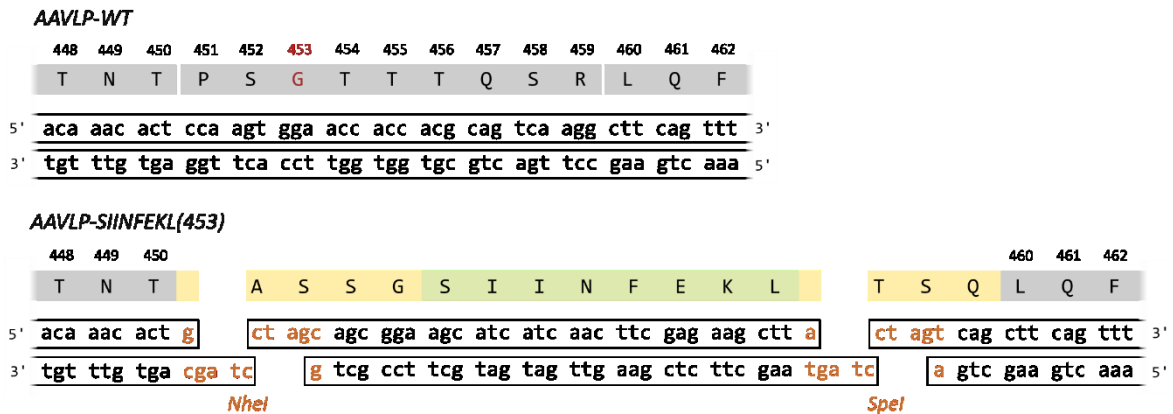


Figure 3.1: Design of peptide insertion site in the AAVLP capsid.

Exemplary insertion of the SIINFEKL antigen into the VR-VIII loop and VR-IV loop. The amino acids highlighted in grey show the wild type sequence of the AAVLP capsid protein VP1 (AAVLP-WT). Sequences highlighted in green and yellow indicate the inserted peptide and additional linker amino acids, respectively.

For peptide insertion, restriction sites (orange) have been inserted into the wild type sequence, excising a portion of the original capsid. Inserts are generated by annealing of complementary oligonucleotides, inducing single-stranded overhangs that match the restriction sites.

Amino acid 588 (aa588) and aa453 (red) represent the peak amino acids of the VR-VIII and VR-IV loop, respectively, and were used to indicate the peptide insertion sites.

Table 3.3: Phosphorylation of DNA oligonucleotides

Component	Volume
ssDNA oligonucleotide [100 μ M]	2.5 μ L
T4 PNK [10000 U/mL]	1.0 μ L
T4 DNA Ligase Reaction Buffer (10x)	1.0 μ L
H ₂ O	5.5 μ L
Reaction at 37° C, 30 min	
Inactivation at 65 °C, 20 min	

Table 3.4: Annealing of DNA oligonucleotides

Component	Volume
ssDNA oligonucleotide fwd [25 μ M]	10 μ L
ssDNA oligonucleotide rev [25 μ M]	10 μ L
NEBuffer 2 (10x)	2.2 μ L
H ₂ O	17.8 μ L

Table 3.5: Linearization of vector DNA

Component	Volume
Vector DNA [1 μ g/ μ L]	3 μ L
Enzyme 1 (NheI or Mlul-HF)	1 μ L
Enzyme 2 (SpeI od AclI)	1 μ L
CutSmart Buffer (10x)	5 μ L
H ₂ O	40 μ L
Reaction at 37 °C, 1 h	

Table 3.6: Ligation of dsDNA oligonucleotides into linearized vector DNA

Component	Volume
dsDNA oligonucleotides [62.5 nM]	1 μ L
Linearized vector DNA [50 ng/ μ L]	1 μ L
T4 DNA Ligase	1 μ L
T4 DNA Ligase Reaction Buffer (10x)	2 μ L
H ₂ O	15 μ L
<i>Reaction at RT, 30 min</i>	
<i>Inactivation at 65 °C, 10 min</i>	

3.3.6 Site-directed mutagenesis (SDM)

Some AAVLP capsids were modified by mutating HD at aa76 to AN (⁷⁶HD/AN), for inactivation of the PLA2 domain. To induce the mutation by SDM, complementary polymerase chain reaction (PCR) primers (P581 + P582) were designed, spanning the target

site, and changing three nucleotides in the original sequence (...GAG **CAC GAC** AAA... to ...GAG **GCC AAC** AAA...). The reaction mix was prepared according to **Table 3.7** and processed in a T3000 Thermocycler (Biometra) using PCR cycles as in **Table 3.8**. After PCR, the product was purified using a QIAquick PCR Purification Kit according to manufacturer's instructions. Purified DNA was transformed into XL1 as described previously (**3.3.3**). Successful mutation was confirmed by restriction digest and sequencing (GENEWIZ, Leipzig, Germany).

Table 3.7: PCR mix for SDM

Component	Volume
Plasmid template [25 ng/ μ L]	1 μ L
Fwd primer [10 μ M]	1 μ L
Rev primer [10 μ M]	1 μ L
dNTP mix [5 mM each]	2.5 μ L
Pfu Buffer (10x)	5 μ L
PfuPlus! DNA polymerase [5 U/ μ L]	0.5 μ L
H ₂ O	39 μ L

Table 3.8: PCR cycles for SDM

Step	Cycles	Temperature	Time
Initial Denaturation	1	95 °C	2 min
Denaturation	40	95 °C	30 sec
Annealing		68 °C	1 min
Extension		68 °C	8.5 min
Final Extension	1	68 °C	7 min

3.3.7 Cloning of BirA expression plasmid

A gene encoding for the *E. coli* biotin ligase (BirA) was cloned into the expression vector pDB2_CMV. PCR primers (P483 + P484) were designed to amplify the BirA sequence from pBS_KSII(+)_IgL-birA-biotin-ligase_KDEL (kindly provided by Frank Momburg, DKFZ, Heidelberg) introducing overhangs with restriction sites for HindIII and XbaI. The reaction mix was prepared according to **Table 3.9** and processed in a T3000 Thermocycler (Biometra) using PCR cycles as in **Table 3.10**. DNA was purified using the QIAquick PCR Purification Kit according to manufacturer's instructions. Purified PCR product and target vector (pDB2_CMV) were digested with restriction enzymes HindIII and XbaI according to **Table 3.11** and **Table 3.12**. The digested PCR product was purified using the QIAquick PCR Purification

Kit, while the vector was loaded on a 1 % agarose gel and separated by electrophoresis (3.3.1). The DNA band of expected size was excised and purified using the QIAquick Gel Extraction Kit according to manufacturer's instructions. Ligation of the insert into the target vector was performed as described previously in 3.3.5 with a stoichiometric insert to vector ratio of 3:1. The ligation product was transformed into XL1 bacteria, amplified, purified by miniprep, and verified by restriction digest and sequencing as described in 3.3.3.

Table 3.9: PCR mix for cloning of BirA

Component	Volume
Plasmid template [25 ng/ μ L]	1 μ L
Fwd primer [10 μ M]	1 μ L
Rev primer [10 μ M]	1 μ L
dNTP mix [5 mM each]	2.5 μ L
Pfu Buffer (10x)	5 μ L
PfuPlus! DNA polymerase [5 U/ μ L]	0.5 μ L
H ₂ O	39 μ L

Table 3.10: PCR cycles for cloning of BirA

Step	Cycles	Temperature	Time
Initial Denaturation	1	95 °C	2 min
Denaturation	30	95 °C	20 sec
Annealing		53 °C	30 sec
Extension		72 °C	60 sec
Final Extension	1	72 °C	7 min

Table 3.11: Restriction digest of PCR product for cloning of BirA

Component	Volume
PCR product	43 μ L
Enzyme 1 (HindIII)	1 μ L
Enzyme 2 (XbaI)	1 μ L
NEBuffer2.1 (10x)	5 μ L
Reaction at 37 °C, 1 h	

Table 3.12: Restriction digest of target vector for insertion of BirA

Component	Volume
Vector DNA [1 µg/µL]	3 µL
Enzyme 1 (HindIII)	1 µL
Enzyme 2 (XbaI)	1 µL
NEBuffer2.1 (10x)	5 µL
H ₂ O	40 µL
Reaction at 37 °C, 1 h	

3.3.8 Cloning of CD40 expression plasmid

Murine CD40 was cloned by PCR from cDNA into the expression vector pDB2_CMV. cDNA was generated from DC2.4 cells using the Maxima H Minus First Strand cDNA Synthesis Kit according to manufacturer's instructions. Briefly, RNA was isolated from cells using the AllPrep DNA/RNA/Protein Mini Kit according to manufacturer's instructions and reverse transcribed by incubating the reaction mix (**Table 3.13**) for 5 min at 25 °C, 60 min at 50 °C and 15 min at 70 °C.

CD40-specific PCR primers (P558 + P559) were designed to contain overhangs with restriction sites for NotI and XbaI and were cloned into pDB2_CMV as described in **3.3.7**.

Table 3.13: Reaction mix for generation of cDNA from DC2.4

Component	Volume
RNA template [300 ng/µL]	0.5 µL
dNTP Mix [10 mM]	2 µL
Random Hexamer Primer [100 µM]	2 µL
RT Buffer (5x)	1 µL
Maxima H Minus Enzyme Mix	2 µL
H ₂ O	23.5 µL

3.3.9 Confirm mutations in B16F10

Mutations in the exome of B16F10 cells that potentially generate neoepitopes were selected from the literature [131], as shown in **Table 3.14**. To confirm mutations in the tested B16F10 cell line, DNA was isolated from B16F10 cells or C57BL/6 wt splenocytes using QIAGEN Dneasy Blood and tissue kit according to manufacturer's instructions. DNA fragments containing the potential mutation or wt sequence were amplified by PCR according to **Table 3.15** and **Table 3.16** using primers as shown in **2.10**. PCR products were loaded on a 1 % agarose gel and separated by electrophoresis. DNA of the predicted band

size was excised and purified using a QIAquick Gel Extraction Kit according to manufacturer's instructions. Purified B16F10 and C57BL/6 wt DNA fragments were sequenced (GENEWIZ, Leipzig, Germany) and compared to confirm mutations.

Table 3.14: Selection of potential mutations in the B16F10 genome

Antigen	Mutation	wt/mut sequence	Sequencing primers
Kif18b	K739N	PSKPSFQEFVDWEKVSPELNSTDQPFL PSKPSFQEFVDWENVSPELNSTDQPFL	P306 + P307
Pbk	V145D	DSGSPFPAAVILRVALHMARGLKYLHQ DSGSPFPAAVILRDALHMARGLKYLHQ	P633 + P634
Ddb1	L438I	LVLSFVGQTRVLMINGEEVEEELMGF LVLSFVGQTRVLMINGEEVEEELMGF	P637 + P638
Dpf2	F275V	GPDGLALPNNYCDFCLGDSKINKKTGQ GPDGLALPNNYCDVCLGDSKINKKTGQ	P639 + P640
Rpl13a	A24G	GRGHLLGRLAAIVAKQVLLGRKVVVVR GRGHLLGRLAAIVGKQVLLGRKVVVVR	P461 + P462
Fat1	I1940M	EKFMSMDHKTGTIAIQNTTQLRSRYELT EKFMSMDHKTGTIAMQNTTQLRSRYELT	P645 + P646
Fzd7	G304A	SGCYFMVAVAHVAGFILLEDRAVCVERF SGCYFMVAVAHVAAFILLEDRAVCVERF	P619 + P620
Golgb1	E2855D	QRAAAPSAASSPAEVQSLKKAMSSLQN QRAAAPSAASSPADVQSLKKAMSSLQN	P623 + P624
Plod2	F530V	STANYNTSHLNNDFWQIFENPVDWKEK STANYNTSHLNNDVWQIFENPVDWKEK	P629 + P630
Orc2	F278V	RVDQKTLHNLLRKFVPSFSAEIERLNQ RVDQKTLHNLLRKVVPFSFAEIERLNQ	P631 + P632
Klhl22	F179V	HLTQQLDITYILKNFVAFSRTDKYRQLP HLTQQLDITYILKNVAFSRTDKYRQLP	P635 + P636
Tm9sf3	Y382H	CGTAFFINFIAIYYHASRAIPFGTMVA CGTAFFINFIAIYHHSRAIPFGTMVA	P481 + P482
Snx5	R373Q	ELINFKRKRVAAFRKNLIEMSELEIKH ELINFKRKRVAAFQKNLIEMSELEIKH	P641 + P642
Armc1	S85I	NREKMKGELGMMLSLQNVIQTTTPGE NREKMKGELGMMLIQLQNVIQTTTPGE	P643 + P644
Eef2	G795A	FVVKAYLPVNESFGFTADLRNNTGGQA FVVKAYLPVNESFAFTADLRNNTGGQA	P621 + P622
Tnpo3	G504A	VVDRNPQFLDPVLGYLMKGLCEKPLAS VVDRNPQFLDPVLAAYLMKGLCEKPLAS	P310 + P311
Atp11a	R522S	SSPDEVALVEGVQRLGFTYLRLKDNYM SSPDEVALVEGVQSLGFTYLRLKDNYM	P625 + P626
Wdr82	I221L	LILISTNGSFIRLIDAFKGVVMHTFGG LILISTNGSFIRLLDAFKGVVMHTFGG	P627 + P628
Cpsf3l	D314N	EFKHIKAFDRTFADNPGPMVVVFATPGM EFKHIKAFDRTFANNPGRPMVVVFATPGM	P308 + P309

Table 3.15: PCR mix for neoantigen confirmation

Component	Volume
Plasmid template [150 ng/ μ L]	1 μ L
Fwd primer [10 μ M]	1 μ L
Rev primer [10 μ M]	1 μ L
dNTP mix [5 mM each]	2.5 μ L
Pfu Buffer (10x)	5 μ L
PfuPlus! DNA polymerase [5 U/ μ L]	0.5 μ L
H ₂ O	39 μ L

Table 3.16: PCR cycles for neoantigen confirmation

Step	Cycles	Temperature	Time
Initial Denaturation	1	95 °C	2 min
Denaturation	30	95 °C	20 sec
Annealing		54 °C	30 sec
Extension		72 °C	60 sec
Final Extension	1	72 °C	7 min

3.4 Production of AAVLPs

AAVLP production was performed in two scales: A small-scale production in 6-well plates, yielding $\sim 5.0 \times 10^9$ capsids per well as a crude lysate, and a large-scale production in several (20-80) 15 cm cell culture dishes, yielding $\sim 1.0 \times 10^{13}$ capsids from 40 dishes. The production yield of crude lysates was estimated in an A20-based sandwich enzyme-linked immunosorbent assay (ELISA), while large-scale productions were purified and titrated by ELISA and quantitative polymerase chain reaction (qPCR).

For AAVLP production, cells were transfected with three DNA plasmids. The plasmid pMT_187_XX2 encoded AAV capsid proteins with respective peptide insertions in the VR-IV loop (aa453) and/or VR-VIII loop (aa588). Plasmid pDGdVP [144] expressed adenoviral helper genes required for AAVLP formation. Plasmid pds-CMV-GFP encoded a green fluorescent protein (GFP) transgene under the *Cytomegalovirus* (CMV) promoter, flanked by ITRs for packaging into AAVLPs [145]. The formation of AAVLPs does not necessarily require integration of a transgene and particles can be assembled solely from the capsid proteins. As pds-CMV-GFP was only included as a reporter gene in some functional assays

and to confirm transfection efficiency during production, pds-CMV-GFP was reduced or absent in some AAVLP productions.

3.4.1 Small-scale production of AAVLPs in crude lysates

HEK293T cells were seeded into 6-well cell culture plates at a density of 3.5E+05 cells per well in 1.5 mL culture medium. The cells were incubated for 48 h under normal cell culture conditions (3.2) and transfected according to *Table 3.17* with pMT_187_XX2, pds-CMV-GFP and pDGdVP. The DNA/OptiMEM mix was supplemented with polyethylenimine (PEI) at a DNA/PEI ratio of 1:4, incubated for 10 min at RT, and added dropwise to the cultured cells. Transfected cells were incubated for 72 h and were harvested by resuspension in the culture medium. After centrifugation at 400 g for 5 min and washing in phosphate-buffered saline (PBS), cell pellets were resuspended in 100 μ L PBS. AAVLPs were released from cells by three cycles of freezing in liquid nitrogen and thawing at 37 °C. Cell debris was removed by centrifugation at 21000 x g for 15 min and AAVLP-containing supernatant was stored at -80 °C.

Table 3.17: Transfection mix for AAVLP small-scale production in 6-well cell culture plate

Component	Volume
Capsid plasmid <i>pMT_187_XX2 (8392 bp)</i> [100 ng/ μ L]	6.3 μ L
GFP plasmid <i>pds-CMV-GFP (5800 bp)</i> [100 ng/ μ L]	4.3 μ L
Ad helper plasmid <i>pDGdVP (20749 bp)</i> [100 ng/ μ L]	15.4 μ L
OptiMEM	170 μ L
PEI [1 mg/mL]	10.4 μ L

3.4.2 Particle titration of AAVLP small-scale productions by sandwich ELISA

The presence of AAVLPs in the small-scale production was confirmed by sandwich ELISA. Wells of a 96-well ELISA plate were coated overnight at 4 °C with undiluted A20 hybridoma supernatant. The wells were washed three times by adding and aspirating PBS containing

0.05 % Tween20 (Washing buffer), blocked for 1 h at room temperature (RT) with Washing buffer containing 3 % BSA and 5 % sucrose (Blocking buffer) and washed again. AAVLP samples were added at a dilution of 1:10 in Blocking buffer and incubated for 1 h at RT, before washing wells. Bound AAVLPs were quantified by successive steps of incubation with A20-Biotin (diluted 1:600) for 1 h at RT, washing, and incubating with HRP-coupled streptavidin (diluted 1:1000) for 1 h at RT. Subsequently, wells were washed three times with Washing buffer and twice with H₂O, before adding 3,3',5,5'-Tetramethylbenzidine (TMB) substrate solution. The color reaction was stopped after 5 min using H₂SO₄ (0.33 M) and quantified at 450 nm with a background subtraction at 650 nm using a spectrophotometer (BioTek Epoch). A reference AAVLP sample was included in all assays to compare productivity between experiments.

3.4.3 Large-scale production of purified AAVLPs

HEK293T cells were seeded into 15 cm cell culture dishes at a density of 5.0E+06 cells in 22 mL culture medium. Cells were incubated under normal cell culture conditions (3.2) for 48 h to reach a confluency of 70 – 80 %. For triple-transfection with pMT_187_XX2, pds-CMV-GFP and pDGdVP, DNA was dissolved in OptiMEM according to **Table 3.18**. Varying amounts of GFP plasmid were added to yield different amounts of full and empty AAVLP capsids (1., 2. or 3.). Unless stated otherwise, AAVLPs were produced according to column 2 in **Table 3.18**. The DNA/OptiMEM mix was supplemented with PEI at a DNA/PEI ratio of 1:4, incubated for 10 min at RT, and added dropwise to the cultured cells.

Table 3.18: Transfection mix for AAVLP large-scale production in 15 cm cell culture dish

	1. Full particles	2. Reduced GFP genomes	3. No GFP genomes
Capsid plasmid <i>pMT_187_XX2 (8392 bp)</i> [1 µg/µL]	10.6 µL	12.1 µL	12.8 µL
GFP plasmid <i>pds-CMV-GFP (5800 bp)</i> [1 µg/µL]	7.3 µL	2.2 µL	/
Ad helper plasmid <i>pDGdVP (20749 bp)</i> [1 µg/µL]	26.1 µL	29.7 µL	31.2 µL
OptiMEM	2.5 mL	2.5 mL	2.5 mL
PEI [1 mg/mL]	176 µL	176 µL	176 µL

Transfected cells were incubated under normal cell culture conditions (**3.2**) for 72 h before harvesting AAVLPs. Cells were flushed off the culture dishes and centrifuged at 400 x g for 20 min. The cell culture supernatant was retained for purification of AAVLPs by polyethylene glycol (PEG) precipitation, while the cell pellet was processed separately.

For precipitation, 40 % PEG 8000 solution (**Table 3.19**) was added to the AAVLP supernatant to a final PEG 8000 concentration of 8 %. After stirring slowly for 1 h at 4 °C, the solution was incubated overnight at 4 °C without stirring. The precipitate was centrifuged at 2800 x g for 15 min at 4 °C and resuspended in 2.5 mL AAVLP lysis buffer per 20 culture dishes (**Table 3.20**).

For processing of AAVLP-containing cells, the cell pellet was washed in PBS and resuspended in 10 mL AAVLP lysis buffer per 20 culture dishes. Cellular membranes were disrupted by three cycles of freezing in liquid nitrogen and thawing at 37 °C, before adding the PEG precipitate of the supernatant. Contaminating DNA and RNA in the sample were removed by treating with 50 U benzonase per mL lysate for 30 min at 37 °C and cell debris was removed by centrifugation at 3800 x g for 20 min.

To purify AAVLPs, lysates were loaded on discontinuous iodixanol gradients for separation by ultracentrifugation. AAVLP lysates from 20 culture dishes, adjusted to 15 mL, were filled into ultracentrifugation tubes and sub-layered with iodixanol phases of 15 % (9 mL), 25 % (6 mL), 40 % (5 mL) and 60 % (4 mL) (**Table 3.21**). Tubes were sealed and centrifuged at 55000 rpm for 3 h at 4 °C in an L8-70M Ultracentrifuge (Beckman) with a Type 70 Ti Rotor. After centrifugation, 3.5 - 4 mL of the 40 % phase were harvested from the tube by aspiration with a needle.

Purified AAVLP samples were further processed by re-buffering and concentration. The samples were diluted to 15 mL (1:4) in AAVLP concentration buffer (**Table 3.22**) [146] and concentrated to roughly 1 mL (15x) in Amicon Ultra-15 (50 kDa) filter units by centrifugation at 2300 x g. Samples were diluted once more in AAVLP concentration buffer (1:15) and centrifuged at 1150 x g until concentrated to 200-300 µL (50x).

Final AAVLP preparations were stored at -80 °C.

Table 3.19: PEG solution for AAVLP precipitation

Component	Concentration
PEG 8000	40 %
NaCl	2.4 %
H ₂ O	
	pH 7.4

Table 3.20: AAVLP lysis buffer

Component	Concentration
Tris/HCl	50 mM
MgCl ₂	2 mM
NaCl	150 mM
H ₂ O	
	pH 8.5

Table 3.21: Iodixanol solutions for AAVLP purification

Component	15 %	25 %	40 %	60 %
PBS (10 x)	5 mL	5 mL	5 mL	-
MgCl ₂ [1 M]	50 µL	50 µL	50 µL	50 µL
KCl [2.5 M]	50 µL	50 µL	50 µL	50 µL
NaCl [5 M]	10 mL	-	-	-
Iodixanol (60 %)	12.5 mL	20 mL	33.3 mL	50 mL
Phenolred (0.5 %)	-	75 µL	-	50 µL
H ₂ O	22.4 mL	24.8 mL	11.6 mL	-

Table 3.22: AAVLP concentration buffer

Component	Concentration
Sodium citrate	100 mM
Tris/HCl	10 mM
Pluronic F68	0.001 %
H ₂ O	
	pH 8.0

3.4.4 Particle titration of AAVLP large-scale productions by ELISA

To determine the particle titer of AAVLP serotype 2, viral preparations were serially diluted 1:2 with a starting dilution of 1:120 in PBS and coated into 96-well ELISA plates overnight at 4 °C. An AAVLP-WT standard of known concentration was included in a 1:2 dilution series with a starting concentration of 5.0E+10 capsids/mL. Wells were washed three times by adding and aspirating PBS containing 0.05 % Tween20 (Washing buffer). After blocking with

Washing buffer containing 3 % BSA and 5 % sucrose (Blocking buffer) for 1 h at RT, A20 hybridoma supernatant was added at a dilution of 1:10 in Blocking buffer and incubated for 1 h at RT. Wells were washed and HRP-coupled anti-mouse immunoglobulin G (IgG) (1:2000 in Blocking buffer) was added to detect A20 binding. After 1 h incubation at RT, wells were washed three times with Washing buffer and twice with H₂O, before adding TMB substrate solution. The color reaction was stopped after 5 min using H₂SO₄ (0.33 M) and quantified at 450 nm with a background subtraction at 650 nm using a spectrophotometer (BioTek Epoch).

The AAVLP titer was determined using the standard AAVLP-WT concentration curve. Sample dilutions within the linear range of the standard curve were used to calculate the titer.

AAVLP serotype 5 was titrated using the AAV5 Titration ELISA (Progen) according to manufacturer's instructions. Briefly, the viral preparation and a standard sample were added to pre-coated ELISA plates, followed by anti-AAV5 biotin conjugate and HRP-coupled streptavidin. Quantification by color reaction occurred as described previously for AAVLP serotype 2.

3.4.5 Genomic titration of AAVLP large-scale productions by qPCR

The genomic titer of AAVLPs was determined by qPCR to detect copy numbers of packaged GFP genes. Vector genomes were extracted from AAVLP preparations using the DNeasy Blood and tissue kit according to manufacturer's instructions for "Isolation of Total DNA from Cultured Animal Cells". As starting material, 2 µL of AAVLP solution were mixed with 198 µL PBS, and isolated DNA was finally eluted in 200 µL 10 mM Tris/HCl pH 8.5. For absolute quantification of AAVLP genomes, a standard GFP plasmid of known concentration was included in the experiment at a 1:10 serial dilution. The qPCR reaction was prepared using qPCRBIO SyGreen Mix Hi-ROX mixed with template DNA and respective primers according to **Table 3.23**. The reaction was carried out at a LightCycler480 II (Roche) according to qPCR cycling program in **Table 3.24**. Specificity of PCR products was confirmed by melting peak analysis.

Table 3.23: Pipetting scheme for qPCR AAVLP titration

Component	Volume
qPCRBIO SyGreen Mix Hi-ROX (2x)	10 μ L
GFP primer fwd [10 μ M]	0.4 μ L
GFP primer rev [10 μ M]	0.4 μ L
AAVLP DNA	4 μ L
H ₂ O	5.2 μ L

Table 3.24: qPCR cycling program

Program	Cycles	Analysis Mode	Target [°C]	Acquisition Mode	Hold [mm:ss]	Ramp Rate [°C/s]	Acquis. [per °C]
Denat.	1	None	95	None	05:00	4.40	
Amplif.	40	Quantification	95	None	00:15	4.40	
			60	None	00:10	2.20	
			72	Single	00:20	4.40	
Melting	1	Melting Curves	95	None	00:01	4.40	
			68	None	00:15	2.20	
			95	Cont.			5
Cooling	1	None	40	None	00:30	2.20	

3.5 Production of AAVLPs with bound anti-CD40

AAVLPs with a capsid-bound anti-CD40 antibody were produced as follows (graphically summarized in *Figure 4.14* on page 77):

3.5.1 Production of biotinylated AAVLPs

For the production of biotinylated AAVLPs, the biotin acceptor peptide (BAP) was cloned into the capsid sequence in the VR-IV loop (aa453) as described previously (**3.3.5**), while SIINFEKL was inserted in the VR-VIII loop (aa588). Particle production in HEK293T cells was carried out as described before (**3.4.3**). In addition to the standard protocol, the culture medium was supplemented with 50 μ M biotin and a fourth plasmid was included in the transfection mix to express BirA (*Table 3.25*). The purification, concentration and titration of viral particles was carried out as for unbiotinylated AAVLPs.

Table 3.25: Transfection mix for biotinylated AAVLP large-scale production in 15 cm cell culture dish

Component	Volume
Capsid plasmid <i>pMT_187_XX2 (8542 bp)</i> [1 µg/µL]	10.3 µL
GFP plasmid <i>pds-CMV-GFP (5800 bp)</i> [1 µg/µL]	2.2 µL
Ad helper plasmid <i>pDGdVP (20749 bp)</i> [1 µg/µL]	25.1 µL
BirA plasmid <i>pDB2_CMV_BirA (5236 bp)</i> [1 µg/µL]	6.3 µL
OptiMEM	2.5 mL
PEI [1 mg/mL]	176 µL

3.5.2 Confirmation of AAVLP-biotinylation by ELISA

To confirm biotinylation, AAVLPs were coated into 96-well ELISA plates as for particle titration (3.4.4). After blocking, HRP-coupled streptavidin was added at a dilution of 1:1000 in Blocking buffer and incubated for 1 h at RT. The wells were washed and developed as described before.

3.5.3 Conjugation of streptavidin to anti-CD40

In order to bind antibodies to biotinylated AAVLPs, streptavidin was conjugated to the antibody using a Streptavidin Conjugation Kit (Abcam) according to manufacturer's instructions. Briefly, 100 µg antibody solution (1 mg/mL) was mixed with 10 µL Modifier reagent and added to the lyophilized Streptavidin Mix. After incubating 3 h at RT, 10 µL Quencher reagent was added and the streptavidin-conjugated antibody was stored at 4 °C.

3.5.4 Confirmation of streptavidin/anti-CD40 conjugation by western blot

Streptavidin conjugation to antibodies was confirmed by western blot. Polyacrylamide gels were casted according to Table 3.26, with a 7 % separating gel and a 4 % stacking gel. Antibody samples (200 ng) were mixed with Sample buffer (Table 3.27) and heated to 95 °C for 5 min. Electrophoresis was performed in Running buffer (Table 3.28) at 80 V for 30 min followed by 130 V for 60 min. After separation, proteins were transferred to a methanol

activated polyvinylidene difluoride (PVDF) membrane via wet electroblotting at 90 V for 2 h in Transfer buffer (**Table 3.29**). The membrane was blocked for 1 h at RT in PBS with 0.1 % Tween20 (PBS-T) containing 5 % milk powder. Proteins on the PVDF membrane were stained overnight at 4 °C with HRP-coupled anti-rat IgG, diluted 1:2500 in PBS-T containing 1 % milk. After washing three times for 5 min, peroxidase substrate solution (Western-Lightning Plus) was added with 0.125 mL/cm² membrane, and chemiluminescence was detected at a Fusion-SL (Vilber Lourmat).

Table 3.26: Non-reducing Tris-Acetate gel

Component	Stacking gel (4 %)	Seperating gel (7 %)
Tris acetate, pH 7.0 [3 M]	0.4 mL	0.76 mL
Acrylamide/bisacrylamide 30% (37.5:1)	0.8 mL	2.36 mL
APS (10 %)	28.6 µL	47.6 µL
TEMED	7.5 µL	12.5 µL
H ₂ O	4.8 mL	7.6 mL

Table 3.27: Sample buffer (4x) for polyacrylamide gel electrophoresis

Component	Concentration
Tris/HCl	250 mM
Glycerol	40 %
SDS	8 %
Bromophenol blue	0.02 %
H ₂ O	
	pH 6.8

Table 3.28: Running buffer (1x) for polyacrylamide gel electrophoresis

Component	Concentration
Tricine	50 mM
Tris	50 mM
SDS	0.1 %
H ₂ O	
	pH 8.2

Table 3.29: Transfer buffer (1x) for wet electroblotting

Component	Concentration
Bis-Tris	25 mM
Bicine	25 mM
EDTA	1 mM
Methanol	20 %
H ₂ O	
	pH 7.2

3.5.5 Binding of streptavidin-conjugated anti-CD40 to biotinylated AAVLPs

Biotinylated AAVLPs ($5.0E+12$ capsids) were mixed with streptavidin-antibodies at a multiplicity of 120 ($6.0E+14$ molecules \cong 160 μ g antibody). The mixture was incubated for 1 h at RT and subsequently stored at 4 °C.

3.5.6 Confirmation of anti-CD40 coupling to AAVLPs by ELISA

The coupling of streptavidin-anti-CD40 to biotinylated AAVLPs was confirmed by ELISA, similar to the previously described A20-sandwich ELISA (3.4.2). Briefly, $1.5E+09$ AAVLPs were added to A20 coated ELISA plates and incubated for 1 h at RT. After washing, HRP-coupled anti-rat IgG antibody was added in Blocking buffer at a dilution of 1:2000 and incubated for 1 h at RT. The wells were washed and developed as described previously.

3.6 In silico prediction of antigens

To determine potential MHC class II epitopes in the AAVLP capsid, the AAVLP-SIINFEKL capsid sequence was analyzed using NetMHCII2.3 [147] and NetMHCIIpan 4.0 [148]. The binding of 15-mers to H-2-IAb was predicted and all strong binders (< 2 % rank) were selected for peptide synthesis. Overlapping 15-mers with the same core sequence were merged into one sequence, resulting in 11 peptides (p1-p11) of 16-27 amino acids (Table 4.2 on page 87). One peptide predicted to be a non-binder was included as a negative control (p0).

Potential CD8+ T cell neoepitopes were selected by predicting MHC class I presentation of 27 amino acid long peptide sequences containing the mutation at the center. Binding of 8- to 11-mers to H2-Kb or H2-Db was analyzed using NetMHC 4.0 [149, 150]. Strong binders (< 0.5 % rank) were selected for the vaccine design.

3.7 *In vitro* experiments

3.7.1 *AAVLP uptake into DC2.4*

To analyze AAVLP-entrance into APCs, $1.0E+05$ DC2.4 cells were seeded in 0.5 mL culture medium into 24-well plates. After adhesion overnight, medium was removed and AAVLPs were added at a concentration of $2.0E+11$ capsids/mL in 0.5 mL serum-free culture medium. Cells were incubated for 4 h under normal cell culture conditions (**3.2**), trypsinized and transferred into round bottom 96-well plates. After washing twice in FACS buffer (centrifugation at $800 \times g$, aspiration and resuspension), cells were fixed and permeabilized using the Cytofix/Cytoperm™ Fixation/Permeabilization Kit according to manufacturer's instructions. To stain internalized AAVLPs, cells were incubated for 20 min at 4°C in BD Perm/Wash buffer containing A20 (1:50). The cells were washed twice in BD Perm/Wash buffer and incubated for 20 min at 4°C with a PE-labeled anti-mouse IgG antibody. After three washing steps in BD Perm/Wash buffer and washing once in FACS buffer, the PE fluorescence intensity was analyzed at a BD FACSCanto II.

3.7.2 *AAVLP-anti-CD40 binding assay*

To analyze the binding of anti-CD40-coupled AAVLPs to CD40 expressing cells, HEK293T cells were transiently transfected with a CD40 expression plasmid (HEK-CD40). Cells were seeded into 6-well cell culture plates with $6.5E+05$ cells per well in 2 mL and incubated for 24 h under normal cell culture conditions (**3.2**). For transfection, 2.6 μg plasmid DNA were dissolved in 170 μL OptiMEM and mixed with 10.4 μL PEI (1 mg/mL). After 10 min incubation at RT, the transfection mix was added dropwise to the cell culture medium and cells were incubated for 72 h.

The expression of CD40 was confirmed after detaching cells using 6.25 mM EDTA and transferring $2.0E+05$ cells into round bottom 96-well plates. Cells were washed in PBS with 1 % BSA and 0.1 % NaN_3 (FACS buffer) and were resuspended in FACS buffer containing PE-labeled anti-CD40 antibody (1:100). After incubating 20 min at 4°C and washing twice in FACS buffer, PE fluorescence intensity was analyzed at a BD FACSCanto II.

The binding of anti-CD40-coupled AAVLPs to HEK-CD40 was shown by seeding $2.5E+05$ transfected cells per well in 100 μL ice-cold culture medium into round-bottom 96-well plates. AAVLPs were added with $1.0E+05$ capsids per cell in 100 μL ice-cold culture medium

and samples were incubated for 1 h at 4 °C. Subsequently, cells were washed twice in cold FACS buffer, and incubated for 30 min at 4 °C in the presence of A20-Biotin (1:100). After washing twice in cold FACS buffer, Alexa Fluor 488-labeled streptavidin, diluted 1:500 in FACS buffer, was added and incubated for 20 min at 4 °C. Samples were washed twice and resuspended in FACS buffer containing DAPI (1:500) to exclude dead cells. Alexa Fluor 488 fluorescence intensity was analyzed at a BD FACSCanto II.

3.8 Animal experiments

Female C57BL/6 mice at 6-8 weeks of age were obtained from Janvier (Le Genest-Saint-Isle, France). Mice were allowed to acclimatize in the local animal facility (IBF, University of Heidelberg) for one week prior to the initiation of an experiment. Experiments were performed according to national guidelines and were approved by the national authority (Regional Authority of Karlsruhe; official approval ID: 35-9185.81/G-84/18).

3.8.1 Vaccination

Unless stated otherwise, $5.0E+11$ AAVLP capsids in 30 μ L PBS were mixed 1:2 with Montanide ISA 51 (60 μ L total) and injected subcutaneously (s.c.) into the hock of mice [151]. Injection occurred under isoflurane anesthesia.

In some mice, AAVLPs were administered s.c. at the tail base or intramuscularly (i.m.) into the quadriceps femoris.

In one experiment, mice received a dose of $1E+11$ viral genomes (VG) in 200 μ L intravenously (i.v.) into the tail vein.

Different adjuvants were tested and AAVLPs were injected s.c. with 7.5 μ g/mouse bis-(3'-5')-cyclic dimeric adenosine monophosphate (c-di-AMP) or 25 μ g/mouse CpG ODN 2395 (CpG), or a combination of either with Montanide ISA 51.

In case of the neoantigen vaccine, mice were vaccinated with four different AAVLPs by injecting two AAVLPs in 60 μ L PBS with Montanide into the left and two AAVLPs into the right hock.

Peptide vaccines consisted of 30 μ g SIINFEKL peptide (Ova₂₅₇₋₂₆₄), 60 μ g of OVAII peptide (Ova₃₂₃₋₃₃₉) or 100 μ g of each neoantigen peptide in Montanide ISA 51 (1:2 in PBS).

3.8.2 Tumor challenge

To analyze primary tumor growth of B16F10 or B16F10-OVA tumors, cultured tumor cells were detached using trypsin, washed twice with PBS and adjusted to a concentration of $2.0E+06$ cells/mL in PBS. Mice were anesthetized with isoflurane and $2.0E+05$ cells were injected s.c. into the right flank. The length and width of developing tumors were determined in blinded measurements three times a week using a caliper. The tumor volume was calculated for each mouse as: $volume = length * width^2 * 0.5236$ [152]. Mice were euthanized when tumors exceeded 12 mm on any side, necrotic wounds developed or mice showed clear signs of distress.

3.8.3 Immune cell depletion

CD4⁺ T cells were depleted in mice by intraperitoneal (i.p.) injection of anti-CD4 (GK1.5), while control mice received rat IgG2b isotype control. Antibodies were injected with a dose of 250 µg per mouse two days before vaccination and 100 µg per mouse one and four days after vaccination. Successful depletion was confirmed by flow cytometry after staining blood lymphocytes with PE anti-mouse CD4 (RM4-4).

B cells were depleted by i.v. injection of anti-CD20 (SA271G2), while control mice received rat IgG2b isotype control. Antibodies were injected with a dose of 185 µg per mouse two days before vaccination. Successful depletion was confirmed by flow cytometry after staining blood lymphocytes with PacificBlue anti-mouse B220 (RA3-6B2).

3.8.4 Intracellular staining (ICS)

Unless stated otherwise, mice were euthanized 3 weeks after vaccination and spleens were isolated and maintained in cold PBS. To obtain a single cell suspension, cells were mashed through a 100 µm cell strainer. Roughly $2.5E+06$ cells per well were seeded into round bottom 96-well plates. Cells were centrifuged at 800 x g for 3 min and resuspended in complete RPMI 1640 Medium supplemented with 50 µM 2-mercaptoethanol and containing 2 µg/mL target peptide for T cell stimulation. Cells were incubated for 1 h under normal cell culture conditions (3.2), before incubating 5 h in the presence of pathway inhibitors brefeldin A (5 µg/mL) and monensin (2 µM). Subsequently, cells were incubated for 10 min at RT in PBS containing Zombie Aqua (1:300) to stain dead cells. The same

volume PBS with 1 % BSA and 0.1 % NaN₃ (FACS buffer) was added and cells were centrifuged at 800 x g for 3 min at 4 °C. Samples were resuspended in FACS buffer containing surface antibodies PerCP/Cy5.5 anti-mouse CD8 (1:100), FITC anti-mouse CD4 (1:200) and PacificBlue anti-mouse B220 (1:100). After 20 min incubation at 4 °C, cells were washed twice with FACS buffer and permeabilized using the Cytofix/Cytoperm™ Fixation/Permeabilization Kit. Antibodies APC anti-mouse IFN γ (1:50) and PE/Cy7 anti-mouse TNF α (1:80) were added for intracellular staining and samples were incubated for 20 min at 4 °C. Cells were washed twice with BD Perm/Wash, resuspended in FACS buffer and analyzed for fluorescence using a BD FACSCanto II. Compensation controls were set up using UltraComp eBeads™ according to manufacturer's instructions.

3.8.5 Tetramer staining

Tetramer staining was performed on immune cells derived from blood, spleen, axillary lymph nodes (AxLN) or inguinal lymph nodes (InLN).

Blood immune cells were obtained by drawing around 50 μ L blood through the facial vein into EDTA-containing tubes (10 μ L, 0.5 M EDTA). Cells were washed in PBS by centrifugation at 400 g for 5 min. Red blood cell (RBC) lysis buffer (1 mL) (**Table 3.30**) was added to the cells, followed by 10 min incubation at RT. Cells were washed in PBS and treated with RBC lysis buffer as before. After washing twice in PBS, cells were transferred into a round bottom 96-well plate for tetramer staining.

Cells from spleen and LNs were obtained by isolating the respective organs from mice and mashing the tissue through a 100 μ m cell strainer. For staining, around 2.5E+06 splenocytes or the entirety of LN cells were transferred into round bottom 96-well plates.

Cells were centrifuged at 800 x g for 3 min and resuspended in PBS containing Zombie Aqua (1:300) to stain dead cells, and 50 nM Dasatinib to prevent TCR downregulation [153]. After 10 min incubation at RT, PBS with 2 % FCS, 0.1 % NaN₃ and 50 nM Dasatinib (Tetramer buffer) containing Mouse BD Fc Block™ (1:100) was added and samples were incubated for additional 5 min. Cells were centrifuged at 800 x g for 3 min and resuspended in Tetramer buffer containing APC-coupled H-2Kb/SIINFEKL MHC Tetramers (1:25). Samples were incubated for 30 min at RT and washed twice in Tetramer buffer, before incubating 20 min at 4 °C in Tetramer buffer containing antibodies FITC anti-mouse CD8 (1:20), PE anti-mouse CD3 (1:100) and PacificBlue anti-mouse B220 (1:100). Cells were washed twice in

Tetramer buffer, resuspended in PBS with 1 % FCS and 2.5 % paraformaldehyde (PFA), and analyzed for fluorescence using a BD FACSCanto II. Compensation controls were set up using UltraComp eBeads™ according to manufacturer's instructions.

Table 3.30: RBC lysis buffer

Component	Concentration
NH ₄ Cl	155 mM
KHCO ₃	10 mM
EDTA	0.1 mM
H ₂ O	23.5 µL

3.8.6 Collecting blood serum samples

Blood samples were collected from vaccinated mice at indicated time points. To this end, 5-10 drops of blood were drawn by puncturing the facial vein and were collected in 1.5 mL reaction tubes. Clotted blood was centrifuged at 1000 x g for 15 min at 4 °C and clear serum was transferred into fresh reaction tubes. After removing residual cells by a second centrifugation step, the serum was stored at –80 °C.

3.8.7 Determine GFP copy numbers in murine tissues by qPCR

Total DNA was isolated from murine tissue samples using QIAGEN DNeasy Blood and tissue kit according to manufacturer's instructions for "Purification of Total DNA from Animal Tissues". Purified DNA was diluted to 25 ng/µL and the GFP copy number in 25 ng tissue DNA was determined by qPCR as described previously (3.4.5).

3.8.8 Peptide ELISA of blood serum samples

To analyze target-specific antibodies in the blood of vaccinated mice, 96-well ELISA plates were coated overnight at 4 °C with a solution of 10 µg/mL target peptide in Carbonate buffer (Table 3.31). Wells were washed three times by adding and aspirating PBS containing 0.05 % Tween20 (Washing buffer) and blocked for 1 h at 37 °C with Washing buffer containing 3 % BSA and 5 % sucrose (Blocking buffer). Murine serum samples were serially diluted 1:2 in Blocking buffer in a dilution range of 1:50 to 1:819200. Sample dilutions were added to the coated plates and incubated for 1 h at 37 °C. After washing, bound serum antibodies were detected with HRP-coupled anti-mouse IgG (1:4000 in Blocking buffer)

incubated 1h at 37 °C. Wells were washed three times with Washing buffer and twice with H₂O, before adding TMB substrate solution. The color reaction was stopped after 5 min using H₂SO₄ (0.33 M) and quantified at 450 nm with a background subtraction at 650 nm using a spectrophotometer (BioTek Epoch). The serum titer of each mouse was determined as the highest dilution factor with a positive signal that was at least two times higher than the absorbance of a blank control.

Table 3.31: Carbonate buffer

Component	Concentration
NaHCO ₃	35 mM
Na ₂ CO ₃	15 mM
H ₂ O	
	pH 9.6

3.8.9 Tumor infiltration of immune cells

The infiltration of immune cells into B16F10 tumor tissue of challenged mice was analyzed at the time of death. Tumors were excised and mashed through a 100 µm cell strainer to obtain a single cell suspension. Cells were seeded into round-bottom 96-well plates at a density of 5.0E+05 cells and centrifuged at 800 x g for 3 min. After resuspension in PBS with Zombie Aqua (1:300), cells were incubated for 10 min at RT. Samples were resuspended in PBS with 1 % BSA and 0.1 % NaN₃ (FACS buffer) containing antibodies APC anti-mouse CD3 (1:50), PerCP/Cy5.5 anti-mouse CD8 (1:100), FITC anti-mouse CD4 (1:200) and PacificBlue anti-mouse B220 (1:100). After 20 min incubation at 4 °C, samples were washed twice with FACS buffer and analyzed for fluorescence, using a BD FACSCanto II. Compensation controls were set up using UltraComp eBeads™ according to manufacturer's instructions.

3.9 Statistical analyses

Statistical analyses were performed using GraphPad Prism 8.0.2.

Normal distribution within groups was analyzed using the Kolmogorov-Smirnov test.

If two groups were compared, significant differences were determined using a Two-tailed t-test.

To calculate significances for three or more normally distributed groups a One-way ANOVA was performed. The ANOVA test was followed by a Tukey's multiple comparison test, if groups were compared to each other, or a Dunnett's multiple comparison test, if the groups were compared to a control group. If samples did not pass the normality test, significances were determined using a Kruskal-Wallis test with a Dunn's multiple comparison test.

If three or more groups were compared, a Two-way ANOVA was performed. This was followed by a Tukey's multiple comparison test to compare all groups with each other, or a Dunnett's multiple comparison test to compare all groups to a control group.

4 Results

4.1 Design and production of AAVLPs

Different recombinant AAVLPs were designed and produced as vaccine candidates during the project. AAVs, or in this case AAVLPs, consist of three capsid proteins (VP1, VP2, VP3), which are encoded by the *cap* gene (Figure 4.1A). VP2 and VP3 are N-terminally truncated versions of VP1 and if peptide sequences are inserted into the VP3 region of the *cap* gene, peptides are presented on all 60 subunits of the particle (Figure 4.1B). The AAVLP vaccine candidates used in this project are shown in Table 4.1.

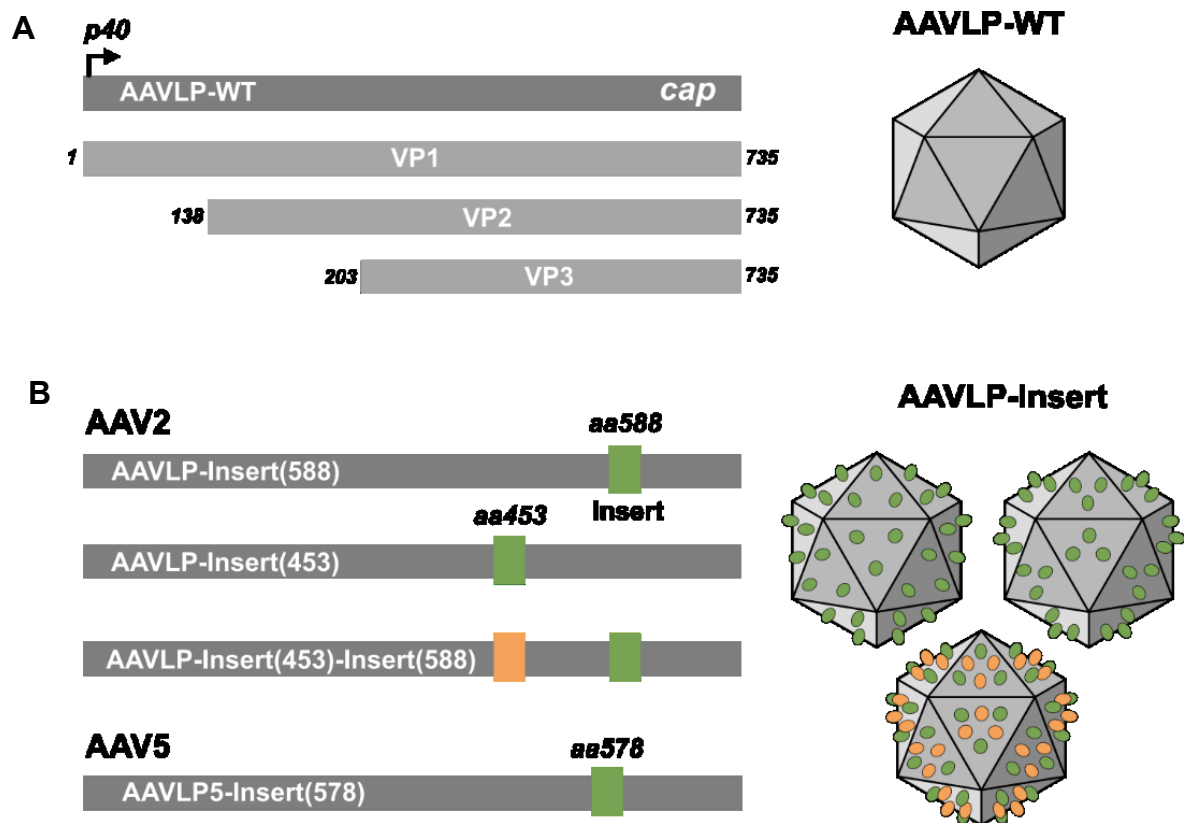


Figure 4.1: Design of AAVLPs.

A) The wild type adeno-associated virus-like particle (AAVLP) consists of three capsid proteins (VP1, VP2, VP3) which are expressed via alternative splicing from the *cap* gene under the p40 promoter. The three proteins assemble in an icosahedral structure of 60 subunits to build the viral capsid. **B)** To display peptides (green) on the capsid surface, the peptide DNA sequence is cloned into the *cap* gene. Insertions into the AAV serotype 2 (AAV2) capsid were achieved by substituting parts of the VR-VIII or VR-IV loop around amino acids 588 (aa588) and aa453 of VP1, respectively. In addition to single peptide insertions around aa588 or aa453, double insertions were designed with an antigen at aa588 and a functional peptide (yellow) at aa453. Corresponding to aa588 of AAV2, AAV5 particles were produced with an antigen insertion in the VR-VIII loop around aa578.

Table 4.1: List of AAVLPs tested during the project. The color code of the different antigens is maintained throughout the thesis.

Target	AAVLP	Serotype	aa453 insertion	aa588 insertion
Controls	AAVLP-WT	2	/	/
	AAVLP-FLAG	2	/	FLAG tag DYKDDDDK
Ovalbumin MHC class I model antigen (SIINFEKL)	AAVLP-SIINFEKL	2	/	Ova ₂₅₇₋₂₆₄ SIINFEKL
	AAVLP-SIINFEKL(453)	2	Ova ₂₅₇₋₂₆₄ SIINFEKL	/
	AAVLP5-SIINFEKL	5	/	Ova ₂₅₇₋₂₆₄ SIINFEKL
	AAVLP-BAP-SIINFEKL	2	BAP GLNDIFEAQKIEWHE	Ova ₂₅₇₋₂₆₄ SIINFEKL
	AAVLP-ICBL-SIINFKEL	2	J-ICBL DLLKNGERIEKVE	Ova ₂₅₇₋₂₆₄ SIINFEKL
Ovalbumin MHC class II model antigen (OVAII)	AAVLP-OVAII	2	/	Ova ₃₂₃₋₃₃₉ (OVAII) ISQAVHAAHAEINEAGR
	AAVLP-OVAII-PLA2mut	2	/	Ova ₃₂₃₋₃₃₉ (OVAII) ISQAVHAAHAEINEAGR
	AAVLP-OVAII(453)	2	Ova ₃₂₃₋₃₃₉ (OVAII) ISQAVHAAHAEINEAGR	/
	AAVLP-OVAII(453)- PLA2mut	2	Ova ₃₂₃₋₃₃₉ (OVAII) ISQAVHAAHAEINEAGR	/
Viral antigens	AAVLP-LCMV	2	/	LCMV NP ₃₉₆₋₄₀₄ FQPQNGQFI
	AAVLP-HPV	2	/	HPV E6 ₄₈₋₅₇ EYDFAFRDL
Neoantigens	AAVLP-Neo(453)	2	14 different neoantigens 21 aa	/
	AAVLP-Neo(588)	2	/	14 different neoantigens 21 aa

The majority of experiments was conducted with AAVLP-SIINFEKL, in which SIINFEKL, a chicken ovalbumin-derived antigen (Ova₂₅₇₋₂₆₄) [154], was inserted into the capsid of AAV2, substituting parts of the VR-VIII loop (**Figure 3.1**). As the VR-VIII loop is located around aa588 of VP1 [63], the insertion site was defined as aa588 in following experiments. Further antigen insertions at aa588 included the MHC class II antigen Ova₃₂₃₋₃₃₉ [155] (AAVLP-OVAII), *lymphocytic choriomeningitis mammarenavirus* (LCMV) NP₃₉₆₋₄₀₄ (AAVLP-LCMV) [156], *human papillomavirus* (HPV) E6₄₈₋₅₇ (AAVLP-HPV) [157], and 14 different neoantigen candidates (AAVLP-Neo). In some experiments, SIINFEKL, OVAII or the neoantigens were inserted into the VR-IV loop around aa453 (AAVLP-SIINFEKL(453), AAVLP-OVAII(453), AAVLP-Neo(453)). AAVLP-OVAII(453) and AAVLP-OVAII(588) were additionally designed to include mutations in the phospholipase A2 (PLA2) domain of the capsid (AAVLP-OVAII-PLA2mut, AAVLP-OVAII(453)-PLA2mut). Some AAVLPs were produced with SIINFEKL at aa588 and a second, functional peptide at aa453, such as the biotin acceptor peptide (BAP) [158, 159] or a β -2-microglobulin-derived peptide (J-ICBL) [160] (AAVLP-BAP-SIINFEKL,

AAVLP-ICBL-SIINFEKL). Next to AAV serotype 2, SIINFEKL was also inserted into the capsid sequence of AAV serotype 5 at the VR-VIII loop around aa578 (AAVLP5-SIINFEKL), the analogous position to aa588 of AAV2. AAVLPs with a wild type (wt) sequence (AAVLP-WT) and AAVLPs displaying a FLAG tag [161] at aa588 (AAVLP-FLAG) were produced as controls for vaccination studies. All recombinant AAVLPs tested in the experiments showed production yields similar to the wild type AAVLP (AAVLP-WT) with around $1.0E+13$ intact capsids from 40 culture dishes.

4.2 General tests of the vaccination strategy (AAVLP-SIINFEKL)

4.2.1 AAVLP-SIINFEKL vaccination induces antigen-specific CD8+ T cells in spleen and blood

An initial experiment with AAVLP-SIINFEKL was performed to estimate the required vaccine dosage for following experiments. The doses ranged from $1.0E+11$ capsids to $1.0E+12$ capsids adjuvanted with or without Montanide ISA 51. The particles were injected s.c. into the hock of C57BL/6 mice, as this injection route has been shown to efficiently drain lymph nodes [151]. Three weeks after vaccination, T cell responses were analyzed by intracellular staining of splenocytes. The cells were stimulated with SIINFEKL peptide, and CD8+ T cells were analyzed for double expression of activation markers TNF α and IFN γ (**Figure 4.1A**)(complete gating strategy in **Appendix 1**). The vaccine showed no T cell induction when AAVLPs were administered without adjuvant (**Figure 4.2B**). Formulation in Montanide ISA 51, on the other hand, induced a distinct, dose-dependent response with an average of 0.10 % and 0.33 % SIINFEKL-specific CD8+ T cells after vaccination with $1.0E+11$ and $3.3E+11$ capsids, respectively. No responses were observed in control groups injected with PBS (0.01 %) and AAVLP-WT (0.01 %), and no significant responses were induced by vaccination with Peptide-SIINFEKL (0.04 %). As expected, no CD4+ T cell responses against SIINFEKL were detected (data not shown).

Due to the dose-dependent effect and a distinct immune response after vaccination with $3.3E+11$ capsids, the standard dose for following experiments was set to $5.0E+11$ capsids per mouse.

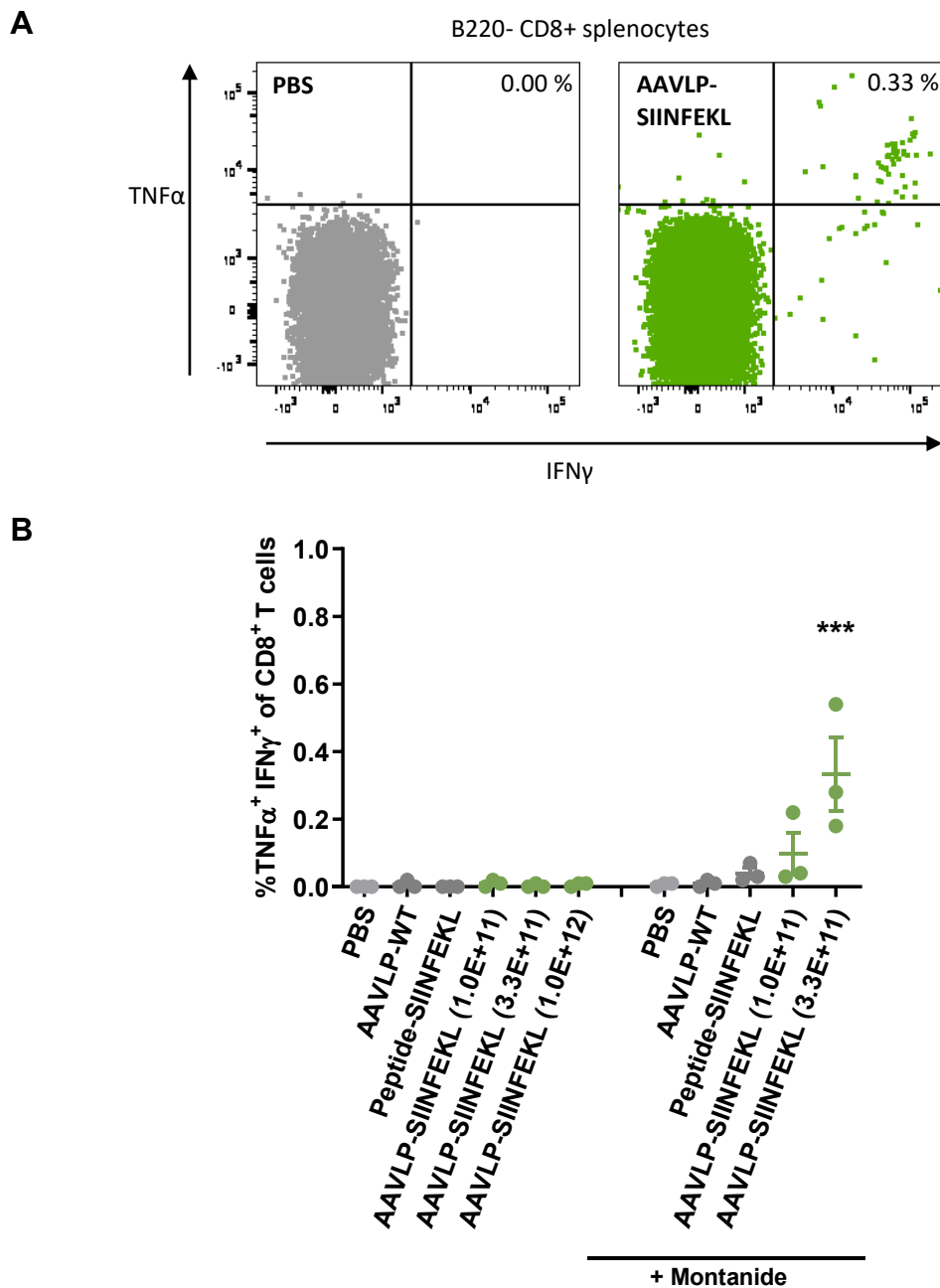


Figure 4.2: Vaccination with AAVLP-SIINFEKL induces antigen-specific CD8+ T cells.

C57BL/6 mice ($n=3$ per group) were vaccinated s.c. into the hock with different doses of AAVLP-SIINFEKL, administered without adjuvant or adjuvanted with Montanide ISA 51 (Montanide). The numbers in brackets indicate the respective dose of injected AAVLPs as viral particles (VP) per mouse. Mice injected with PBS, AAVLP-WT ($1.0E+11$ VP/mouse) and Peptide-SIINFEKL ($30 \mu\text{g}/\text{mouse}$) served as controls. To detect antigen-specific CD8+ T cells 3 weeks after vaccination, splenocytes were stimulated with SIINFEKL peptide for 6h in the presence of Monensin and Brefeldin A, and were subsequently analyzed by intracellular staining (ICS) and flow cytometry for the activation markers TNF α and IFN γ . **A**) Gating of live B220- CD8+ splenocytes for flow cytometry analysis after intracellular staining. **B**) Frequencies of antigen-specific CD8+ T cells. Horizontal bars indicate the mean of each group with the standard error of mean (SEM). Significant differences between groups were determined using a One-way ANOVA with a Tukey's multiple comparison test. Asterisks indicate significant difference to all other groups with *** ($P \leq 0.001$).

To analyze the induction of T cell responses in different organs, the spleen, inguinal lymph node (InLN) and axillary lymph node (AxLN) were analyzed three weeks after vaccination. In addition, blood samples of vaccinated mice were analyzed for CD8⁺ T cell responses. Splenocytes were analyzed either by intracellular staining of peptide-stimulated cells or by H2-Kb-SIINFEKL tetramer staining together with samples from InLN, AxLN and blood. The gating of tetramer positive cells is shown in **Figure 4.3A**, while a complete gating strategy is shown in **Appendix 2**.

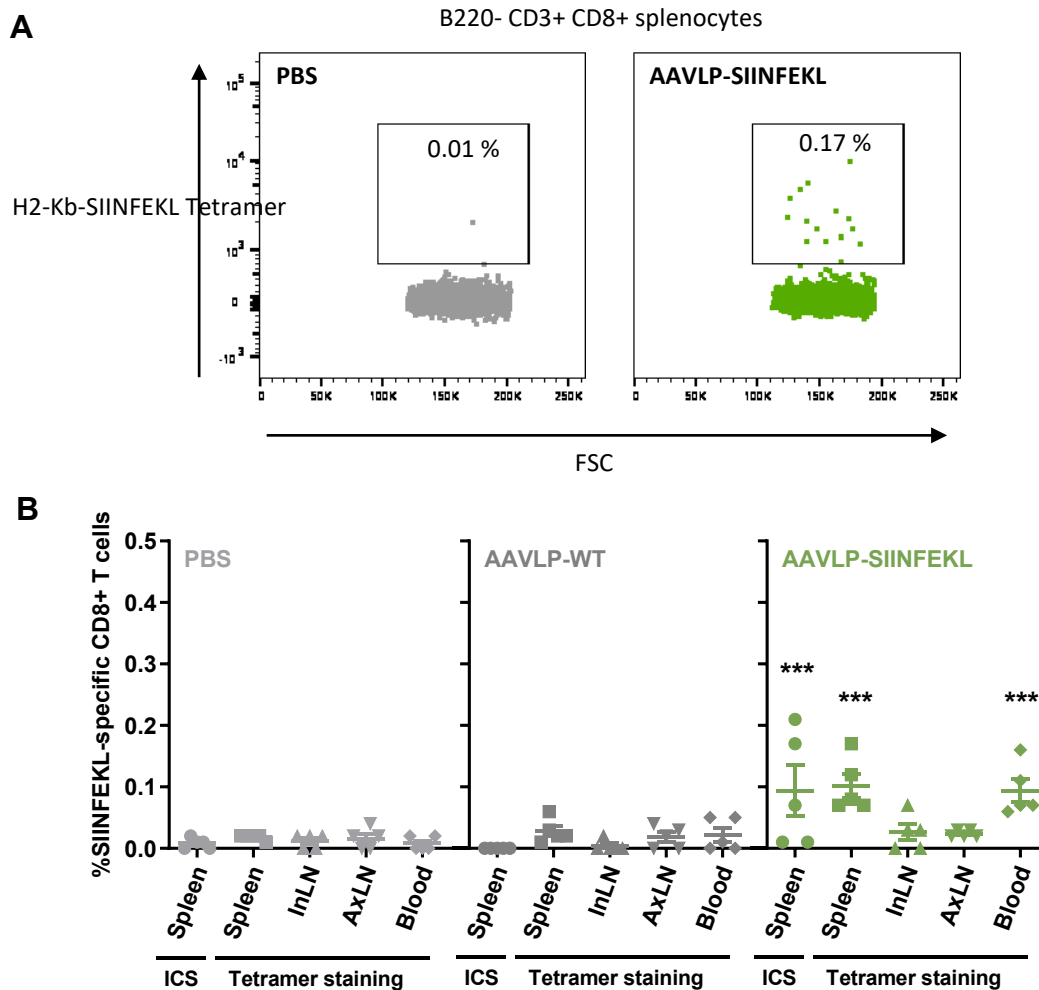


Figure 4.3: Tetramer staining reveals antigen-specific CD8⁺ T cells in the spleen and blood of AAVLP-SIINFEKL vaccinated mice.

C57BL/6 mice ($n=5$ per group) were vaccinated s.c. into the hock with AAVLP-SIINFEKL. Mice injected with PBS or AAVLP-WT served as negative controls. Three weeks after vaccination, cells were extracted from the spleen, the inguinal lymph node (InLN), the axillary lymph node (AxLN) and the blood. Antigen-specific CD8⁺ T cells in the spleen were detected by stimulating splenocytes with SIINFEKL peptide for 6h in the presence of Monensin and Brefeldin A and subsequent analysis by intracellular staining (ICS) and flow cytometry for the activation markers TNF α and IFN γ . Alternatively, cells from the spleen, the LNs and the blood were analyzed for the presence of antigen-specific CD8⁺ T cells using fluorescent-labeled H-2Kb/SIINFEKL MHC Tetramers (Tetramer staining). **A**) Gating of live B220- CD3⁺ CD8⁺ splenocytes for flow cytometry analysis of tetramer staining. **B**) Frequencies of antigen-specific CD8⁺ T cells. Horizontal bars indicate the mean of each group with SEM. Significant differences to the PBS group were determined using a Two-way ANOVA with a Dunnett's multiple comparisons test. Asterisks indicate significant difference to the PBS group with *** ($P \leq 0.001$).

As before, PBS and AAVLP-WT controls did not show any antigen-specific T cells (0.00 % - 0.02 %) (*Figure 4.3B*). In AAVLP-SIINFEKL vaccinated mice, both the intracellular cytokine staining and tetramer staining showed a mean of 0.10 % SIINFEKL-specific CD8+ T cells in the spleen, indicating comparability between both assays. A similar rate of specific CD8+ T cells (0.09 %) was also observed in blood samples. However, no SIINFEKL-specific T cells were detectable in the lymph nodes of vaccinated mice (0.02 %).

Taken together, a dose of 5.0E+11 AAVLP-SIINFEKL per mouse induced SIINFEKL-specific CD8+ T cell responses detectable in the spleen and blood but not in the lymph nodes. Based on these results, following experiments were mainly evaluated by measuring antigen-specific T cell responses in the spleen through intracellular staining of peptide stimulated cells.

4.2.2 AAVLP-SIINFEKL induces long lasting CD8+ T cell responses with a peak after 3 weeks

In the previous experiment, T cell responses were only measured three weeks after vaccination. To analyze the level of antigen-specific T cells over time, mice were vaccinated with AAVLP-SIINFEKL at different time points (1-10 weeks) before harvesting the spleen. While no SIINFEKL-specific CD8+ T cell responses were observed after 1 week (0.00 %), first responses emerged 2 weeks after vaccination (0.02 %) finally leading to a peak of 0.10 % after 3 weeks (*Figure 4.4A*). Subsequently, the T cell level decreased to 0.05 % at 4 weeks after vaccination, while a base level of 0.03 % lasted up to 10 weeks.

A similar result was observed in a second experiment, in which the blood of vaccinated mice was analyzed every week by H2-Kb-SIINFEKL tetramer staining. First responses emerged after 2 weeks and reached 0.10 % at 3 weeks after vaccination (*Figure 4.4B*).

In conclusion, the experiments showed highest CD8+ T cell responses 3 weeks after vaccination with AAVLPs, which was thereafter set as a readout time point for following experiments.

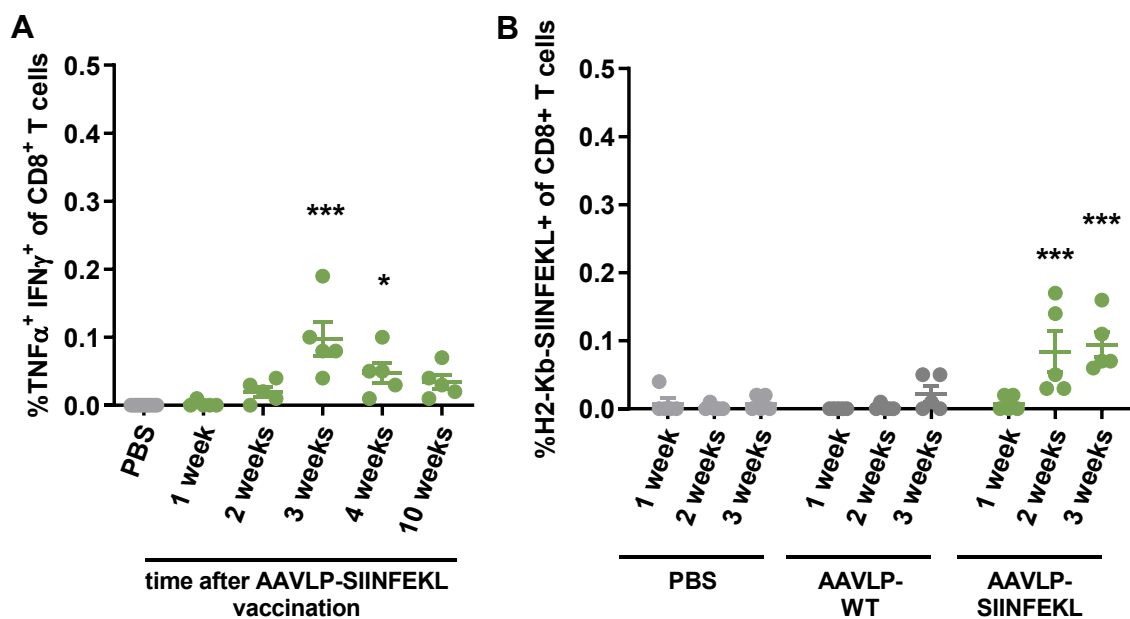


Figure 4.4: CD8⁺ T cell responses after AAVLP-SIINFEKL vaccination are long-lasting and peak around 3 weeks.

C57BL/6 mice (n=5 per group) were vaccinated s.c. into the hock with AAVLP-SIINFEKL. Mice injected with PBS or AAVLP-WT served as negative controls. **A)** Mice were vaccinated one, two, three or ten weeks before extracting the splenocytes. Antigen-specific CD8⁺ T cells in the spleen were detected by stimulating splenocytes with SIINFEKL peptide for 6h in the presence of Monensin and Brefeldin A, followed by intracellular staining (ICS) and flow cytometry analysis of activation markers TNFα and IFNγ. Horizontal bars indicate the mean of each group with SEM. Significant differences to the PBS group were determined using a One-way ANOVA with a Dunnett's multiple comparison test. Asterisks indicate significant difference with * (P ≤ 0.05); *** (P ≤ 0.001). **B)** Blood lymphocytes from vaccinated and control mice were analyzed weekly for the presence of antigen-specific CD8⁺ T cells (B220⁻, CD3⁺) using fluorescent-labeled H-2Kb/SIINFEKL MHC Tetramers (Tetramer staining). Horizontal bars indicate the mean of each group with SEM. Significant differences to the PBS group were determined using a Two-way ANOVA with a Dunnett's multiple comparisons test. Asterisks indicate significant difference to the PBS group with *** (P ≤ 0.001).

4.2.3 AAVLP-SIINFEKL vaccination via s.c. but not i.m. injection route induces CD8⁺ T cell responses

So far, the vaccine was administered s.c. into the hock of mice. To compare different injection routes, mice were vaccinated by injecting AAVLP-SIINFEKL s.c. into the hock, s.c. at the tailbase or i.m. into the thigh muscle. While s.c. injection into the hock and at the tailbase induced comparable antigen-specific CD8⁺ T cell responses with a mean of 0.23 % and 0.19 %, respectively, i.m. injection did not induce detectable responses (0.03 %) (**Figure 4.5**). Based on these results, following vaccinations were administered s.c. into the hock of mice.

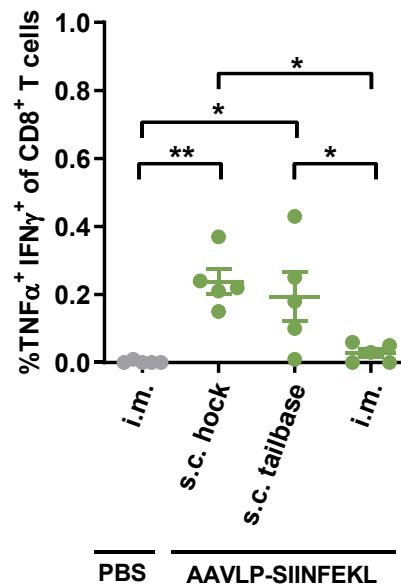


Figure 4.5: CD8+ T cell responses are generated after s.c. but not i.m. injection of AAVLP-SIINFEKL.

C57BL/6 mice (n=5 per group) were vaccinated with AAVLP-SIINFEKL via different injection routes. AAVLP-SIINFEKL adjuvanted with Montanide ISA 51 was administered s.c. into the hock, s.c. at the tailbase or i.m. into the thigh muscle. Mice injected i.m. with PBS served as negative controls. In order to detect antigen-specific CD8+ T cells 3 weeks after vaccination, splenocytes were stimulated with SIINFEKL peptide for 6h in the presence of Monensin and Brefeldin A, and were subsequently analyzed by intracellular staining (ICS) and flow cytometry for activation markers TNFα and IFNγ. Horizontal bars indicate the mean of each group with SEM. Significant differences between groups were determined using a One-way ANOVA with a Tukey's multiple comparison test. Asterisks indicate significant difference with * ($P \leq 0.05$); ** ($P \leq 0.01$).

4.2.4 High local concentration of AAVLP-SIINFEKL promotes generation of CD8+ T cell responses

The observation that T cell responses induced by the AAVLP vaccine require Montanide ISA 51 indicates that the depot effect of the adjuvant and thus concentration of AAVLPs at the injection site is of importance. In order to analyze the effect of local concentration, a dose of $5.0E+11$ AAVLPs was injected either into one hock of mice (one injection site; $5.0E+11$ in 60 μ L) or distributed between two hocks (two injection sites; $2 \times 2.5E+11$ in 60 μ L). Significantly higher responses were detected when the vaccine was injected at one site only (0.24 %), instead of two sites (0.08 %) (Figure 4.6).

These results show that a high local concentration of AAVLPs is needed for the induction of T cell responses, even if the dose per animal is kept constant.

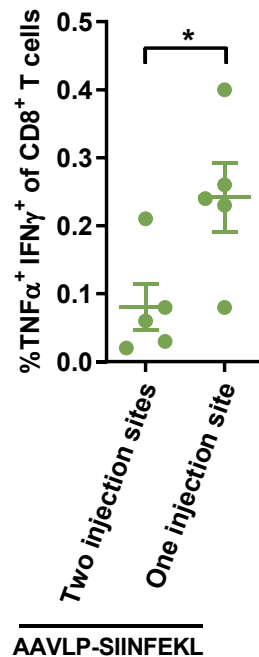


Figure 4.6: A high local concentration of AAVLP-SIINFEKL increases CD8+ T cell responses.

C57BL/6 mice (n=5 per group) were vaccinated with AAVLP-SIINFEKL. A set dose of 5E+11 capsids AAVLP was either injected in 60 μ L into the hock of one leg (one injection site) or distributed into both legs with 2.5E+11 capsids in 60 μ L each (two injection sites). In order to detect antigen-specific CD8+ T cells 3 weeks after vaccination, splenocytes were stimulated with SIINFEKL peptide for 6h in the presence of Monensin and Brefeldin A, and were subsequently analyzed by intracellular staining (ICS) and flow cytometry for activation markers TNF α and IFN γ . Horizontal bars indicate the mean of each group with SEM. Significant differences between groups were determined using a Two-tailed t-test. Asterisks indicate significant difference with * (P \leq 0.05).

4.2.5 Adjuvants Montanide ISA 51 but not CpG ODNs or c-di-AMP promote induction of CD8+ T cells by AAVLP-SIINFEKL

The initial experiment showed only detectable T cell responses when AAVLP-SIINFEKL was adjuvanted with Montanice ISA 51 (**Figure 4.2**). In an attempt to further increase responses, different adjuvants were tested for the vaccination strategy. Next to Montanide ISA 51 [162, 163], bis-(3',5')-cyclic dimeric adenosine monophosphate (c-di-AMP) [164], CpG ODN 2395 (CpG) [162], or a combination of Montanide ISA 51 with either c-di-AMP or CpG was tested. Only Montanide ISA 51 induced significant T cell responses with 0.21 % SIINFEKL-specific CD8+ T cells (**Figure 4.7**). Neither c-di-AMP (0.01 %), nor CpG (0.01 %) promoted detectable responses. Furthermore, c-di-AMP and CpG had a negative effect on the

adjuvancy of Montanide ISA 51. Both reduced the CD8⁺ T cell level induced by AAVLP-SIINFELK in Montanide ISA 51 (0.21 %) to 0.04 % and 0.06 %, respectively.

In conclusion, vaccination with AAVLP-SIINFELK requires formulation with an adjuvant to generate CD8⁺ T cell responses. Only Montanide ISA 51 was able to achieve the desired effect and was chosen as the standard formulation for following experiments.

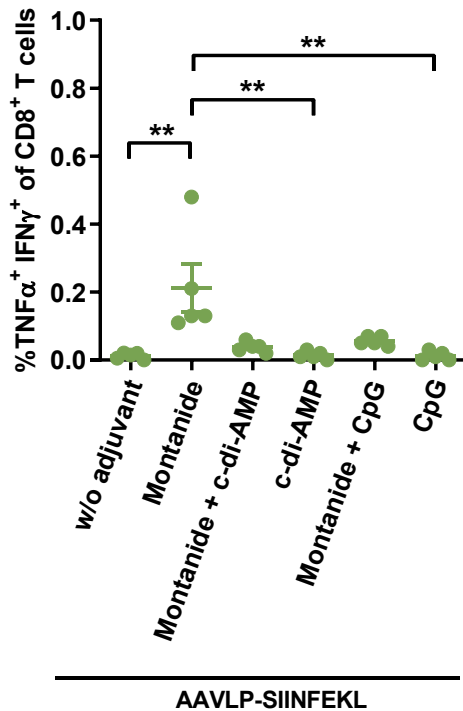


Figure 4.7: CD8⁺ T cell responses are only generated when AAVLP-SIINFELK is adjuvanted with Montanide ISA 51.

C57BL/6 mice (n=5 per group) were s.c. vaccinated with AAVLP-SIINFELK without adjuvant (w/o adjuvant) or adjuvanted with Montanide, c-di-AMP, CpG or combinations thereof. In order to detect antigen-specific CD8⁺ T cells 3 weeks after vaccination, splenocytes were stimulated with SIINFELK peptide for 6h in the presence of Monensin and Brefeldin A, and were subsequently analyzed by intracellular staining (ICS) and flow cytometry for activation markers TNF α and IFN γ . Horizontal bars indicate the mean of each group with SEM. Significant differences between groups were determined using a Kruskal-Wallis test with Dunn's multiple comparisons test. Asterisks indicate significant difference with ** (P ≤ 0.01).

4.2.6 DNA packaged in AAVLP-SIINFELK particles increases CD8⁺ T cell responses

Previous studies suggested that the presence of DNA within AAVLPs could influence the immunogenicity of the particles [113, 116]. To test this, AAVLP-SIINFELK particles were produced with varying amounts of packaged GFP genomes. This included a production with a genome to capsid ratio of 1:10, a reduced genome to capsid ratio of 1:16 and empty particles (no genome). Mice were vaccinated with the different AAVLP-SIINFELK productions and antigen-specific CD8⁺ T cells were analyzed after 3 weeks. While differences were not significant, a tendency of reduced T cell responses after vaccination with empty particles was observed (*Figure 4.8*). Measured T cell responses were 0.09 %, 0.08 % and 0.04 % SIINFELK-specific CD8⁺ T cells for 1:10, 1:16 and empty particle

productions, respectively. These results support the role of packaged DNA in the augmentation of immune responses.

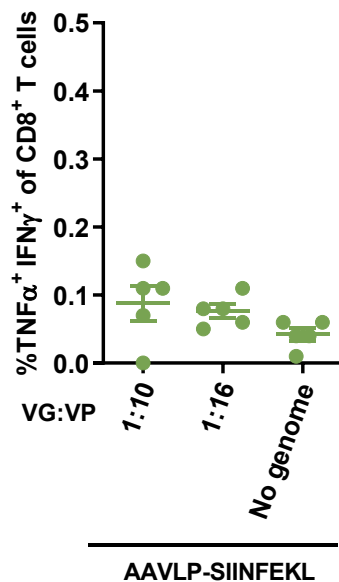


Figure 4.8: Higher CD8+ T cell responses are achieved when AAVLP-SIINFEKL particles contain genomic DNA. C57BL/6 mice (n=5 per group) were s.c. vaccinated with AAVLP-SIINFEKL with different contents of genomic DNA. AAVLP preparations contained a genome to capsid ratio of 1:10, a reduced genome to capsid ratio of 1:16 or empty particles (no genome). In order to detect antigen-specific CD8+ T cells 3 weeks after vaccination, splenocytes were stimulated with SIINFEKL peptide for 6h in the presence of Monensin and Brefeldin A, and were subsequently analyzed by intracellular staining (ICS) and flow cytometry for activation markers TNF α and IFN γ . Horizontal bars indicate the mean of each group with SEM. Significant differences between groups were determined using a One-way ANOVA with a Tukey's multiple comparison test. No significant difference were detected.

4.2.7 Insertion of SIINFEKL in the VR-IV loop (aa453) of AAVLPs yields higher CD8+ T cell responses than VR-VIII loop (aa588) insertion

The AAVLP capsid offers the possibility to insert peptides at various sites of the VP sequence [58-60, 62, 63] and the choice of insertion site can influence the tropism of viral particles. In the preceding experiments, substitution in the VR-VIII loop around aa588 (AAVLP-SIINFEKL(588)) removed the heparin-binding motif of AAV2, which prevents binding to the universal HSPG receptor [58-60]. As the tropism of AAVLPs could also influence the entry into APCs for antigen presentation, an alternative insertion site was tested and SIINFEKL was inserted into the VR-IV loop around aa453 (AAVLP-SIINFEKL(453)).

To test the cell entry *in vitro*, HEK293T cells or the dendritic cell line DC2.4 were incubated with AAVLPs containing SIINFEKL in the VR-IV or VR-VIII loop. Internalized AAVLPs were detected by flow cytometry after intracellular staining of intact particles with A20 antibody. AAVLP-WT, with a natural tropism, entered both cell types and served as a positive control (**Figure 4.9**). Cell entry was less efficient in DC2.4 cells compared to HEK293T cells. AAVLP-SIINFEKL(588), used in the previous experiments, did not show any sign of internalization and was comparable to a negative control without AAVLPs. For AAVLP-SIINFEKL(453) the increased cell entry was not as distinct as for AAVLP-WT but still significant in both cell types. The increased internalization was likely due to more efficient cell binding by AAVLPs, as a cell-binding assay showed the same tendencies (**Appendix 3**).

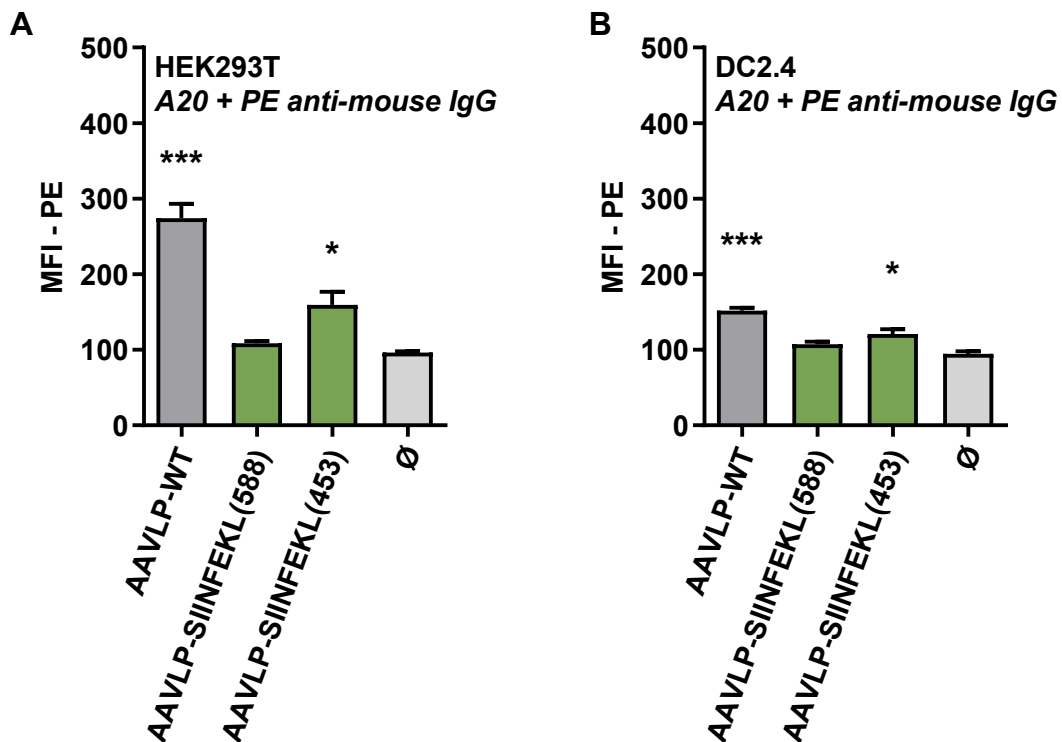


Figure 4.9: AAVLP-SIINFEKL enters APCs more efficiently when the antigen is inserted into the VR-IV loop instead of the VR-VIII loop.

Two AAVLP-SIINFEKL variants were compared, in which SIINFEKL was substituted for parts of the VR-VIII loop around aa588 (AAVLP-SIINFEKL(588)) or the VR-IV loop around aa453 (AAVLP-SIINFEKL(453)) of the capsid protein VP1. In order to analyze potential AAVLP entry into APCs, HEK293T (**A**) and DC2.4 cells (**B**) were incubated with either variant of AAVLP-SIINFEKL or AAVLP-WT. Cells without AAVLPs served as negative controls (Ø). After 4h incubation, cells were detached with trypsin, permeabilized and stained intracellularly for the presence of AAV particles using A20 with a PE-labeled secondary antibody. The graph shows the mean fluorescence intensity (MFI) of PE in each sample, measured by flow cytometry. Each bar represents the mean of three independent experiments including SEM. Significant differences to the negative control were determined using a One-way ANOVA with a Dunnett's multiple comparison test. Asterisks indicate significant difference with * ($P \leq 0.05$); *** ($P \leq 0.001$).

The altered tissue tropism of AAVLPs with a VR-VIII loop (aa588) insertion was tested *in vivo* by i.v. injection of GFP-encoding particles. The GFP copy number and thus number of AAVLPs in target tissues was analyzed by qPCR (Figure 4.10). The majority of AAVLP-WT particles located to the liver and a distinct proportion was found in the spleen. A minor fraction of GFP was observed in the kidney, while being absent in the lung, heart and thigh muscle tissue. AAVLPs with an antigen-insertion in the VR-VIII loop (aa588) (AAVLP-SIINFEKL) lost the liver tropism entirely but were still present in the spleen at a comparable level to AAVLP-WT.

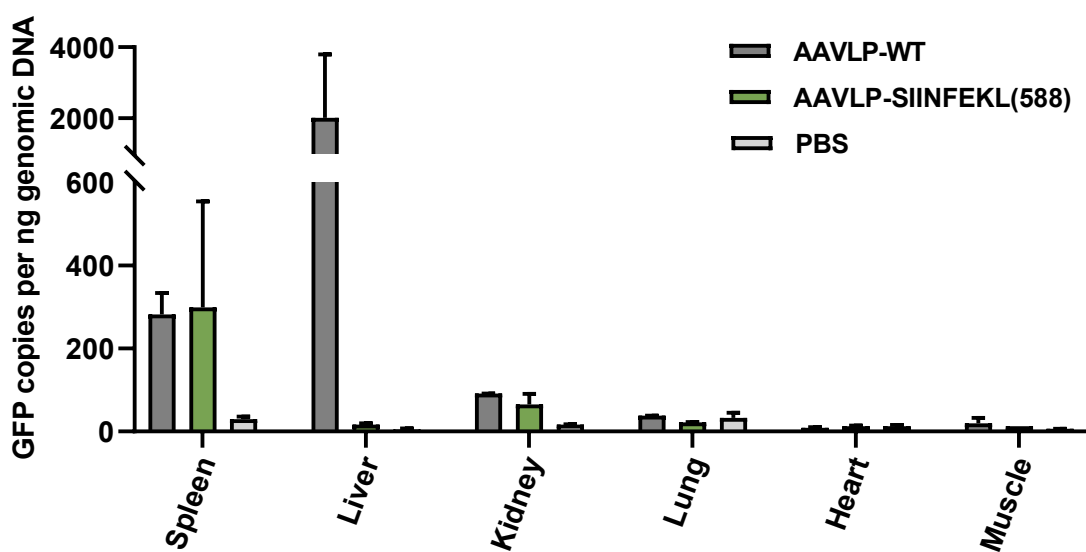


Figure 4.10: Antigen-insertion in the VR-VIII loop of AAVLPs disrupts liver tropism but sustains localization to the spleen.

C57BL/6 mice (n=2 per group) were injected i.v. with $1E+11$ VG per mouse of AAVLP-WT or AAVLP-SIINFEKL packaged with a GFP gene under the CMV promoter. PBS injected mice served as negative controls. Localization of AAVLPs to the spleen, liver, kidney, lung, heart and thigh muscle was analyzed by qPCR. DNA was isolated from the tissue and copy numbers of the GFP gene were determined with respective qPCR primers. The graph shows the GFP copy number per ng of genomic tissue DNA.

To analyze an effect on CD8⁺ T cell responses *in vivo*, mice were vaccinated with AAVLP-SIINFEKL(588) or AAVLP-SIINFEKL(453). As before, AAVLP-SIINFEKL(588) induced responses with a mean of 0.17 % SIINFEKL-specific CD8⁺ T cells (Figure 4.11). Insertion of SIINFEKL in the VR-IV loop (aa453), on the other hand, increased responses significantly to 0.48 %.

In conclusion, these experiments point towards an advantage of maintaining the natural tropism of AAVLPs by antigen insertion around aa453. While most of the preceding experiments were carried out with VR-VIII loop (aa588) insertions, the final neoantigen vaccine was designed to contain antigens in the VR-IV loop (aa453).

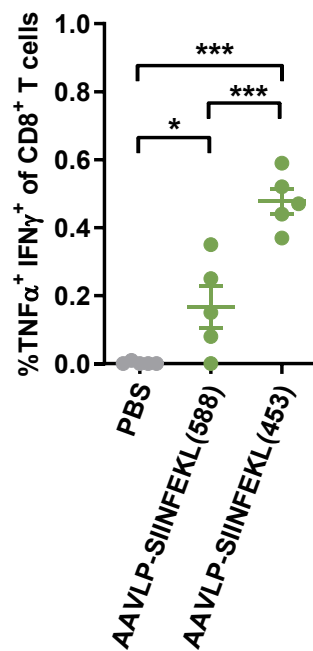


Figure 4.11: AAVLP-SIINFEKL induces stronger immune responses when the antigen is inserted in the VR-IV loop instead of the VR-VIII loop.

SIINFEKL was substituted for parts of the VR-VIII loop around aa588 (AAVLP-SIINFEKL(588)) or the VR-IV loop around aa453 (AAVLP-SIINFEKL(453)) of the capsid protein VP1. C57BL/6 mice (n=5 per group) were vaccinated with either insertion variant of AAVLP-SIINFEKL. PBS injected mice served as negative controls. In order to detect antigen-specific CD8⁺ T cells 3 weeks after vaccination, splenocytes were stimulated with SIINFEKL peptide for 6h in the presence of Monensin and Brefeldin A, and were subsequently analyzed by intracellular staining (ICS) and flow cytometry for activation markers TNF α and IFN γ . Horizontal bars indicate the mean of each group with SEM. Significant differences between groups were determined using a One-way ANOVA with a Tukey's multiple comparison test. Asterisks indicate significant difference with * ($P \leq 0.05$); *** ($P \leq 0.001$).

4.2.8 Neither homologous nor heterologous prime-boost strategies improve AAVLP-SIINFEKL vaccination

Prime-boost strategies are commonly used to increase immune responses in vaccination approaches [92, 94, 95, 165-167]. Thus, homologous and heterologous prime-boost strategies were tested in mice. Prime injections with PBS, AAVLP-WT or AAVLP-SIINFEKL of serotype 2 (AAVLP2) were followed after three weeks by injections with AAVLP-SIINFEKL of serotype 2 or serotype 5 (AAVLP5). SIINFEKL-specific T cell responses were evaluated 3 weeks after the second vaccination. Differences between groups were not significant but clear tendencies were observed (*Figure 4.12*). The combination of PBS prime and AAVLP2-SIINFEKL boost (PBS + AAVLP2-SIINFEKL) corresponds to previous experiments with a single injection dose and yielded similar results with a mean of 0.19 % SIINFEKL-specific CD8⁺ T

cells. Pre-existing immune responses due to a prime with AAVLP2-WT reduced responses of AAVLP2-SIINFEKL to 0.04 % (AAVLP2-WT + AAVLP2-SIINFEKL). The effect of pre-existing immunity was not as strong after AAVLP2-SIINFEKL prime (AAVLP2-SIINFEKL + AAVLP2-SIINFEKL), yielding a mean of 0.16 % SIINFEKL-specific CD8⁺ T cells. After a single injection of AAVLP5-SIINFEKL (PBS + AAVLP5-SIINFEKL), induced antigen-specific CD8⁺ T cells of 0.12 % were slightly lower than for AAVLP2-SIINFEKL. Yet, the effect of pre-existing immune responses due to AAVLP2-WT prime (AAVLP2-WT + AAVLP5-SIINFEKL) was not as prominent with a mean of 0.08 % antigen-specific CD8⁺ T cells. Additionally, a slight boost effect of AAVLP5-SIINFEKL after AAVLP2-SIINFEKL prime was observed (AAVLP2-SIINFEKL + AAVLP5-SIINFEKL), but with a mean of 0.21 % SIINFEKL-specific CD8⁺ T cells, the level was not considerably elevated above a single injection of AAVLP2-SIINFEKL (0.19 %).

In conclusion, the results showed that the tested prime-boost strategies are not beneficial for the vaccination strategy. In addition, pre-existing immune responses influence the efficacy of the vaccine.

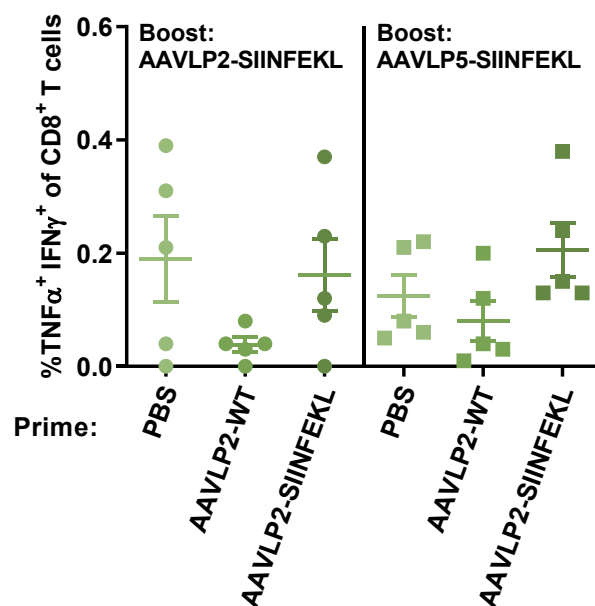


Figure 4.12: Pre-existing immune responses against AAV particles reduce the effect of the vaccine, and a heterologous prime-boost vaccination does not improve CD8⁺ T cell responses.

Mice (n=5 per group) were immunized with AAVLP-SIINFEKL in different prime-boost regimens. As a prime injection, mice received either PBS, AAVLP-WT or AAVLP-SIINFEKL of serotype 2 (AAVLP2). Three weeks later, primed animals received a second vaccination with AAVLP-SIINFEKL, based on serotype 2 or serotype 5 (AAVLP5). In order to detect antigen-specific CD8⁺ T cells 3 weeks after the second vaccination, splenocytes were stimulated with SIINFEKL peptide for 6h in the presence of Monensin and Brefeldin A, and were subsequently analyzed by intracellular staining (ICS) and flow cytometry for activation markers TNF α and IFN γ . Horizontal bars indicate the mean of each group with SEM. Significant differences between groups were determined using a One-way ANOVA with a Tukey's multiple comparison test. No significant differences were detected.

4.2.9 CD8+ T cells induced by AAVLP-SIINFEKL are able to prevent B16F10-OVA tumor growth in mice

In the previous experiments, antigen-specific CD8+ T cells were analyzed merely quantitatively as a percentage in the CD8+ T cell population. To evaluate the T cell responses qualitatively, the ability of the vaccine to prevent tumor growth was analyzed. Mice were challenged 3 weeks after AAVLP-SIINFEKL vaccination by injecting SIINFEKL-expressing B16F10-OVA cells s.c. into the flank, and tumor growth was measured every 2-3 days. Both the growth curves of tumors in individual mice (*Figure 4.13A*), as well as the survival curves (*Figure 4.13B*), showed clear protection by the vaccine. While mice injected with PBS or AAVLP-WT developed tumors that lead to the death within 15-22 days, AAVLP-SIINFEKL vaccination protected 6 of 7 mice, which remained tumor-free. Only one vaccinated mouse developed a slow growing tumor.

To analyze long-term protection, mice were challenged 10 weeks after vaccination. The effect was the same as 3 weeks after vaccination, with 6 of 7 tumor-free mice in the AAVLP-SIINFEKL vaccinated group (*Figure 4.13C+D*).

In conclusion, these experiments showed that induced T cells are functional and able to facilitate long-term tumor protection.

To summarize the results of the chapter **4.2** (General tests of the vaccination strategy), vaccination with AAVLP-SIINFEKL at a dose of $5.0E+11$ particles per mouse induced functional T cell responses peaking around 3 weeks that protected animals from tumor growth. Highest CD8+ T cell responses were achieved when the vaccine was I) injected s.c. in the hock, II) adjuvanted with Montanide ISA 51, III) injected at a high local concentration, IV) composed of vector DNA-containing particles that V) display the antigen in the VR-IV loop (aa453) of the VP protein.

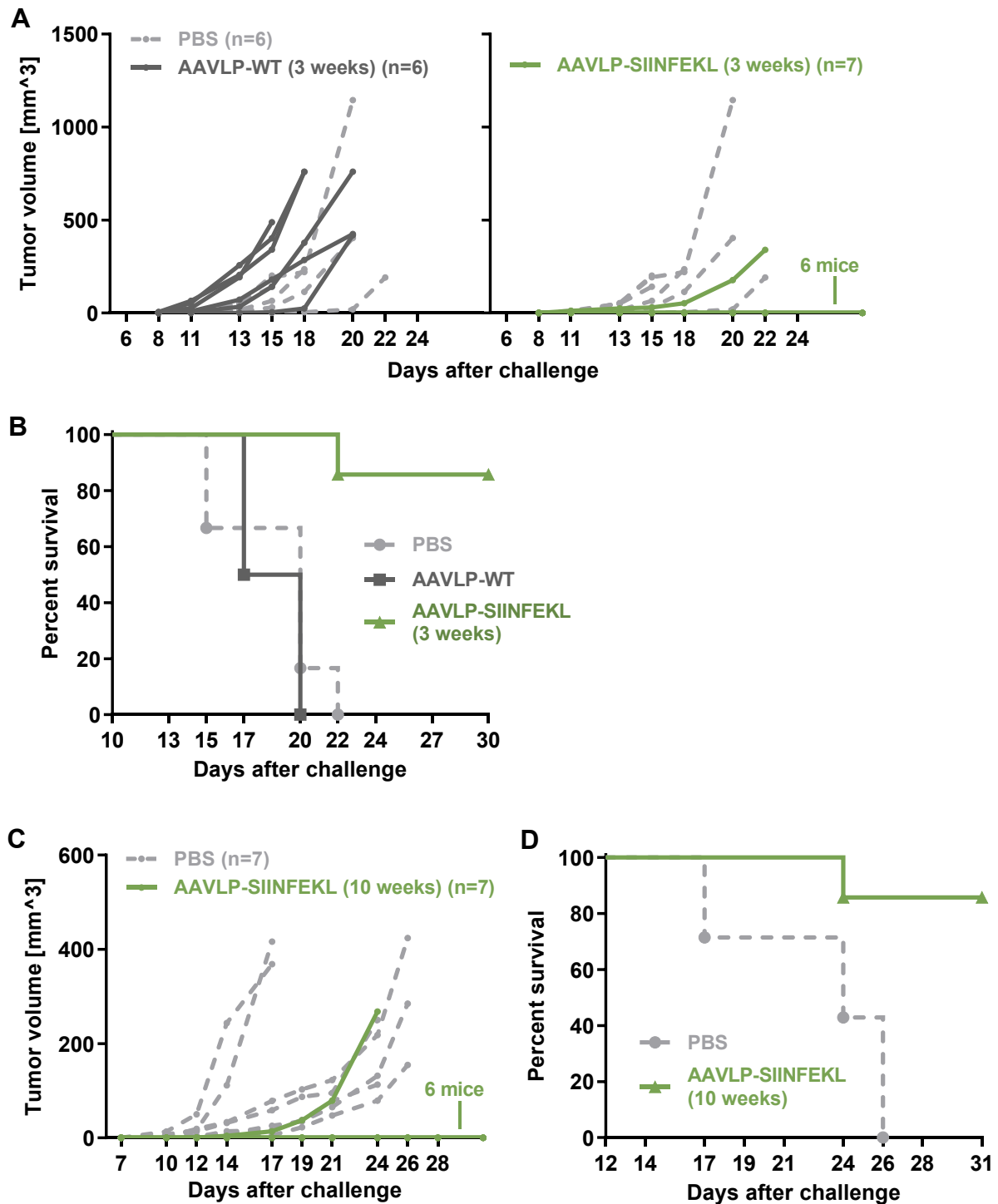


Figure 4.13: Vaccination with AAVLP-SIINFEKL protects mice from tumor growth after s.c. B16F10-OVA challenge.

AAVLP-SIINFEKL vaccinated mice were challenged s.c. with 2.0×10^5 B16F10-OVA cells, 3 weeks (A+B) or 10 weeks (C+D) after vaccination. A+C) Individual tumor growth curves in each mouse of the AAVLP-WT and AAVLP-SIINFEKL vaccinated group. For comparison, the growth curves of PBS-injected mice are shown as dashed, light-grey lines. B+D) Survival curves comparing AAVLP-SIINFEKL vaccinated mice to the control groups. The graphs show the percentage of live animals on each day.

4.3 Improvement strategies (AAVLP-SIINFEKL)

The previous experiments showed that functional T cell responses were induced by the AAVLP vaccine, but compared to other studies [112, 165, 168, 169] the level of antigen-specific T cells was rather low for a highly immunogenic antigen like SIINFEKL. Two strategies were tested to potentially increase CD8+ T cell responses. An agonistic anti-CD40 antibody was coupled to AAVLP-SIINFEKL particles for directed targeting and activation of CD40-expressing DCs [170, 171]. Another strategy was co-display of a β -2-microglobulin peptide [160] on AAVLPs, together with the SIINFEKL antigen.

4.3.1 Generation of anti-CD40-coupled AAVLPs

The generation of anti-CD40-coupled AAVLPs included three steps: I) Biotinylation of AAVLPs, II) conjugation of streptavidin to anti-CD40 antibodies and III) fusion of biotinylated AAVLPs with streptavidin-anti-CD40 (*Figure 4.14*).

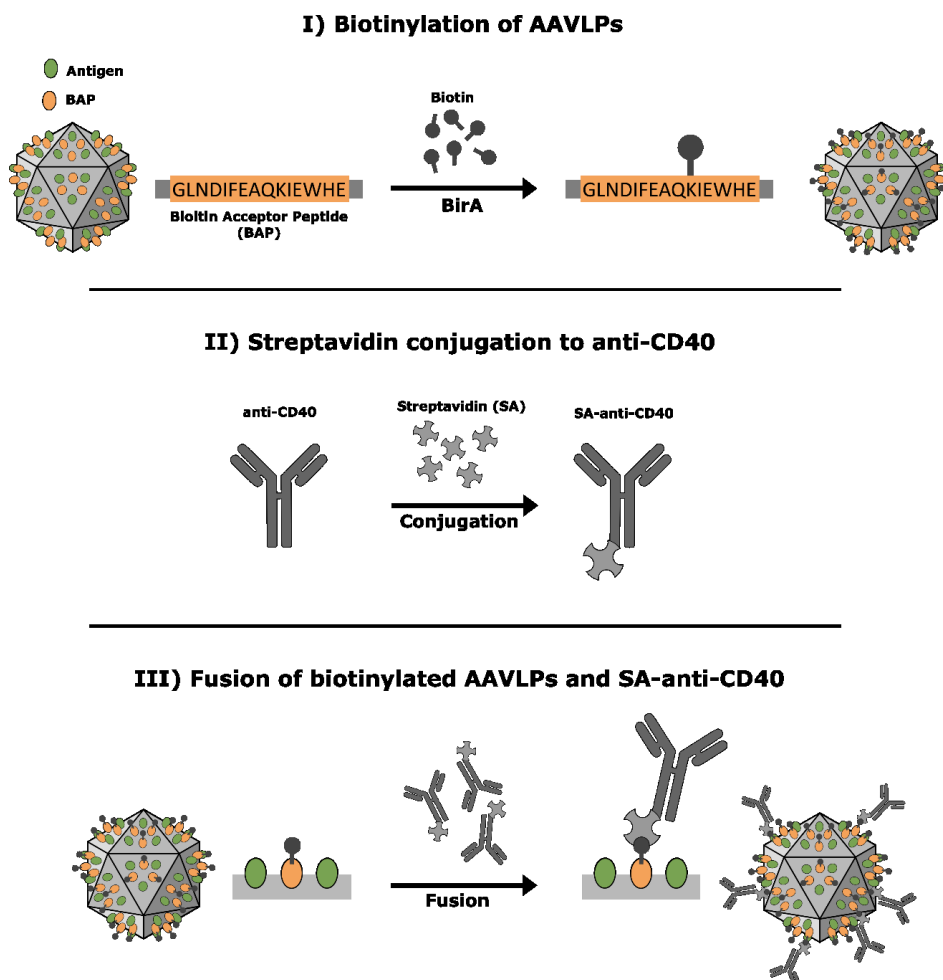


Figure 4.14: Generation of AAVLPs with bound anti-CD40.

Biotinylation of AAVLPs was achieved by inserting BAP into the VR-IV loop (aa453) of AAVLP-SIINFEKL (SIINFEKL in the VR-VIII loop around aa588). AAVLP production was conducted in the presence of biotin and the biotin ligase BirA, which attaches biotin to BAP, as described in **3.5.1**. Biotinylation was confirmed by coating AAVLPs on ELISA plates and detecting bound biotin with HRP-coupled streptavidin. A clear signal was observed for biotinylated AAVLPs (AAVLP-BAP-SIINFEKL) but not for unbiotinylated particles of AAVLP-WT (*Figure 4.15A*).

Streptavidin coupling to anti-CD40 was achieved using a streptavidin conjugation kit, as described in **3.5.3**, and was confirmed by non-reducing WB analysis with an anti-IgG antibody. Unconjugated anti-CD40 (α CD40) showed one distinct band with the expected size of 160 kDa (IgG2a) (*Figure 4.15B*). Conjugated anti-CD40 (α CD40 + SA) showed additional bands around the calculated sizes of 213 kDa, 266 kDa and 319 kDa, corresponding to 1, 2 or 3 bound streptavidin molecules, respectively (indicated by arrows). Additional bands were observed which likely originate from antibody cleavage products that were streptavidin-conjugated.

After fusion of streptavidin-anti-CD40 with biotinylated AAVLPs, successful coupling of anti-CD40 to AAVLPs was confirmed by ELISA. To this end, AAVLPs were fixed on A20-coated ELISA plates and were analyzed with an anti-rat IgG antibody for detection of bound anti-CD40 (rat IgG2a). Anti-CD40-coupled AAVLPs (AAVLP-BAP-SIINFEKL + anti-CD40) showed a clear signal, which was not detectable in AAVLPs without antibody conjugation (AAVLP-SIINFEKL, AAVLP-BAP-SIINFEKL) or unbiotinylated AAVLPs mixed with anti-CD40 (AAVLP-SIINFEKL + anti-CD40) (*Figure 4.15C*).

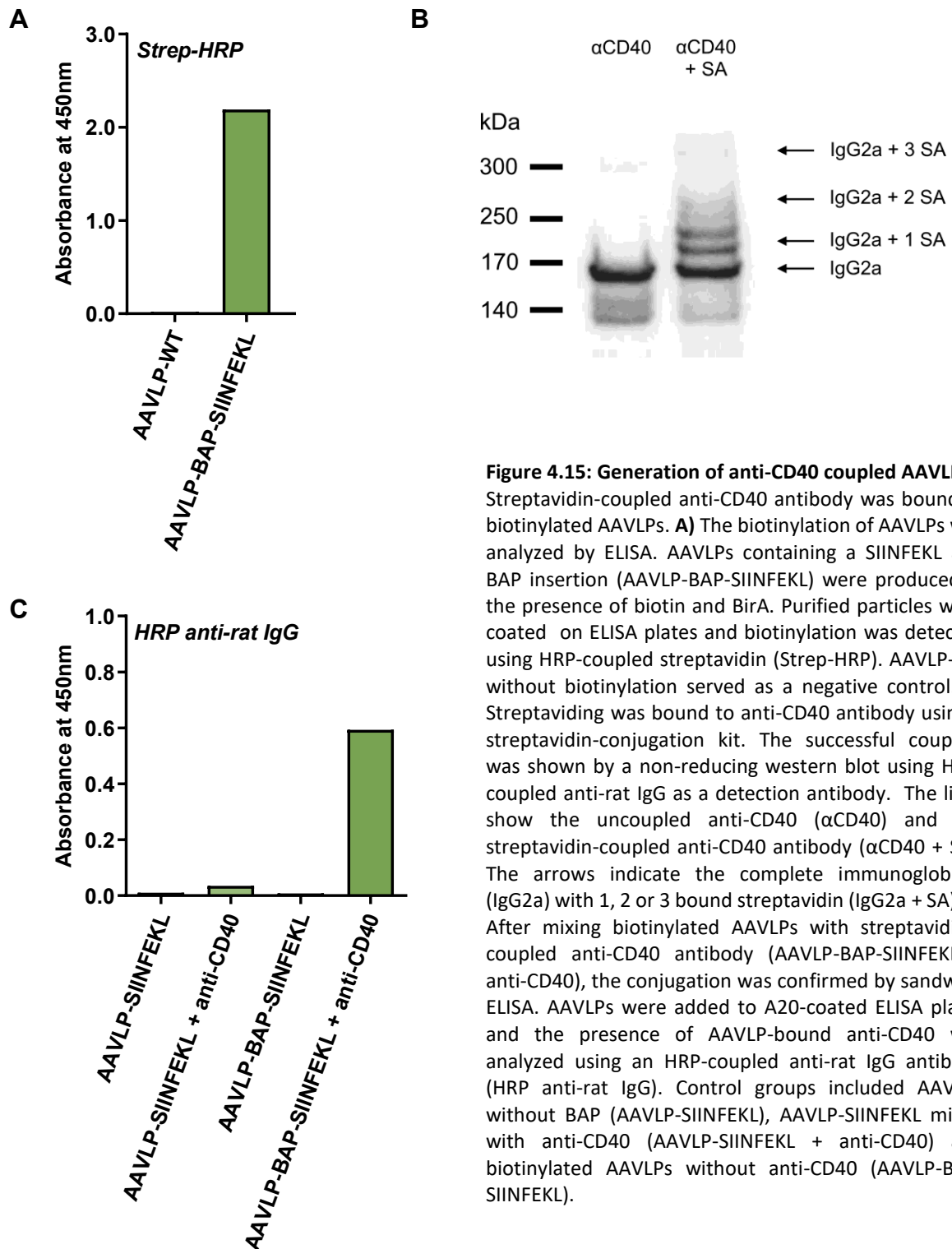


Figure 4.15: Generation of anti-CD40 coupled AAVLPs.

Streptavidin-coupled anti-CD40 antibody was bound to biotinylated AAVLPs. **A)** The biotinylation of AAVLPs was analyzed by ELISA. AAVLPs containing a SIINFEKL and BAP insertion (AAVLP-BAP-SIINFEKL) were produced in the presence of biotin and BirA. Purified particles were coated on ELISA plates and biotinylation was detected using HRP-coupled streptavidin (Strep-HRP). AAVLP-WT without biotinylation served as a negative control. **B)** Streptavidin was bound to anti-CD40 antibody using a streptavidin-conjugation kit. The successful coupling was shown by a non-reducing western blot using HRP-coupled anti-rat IgG as a detection antibody. The lines show the uncoupled anti-CD40 (α CD40) and the streptavidin-coupled anti-CD40 antibody (α CD40 + SA). The arrows indicate the complete immunoglobulin (IgG2a) with 1, 2 or 3 bound streptavidin (IgG2a + SA). **C)** After mixing biotinylated AAVLPs with streptavidin-coupled anti-CD40 antibody (AAVLP-BAP-SIINFEKL + anti-CD40), the conjugation was confirmed by sandwich ELISA. AAVLPs were added to A20-coated ELISA plates and the presence of AAVLP-bound anti-CD40 was analyzed using an HRP-coupled anti-rat IgG antibody (HRP anti-rat IgG). Control groups included AAVLPs without BAP (AAVLP-SIINFEKL), AAVLP-SIINFEKL mixed with anti-CD40 (AAVLP-SIINFEKL + anti-CD40) and biotinylated AAVLPs without anti-CD40 (AAVLP-BAP-SIINFEKL).

4.3.2 Anti-CD40-coupled AAVLPs bind to CD40-expressing cells

The ability of AAVLP-BAP-SIINFEKL with bound anti-CD40 antibody to target CD40-expressing cells was analyzed.

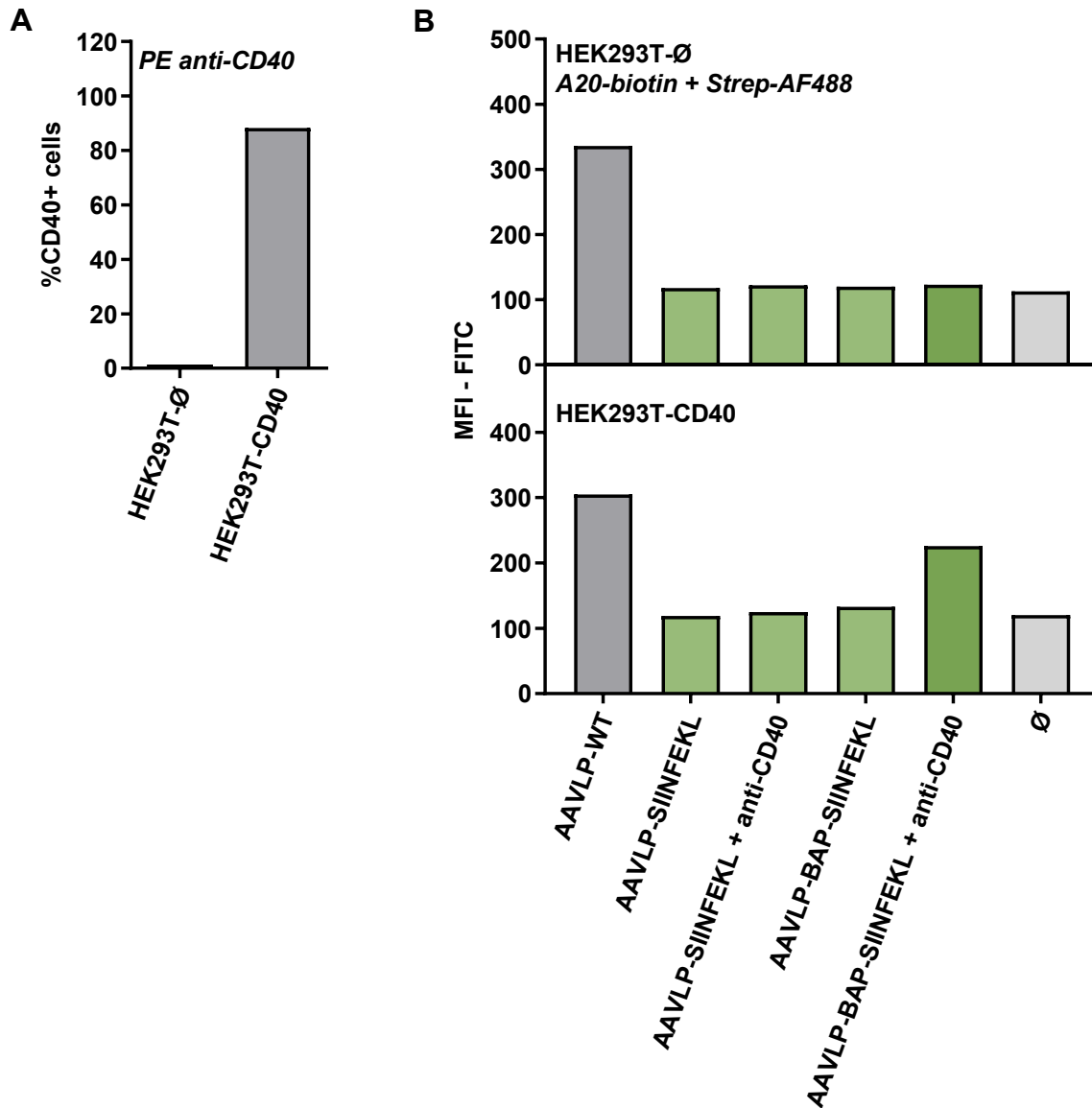


Figure 4.16: Coupling of anti-CD40 to AAVLPs increases the ability to target CD40-expressing cells.

A) HEK293T cells were transiently transfected with CD40. The expression was analyzed by flow cytometry using a PE-labeled antibody against CD40 (PE anti-CD40). The graph shows the percentage of CD40 expressing cells. **B)** The ability of anti-CD40-coupled AAVLPs (AAVLP-BAP-SIINFEKL + anti-CD40) to bind wt (HEK293T-Ø) or CD40-expressing cells (HEK293T-CD40) was analyzed after 4 h incubation by staining with a biotinylated A20 antibody (A20-biotin), followed by Alexa Fluor 488-tagged streptavidin (Strep-AF488). The graph shows the mean fluorescence intensity (MFI) of FITC. AAVLP-WT with a natural tropism served as a positive control, while negative controls included unbiotinylated AAVLP-SIINFEKL without anti-CD40 (AAVLP-SIINFEKL) or mixed with anti-CD40 (AAVLP-SIINFEKL + anti-CD40), as well as biotinylated AAVLP-SIINFEKL without coupled antibody (AAVLP-BAP-SIINFEKL).

The expression of CD40 on transfected HEK293T cells was confirmed by staining with a PE-labeled anti-CD40 antibody (*Figure 4.16A*).

Binding of AAVLPs to target cells was analyzed by staining cell-bound particles with a biotin-conjugated A20 antibody, which was detected by flow cytometry after incubation with streptavidin-AlexaFluor 488. AAVLP-WT with a natural tropism was included as a positive control.

While AAVLPs without bound anti-CD40 (AAVLP-SIINFEKL, AAVLP-SIINFEKL + anti-CD40, AAVLP-BAP-SIINFEKL) did not attach to the cells, coupling anti-CD40 to AAVLPs (AAVLP-BAP-SIINFEKL + anti-CD40) facilitated binding to CD40-expressing target cells (HEK293T-CD40), but not untransfected cells (HEK293T- \emptyset) (*Figure 4.16B*). Binding of AAVLP-WT to HEK293T-CD40 was stronger, but not CD40-specific, as particles attached similarly to CD40-negative HEK293T cells.

4.3.3 Coupling anti-CD40 to AAVLP-SIINFEKL does not improve CD8⁺ T cell responses

To determine if anti-CD40 can increase T cell responses induced by the vaccine, mice were vaccinated with AAVLP-SIINFEKL mixed with anti-CD40 (AAVLP-SIINFEKL + aCD40) or with biotinylated AAVLP-BAP-SIINFEKL with bound anti-CD40 (AAVLP-SIINFEKL-aCD40). AAVLP-SIINFEKL and biotinylated AAVLP-SIINFEKL (AAVLP-SIINFEKL-B) served as base level controls. CD8⁺ T cell responses were analyzed after 1 week in the blood of mice by tetramer staining or after 3 weeks by intracellular staining (ICS) of activation markers in stimulated splenocytes.

Generally, T cell responses were rather low compared to previous experiments, but first responses were already observed after 1 week (vs. 2 weeks in previous experiments). After 1 week, antigen-specific CD8⁺ T cell responses were highest in the group of AAVLP-SIINFEKL mixed with anti-CD40 (AAVLP-SIINFEKL + aCD40) (0.08 %) (*Figure 4.17A*). In addition, anti-CD40-coupled AAVLPs (AAVLP-SIINFEKL-aCD40) showed slightly but not significantly increased responses (0.05 %) compared to groups without antibody (AAVLP-SIINFEKL, AAVLP-SIINFEKL-B) (0.03 % each).

After 3 weeks, the beneficial effect of anti-CD40 was no longer explicit. AAVLP-SIINFEKL administered with anti-CD40 (AAVLP-SIINFEKL + aCD40) showed responses of 0.09 % antigen-specific CD8⁺ T cells compared to 0.06 % induced by AAVLP-SIINFEKL (*Figure 4.17B*). However, these differences were not significant. Higher responses of 0.14 % were induced

by anti-CD40-coupled AAVLP-SIINFEKL (AAVLP-SIINFEKL-aCD40). Yet, the highest responses were observed for biotinylated AAVLPs without antibody (AAVLP-SIINFEKL-B) (0.20 %) which were significantly higher than responses induced by AAVLP-SIINFEKL.

In conclusion, anti-CD40 had an early effect on induced CD8⁺ T cell responses but no long-term advantage. On the other side, biotinylation itself increased immune responses of the AAVLP vaccine.

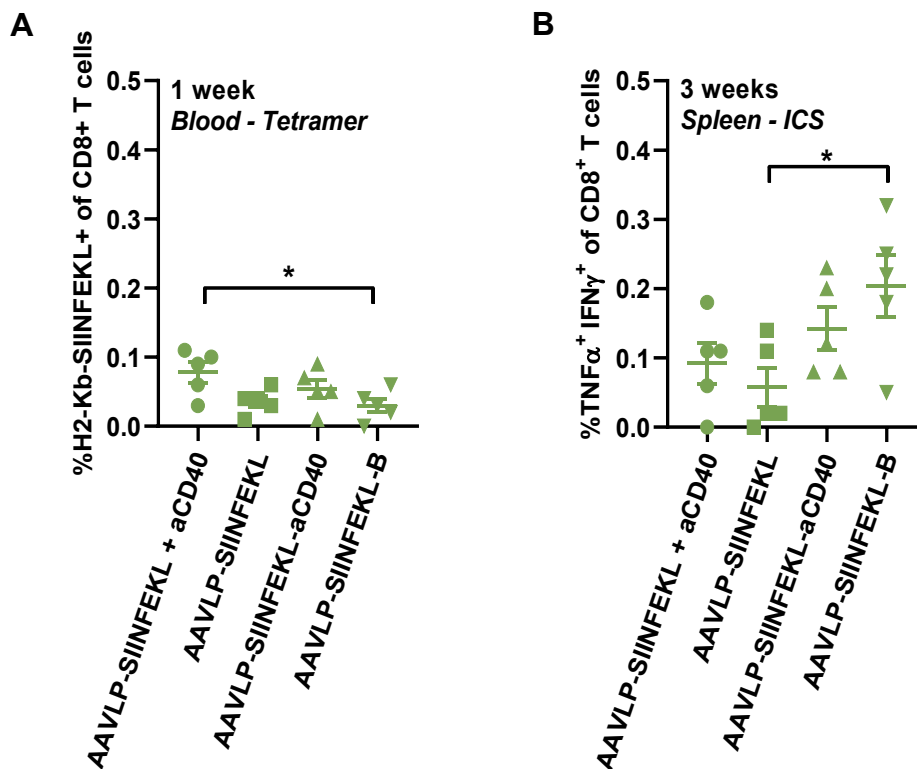


Figure 4.17: Binding of anti-CD40 to AAVLPs does not improve immune responses but biotinylation has an advantageous effect.

C57BL/6 mice (n=5 per group) were vaccinated with AAVLP-SIINFEKL in combination with an anti-CD40 antibody. AAVLP-SIINFEKL was either mixed with the antibody (AAVLP-SIINFEKL + aCD40) or a streptavidin-conjugated anti-CD40 was bound to biotinylated AAVLPs (AAVLP-SIINFEKL-aCD40). AAVLP-SIINFEKL and biotinylated AAVLP-SIINFEKL (AAVLP-SIINFEKL-B) without antibody served as controls. **A**) One week after vaccination, the presence of antigen-specific CD8⁺ T cells in the blood was analyzed by staining with fluorescent-labeled H-2Kb/SIINFEKL tetramers. **B**) Three weeks after vaccination, CD8⁺ T cells in the spleen were analyzed by stimulating splenocytes with SIINFEKL peptide for 6h in the presence of Monensin and Brefeldin A, and intracellular staining (ICS) for activation markers TNFα and IFNγ. Horizontal bars indicate the mean of each group with SEM. Significant differences between groups were determined using a One-way ANOVA with a Tukey's multiple comparison test. Asterisks indicate significant difference with * (P ≤ 0.05).

4.3.4 Co-display of ICBL on AAVLP-SIINFELK increases CD8+ T cell responses

An alternative strategy to improve CD8+ T cell responses induced by the AAVLP vaccine included co-display of an immune stimulatory peptide. The J-immune cell binding ligand (J-ICBL) is a β -2-microglobulin-derived peptide [160], which is known to induce DC maturation and activation of T helper 1 (Th1) responses [172, 173]. While SIINFELK was inserted into the VR-VIII loop (aa588) of the AAVLP capsid, J-ICBL was inserted in the VR-IV loop (aa453) (AAVLP-ICBL-SIINFELK). Mice were vaccinated with AAVLP-ICBL-SIINFELK or AAVLP-SIINFELK as a control. AAVLP-SIINFELK induced 0.17 % antigen-specific CD8+ T cells, while co-display of ICBL increased the responses significantly to a mean of 0.57 % (Figure 4.18). These were the highest CD8+ T cell responses measured throughout the project.

In conclusion, co-display of immune stimulatory peptides in general, and J-ICBL specifically, can improve CD8+ T cell responses and is worth considering for future strategies.

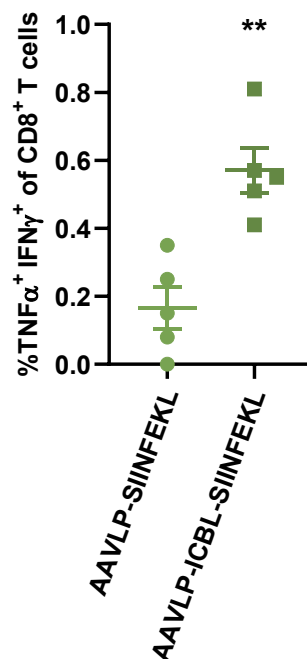


Figure 4.18: Displaying a β -2-microglobulin peptide on AAVLP-SIINFELK increases CD8+ T cell responses. C57BL/6 mice (n=5 per group) were vaccinated with AAVLPs displaying only SIINFELK at amino acid 588 (AAVLP-SIINFELK) or a combination of SIINFELK at amino acid 588 and a β -2-microglobulin peptide (ICBL) at amino acid 453 (AAVLP-ICBL-SIINFELK). In order to detect antigen-specific CD8+ T cells 3 weeks after vaccination, splenocytes were stimulated with SIINFELK peptide for 6h in the presence of Monensin and Brefeldin A, and were subsequently analyzed by intracellular staining (ICS) and flow cytometry for activation markers TNF α and IFN γ . Horizontal bars indicate the mean of each group with the SEM. Significant differences between groups were determined using a Two-tailed t-test. Asterisks indicate significant difference with ** (P \leq 0.01).

4.4 The role of B cells (AAVLP-SIINFEKL)

4.4.1 Absence of B cells increases CD8+ T cell responses induced by AAVLP-SIINFEKL

To analyze if B cells play a role in the induction of CD8+ T cell responses after AAVLP vaccination, B cells were depleted during vaccination by injection of anti-CD20 antibodies. Successful depletion was confirmed by flow cytometry. Control mice injected with an IgG isotype control had a level of 40 % B220+ B cells in the blood and spleen. B cells were reduced to 0.5 - 1.0 % upon anti-CD20 injection and were absent until euthanasia of mice (*Appendix 5A,B*).

Despite almost complete depletion of B cells, antibodies against the capsid of AAVLPs were still detectable in anti-CD20-injected mice, although to a lesser extent than in B cell-carrying control mice (*Appendix 5C*).

B cell depletion during AAVLP-SIINFEKL vaccination caused a significant increase in SIINFEKL-specific CD8+ T cell responses. While vaccinated mice injected with an IgG isotype control showed a mean of 0.21 % antigen-specific CD8+ T cells, B cell-depleted mice developed an average of 0.52 % SIINFEKL-specific CD8+ T cells (*Figure 4.19*).

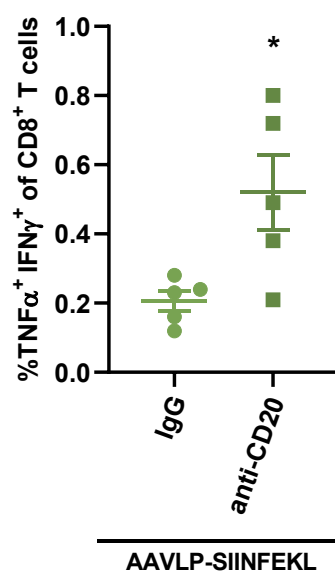


Figure 4.19: Depletion of B cells improves CD8+ T cell responses induced by AAVLP-SIINFEKL.

C57BL/6 mice (n=5 per group) were vaccinated with AAVLP-SIINFEKL upon injection of a depleting anti-CD20 antibody or an IgG isotype control. In order to detect antigen-specific CD8+ T cells 3 weeks after vaccination, splenocytes were stimulated with SIINFEKL peptide for 6h in the presence of Monensin and Brefeldin A, and were subsequently analyzed by intracellular staining (ICS) and flow cytometry for the activation markers TNF α and IFN γ . Horizontal bars indicate the mean of each group with SEM. Significant differences between groups were determined using a Two-tailed t-test. Asterisks indicate significant difference with * ($P \leq 0.05$).

4.5 The role of CD4+ T cells (AAVLP-SIINFEKL)

4.5.1 Presence of CD4+ T cells is required for CD8+ T cell responses induced by AAVLP-SIINFEKL

In this chapter, the role of CD4+ T cells in the vaccination strategy was examined.

To analyze if CD4+ T cells are required for vaccine efficacy, CD4+ T cells were depleted during vaccination by injecting an anti-CD4 antibody. Successful depletion was confirmed by flow cytometry (*Appendix 4*).

The effect of CD4+ T cells was first analyzed by challenging AAVLP-SIINFEKL vaccinated mice with B16F10-OVA cells in the presence or absence of CD4+ T cells (*Figure 4.20A+B*). AAVLP-SIINFEKL vaccination in combination with an IgG isotype control (AAVLP-SIINFEKL + IgG) prevented tumor growth in 6 of 7 mice, as seen before (*Figure 4.13*). In CD4+ T cell depleted mice (AAVLP-SIINFEKL + anti-CD4), the protection was completely abrogated and mice developed rapid tumor growth comparable to a PBS-injected control group.

The dependence on CD4+ T cells for vaccine efficacy was further confirmed by analyzing induction of CD8+ T cell responses as in previous experiments (**4.2**). Without depletion, AAVLP-SIINFEKL vaccinated mice developed 0.24 % antigen-specific CD8+ T cells. Depletion of CD4+ T cells by anti-CD4 injection prevented the effect of the vaccine entirely with 0.02 % SIINFEKL-specific CD8+ T cells (*Figure 4.20C*).

These results showed that presence of CD4+ T cells is required for AAVLP vaccine efficacy.

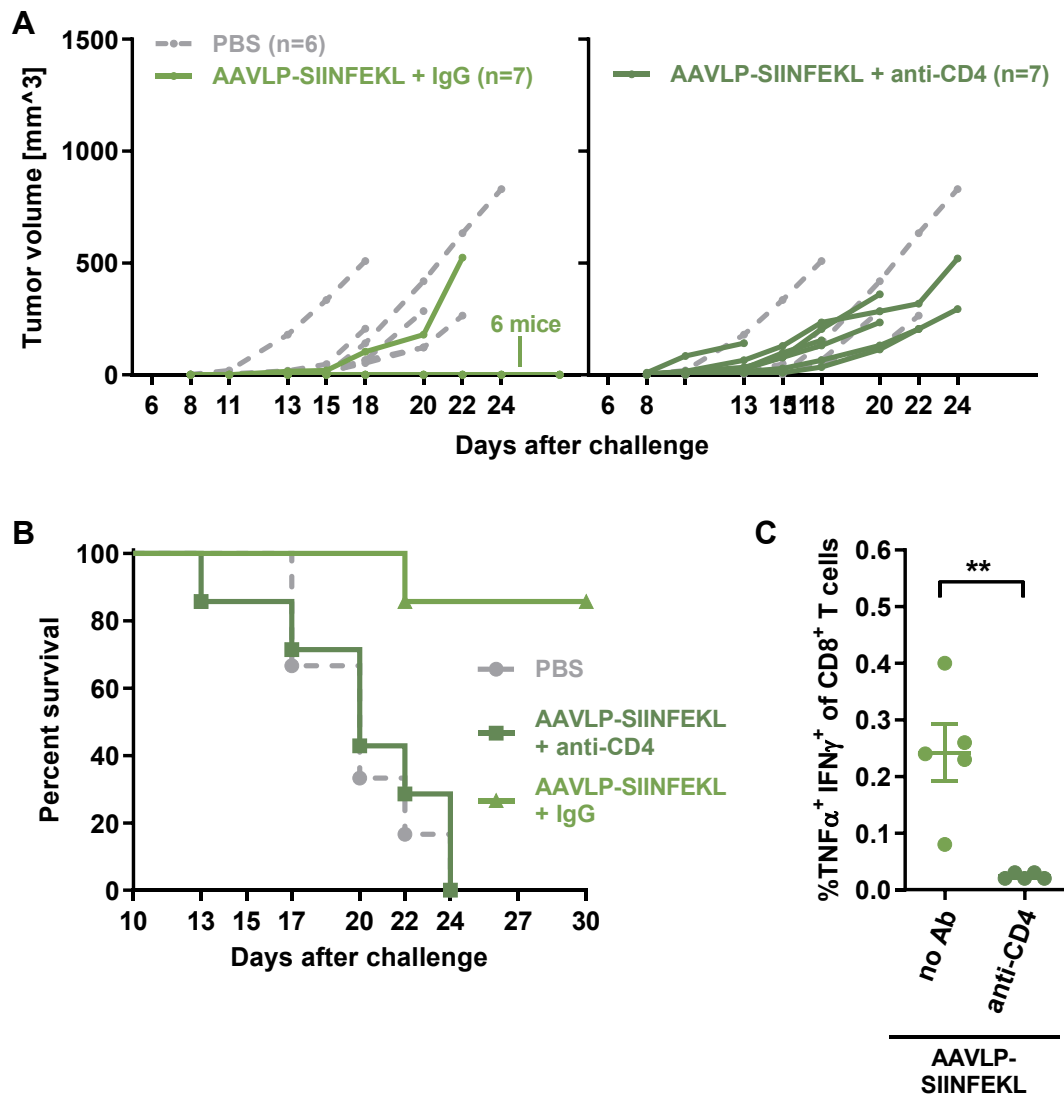


Figure 4.20: Tumor protection and induction of CD8+ T cell responses after AAVLP-SIINFEKL vaccination depend on presence of CD4+ T cells.

Mice were vaccinated with AAVLP-SIINFEKL and additionally treated with a depleting anti-CD4 antibody or an isotype control (IgG) **A+B**) Three weeks after vaccination and anti-CD4 treatment, mice were challenged s.c. with B16F10-OVA cells. **A**) Individual tumor growth curves for each mouse of AAVLP-SIINFEKL vaccinated groups that were co-injected with an IgG isotype control (left) or anti-CD4 (right). As controls, the growth curves of PBS-injected mice are shown as dashed, light-grey lines. **B**) Survival curves of AAVLP-SIINFEKL vaccinated mice with or without anti-CD4 injection compared to the control groups. The graph shows the percentage of live animals on each day. **C**) Spleens were isolated three weeks after mice (n=5 per group) were vaccinated with AAVLP-SIINFEKL under treatment with anti-CD4. In order to detect antigen-specific CD8+ T cells, splenocytes were stimulated with SIINFEKL peptide for 6h in the presence of Monensin and Brefeldin A, and were subsequently analyzed by intracellular staining (ICS) and flow cytometry for the activation markers TNF α and IFN γ . Horizontal bars indicate the mean of each group with SEM. Significant differences between groups were determined using a One-way ANOVA with a Tukey's multiple comparison test. Asterisks indicate significant difference with ** ($P \leq 0.01$).

4.5.2 Identification of potential helper epitopes in the AAVLP capsid

The observed dependence on CD4+ T cells (*Figure 4.20*) indicated the presence of T helper epitopes in the AAVLP capsid itself. Therefore, MHC class II epitopes in the AAVLP-SIINFEKL capsid sequence were predicted *in silico* using NetMHCII2.3 [147] and NetMHCIIpan 4.0 [148]. Both servers predicted similar 15-mer epitopes as strong binders (< 2 % rank) (*Table 4.2*). Overlapping predictions with the same core sequence were merged, yielding 11 peptides of 16-27 amino acids (p1-p11) displayed in *Table 4.2*. One peptide that was predicted to be an MHC class II non-binder was additionally included as a negative control (p0).

Table 4.2: *In silico* predicted helper epitopes in the AAVLP capsid sequence.

Potential AAVLP helper epitopes in AAVLP-SIINFEKL were predicted using NetMHCII 2.3 and NetMHCIIpan 4.0. The table shows peptide sequences with the corresponding position in AAVLP-WT or AAVLP-SIINFEKL capsid. The last two columns indicate the best binding score (% rank) within the peptides as predicted by NetMHCII 2.3 and NetMHCIIpan 4.0. Bold numbers mark predicted strong binders (< 2 % rank).

	Position in VP1 of AAVLP-WT / AAVLP-SIINFEKL	Sequence	NetMHCII 2.3 (% rank)	NetMHCIIpan 4.0 (% rank)
p0	30-46	PPPKPAERHKDDSRGLV	95.00	71.40
p1	88-104	NPYLKYNHADAEFQERL	14.00	0.89
p2	342-361	VFTDSEYQLPYVLGSAHQGC	3.50	0.07
p3	414-432	TFEDVPPFHSSYAHSQSLDR	1.20	0.18
p4	440-455	QYLYLSRTNTPSGTT	1.70	6.32
p5	455-473	TTQSRLQFSQAGASDIRDQ	0.40	1.17
p6	511-529	NGRDSLVPNGPAMASHKDD	0.50	0.46
p7	560-577	TDEEEIRTTNPVATEQYG	1.40	1.70
p8	571-582 / 571-590	VATEQYGSVSTNASASIINF	1.00	0.88
p9	646-672 / 654-680	ILIKNTPVPANPSTTFSAAKFASFITQ	1.30	5.46
p10	669-684 / 677-692	FITQYSTGQVSVEIEW	3.50	1.52
p11	714-732 / 722-740	VDTNGVYSEPRPIGTRYLT	5.00	0.10

To confirm the predicted helper epitopes, mice were vaccinated with AAVLP-WT or AAVLP-SIINFEKL and analyzed for CD4⁺ T cell responses against the selected epitopes. While PBS-injected control mice did not show responses to any of the peptides, the AAVLP-injected groups showed CD4⁺ T cell responses against four peptides (p2, p5, p6, p11) (*Figure 4.21*). In general, responses were stronger and more significant in mice injected with AAVLP-WT with 0.06 %, 0.06 %, 0.15 % and 0.26 % for p2, p5, p6 and p11, respectively. AAVLP-SIINFEKL showed the same tendencies but only two peptides (p2, p11) showed significant CD4⁺ T cell responses with 0.05 % and 0.07 % for p2 and p11, respectively. The confirmed CD4⁺ T cell epitopes are located in the regions of aa342-361 (p2), aa455-473 (p5), aa511-529 (p6) and aa714-732 (p11) of the wild type AAV VP1 sequence.

The sequence of the predicted peptide p8 was not entirely present in AAVLP-WT, but included parts of the inserted SIINFEKL antigen of AAVLP-SIINFEKL. While weak CD4⁺ T cell responses against p8 were detected only in the AAVLP-SIINFEKL vaccinated group, responses were not significant.

In conclusion, four of the predicted helper epitopes in the AAVLP capsid sequence induced CD4⁺ T cell responses after vaccination with AAVLPs and might be responsible for vaccine efficacy.

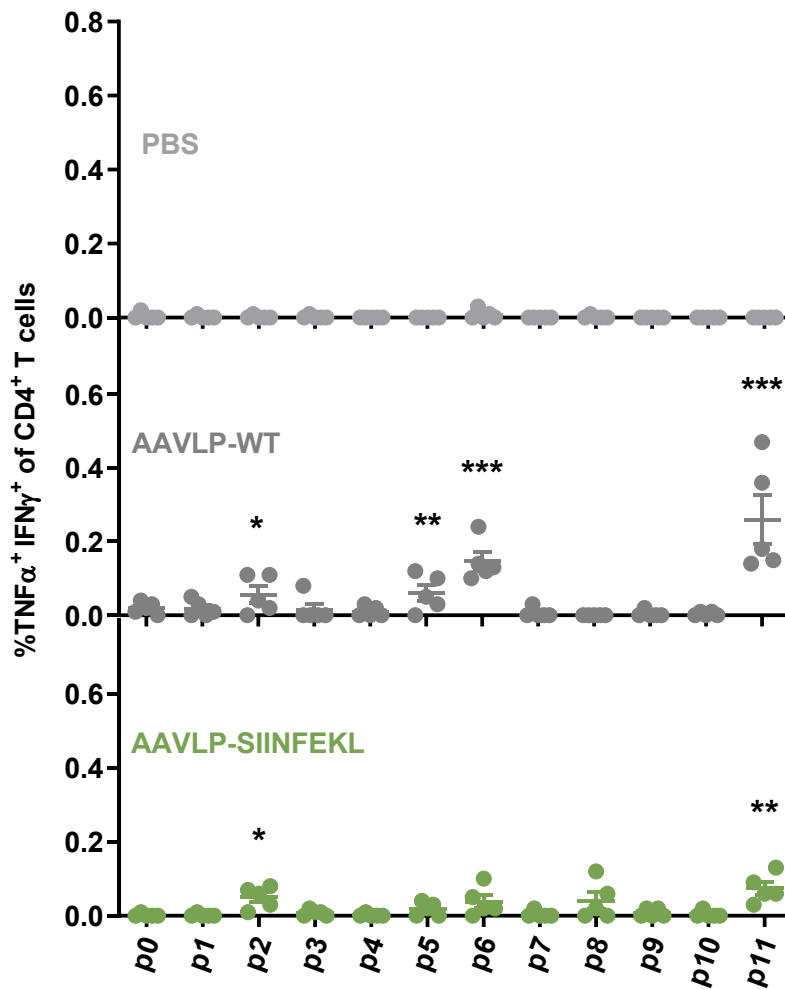


Figure 4.21: Identification of potential T helper epitopes in AAVLPs.

Mice (n=5 per group) injected with PBS, AAVLP-WT or AAVLP-SIINFEKL were analyzed for the presence of AAV-specific CD4⁺ T cells. Three weeks after vaccination, splenocytes were stimulated with AAV capsid-derived peptides with a predicted presentation on MHC class II (p1-p11). p0 was selected as a negative control, based on a predictively weak MHC class II presentation. After 6h incubation with the peptides in the presence of Monensin and Brefeldin A, splenocytes were analyzed by intracellular staining (ICS) and flow cytometry for activation markers TNF α and IFN γ . Horizontal bars indicate the mean of each group with SEM. Significant differences to the control peptide p0 were determined in each group using a One-way ANOVA with a Dunnett's multiple comparison test. Asterisks indicate significant difference to the control peptide p0 with * ($P \leq 0.05$); ** ($P \leq 0.01$); *** ($P \leq 0.001$).

4.6 Targeted induction of antibody and CD4⁺ T cell responses (AAVLP-OVAII)

The previous results suggested that helper epitopes within the AAVLPs are able to induce CD4⁺ T cell responses. To analyze if a displayed MHC class II epitope is able to induce directed antibody and/or CD4⁺ T cell responses, the I-Ab presented ovalbumin peptide OVAII (Ova₃₂₃₋₃₃₉) [155] was inserted into the AAVLP capsid (AAVLP-OVAII).

4.6.1 Vaccination with AAVLP-OVAII induces strong antibody responses against the target antigen

Antibody responses in AAVLP-OVAII or Peptide-OVAII vaccinated mice were analyzed by ELISA for binding to OVAII peptide. The titers of antibodies in the blood were determined weekly for three weeks as the highest serum dilution with still detectable antibody responses in the assay. The baseline titer in unvaccinated mice was 1:200 (**Figure 4.22**). Mice vaccinated with OVAII peptide developed antibody responses after 2 weeks with a mean titer of 1:1571, reaching a titer of 1:44400 after 3 weeks. Responses induced by AAVLP-OVAII were significantly higher than in Peptide-OVAII vaccinated and control mice, with mean titers of 1:3314 and 1:215771 after 2 and 3 weeks, respectively.

In conclusion, the results showed that AAVLPs displaying B cell epitopes are able to induce strong antibody responses, which is in accordance to previous reports [107, 109-111].

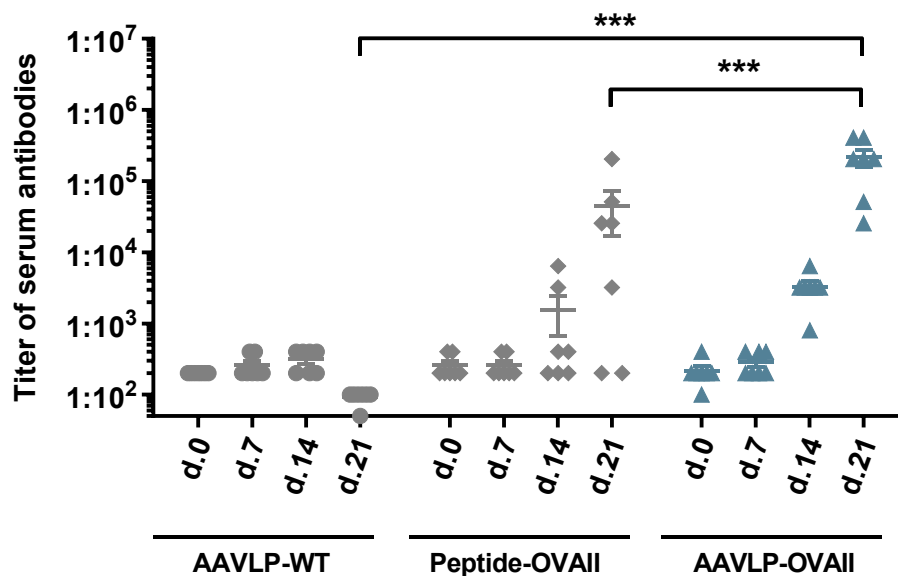


Figure 4.22: Vaccination with AAVLP-OVAII induces high serum titers of OVAII-specific antibodies. C57BL/6 mice (n=5) were vaccinated with AAVLP-OVAII. Blood serum was collected every week and analyzed for the presence of OVAII-specific antibodies by ELISA. The graph shows the serum antibody titers for each animal at the indicated days after vaccination (d.0-d.21). Titers were determined as the highest serum dilution at which antibodies were still detectable. Mice injected with AAVLP-WT or Peptide-OVAII served as controls. Horizontal bars indicate the mean of each group with SEM. Significant differences were determined using a Two-way ANOVA with a Dunnett's multiple comparisons test. Asterisks indicate significant difference between groups with *** ($P \leq 0.001$).

4.6.2 Vaccination with AAVLP-OVAII does not induce CD4⁺ T cell responses against the target antigen

To test if the AAVLP vaccine is able to induce CD4⁺ T cell responses against a target antigen, mice were vaccinated with OVAII-displaying AAVLPs. Four different AAVLP-OVAII variants were tested: AAVLP-OVAII(588), AAVLP-OVAII(588)-PLA2mut, AAVLP-OVAII(453) and AAVLP-OVAII(453)-PLA2mut. In addition to antigen insertions into the VR-VIII loop (aa588) or the VR-IV loop (aa453), two AAVLP variants included a mutation of the phospholipase A2 (PLA2) domain. The mutation was included, as it has been shown to affect intracellular trafficking of AAVs [51], which in turn might influence MHC class II presentation and thus induction of T cell responses [114, 116]. If PLA2 inactivation retains particles in the endosomal/lysosomal compartment, an augmented loading onto MHC class II molecules might occur.

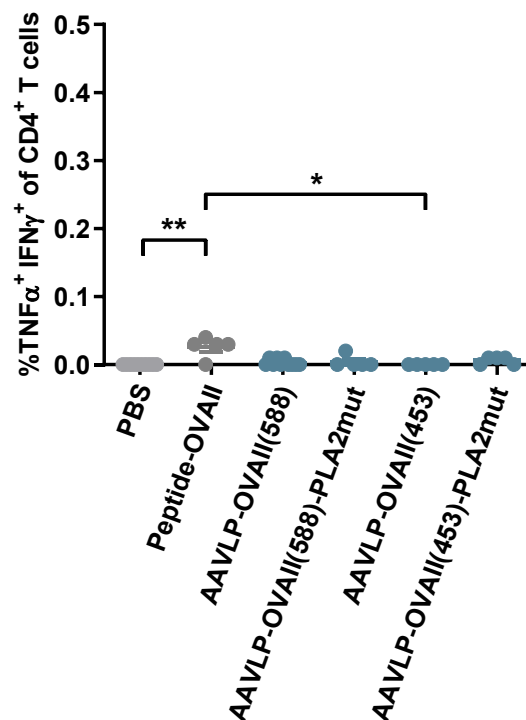


Figure 4.23: Vaccination with AAVLP-OVAII does not induce antigen-specific CD4⁺ T cell responses.

C57BL/6 mice (n=5 per group) were vaccinated with four different AAVLP-OVAII candidates. The target antigen OVAII was inserted at amino acid 588 (588) or 453 (453) of the AAV capsid protein VP. In addition, the PLA2 domain in VP was mutated in either of the insertion variants (PLA2mut). Mice injected with PBS or Peptide-OVAII served as controls. In order to detect antigen-specific CD4⁺ T cells 3 weeks after vaccination, splenocytes were stimulated with OVAII peptide for 6h in the presence of Monensin and Brefeldin A, and were subsequently analyzed by intracellular staining (ICS) and flow cytometry for activation markers TNF α and IFN γ . Horizontal bars indicate the mean of each group with SEM. Significant differences between groups were determined using a Kruskal-Wallis test with a Dunn's multiple comparison test. Asterisks indicate significant difference with * ($P \leq 0.05$); ** ($P \leq 0.01$).

While Peptide-OVAII generated weak but significant OVAII-specific CD4+ T cell responses (0.03 %), none of the AAVLP-OVAII candidates induced any detectable CD4+ T cell responses (*Figure 4.23*). Accordingly, in a B16F10-OVA tumor model, AAVLP-OVAII(588) had no effect on tumor growth while 4 of 7 Peptide-OVAII vaccinated mice remained tumor-free (*Figure 4.24*).

In conclusion, display of the MHC class II model antigen OVAII on AAVLPs did not generate detectable CD4+ T cell responses.

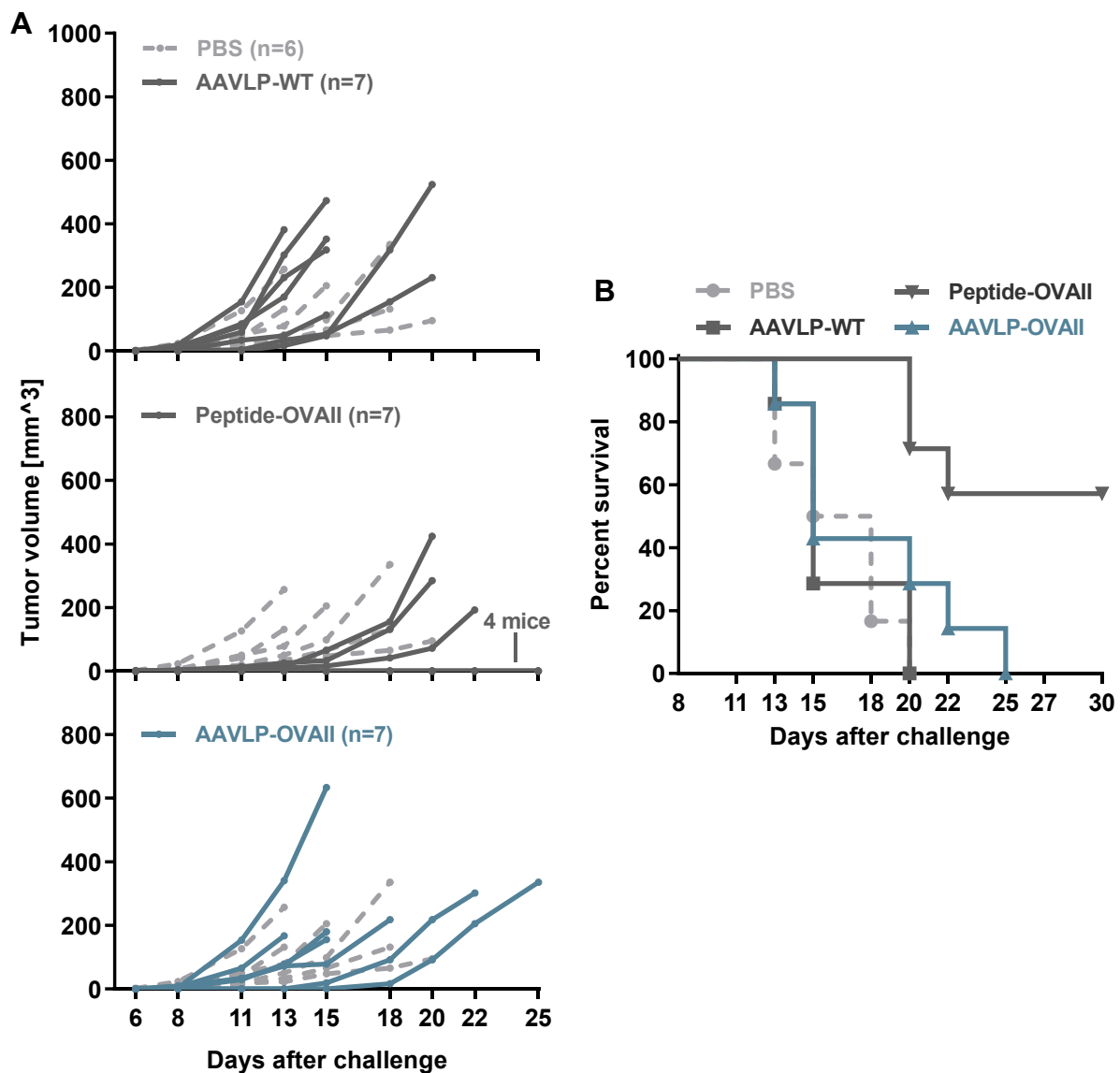


Figure 4.24: Presentation of an ovalbumin MHC class II epitope on AAVLP-OVAII does not protect mice after B16F10-OVA challenge.

AAVLP-OVAII vaccinated mice were challenged s.c. with 2.0×10^5 B16F10-OVA cells, 3 weeks after vaccination. **A)** Individual tumor growth curves in each mouse of the AAVLP-WT (top), Peptide-OVAII (middle) and AAVLP-OVAII (bottom) vaccinated group. For comparison, the growth curves of PBS-injected mice are shown as dashed, light-grey lines. **B)** Survival curves comparing AAVLP-OVAII vaccinated mice to the control groups. The graph shows the percentage of live animals on each day after the challenge.

4.7 Testing alternative CD8+ T cell epitopes (AAVLP-LCMV and AAVLP-HPV)

4.7.1 Vaccination with AAVLPs displaying an LCMV but not HPV antigen induces antigen-specific CD8+ T cell responses

Previous experiments were solely conducted with model antigens derived from chicken ovalbumin. To test alternative antigens for the induction of CD8+ T cell responses, seven viral antigens, which have been shown to induce T cell responses, were cloned into the VR-VIII loop (aa588): LCMV GP₃₃₋₄₁ [156], LCMV NP₃₉₆₋₄₀₄ [156], *mouse mammary tumor virus* (MMTV) Env₅₄₄₋₅₅₁ [174], *murine leukemia virus* (MuLV) Gag₈₅₋₉₃ [175], MuLV p15E₆₀₄₋₆₁₁ [176], HPV E₆₄₈₋₅₇ [157], and HPV E7₄₉₋₅₇ [177]. Notably, only insertion of LCMV NP₃₉₆₋₄₀₄ and HPV E₆₄₈₋₅₇ resulted in AAVLPs (AAVLP-LCMV and AAVLP-HPV) that yielded sufficient particle amounts for vaccination, while the other antigens led to AAVLP preparations with low or no detectable titers.

Mice were vaccinated with the two AAVLP vaccine candidates or a control AAVLP with an inserted FLAG tag (AAVLP-FLAG). Three weeks after vaccination, splenocytes were stimulated with peptides (FLAG tag, LCMV NP₃₉₆₋₄₀₄ or HPV E₆₄₈₋₅₇) and were analyzed for activated CD8+ T cells. As expected, the low immunogenic FLAG tag did not induce CD8+ T cells (**Figure 4.25**). While significant responses of 0.15 % antigen-specific CD8+ T cells were observed after AAVLP-LCMV vaccination, no detectable T cells were induced by AAVLP-HPV vaccination.

In conclusion, the results showed that antigens other than SIINFEKL can be inserted into AAVLPs for generation of specific CD8+ T cell responses. However, not every vaccine candidate showed efficacy and several antigen insertions disrupted formation of AAVLPs.

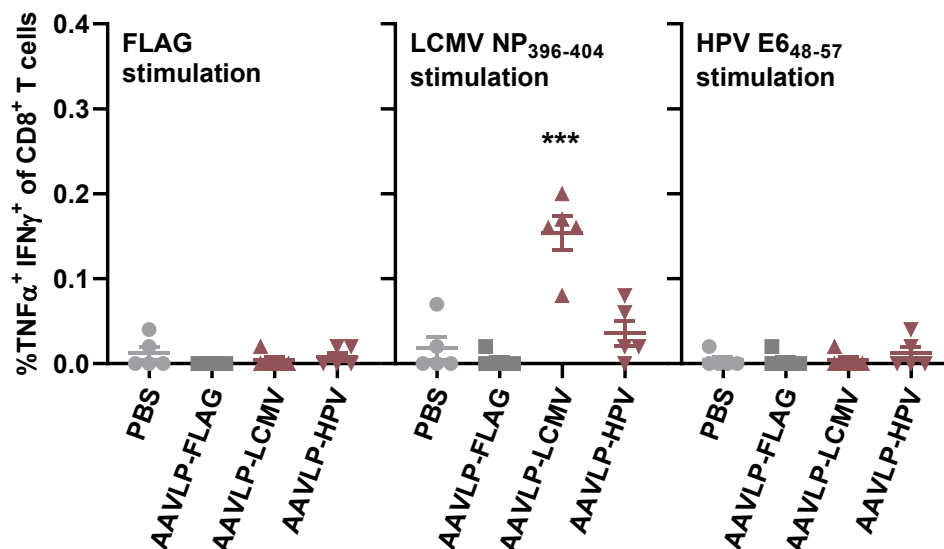


Figure 4.25: Vaccination with AAVLPs displaying an LCMV epitope induces antigen-specific CD8⁺ T cell responses.

C57BL/6 mice (n=5 per group) were vaccinated with AAVLPs displaying viral antigens. Vaccine candidates were AAVLPs with an inserted LCMV NP₃₉₆₋₄₀₄ antigen (AAVLP-LCMV) or an inserted HPV E₆₄₈₋₅₇ antigen (AAVLP-HPV). Mice injected with PBS or AAVLPs displaying a FLAG-tag sequence (AAVLP-FLAG) served as negative controls. In order to detect antigen-specific CD8⁺ T cells 3 weeks after vaccination, splenocytes were stimulated with FLAG, LCMV NP₃₉₆₋₄₀₄ or HPV E₆₄₈₋₅₇ peptide for 6h in the presence of Monensin and Brefeldin A, and were subsequently analyzed by intracellular staining (ICS) and flow cytometry for activation markers TNF α and IFN γ . Horizontal bars indicate the mean of each group with SEM. Significant differences to the PBS group were determined using a One-way ANOVA with a Dunnett's multiple comparison test. Asterisks indicate significant difference with *** (P \leq 0.001).

4.8 Targeting neoantigens (AAVLP-Neo)

Having characterized the AAVLP vaccine with inserted model epitopes, the next step included translation of the strategy to a personalized cancer vaccination. To this end, neoantigen candidates were selected and presented on AAVLPs for the induction of tumor-specific CD8⁺ T cell responses.

4.8.1 Selection of neoantigens for the AAVLP-Neo vaccine

Castle et al. published 50 potential neoantigens in the B16F10 tumor cell line [131], which served as a starting point to design the neoantigen-displaying vaccine AAVLP-Neo. A first selection of antigens included the prediction of MHC class I presentation using the NetMHC 4.0 server [149, 150]. A selection of 19 antigen peptides with 21 amino acids was defined

by a predictively strong binding to the murine MHC class I molecules H2-Kb or H2-Db (**Table 4.3**). Two exceptions to the predicted MHC class I binding were the neoantigens Kif18b and Tm9sf3, which showed anti-tumor effects in Castle et al. [131] but were no predicted strong MHC class I binders.

From 19 selected neoantigen mutations, 16 could be confirmed by genome sequencing in the cultured B16F10 cell line (**Table 4.3, Figure 4.26A**).

Table 4.3: Neoantigen selection.

Neoantigens were selected based on predicted MHC class I presentation (< 0.5 % rank at NetMHC 4.0). Underlined values were not predicted as strong binders by NetMHC 4.0 but were included in the selection due to reported anti-tumor efficacy [131]. Mutations were confirmed in the cultured B16F10 cell line (+) by sequencing (**3.3.9**).

Gene	Mutation	Neoepitope sequence (21 aa)	NetMHC 4.0 (% rank)	Confirmed in B16F10
Kif18b	K739N	PSFQEFVDWENVSPELNSTDQ	<u>1.70</u>	+
Pbk	V145D	SPFPAAVILRDALHMARGLKY	0.12	+
Ddb1	L438I	SFVGQTRVLMINGEEVEEEL	0.15	+
Dpf2	F275V	GLALPNNYCDVCLGDSKINKK	0.50	+
Rpl13a	A24G	HLLGRLAAIVGKQVLLGRKVV	0.25	+
Fat1	I1940M	SMDHKTGTIAMQNTTQLRSRY	0.01	+
Fzd7	G304A	YFMVAVAHVAAFLLEDRAVCV	0.25	+
Golgb1	E2855D	AAPSAASSPADVQSLKKAMSS	0.50	+
Plod2	F530V	NYNTSHLNNDVWQIFENPVDW	0.50	+
Orc2	F278V	QKTLHNLLRKVVPSFSAEIER	0.10	+
Klh122	F179V	QQLDITYILKNVVAFSRTDKYR	0.25	+
Tm9sf3	Y382H	AFFINFIAIYHHSRAIPFGT	<u>1.00</u>	+
Snx5	R373Q	NFKRKRVAAFQKNLIEMSELE	0.07	+
Armc1	S85I	KMKGELGMMLILQNVIQKTTT	0.30	+
Eef2	G795A	KAYLPVNESFAFTADLRNNTG	0.15	-
Tnpo3	G504A	RNPQFLDPVLAYLMKGLCEKP	0.17	+
Atp11a	R522S	DEVALVEGVQSLGFTYLRLKD	0.02	-
Wdr82	I221L	ISTNGSFIRLLDAFKGVVMHT	0.50	-
Cpsf3l	D314N	HIKAFDRTFANNPQPMVVFAT	0.30	+

The 21 amino acid long sequences (mutation at the center of the sequence) were inserted into the AAVLP capsid at the VR-IV (aa453) or VR-VIII loop (aa588), as described before (**3.3.5**). To test which of the neoantigen insertions are tolerated during AAVLP formation, the candidates were first produced in a small scale as crude-lysates. Assembly of intact particles was confirmed by A20-sandwich ELISA, showing that 4 of 14 antigens inserted in the VR-IV loop (aa453) region were tolerated and led to AAVLP titers detectable over background, while 5 of 14 insertions in the VR-VIII loop (aa588) yielded intact AAVLPs (*Figure 4.26B*). Two neoantigens, Tnp03 and Cpsf3l, were excluded from the small-scale production, as a pilot experiment showed undetectable AAVLP levels after small-scale production (data not shown).

As several AAVLPs with long insertions of 21 amino acids showed poor production yields, another attempt was insertion of shorter antigens (8-11 amino acids) into the VR-VIII loop (aa588) of the AAVLP capsid. In this case 13 of 16 antigen insertions yielded AAVLPs detectable over background (*Appendix 6*).

The final selection of antigens for AAVLP-Neo were Kif18b, Ddb1, Golgb1 and Snx5 inserted into the VR-IV loop (aa453), as this position was previously shown to induce higher T cell responses than the VR-VIII loop (aa588) (**4.2.7**). Insertions of 21 amino acids were used, because longer sequences have the potential to contain additional, unpredicted T cell epitopes.

In the large-scale production, AAVLP-Kif18b, AAVLP-Ddb1 and AAVLP-Golgb1 yielded sufficient titers, while AAVLP-Snx5 showed poor yields, which was in accordance to the small-scale production (*Figure 4.26*).

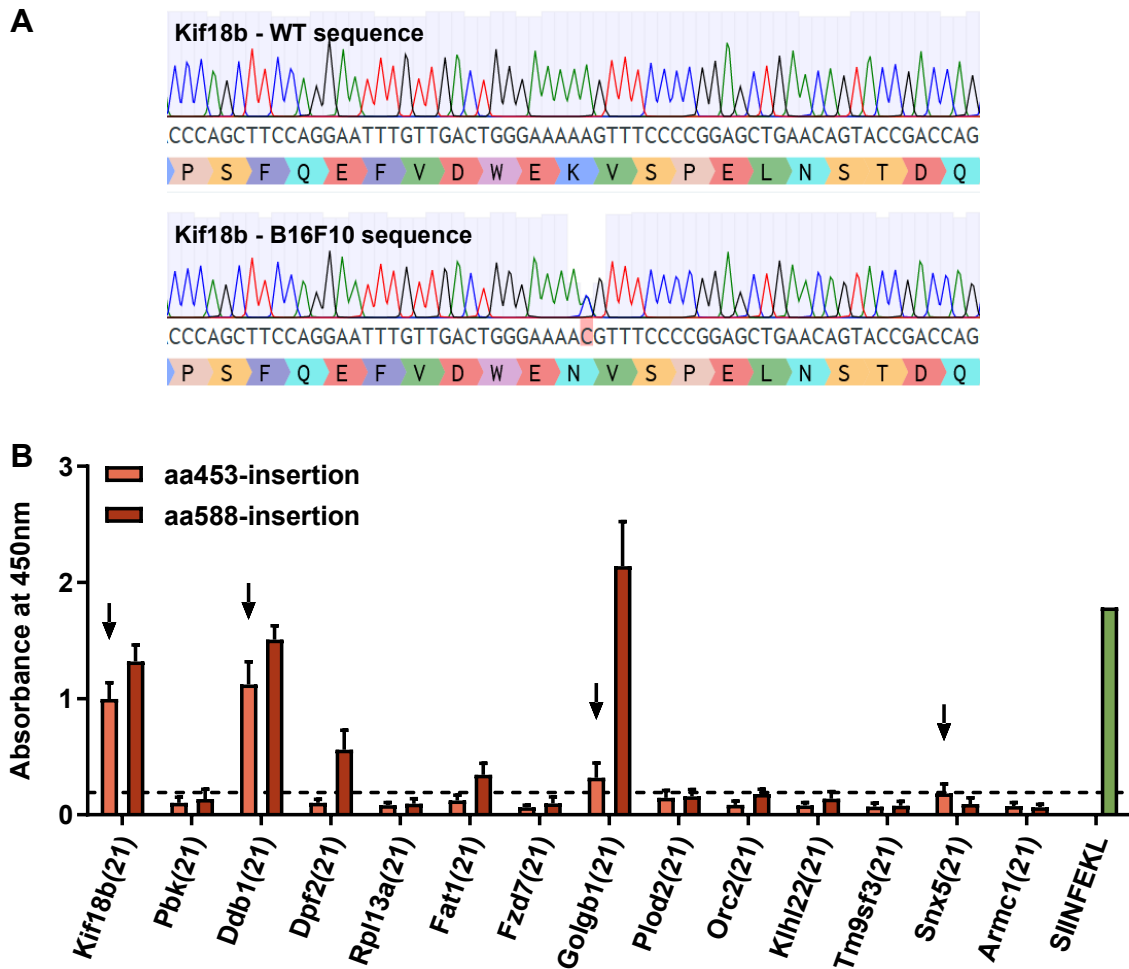


Figure 4.26: Selection of neoantigens for AAVLP-Neo.

A) Representative result of mutation scanning. DNA amplified by PCR from wt CD57BL/6 mouse cells (splenocytes) or the melanoma cell line B16F10 was sequenced. The mutation from nucleotide A to C is shown in a red box. **B)** Ability to produce intact AAVLPs after insertion of different neoantigens into the capsid sequence. 14 neoantigen sequences with a length of 21 amino acids were cloned into the AAVLP capsid sequence in the VR-IV loop (aa453-insertion) or the VR-VIII loop (aa588-insertion). After production in 6-well plates, AAVLP preparations were analyzed for intact particles by A20 sandwich ELISA (3.4.2). AAVLP-SIINFEKL (SIINFEKL) served as a positive control. The dashed line shows the threshold of three times the background value. Arrows indicate the AAVLP-candidates used as AAVLP-Neo in the following experiments to vaccinate mice. The bars show the mean values of three experiments with SEM. The values of different experiments were normalized to the SIINFEKL reference sample.

4.8.2 Vaccination with AAVLP-Neo does not induce detectable CD8+ T cell responses

Mice were vaccinated with AAVLP-Neo, a combination of four AAVLPs: AAVLP-Ddb1, AAVLP-Golgb1 and AAVLP-Kif18b were administered at a dose of $5.0E+11$ particles, while AAVLP-Snx5 was administered at a reduced dose of $1.3E+11$ particles per mouse, owing to its low titer. To compare AAVLP-Neo to a current standard vaccination strategy, 21 amino acid long peptides of the same neoantigens (Peptide-Neo) were administered.

The induction of CD8⁺ T cell responses three weeks after vaccination was analyzed by stimulating splenocytes with neoantigen peptides and determining T cell activation by intracellular cytokine staining. To confirm specificity of neoantigen responses, splenocytes were also stimulated with wt peptides without mutations. None of the AAVLP-Neo vaccinated mice showed detectable T cell responses to any of the four peptides (**Figure 4.27**). The only detectable response was induced by the peptide vaccine in which CD8⁺ T cells against the Snx5 neoantigen were detected. No CD4⁺ T cell responses were measured in any of the groups (data not shown).

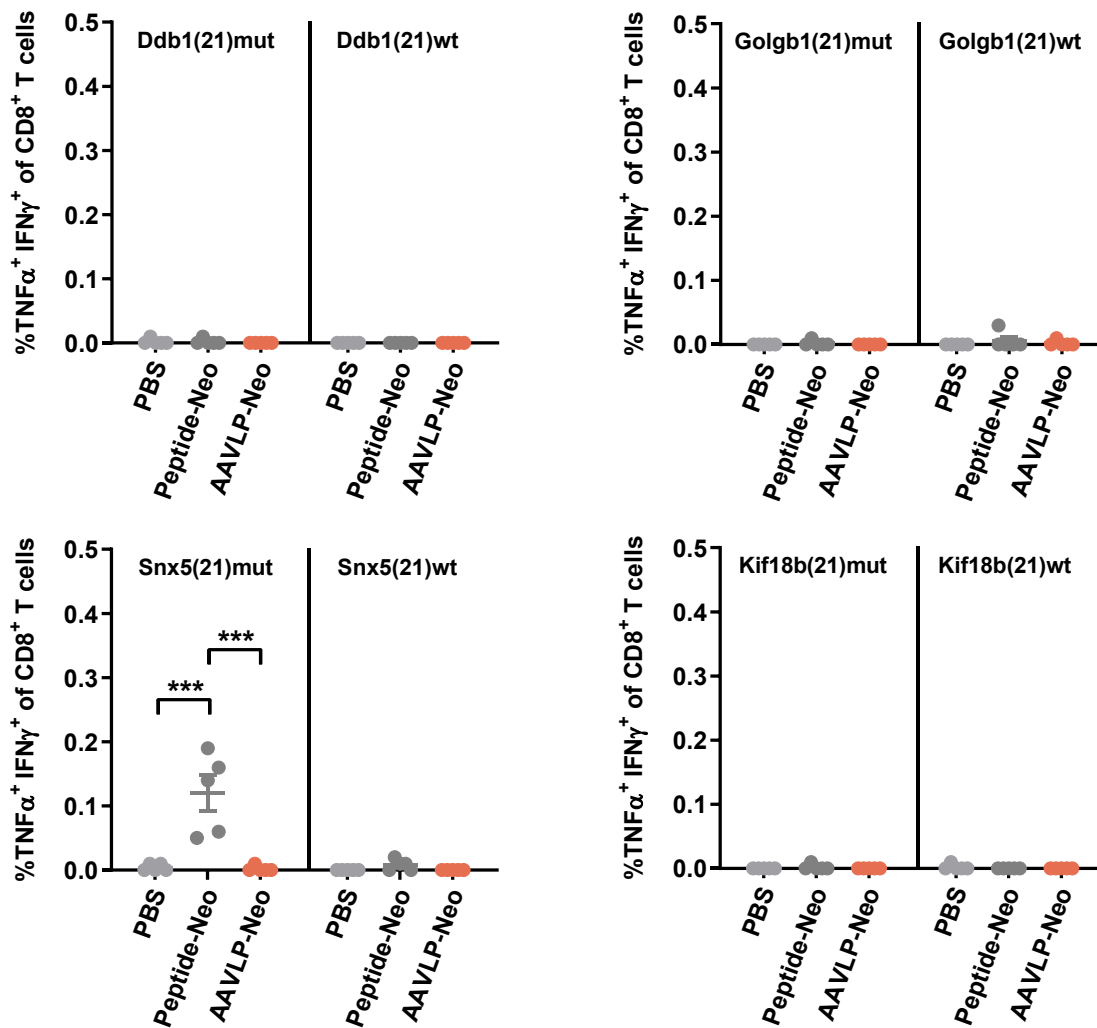


Figure 4.27: AAVLP-Neo does not induce detectable neoantigen-specific CD8⁺ T cell responses.

C57BL/6 mice (n=5) were vaccinated with a neoantigen vaccine (AAVLP-Neo) consisting of AAVLP-Ddb1, AAVLP-Golgb1, AAVLP-Snx5 and AAVLP-Kif18b. AAVLP-Snx5 was administered at a dose of 1.3E+11 capsids per mouse, while the other AAVLPs were administered with 5.0E+11 capsids per mouse. A peptide vaccine (Peptide-Neo) consisting of the same 21 amino acid long sequences served as a control. In order to detect antigen-specific CD8⁺ T cells 3 weeks after vaccination, splenocytes were stimulated with either neoantigen peptide or respective wt sequence for 6h in the presence of Monensin and Brefeldin A, and were subsequently analyzed by intracellular staining (ICS) and flow cytometry for the activation markers TNFα and IFNγ. Horizontal bars indicate the mean of each group with SEM. Significant differences between groups were determined using a One-way ANOVA with a Tukey's multiple comparison test. Asterisks indicate significant difference with *** (P ≤ 0.001).

4.8.3 Vaccination with AAVLP-Neo induces antibody responses against the mutated and wild type peptide

Previous experiments with OVAII showed that strong antibody responses could be induced by the AAVLP vaccine. To detect neoantigen-specific antibodies, pooled serum samples of mice were analyzed by ELISA for responses against the four neoantigen peptides or their wt counterpart.

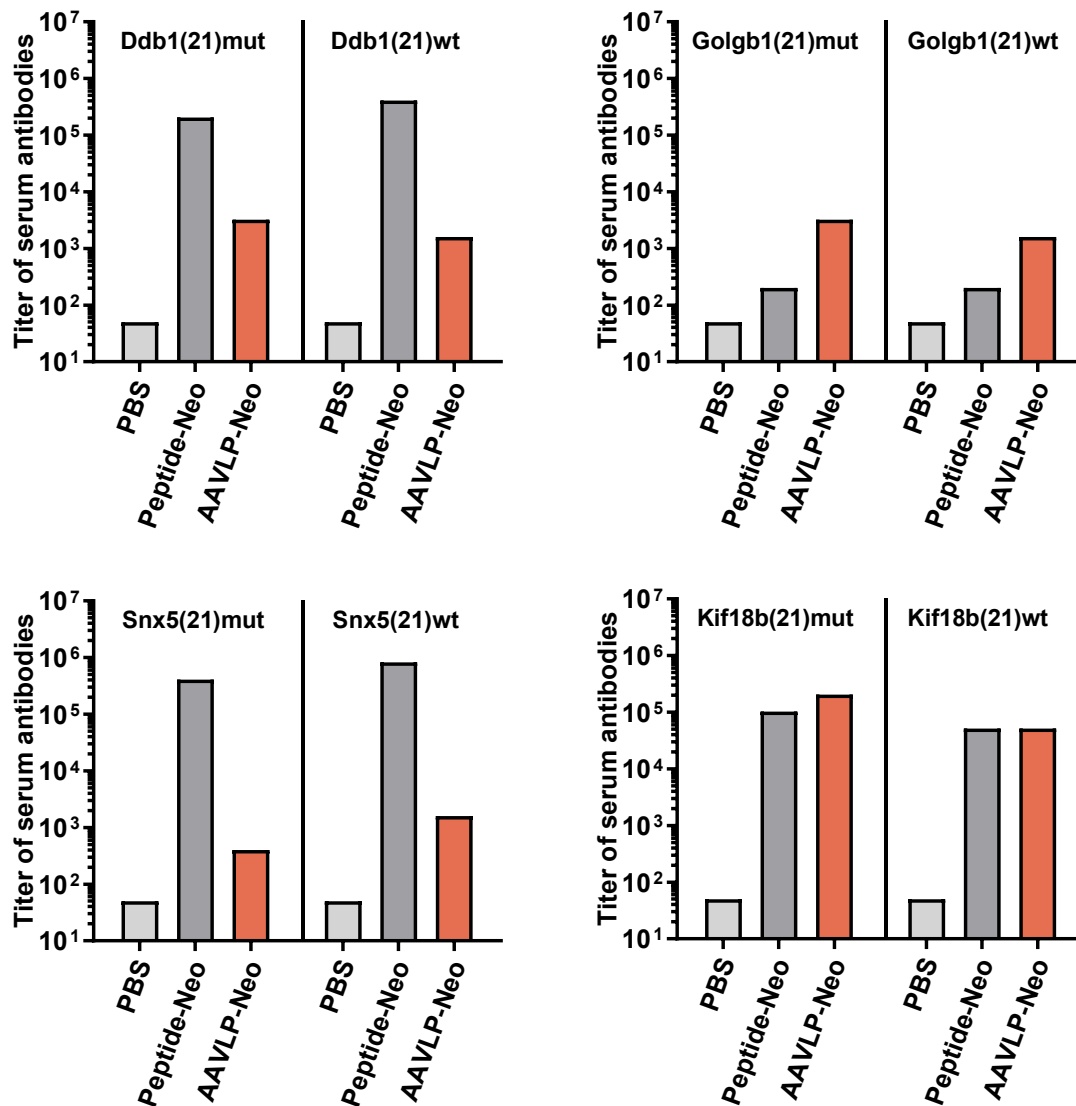


Figure 4.28: Vaccination with AAVLP-Neo induces antibody responses against neoantigens.

C57BL/6 mice were vaccinated as in **Figure 4.27** with AAVLP-Neo or Peptide-Neo, while PBS-injected mice served as negative controls. Blood serum collected after three weeks was analyzed for the presence of neoantigen-specific antibodies. ELISA plates were coated with neoantigen peptides (mut) or their wt counterpart (wt). Serum samples were pooled within a group (n=12) and analyzed for binding to each peptide. The graph shows the serum antibody titers, which were determined as the highest serum dilution with detectable antibody binding.

Titers were determined as highest serum dilutions with still detectable antibody responses. In general, titers against mutated and wt sequences were in the same magnitude, indicating no mutation-specific antibody responses (*Figure 4.28*). The peptide vaccine induced higher titers against Ddb1 and Snx5 than the AAVLP vaccine. Titers against Kif18b were in the same range, while AAVLP-Neo induced higher titers against Golgb1 than Peptide-Neo.

4.8.4 Vaccination with AAVLP-Neo reduces B16F10 tumor growth in mice

Despite no detectable CD8+ T cell responses, anti-tumor efficacy of AAVLP-Neo was analyzed. Mice were challenged three weeks after vaccination s.c. with B16F10 tumor cells. Considering the individual growth curves in each group, a tendency of reduced tumor growth was observed in AAVLP-Neo vaccinated mice compared to PBS-injected and Peptide-Neo vaccinated animals (*Figure 4.29A*). The effect was not as clear in the survival curves, in which the effect of AAVLP-Neo was only marginally visible (*Figure 4.29B*). Yet, this discrepancy is likely due to necrotic events in B16F10 challenged mice. In all groups, mice had mostly been euthanized due to development of necrotic wounds, rather than reaching the maximum tumor size. The tumor volume at the point of necrosis was significantly smaller in AAVLP-Neo vaccinated mice compared to the PBS and Peptide-Neo groups (*Appendix 7*). To show the effect of the vaccine on tumor growth irrespective of the survival, the growth rate was shown as the time until reaching a volume of 100 mm³. AAVLP-Neo vaccinated mice reached this volume at significantly later time points compared to the control groups (*Figure 4.29C*).

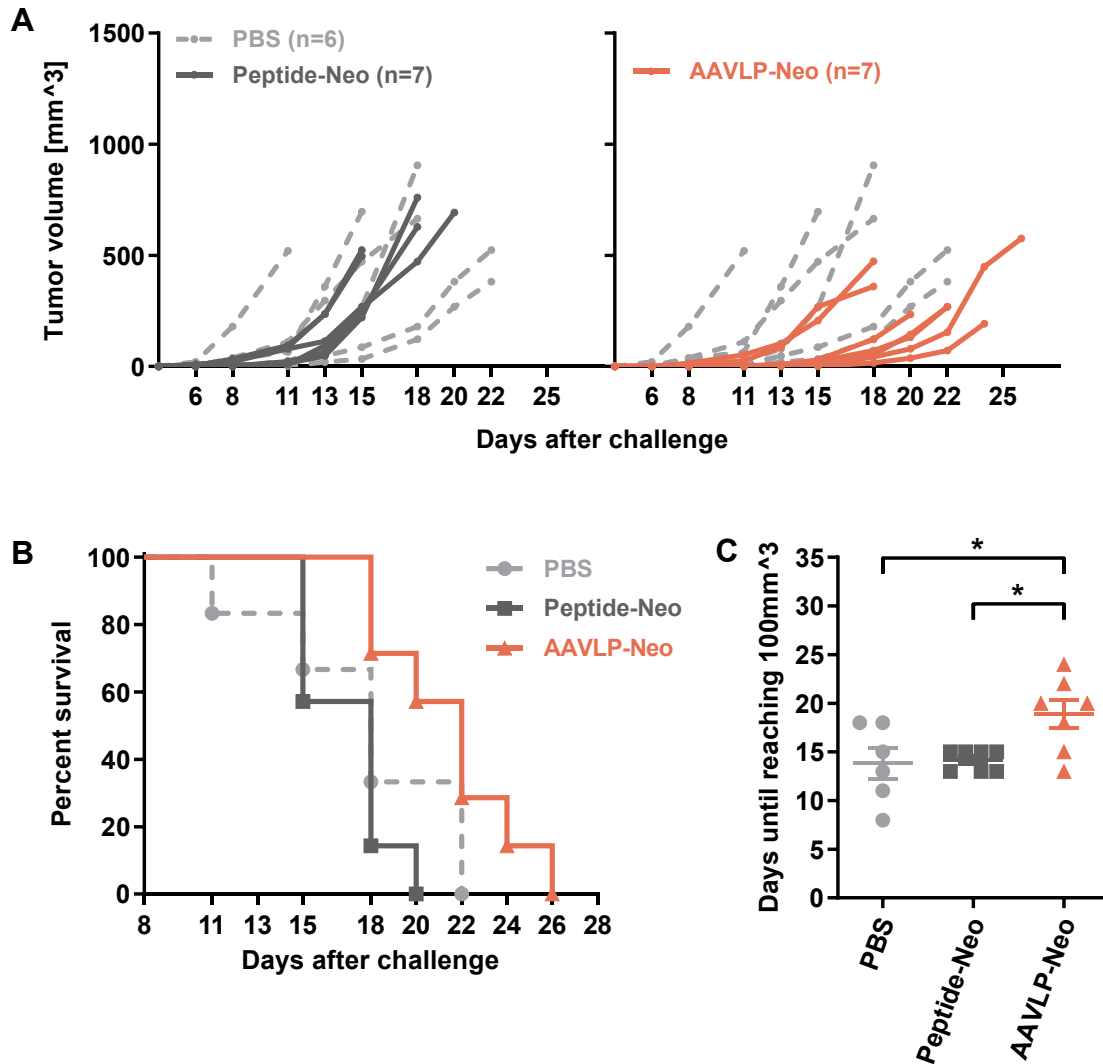


Figure 4.29: Vaccination with AAVLP-Neo reduces tumor growth rate after s.c. B16F10 challenge. C57BL/6 mice vaccinated with AAVLP-Neo or Peptide-Neo were challenged s.c. with B16F10 cells. PBS-injected mice served as negative-controls. **A)** Individual tumor growth curves in each mouse of the Peptide-Neo (left) and AAVLP-Neo (right) vaccinated group. For comparison, the growth curves of PBS-injected mice are shown as dashed, light-grey lines. **B)** Survival curves comparing AAVLP-Neo vaccinated mice to the control groups. The graph shows the percentage of live animals on each day after challenge. **C)** Comparison of tumor growth rates between the vaccine and control groups. The indicated values show the time after challenge until individual tumors reached a volume of 100mm^3 . Horizontal bars indicate the mean of each group with SEM. Significant differences between groups were determined using a One-way ANOVA with a Tukey's multiple comparison test. Asterisks indicate significant difference with * ($P \leq 0.05$).

4.8.5 Vaccination with AAVLP-Neo increases immune cell infiltration into tumor tissue

As the AAVLP-Neo vaccine showed an effect on tumor growth, the infiltration of immune cells into the tumor tissue was analyzed. B220+, CD3+, CD4+ and CD8+ cells within tumors were stained at the point of death and analyzed by flow cytometry. B220+ cells, which mark the B cell subset, were not distinctly increased after AAVLP-Neo vaccination compared to the control groups (*Figure 4.30*). On the other hand, CD4+, CD8+ and thus also CD3+ T cells in general, showed a tendency of elevated levels within the tumors of AAVLP-Neo vaccinated mice.

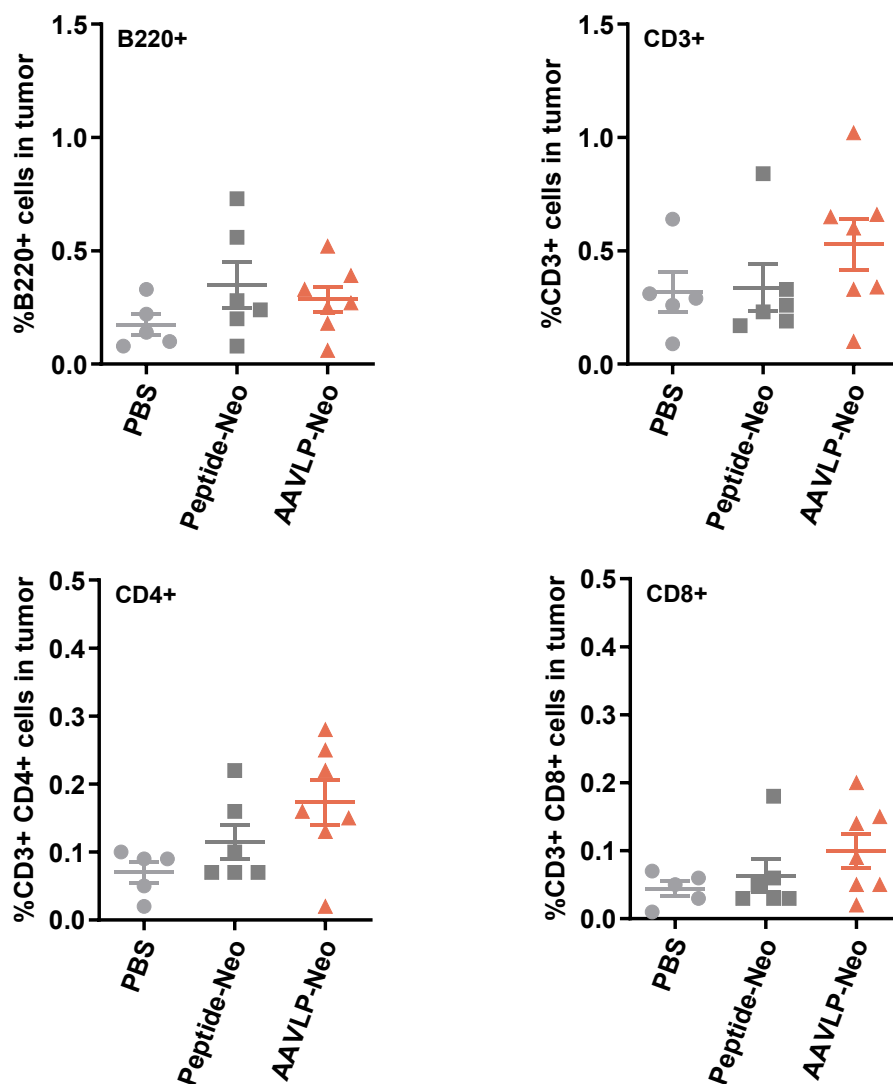


Figure 4.30: Tendency of increased immune cell infiltration into tumor tissue of AAVLP-Neo vaccinated mice.

C57BL/6 mice vaccinated with AAVLP-Neo or Peptide-Neo were challenged s.c. with B16F10 cells. PBS-injected mice served as negative-controls. At the point of death, tumor tissue was isolated, and dissected into a single-cell suspension. The presence of immune cells was analyzed by staining the cells with fluorescent-labeled antibodies for B220, CD3, CD4 and CD8. The graphs show the percent of respective cells in the tumor tissue. Horizontal bars indicate the mean of each group with SEM. Significant differences between groups were determined using a Kruskal-Wallis test with Dunn's multiple comparisons test. No significant differences were detected.

Considering the smaller tumor size at the point of death in AAVLP-Neo vaccinated mice compared to the other groups (*Appendix 7*), the observation could also be an unspecific effect due to the tumor size. A significant negative correlation between the tumor volume at the point of death and the rate of infiltrated immune cells was detected for CD4+ T cells and CD3+ T cells, while no significant correlation was observed for B220+ B cells or CD8+ T cells (*Figure 4.31*).

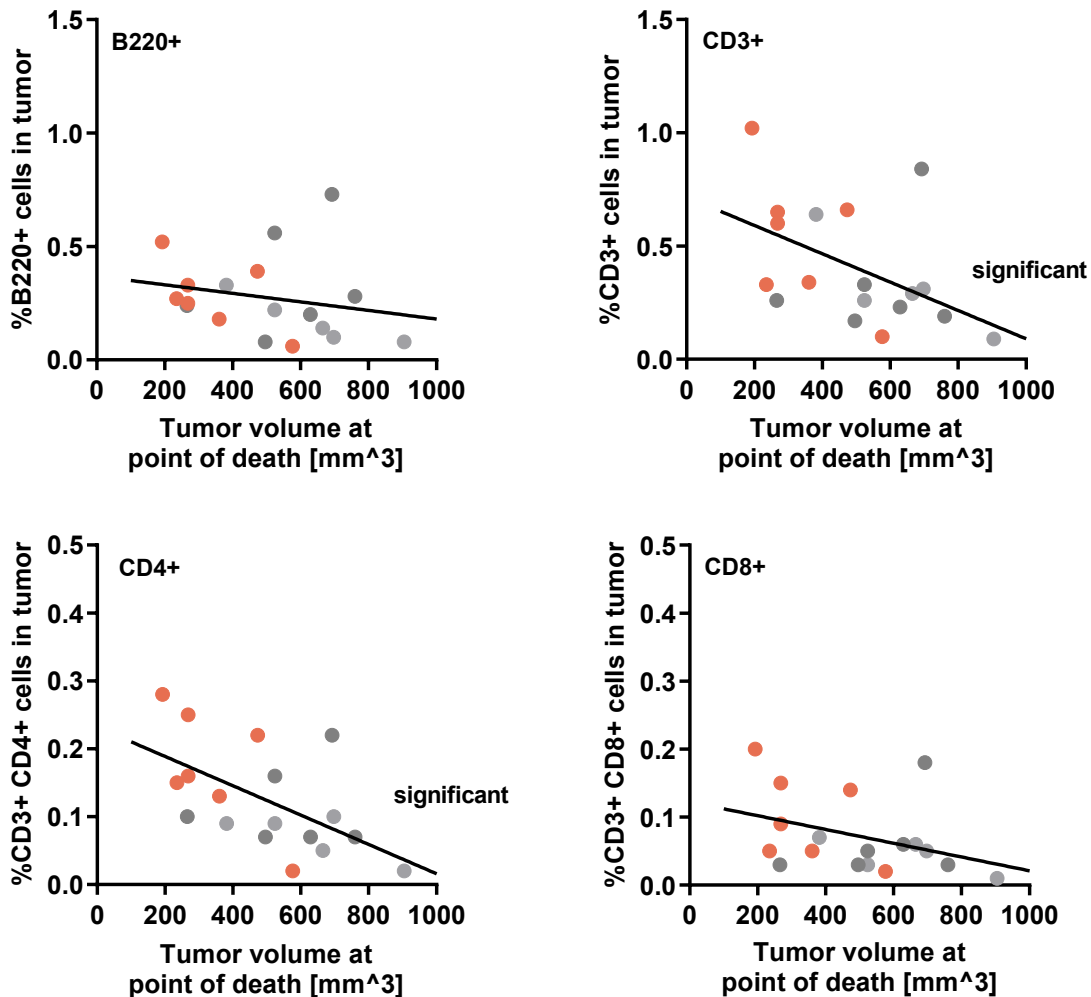


Figure 4.31: Negative correlation between tumor volume and rate of immune cell infiltration.

A correlation analysis between the tumor volume at point of death (*Appendix 7*) and the measured rate of infiltrated B220+, CD3+, CD4+ or CD8+ immune cells (*Figure 4.30*) is shown. Red dots are AAVLP-Neo vaccinated mice, dark grey dots are Peptide-Neo vaccinated mice and light grey dots are PBS-injected mice. Significance determined by linear regression using GraphPad Prims 8.0.2.

Taken together, the results in this chapter showed that despite undetectable neoantigen-specific CD8+ T cell responses, AAVLP-Neo had a reducing effect on tumor growth, which goes along with increased infiltration of T cells into the tumor tissue.

5 Discussion

The aim of this project was the development of a personalized vaccination strategy based on AAVLPs displaying cancer neoantigens. As AAVLPs were not yet well defined regarding the induction of CD8+ T cell responses in a vaccination approach, initial experiments were set up to define general properties of the vaccine. In the following chapters, results obtained with SIINFEKL and other peptides as model antigens will be discussed regarding the induction of immune responses in general (5.1), optimization of the vaccination strategy (5.2), mechanistic analysis (5.3) and targeting of neoantigens (5.4).

5.1 AAVLPs as a vaccine platform

The purpose of a vaccine is activation of humoral and/or cellular immune responses. Depending on the pathogen, either antibody or CTL responses against a target protein are required for protection.

A straightforward design is incorporation of whole proteins in the vaccine formulation, to achieve a universal response against multiple epitopes. Opposed to that, epitope-directed vaccines may include only minimal B cell or T cell epitopes. Both strategies have their advantages: While the whole-protein vaccine does not require prior identification of immunogenic epitopes, a risk remains of inducing immune responses against irrelevant epitopes or even cross-reactive responses against self-antigens. The epitope-directed vaccine requires prior identification of B cell or T cell epitopes, but responses are more focused. The focus on single epitopes is especially advantageous for a neoantigen vaccine, in which immune responses need to be directed towards a single mutation. In the current strategy, known or predicted immunogenic epitopes were displayed on AAVLPs and antigen-directed immune responses were analyzed regarding induction of I) CD8+ T cells, II) CD4+ T cells and III) antibodies.

I) CD8+ T cell responses:

Previous studies, in which SIINFEKL was displayed on AAV particles for the analysis of T cell responses, showed varying results from minor [112, 113] to high T cell levels [62]. These studies already indicated that general differences in the AAVLP design and vaccination

strategy, such as capsid-insertion site or route of injection, influence the induced immune responses. Accordingly, several factors were tested during this work and will be discussed in the chapters about the injection route and local concentration (5.2.1), external and internal adjuvants (5.2.2), AAVLP tropism (5.2.3), and prime-boost strategies (5.2.4).

The initial experiments conducted in this study revealed antigen-specific responses in the spleen and blood (4.2.1), which were strongest three weeks after vaccination and lasted for at least 10 weeks (4.2.2). Throughout the project, responses induced by the standard AAVLP-SIINFEKL vaccine (SIINFEKL in the VR-VIII loop) varied between experiments in a range of 0.1 % to 0.3 % antigen-specific T cells. As the effect of the vaccine on T cell responses was observed to be dose-dependent (4.2.1), differences between experiments might be explained by batch-to-batch titer variations of AAVLPs. Alternatively, impurities of AAVLP preparations could have affected the vaccine in a positive or negative way.

Compared to other vaccination studies [89, 112, 165, 169], the AAVLP vaccine-induced responses were rather low in this project, especially for a highly immunogenic epitope like SIINFEKL. A lack of assay sensitivity is unlikely, as both ICS and tetramer staining showed comparable results (4.2.1). Yet, the comparison between the two assays provided a first estimation of T cell quality. The ICS assay detects only functional T cells that are activated upon stimulation with the antigen, while the tetramer staining reveals all antigen-specific T cells, irrespective of their activation. Comparison of both assays, with similar results, indicates a high frequency of functional and active T cells, while excluding the presence of exhausted or anergic T cells [178]. Another evidence for the potency of vaccine-induced responses was provided by the protection of mice after challenge with an aggressive tumor model (4.2.9).

Typical CD8⁺ T cell responses after vaccinations or natural infections show a peak around 7-15 days. Subsequently, 90-95 % of the T cells die and a memory T cell subset remains [179]. Thus, CD8⁺ T cell responses induced by AAVLP-SIINFEKL, which were first detectable 2 weeks after vaccination and peaked around 3 weeks, emerged rather late. In contrast to that, previous studies of vaccination with SIINFEKL peptides [168] or alternatively designed AAVs [87, 180] showed that T cell responses had already been vanished after 3 weeks. An explanation for the late response to AAVLP-SIINFEKL could be a “trapping” effect by the Montanide ISA 51 adjuvant, which forms a depot [162] and potentially delays APC

encounter. Another explanation might be the later discussed requirement for CD4⁺ T cells (5.3) that need to be induced before CD8⁺ T cells are able to expand.

The period until immune responses are functional is relevant for tumor protection. In the experiments of B16F10-OVA challenge, the AAVLP-SIINFEKL model vaccine was only tested in a prophylactic but not therapeutic tumor setting (4.2.9). The reason for this decision was the rather late emergence of CD8⁺ T cell responses, which would unlikely have an effect on the rapidly growing tumors that lead to the death of mice within 3-4 weeks. A potential solution to this circumstance is the combination with additional treatment modalities. Thus, combination with checkpoint inhibitors could decelerate tumor progression and promote efficacy of the AAVLP vaccine in a therapeutic setting. In addition, the vaccine could be tested as an adjuvant after excision of primary tumors to prevent relapse and/or development of metastases.

The long-lasting T cell responses, which were even detectable 10 weeks following vaccination and were still functional to prevent tumor growth, are an indicator for a memory T cell subset. Alternatively, the long-lasting responses could be due to a prolonged persistence of antigens at the injection site that constantly induce T cell responses. After systemic injection of AAVs into mice, viral particles are detectable for several weeks to months [112, 116, 181], which is likely even extended after s.c. injection in the depot-forming Montanide ISA 51 [162]. However, a counter-argument to this explanation is that a locally persistent, excessive antigen source has been reported to cause exhaustion and apoptosis of CTLs [168, 182, 183]. As T cells were still activated by peptide stimulation in the ICS assay and the tumor protection was not affected even after 10 weeks, the presence of a profound memory response is more plausible than a likely exhausted CD8⁺ T cell subset. This should be further confirmed by analyzing memory T cell markers on the induced CD8⁺ T cells. In addition, analysis of tumor protection after an even longer time span would be of interest to confirm a potential life-long protection.

II) CD4⁺ T cell responses:

Not only CD8⁺ T cells but also CD4⁺ T cells could be the aim of a vaccination regimen. It has been shown that CD4⁺ T cells against neoantigens can have a substantial effect in the eradication of tumors [132, 184, 185]. If tumors are MHC class II positive, CD4⁺ T cells can have a direct cytotoxic effect on cancer cells [186, 187]. Also MHC class II-deficient tumors

benefit from activated CD4⁺ T cells, which promote an inflammatory microenvironment and interacting with different immune cells, such as cancer antigen-presenting DCs, B cells and CD8⁺ T cells [188]. Following activation of the immune system, further immune cells infiltrate to induce a potent CTL response and even initiate responses against vaccine-unrelated antigens [132]. In addition, cytokines like IFN- γ , which is released by CD4⁺ T cells, upregulate MHC class I on tumor cells and facilitate killing by CD8⁺ T cells [130].

In the current experiments, attempts to prime CD4⁺ T cells against an MHC class II-presented ovalbumin model antigen (OVAII) were unsuccessful (**4.6.2**). This was peculiar, as later experiments in this project (**4.5.1, 5.3**) but also results from previous studies [155, 189] showed a distinct CD4⁺ T cell response against capsid antigens. OVAII is a well-defined MHC class II-presented epitope in C57BL/6 mice and CD4⁺ T cell responses would have been expected [155, 189]. Thus, a potential explanation for the lack of specific CD4⁺ T cells can only be a deficiency in antigen processing due to AAVLP integration or an insufficient quantity of antigens. Yet, the presence of capsid-specific CD4⁺ T cells rejects any potential explanation.

Alternative strategies were tested to yield CD4⁺ T cells against the displayed antigen (**4.6.2**). OVAII was inserted at different sites of the AAVLP capsid, in order to alter the tropism of particles for a more efficient internalization into APCs (discussed in **5.2.3**). Although the location within a protein has been shown to be irrelevant for induction of CD4⁺ T cell responses [190], the differential effect of an alternative amino acid surrounding was additionally considered through this strategy. Yet, no benefit was observed by alternating the epitope insertion site and surrounding amino acids (**4.6.2**). Another attempt was the retention of AAVLPs in the acidic endosomal compartment where loading of extracellular antigens on MHC class II occurs [191]. This was achieved by an inactivating mutation in the PLA2 domain, which has been shown to be required for endosomal escape of AAV particles [51]. Yet again, this modification did not have a positive effect on the induction of OVAII-specific CD4⁺ T cell responses (**4.6.2**).

As no antigen-specific CD4⁺ T cells could be induced by AAVLP vaccination, the focus of the project remained on targeting CD8⁺ T cells.

III) Antibody responses:

The induction of antibodies against B cell epitopes presented on AAVLPs has been previously shown in several vaccination studies [91, 107, 108, 110, 111]. The results were confirmed in the current experiments by showing high antibody levels against OVAII after vaccination with respective AAVLPs (**4.6.1**). Yet, the induction of antibody responses was not the primary focus of this project. Tumors can be targeted by treatment with monoclonal antibodies [122, 123] but this strategy is not very well applicable to neoantigens. It would require mutated target proteins to be expressed on the cancer cell surface and accessibility of the mutations at the protein exterior. In addition, an antibody response specific for the mutation is difficult to generate. In the current experiments, AAVLP-induced antibodies against neoantigens did not only bind the mutated peptides but also the wt sequences (**4.8.3**), which generates a potential risk of autoimmune reactions.

A rational approach to target intracellular neoantigens would be the induction of antibodies against neoepitopes presented on MHC molecules [192-194]. However, such TCR-mimic antibodies are difficult to predict and produce, and would not be readily generated by displaying peptides on AAVLPs.

In conclusion, the experiments showed that AAVLPs are well suited to induce strong antibody responses against displayed epitopes. However, due to their minor relevance for a personalized vaccination strategy against neoantigens, antibody responses were not in the focus of this project.

5.2 Optimizing AAVLP vaccination

As the focus of the vaccine was set on the induction of CTLs, different strategies were tested to increase CD8+ T cell responses.

5.2.1 The effect of injection route and local concentration

The injection route of a vaccine is of importance as it determines successful encounter with APCs. VLP-based vaccines generally benefit from s.c. or i.m. injection routes. Due to their size between 20 and 200 nm, the particles efficiently enter the lymphatic system to reach draining lymph nodes [4, 6, 13, 14]. In addition, VLPs ingested by DCs and macrophages are actively transported to the lymphoid organs [6, 15]. This is in contrast to peptide vaccines,

which are rather lost in the blood circulation due to their smaller size and are removed by renal clearance before encountering APCs [195]. While peptide dispersion can be circumvented by administration in depot-forming adjuvants like incomplete Freund's adjuvant or Montanide ISA 51 [168, 183], AAVLPs are presumably still ingested more efficiently by APCs due to the greater size and viral resemblance [4, 15-17].

S.c. injection into the hock of mice was tested in initial experiments, as this route was reported to efficiently drain the local inguinal lymph nodes, while being less invasive than foot pad injection [151]. Despite no detectable antigen-specific T cells in the draining lymph nodes (**4.2.1**), s.c. injection of AAVLP-SIINFEKL into the hock induced reliable T cell responses and was defined as the standard injection route.

For an effective immune activation, vaccine particles do not only need to traffic to lymphoid organs but also have to be captured there. Otherwise, antigens are flushed through and eventually enter systemic circulation through the thoracic duct [196]. Thus, the absence of antigen-specific T cells in lymph nodes might be a consequence of deficient AAVLP homing to the lymphoid organs. Instead, the particles might have entered the blood circulation and reached the spleen, where antigen presentation occurred. In fact, the particles used for vaccination were shown to efficiently localize to the spleen upon systemic administration (**4.2.7**). The circumstance of AAVLP localization should be further tested by analyzing the presence of AAVLPs in the lymph nodes and blood a few hours to days after injection.

It was startling that CD8⁺ T cell responses were only observed after s.c. but not i.m. injection. Previous studies reported conflictive results after i.m. injection of AAVs, from profound [68] to undetectable [112] capsid-directed CTL responses. As the studies were performed in BALB/c mice and C57BL/6 mice, respectively, AAVs might have a different immunogenicity depending on the mouse strain. In another study, a genetic vaccine of ovalbumin-encoding AAV vectors was tested at different injection routes [86]. While strong ovalbumin-directed CTL responses were induced after s.c., i.v. and i.p. injection, only minor responses were detectable after i.m. injection, indicating general differences of AAV processing and immunogenicity for the different injection routes. Thus, different theories could explain the current observations: 1) A first explanation might be the higher blood supply in the muscle tissue compared to the s.c. space. Experiments during this project showed that a high local AAVLP concentration is essential for the induction of T cell responses (**4.2.4**). The increased blood circulation in combination with muscle contraction

might account for a more rapid dispersion of the vaccine. II) Another explanation could be the timing of T cell measurement. T cell kinetics showed a peak around 3 weeks after s.c. injection, which was subsequently defined as the readout time point. However, the T cell kinetics could be different after i.m. injection, so that responses induced at an earlier time point might be no longer detectable 3 weeks after vaccination. This is supported by a report in which capsid-specific T cell responses after i.m. vaccination peaked around one week and rapidly decreased thereafter [79, 180]. III) A third explanation for distinct efficacy of the two injection routes might be the general difference in immune competence. Thus, draining to proximal lymph nodes occurs more efficiently after s.c. injection than i.m. injection and the skin contains a more diverse set of APCs than the muscle tissue [197]. In the current experiments, s.c. injections were only compared to i.m. injections. Intravenous (i.v.) vaccinations were neglected, as a rapid clearance of the particles in the blood stream was expected due to the inability of tropism-modified particles to enter tissue cells (further discussed in **5.2.3**). Several studies showed efficient antigen presentation on DCs [62, 112, 113, 115, 116, 181] and induction of antigen-specific T cells [62] after i.v. injection of particles with intact HSPG-directed tissue tropism. On the other hand, alternative results showed that weaker capsid-specific T cell responses were observed after i.v. than i.m. injection of AAVLP particles [79]. Thus, in future experiments, alternative strategies should be considered next to the s.c. injection to confirm the best suited vaccination route. However, since s.c. vaccination into the hock yielded reliable results, this route was chosen as the standard in this project.

As mentioned before, not only the dose of the vaccine but also the local AAVLP concentration is of relevance. This was shown by the observation that a set dose of AAVLPs in one injection site ($5E+11$ capsids in $60 \mu\text{L}$) was more effective than the same dose distributed between two sites ($2 \times 2.5E+11$ capsids in $60 \mu\text{L}$) (**4.2.4**).

A single peptide-MHC complex suffices to induce CD8⁺ T cell responses [198] and one AAVLP particle alone, containing 60 antigens, would likely increase the capacity of T cell activation. Yet, the encounter of APCs with antigen-specific T cells is a stochastic effect, and the probability of interaction is significantly increased at higher antigen concentration. In addition, previous studies showed that a low amount of antigen might cause T cell anergy [199], indicating the importance of a certain antigen concentration.

Another factor that could explain the beneficial effect of high vaccine concentration is the local inflammatory response induced by AAVLPs. With more particles, a stronger innate immune activation through TLR2 [67] and TLR9 [68] is expected, which positively affects the adaptive responses.

While the exact mechanisms are unknown of how the concentration affects AAVLP trafficking and APC presentation, the results clearly show that the local dose of antigens can shape the T cell response.

5.2.2 Effects of external and internal adjuvants

Induction of strong and long-lasting T cell responses requires activation of the innate and adaptive immune system. To increase immune stimulation of vaccines, co-administration of adjuvants is often useful or even required [200]. The mode of action and the finally induced immune responses vary with the type of adjuvant. Common mechanisms include the formation of antigen depots for sustained release of antigens, generation of an inflammatory milieu, and activation of APCs [200]. Next to externally administered adjuvants, the vaccine itself can have internal adjuvancy. Most viral vectors are immune stimulatory on their own by activating innate immunity through PAMPs [201]. AAVLPs have a reported ability to activate innate responses via TLR2 [67] and TLR9 [68-70]. The latter detects unmethylated CpG DNA within AAVLP particles and activates innate immune responses [68-70, 113] via signaling through MyD88 and NF- κ B for the release of IFNs [68]. Rogers et al. suggested that AAV recognition via TLR9 occurs in plasmacytoid DCs (pDCs), which in turn activate conventional DCs (cDCs) for the cross-priming of capsid-specific CD8⁺ T cells [202]. The current experiments confirmed a partial importance of AAVLP-packaged DNA, as higher CD8⁺ T cell responses were observed by increasing the genomic content (4.2.6). Yet, even empty particles induced a certain level of CD8⁺ T cells, indicating that the AAVLP genome is only supporting but not required for the T cell responses.

In most of the experiments, only 1 in 16 AAVLPs contained a GFP gene flanked by ITRs. While a higher content of 1 genome per 10 AAVLPs increased the immune responses only marginally, an interesting and rational approach would be inclusion of specifically designed DNA with a high content of CpG motifs to further increase immune responses. This would be an opposite approach to previously published strategies, in which CpG-depleted AAVs were designed to circumvent immune responses during gene therapy [70, 113].

In the attempt to further boost immune responses, AAVLPs were administered in combination with different adjuvants. Montanide ISA 51 is a water-in-oil emulsion that does not only create an antigen depot, but also attracts immune cells and activates phagocytosis by APCs [162, 163]. CpG containing oligodeoxynucleotides (CpG ODNs) and c-di-AMP activate innate immune response by interaction with the TLR9 [162] and stimulator of interferon genes (STING) pathway [164] in APCs, respectively.

Depending on the antigen formulation, adjuvants are not always beneficial and can even have detrimental effects. Usually, a prolonged presentation of antigens is beneficial or even required for the induction of T cell responses [203]. Yet, depot formation by incomplete Freund's adjuvant have been reported to be disadvantages for peptide vaccines against cancer antigens. Immune cells are withdrawn from tumors and accumulate over a long time at the vaccine injection site, finally leading to exhaustion and apoptosis of T cells [168, 183]. Nevertheless, the current AAVLP-based vaccine profited from administration in Montanide ISA 51, and induction of CTL responses even depended on the adjuvant (**4.2.1, 4.2.5**). On the contrary, the two alternative adjuvants CpG ODNs and c-di-AMP had no effect on the induction of CD8⁺ T cell responses and even impaired responses in combination with Montanide ISA 51 (**4.2.5**). This observation was peculiar, as CpG DNA within AAVLPs showed a beneficial effect by activating the TLR9 pathway [68-70, 113, 202]. A similar observation has been reported before in the context of peptide and protein vaccines, as a combination of Montanide with CpG ODNs cancelled out the effect of each adjuvant alone [162, 204]. This was explained by a Th2 bias at the cost of Th1 responses, required for CD8⁺ T cell induction [162]. In addition, differences in the kinetics of CD8⁺ T cell responses could explain the negative effect of combining adjuvants. CpG ODNs and c-di-AMP might promote a faster but shorter response to the AAVLP delivered antigens, so that CD8⁺ T cells have been vanished already before the readout at 3 weeks after vaccination. This could be tested by analyzing the presence of antigen-specific T cells at earlier time points after vaccination.

In conclusion, Montanide ISA 51 proved to be an efficient adjuvant to the AAVLP vaccine. Yet, the repertoire of adjuvants is far from being exhausted [205] and alternatives should be considered as well for the vaccination strategy.

5.2.3 The role of AAVLP tropism and endosomal escape

Different sites in the AAVLP capsid tolerate peptide insertions without affecting viral assembly. Common insertion sites include the VR-IV loop, which is the highest peak spiking from the particle surface around aa453 [58], the second highest peak of the VR-VIII loop around aa588 [58-60] or the HI loop around aa660 [62, 180]. While insertions in the VR-IV loop or the HI loop do not affect the tropism of AAVs, insertions in the VR-VIII loop have a high probability of disrupting the HSPG binding site and thus the natural tropism [58-60]. As the *in vivo* localization and cell tropism of vaccine particles can have detrimental effects on induced immune responses, two different capsid insertion sites were compared for the AAVLP vaccine.

Most experiments in this project were conducted with antigen insertions in the VR-VIII loop (aa588). The rationale behind this decision was to prevent random entry and distribution into tissue cells and thus dilution of antigen concentration at the injection site. A higher amount of free antigen was expected to be beneficial for internalization by APCs, promoting efficient antigen presentation. However, a head-to-head comparison showed a clear advantage of retaining an intact tissue tropism by inserting the SIINFEKL antigen in the VR-IV loop (aa453) instead of the VR-VIII loop (aa588) (**4.2.7**). This is in line with other studies, in which the HSPG binding of AAVs was important for generation of capsid-directed T cells [85]. In these studies, AAVs with intact tropism were even able to induce capsid-specific responses after i.m. injection [85, 180], which was not observed in the current setting for tropism-modified AAVs. A possible effect might be the entry of AAVLPs into muscle cells, which are subsequently phagocytosed by APCs for cross-presentation of antigens on MHC class I.

One advantage of retaining cell entry via AAV's natural receptors is the following intracellular migration of AAVs. Thus, the endosomal/lysosomal escape and proteasomal degradation was shown to promote capsid antigen presentation in APCs [114, 116]. Exogenous antigens are usually cross-presented by DCs for the activation of CD8+ T cell responses. While a small fraction of antigens is loaded on MHC class I in acidic endosomes, the majority of antigens enters the cytosol for proteasomal degradation and transporter associated with antigen processing (TAP)-dependent MHC class I loading [51]. Endosomal escape of AAV particles likely promote cross-presentation by active transition into the cytosol for further processing [116]. This theory is promoted by the comparison of full and

empty capsids in the intracellular migration. The DNA content in AAVs is required for conformational changes of the particles in acidic endosomes [206], which lead to an externalization of VP1 and VP2 N-terminal tails through pore complexes in the capsid [207]. By revealing the N-terminal PLA2 domain, endosomal escape is facilitated by lipolytic pore formation [51]. While full AAV particles that reach the cytosol are presented via the cytosolic pathway, empty particles shift to an endocytic antigen presentation pathway with a different T cell kinetic [116]. As capsid-modified AAVs that are deficient in HSPG-binding can interact with non-natural receptors and enter cells via a different pathway than HSPG-binding AAVs [46], they may be unable to escape endosomes and are rather presented like empty particles. Thus, next to determining the target cell type, an altered tropism of AAVLPs presumably also affects processing of capsid antigens in the cytosol.

Not only is the entry into APCs of importance for successful antigen presentation but also the homing of particles to lymphoid organs, as discussed in the context of injection route (5.2.1). While AAVLPs that are phagocytosed at the vaccine injection site are transported to the draining lymph nodes within APCs, the particles alone can also be drained to the lymphoid organs via the lymphatic system. Particles of 50-100 nm are retained in lymph nodes due to their size alone [208]. Smaller particles, however, which are in the range of the 20 nm AAVLPs, have been shown to be cleared from the lymph nodes [196, 208], which is in accordance with absence of T cell responses in these organs (4.2.1). Thus, an intact tropism might be detrimental for retention and antigen-presentation in the lymphoid organs. Nevertheless, even particles that are potentially flushed into the systemic circulation are able to enter the spleen for induction of CD8⁺ T cell responses. This was shown by comparing the tissue tropism of HSPG-deficient and WT AAVLPs upon i.v. injection (4.2.7). While the natural liver tropism of WT AAVLPs was completely abolished, homing and retention in the spleen was not affected by HSPG-binding inability.

In conclusion, the tropism of AAVLPs is of high importance for antigen processing and presentation. Intact HSPG-binding positively affects immune responses induced by the AAVLP vaccine and should be considered in future vaccine trials.

5.2.4 Prime-boost strategies and pre-existing immune responses

By testing combinations of SIINFEKL-displaying AAVLPs of serotype 2 (AAVLP2) and serotype 5 (AAVLP5), different prime-boost strategies were evaluated. Simultaneously, the

effect of pre-existing immune responses was analyzed by vaccinating mice that were pre-immunized with wild type (wt) AAVLP2.

The repeated administration of vaccines is a common strategy to increase immune responses [92, 94, 95, 165, 166, 209, 210]. While a first vaccination primes the immune system, following vaccinations provide a boost and initiate expansion of already existing immune cells. Prime-boost strategies can be designed with a homologous boost, in which the same vaccine is administered repeatedly, or a heterologous boost in which different vaccine formulations, platforms or vectors against the same target antigen are administered at defined time points [211]. Especially in the case of homologous prime-boost strategies, there is a thin line between beneficial effects of increasing target immune responses and inhibiting effects through pre-existing vector immunity. For other VLP-based strategies, vector-directed immune responses that were induced during a prime did not affect repeated booster vaccinations [209, 210]. Yet, in the current experiments, there was a negative effect of AAV-directed immunity due to pre-immunization with wt AAVLPs (**4.2.8**). The observation that effects of pre-existing immune responses were less severe in mice primed with AAVLP2-SIINFEKL instead of wt AAVLPs, could be explained by lower capsid-directed immune responses. As AAVLP2-SIINFEKL had an altered tropism due to the antigen insertion, lower responses were expected, as discussed previously (**5.2.3**). Another explanation might be the originally intended boosting effect of the second AAVLP2-SIINFEKL vaccination that compensated for the negative effect of pre-existing capsid responses. However, as no considerable boosting effect was observed, the intended effect of a prime-boost strategy was not accomplished. Even the heterologous prime-boost of AAVLP2 followed by AAVLP5 did not improve the responses considerably, although effects of capsid-directed responses were apparently less severe (**4.2.8**).

Despite no success regarding a boosting strategy, the experiment gave insight into the importance of pre-existing immune responses for the AAVLP vaccine [86]. Since little is known about the actual mechanism of AAVLP antigen presentation and the involvement of different immune cells, it can only be speculated which aspects of the adaptive immune response played a role in the reduction of vaccine immunogenicity.

CTLs might affect antigen-presentation by removing AAVLP-containing cells. However, no capsid-directed CD8⁺ T cell responses were observed in the current experiments (tested by stimulating splenocytes of vaccinated mice with denatured AAVLP proteins; data not

shown). In addition, previous studies showed that CTLs induced by AAVs were unable to eradicate AAV-transduced cells in mice [75, 79, 80], which therefore unlikely have an effect on AAVLP antigen presentation.

AAVLP-binding antibodies could facilitate recognition and phagocytosis of the particles by cells expressing Fc receptors, such as macrophages or B cells [71, 212]. Usually this would increase immune activation and antigen presentation [16]. However, as Rogers et al. showed that the primary mechanism of capsid-specific T cell induction was mediated by antigen presentation on cDCs [202], increased internalization by other immune cells might be disadvantageous for AAVLP antigen presentation. In addition, neutralizing antibodies might cause removal of injected AAVLPs before even encountering APCs. Accordingly, depletion of B cells and thus antibodies during AAVLP-SIINFEKL vaccination improved the CD8+ T cell responses (4.4), as discussed later (5.3).

Responses induced after AAVLP-WT injection were described in here as pre-existing immune responses. Yet, a natural infection with AAVs would likely have a different characteristic, since co-infection with helper viruses shape the immune responses against the AAV capsid in an adjuvant-like manner [82]. The effect of pre-existing immune responses need to be considered carefully for vaccination attempts, as up to 80 % of the human population are seropositive for AAVs [73]. Every second human has antibodies against AAV serotype 2 alone [82]. A solution to circumvent pre-existing immune responses is the choice of alternative serotypes. Thus, AAVrh32.33, derived from rhesus macaques, has no neutralizing antibodies in the human population [73]. In addition, AAVrh32.33 contains a T cell activating domain [213], which makes it more immunogenic than other serotypes [101, 214] and a good candidate for future vaccination trials.

In conclusion, repeated administration of AAVLPs in a prime-boost strategy was not beneficial for CD8+ T cell expansion, most likely due to induction of capsid-directed antibody responses. However, it might be worth considering alternative vaccine platforms, based on peptides, RNA, DNA or other VLPs, for combination with AAVLPs in a prime-boost strategy.

5.2.5 Improvement strategies of AAVLP vaccines

Despite the induction of sufficient CD8+ T cell responses against SIINFEKL, additional improvement strategies of the AAVLP vaccine might be beneficial to target less

immunogenic antigens. Several strategies were approached during this project, such as co-display of the DC-stimulating peptide Hp91 [215, 216] on the capsid, linkage of immunostimulatory factors (e.g. CD40L [217, 218] or GM-CSF [217, 219]) to the N-terminal end of VP2 proteins [56] or to the capsid surface via SpyTag/SpyCatcher binding [220, 221], and a reported DC-targeting mutation S662V [222]. Unfortunately, these strategies had to be discontinued because modified AAVLPs were not producible or initial experiments showed no benefit. Two strategies promised technical feasibility, as well as potential benefit for the immunization, and were therefore tested for *in vivo* efficacy in mice: I) coupling of anti-CD40 to AAVLPs and II) co-display of the J-immune cell binding ligand (J-ICBL).

CD40 is a receptor on DCs and CD8+ T cells, which is stimulated by CD40L expressed on CD4+ T cells [223-225]. Activation of CD40 leads to upregulation of costimulatory receptors and cytokines essential for CD8+ T cell priming [223]. A requirement for CD40/CD40L signaling has also been shown for the induction of AAV capsid specific CD8+ T cell [180]. Thus, an improvement strategy for increased antigen presentation was targeting of AAVLPs to CD40-expressing DCs by displaying an anti-CD40 antibody on the capsid surface. Technically, this was achieved by attaching streptavidin-coupled antibodies to biotinylated AAVLPs containing a biotin-acceptor peptide (BAP) (**Figure 4.14**). Directing vaccine particles to CD40 has been shown to increase both B cell [226], as well as T cell responses [227], whereas the latter were of higher interest for the current AAVLP strategy. As the displayed anti-CD40 antibody had an agonistic effect on CD40, additional activation of DCs through this pathway was predicted. Additionally, the CD4+ T cell requirement in the induction of CD8+ T cells (discussed in **5.3**) can be substituted by agonistic CD40 antibodies [224, 225]. While similar strategies reported efficacy after coupling CD40L to antigens [217, 218], display of anti-CD40 on AAVLPs had no distinct effect on CD8+ T cell responses (**4.3.3**). A tendency of early increased CD8+ T cell responses was observed in the blood, but the effect did not last above one week after vaccination. The responses were also more likely accountable to general DC activation by anti-CD40 instead of an improved targeting, as AAVLPs administered with free (unbound) anti-CD40 showed even higher responses. A similar effect has been shown for a peptide vaccine adjuvanted with anti-CD40 antibodies, in which increased responses were observed early after vaccination but vanished shortly after [183]. The reason for failure of the CD40-targeting strategy can only be speculated.

Eventually, coupling of anti-CD40 was not efficient enough and not all AAVLPs displayed the antibody on their capsid surface. In addition, only the binding to target cells by anti-CD40-coupled AAVLPs was analyzed but not the internalization, which might be impeded due to structural changes of the AAV particle. Finally, a high amount of uncoupled anti-CD40 in the vaccine preparation might have blocked interaction of AAVLPs with DCs.

A side observation of the experiment was that biotinylated AAVLPs showed higher CD8⁺ T cell responses than unbiotinylated particles. A similar effect has been reported before, in which biotinylation of vaccine particles increased immune responses [167]. This was explained by a maturation of APC, causing MHC class II and CD40 upregulation [167]. APC maturation could also explain the current observations, as MHC class II upregulation might enhance CD4⁺ T cell help, while CD40 leads to increased DC activity. Further studies reported effects of biotin on immune cells, but these were rather induced by free biotin acting on metabolic processes [228, 229].

In general, the observed effect of biotin has to be evaluated with caution. In this specific experiment, biotinylated AAVLPs induced higher responses than unbiotinylated AAVLPs, but the two vaccines originated from different productions. Previous experiments showed that the level of CD8⁺ T cells varied between experiments and vaccine batches. The observed level of 0.2 % antigen-specific CD8⁺ T cells for biotinylated AAVLPs was also reached by unbiotinylated AAVLPs in other experiments. Thus, further experiments should be performed to confirm the theory.

In conclusion, the attempt to target AAVLPs to CD40 expressing DCs did not yield satisfying results. While co-administration of anti-CD40 or biotinylation of AAVLP particles might have minor effects on the priming of CD8⁺ T cells, both strategies are likely not suited to substantially increase immune responses.

A more successful approach was the co-display of an immune stimulatory peptide on the capsid surface. The J-immune cell binding ligand (J-ICBL) is a β -2-microglobulin-derived peptide used in a strategy called ligand epitope antigen presentation system (LEAPS) [160]. J-ICBL is coupled to an antigenic peptide [160, 230, 231] to induce immune responses against different targets [230, 232-235]. The effect of the immune stimulatory peptide is a maturation of DC precursors into IL12-producing DCs and activation of Th1 responses [172, 173]. As this could also benefit AAVLP vaccination, J-ICBL was inserted into the capsid

sequence, which co-displayed the target antigen SIINFEKL. The assumption was confirmed by the results, as the induced CD8⁺ T cell responses were the highest throughout the whole project.

J-ICBL originates from a β -2-microglobulin sequence that corresponds to the binding site of CD8 [160]. In addition to a direct activation of CD8⁺ T cells, an effect on CD8⁺ DCs is possible. CD8⁺ DCs are essential for cross-presentation of exogenous antigens [236] and interaction through J-ICBL could promote cross-presentation of AAVLPs.

Despite a beneficial effect, the additional inclusion of the J-ICBL peptide also generates further limits. Some AAVLPs are already difficult to produce in sufficient amounts if a single peptide is inserted into the capsid. A second insertion provides even more tension in the particle and restricts correct AAVLP assembly.

Despite a clear advantage of J-ICBL inclusion in the AAVLP vaccination strategy, little is known about the mechanistic effects in this context. Future experiments have to show the influence on different immune cells (DC maturation, T cell activation) and reveal the potential and limits of this strategy.

5.3 Role of helper T cells and B cells in AAVLP-induced CD8⁺ T cell responses

While the first parts of the project focused on the general induction and improvement of CD8⁺ T cell responses, this chapter includes a mechanistic analysis. More specifically, the roles of helper T cells and B cells in the promotion of CD8⁺ T cell responses were analyzed (*Figure 5.1*).

Usually, CD4⁺ T cell help is less essential for initial CD8⁺ T cell responses but rather important for CD8⁺ T cell memory [237, 238]. However, in the current experiments, but also previous studies [180, 214], a requirement for CD4⁺ T cells was detected in order to initiate a CD8⁺ T cell response against AAVLP antigens and protect mice after tumor challenge (**4.5.1**). This is a phenomenon also known from other vaccination strategies [169, 178, 223], in which the absence of CD4⁺ T cells prevented CD8⁺ T cell priming or caused dysfunctional CD8⁺ T cells.

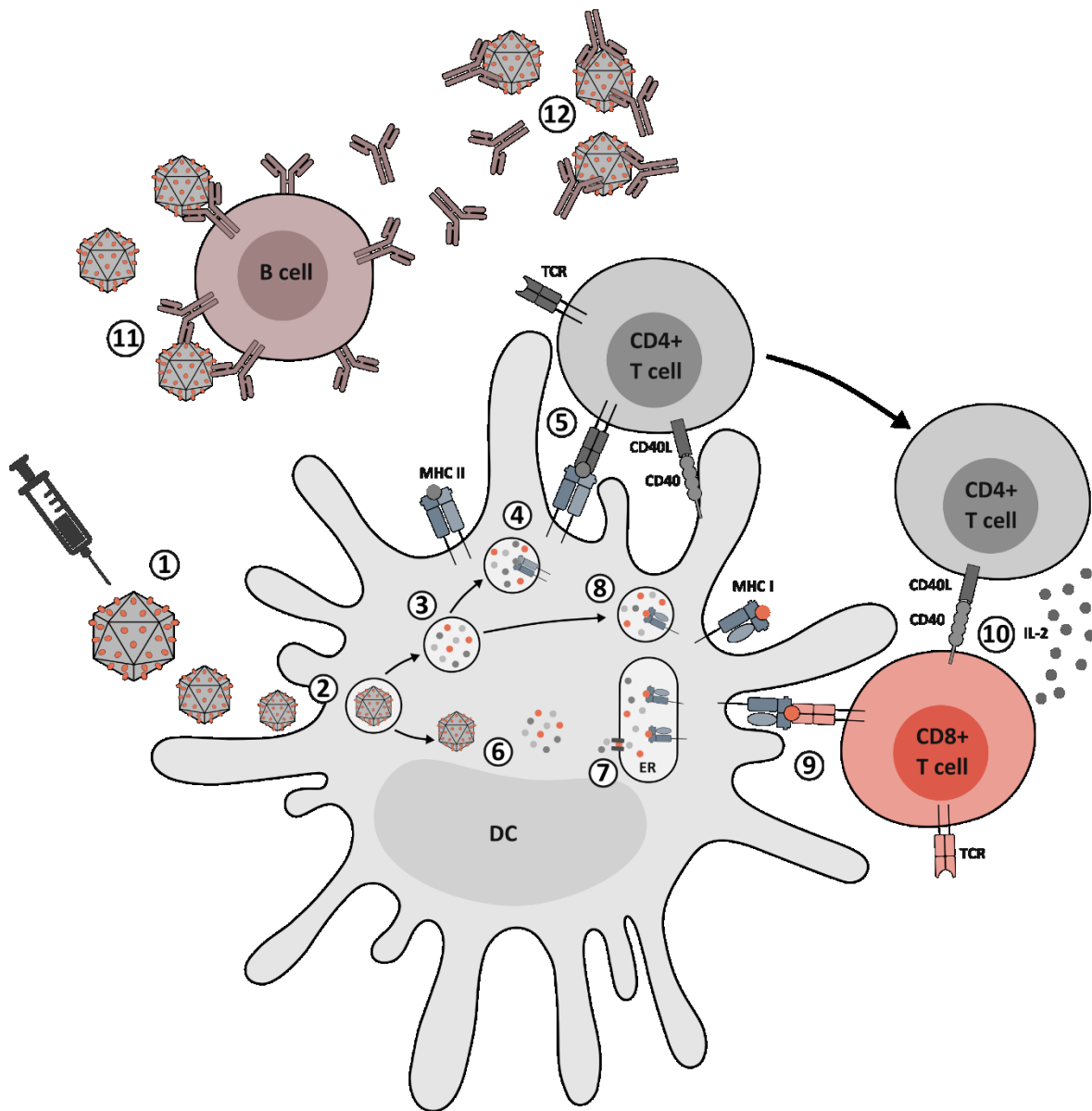


Figure 5.1: Model of AAVLP induced immune responses.

AAVLPs displaying an antigen epitope are injected (1) and ingested by APCs, presumably cDC (2). Endocytosis into the cells can occur via the natural tropism of AAVs or by undirected macropinocytosis. AAVLPs are retained and lysed in acidic endosomes (3). In the antigen-processing compartment, antigenic epitopes are loaded on MHC class II molecules (MHC II) (4), are presented on the cell surface and activate CD4+ T cells (5). CD4+ T cells in turn, activate the cDCs via CD40/CD40L signaling for cross-presentation of antigens on MHC class I. Alternatively, AAVLPs escape endosomes and are proteasomally degraded in the cytosol (6). Antigen peptides are transported into the endoplasmic reticulum (ER) via the transporter associated with antigen processing (TAP), where MHC class I loading takes place (7). In addition, AAVLP antigens degraded in endosomes can be loaded on MHC class I in late endosomes and lysosomes (8). MHC class I-presented antigens induce CD8+ T cells (9), which is promoted by activation signals, such as CD40/CD40L or IL-2, delivered by CD4+ T cells (10). In addition to T cell responses, AAVLPs encounter B cells and induce antibody production against the AAVLP capsid and displayed antigens (11). Antibodies binding to AAVLPs (12) inhibit antigen presentation and induction of CD8+ T cells via an unknown mechanism.

The CD4⁺ T cell-mediated help for CD8⁺ T cell priming and expansion is multifaceted and regulated on several levels. A common concept is that CD4⁺ T cells interact directly with both antigen-presenting cells, such as DCs, and CD8⁺ T cells. Thus, DCs that present a foreign antigen on MHC class II are recognized by helper T cells via the TCR. CD40L, expressed on CD4⁺ T cells, binds to CD40 on DCs and licenses them for increased antigen-presentation to CD8⁺ T cells [239]. Direct interaction between CD4⁺ and CD8⁺ T cells can also occur via CD40L/CD40 binding. In addition, cytokines like IL-2, released from helper T cells, provide survival signals to CD8⁺ T cells [239] (*Figure 5.1*).

In case of AAVs, Shirley et al. showed that cross-priming of CD8⁺ T cells required activation of cDCs through Type I IFN signaling and CD4⁺ T cell interaction [180]. More specifically, pDCs that were activated by innate immune mechanisms, such as TLR9-recognition of AAV genomes, released Type I IFNs and activated cDCs. In addition, co-stimulation by CD4⁺ T cells via CD40L/CD40 signaling was a requirement for priming of CD8⁺ T cells by cDCs [180]. The dependence on CD4⁺ T cells for CD8⁺ T cell activation suggested that AAVLP particles themselves contain helper epitopes. These would be presented on MHC class II and initiate CD4⁺ T cell-mediated DC licensing for priming of CD8⁺ T cell responses. In the current project, four CD4⁺ T cell epitopes in the AAVLP capsid sequence were identified for C57BL/6 mice. The observation that capsid-directed CD4⁺ T cell responses were stronger in AAVLP-WT than AAVLP-SIINFEKL vaccinated mice is likely ascribable to the intact tropism of AAVLP-WT, which is absent in AAVLP-SIINFEKL (discussed in **5.2.3**).

Helper epitopes have been identified before in the C3H mouse strain [240], but due to an alternative MHC haplotype, the epitopes differed from the ones detected in the current experiments. Nevertheless, the results confirmed general presence of helper epitopes in the AAV capsid. Further experiments can be performed to confirm the role of individual epitopes on the induction of CD8⁺ T cell responses, by inducing non-immunogenic mutations in single or multiple epitopes.

The presence of helper epitopes in the AAV capsid sequence has advantages for vaccine approaches. Peptide vaccines usually require fusion or addition of CD4⁺ T cell epitopes, in order to induce long-lasting CD8⁺ T cell responses. Since the CD4⁺ T cell help is included in the AAVLP sequence, minimal CD8⁺ T cell epitopes can be inserted without the need for additional helper epitopes.

Another possible application of the discovered helper epitopes lies in the field of gene therapy. If epitopes presented on common HLA molecules are identified, these could be silenced in AAV vectors to prevent capsid-induced immune responses and killing of transduced cells by CD8+ T cells [81].

In conclusion, the experiments showed that CD4+ T cells are essential for the induction of CD8+ T cell responses after AAVLP vaccination. The T helper epitopes in the AAVLP capsid represent an advantage for the vaccination strategy by generating CD4+ T cells that help priming target-specific CTLs.

The role of B cells in the induction of CD8+ T cell responses was analyzed by injection of depleting anti-CD20 antibodies. It was surprising that depletion of B cells improved immune responses (**4.4**). Usually, the presence of B cells as additional APCs should be beneficial for responses against pathogens and vaccines [241]. Furthermore, B cell-released antibodies promote antigen ingestion by APCs through interaction with Fc receptors [242, 243].

The negative effect of B cells on the AAVLP-induced CD8+ T cells was most likely a consequence of capsid-directed antibody responses. Neutralizing antibodies might have prevented antigen presentation, as observed for other VLP-based vaccines [244]. This would also be in accordance with the observed negative effect of pre-existing immune responses in a prime-boost strategy (**4.2.8**). The exact mechanism of inhibition is unknown, but bound antibodies might facilitate destruction of VLPs by opsonization, targeting to different protein processing pathways that prevent MHC class I presentation, or targeting to alternative cell types. Fitzpatrick et al. showed that binding of neutralizing antibodies (NAbs) alters the tropism of AAVs to mostly lymphoid organs [245]. This would initially be beneficial for a vaccination approach, but additional *in vitro* experiments showed that although cell entry was still functional, gene expression was defective in the presence of NAbs [245]. This shows that also intracellular trafficking of the particles is affected by bound antibodies. Thus, in the context of AAVLP vaccines, an altered antigen processing pathway could be unfavorable for CD8+ T cell induction.

The antibody responses were not entirely abrogated by anti-CD20 injection, and residual AAVLP-directed antibodies were even observed in B cell-depleted mice (**Appendix 5**). This was likely due to residual levels of B cells (up to 1 %) (**Appendix 5**). Therefore, the extent of capsid-antibodies might be a critical factor for AAVLP antigen presentation. While low

levels of antibodies could promote particle ingestion and presentation in APCs, high serum titers might cause rapid eradication of injected AAVLPs. This can be tested in mice that are passively immunized through injection of AAVLP-antibodies at different concentrations.

The acquired B cell data is in slight contrast to previous studies, in which no effect of B cells on AAV-induced T cell responses was observed [202]. Yet again, the results were generated in a different setting and HSPG-binding particles were injected i.m. at a higher dose, which might alter the outcome.

As very little is known about the antigen processing mechanisms of AAVLPs, future experiments need to uncover in detail how B cells and released antibodies affect the induction of CD8+ T cell responses.

5.4 Targeting neoantigens with AAVLP-based vaccines

The original aim of the project was to generate anti-tumor responses by targeting neoantigens with the AAVLP vaccine, which will be discussed in this chapter.

The AAVLP vaccine worked well in the SIINFEKL-expressing melanoma model (**4.2.9**). However, SIINFEKL is a rather insufficient model for tumor targeting, because the artificial antigen neglects the central tolerance observed for native tumor antigens [246]. Multiple immunogenic tumor-associated antigens have been described in mice [55, 168, 247-251], representing a more realistic tumor setting to test vaccination strategies. However, approaches with Trp2 [247] or endogenous retroviral antigens [55] failed, because vaccines were not producible upon antigen insertion into the AAVLP capsid (data not shown). Therefore, general feasibility of the vaccine was confirmed with viral antigens (**4.7**) and the vaccination strategy was immediately tested for neoantigen targets (**4.8**).

The first challenge in targeting neoantigens by vaccination is the choice of suitable antigens. Usually, the whole exome of a patient's tumor needs to be sequenced and compared to a healthy reference genome, in order to detect mutations [124, 130]. This step was cut short in the current project, as Castle et al. published mutations and potential neoantigens that are expressed in the B16F10 tumor cell line [131]. As the AAVLP vaccine was only able to induce targeted CD8+ T cell responses (tested for SIINFEKL and LCMV) but not CD4+ T cell responses (tested for OVAII), the selection of neoantigens was reduced to predicted MHC

class I presented epitopes. As discussed in a previous chapter (5.1), CD4+ T cells can be equally important as CD8+ T cells for targeting malignant cells [132, 184-188] and a majority of B16F10 neoantigens in previous studies were effective by inducing CD4+ T cell responses [132]. CD4+ T cells recognize their target antigen presented on APCs in the tumor vicinity. Stimulated CD4+ T cells induce an inflammatory microenvironment and activate DCs for presenting further cancer antigens [188], finally leading to antigen spreading [132]. Nevertheless, CD8+ T cells are essential for direct killing of tumor cells, and neoepitope-directed CD8+ T cells are a valuable tool in the containment of malignant cells.

A bottleneck in the vaccination strategy emerged as the majority of selected 21 amino acid-long neoepitopes disrupted particle assembly upon insertion into the AAVLP capsid (4.8.1). Consequently, the antigen selection was rather defined by inability to produce the vaccine rather than selecting antigens with a previously reported immunogenicity [131]. While three of the selected neoepitopes were predicted MHC class I binders, one neoantigen (Kif18b) was predictively not presented on MHC class I but was included in the experiment due to high efficacy as a peptide vaccine in the study by Castle et al. [131].

The AAVLP-Neo vaccine consisting of the four neoantigen-presenting AAVLPs induced partial tumor-protection in mice (4.8.4). The observed effect was unlikely induced by antibody responses, as peptide vaccinated mice showed similar or even higher responses against the epitopes (4.8.3) but no tumor protection. In general, targeting neoantigens with antibodies is difficult to achieve, as the mutated proteins are rather retained intracellularly or mutations are not accessible on the protein surface.

The anti-tumor effect was more likely induced by T cell responses. These were not detectable by intracellular staining of activation markers in stimulated splenocytes (4.8.2), but this could simply mark a limit of the detection method. Longer *in vitro* re-stimulation and expansion of T cells or more sensitive assays like the enzyme-linked immune absorbent spot (ELISPOT) assay might be required to detect neoantigen-specific T cells. Despite undetectable responses, a low level of T cells might have initiated a first response against the tumor cells and shaped an inflammatory microenvironment, leading to the observed immune cell infiltration into the tumor tissue (4.8.5).

Yet, the observed infiltration of T cells has to be evaluated with caution. Most mice were euthanized due to development of necrosis, rather than reaching the endpoint by tumor size. Based on this, all tumors analyzed for immune cell infiltration had different sizes, while

tumors in the AAVLP-Neo-vaccinated group were significantly smaller when developing necrotic wounds (*Appendix 7*). It is possible that the increased infiltration of T cells led to an earlier necrosis in small tumors due to cell lysis. Alternatively, a smaller tumor size and corresponding vascularization at the point of death could account for the higher rate of T cells detected in the tumor. In fact, a negative correlation has been observed (**4.8.5**), showing that with increasing tumor volumes the rate of infiltrated T cells decreased. However, an unspecific infiltration would affect all immune cell alike. Yet, the rate of B cells remained the same between groups, indicating that the increased T cell infiltration in the AAVLP-Neo group could indeed be a consequence of the vaccine.

An open question remains as to why no tumor protection was observed in peptide-vaccinated mice (**4.8.4**), although strong CD8+ T cell responses were observed against the Snx5 neoantigen (**4.8.2**). In a second experiment (data not shown), the peptide-based neoantigen vaccine even caused faster tumor progression in mice, which can be explained with an effect observed by Hailemichael et al.. Antigenic peptides that are locally persistent at the injection site due to a depot-forming adjuvant (in this case Montanide IS 51), caused accumulation of immune cells and distracted T cells from the tumor. In addition, the excessive, long-lasting antigen source caused exhaustion and apoptosis of CTLs [168, 183]. In theory, this should also be the case for the AAVLP vaccine, which likewise persists in Montanide ISA 51 at the injection site. Nevertheless, the lower antigen load compared to the peptide vaccine (~900 times lower), might have had a lesser effect on T cell exhaustion. Exhaustion of T cells [252] is only one of the difficulties in cancer immunotherapy, which needs to be considered when treating tumors by vaccination.

Several other factors are known by which cancer cells induce peripheral tolerance and escape immune surveillance [246], which is also relevant for the AAVLP vaccine.

Malignant cells can reduce antigen expression or lose MHC class I on the cell surface [253]. The outgrowth of neoantigen-loss variants can usually be compensated by including a higher number of antigens in the immunization regimen [130]. In addition, MHC class I downregulation is not necessarily a criterion for failure of the AAVLP vaccine. If tumors are removed by surgery, radiation or chemotherapy, remnants of dead tumor cells are presented on APCs. These attract vaccine-induced immune cells, which in turn cause a pro-inflammatory milieu [130]. In this scenario, the vaccine overcomes the immunosuppressive

environment, in which tumor cells release cytokines and chemokines to attract suppressive immune cells [254].

Further immunosuppression by cancer cells is mediated through expression of immune checkpoint molecules [118, 124, 130]. To circumvent immune cell inactivation by this mechanism, checkpoint inhibitors like anti-PD1, anti-PDL1 or anti-CTLA4 can be administered in addition and likely increase efficacy of the AAVLP vaccine.

An entirely different factor that needs to be considered for a vaccination strategy is the turnaround time from identifying mutations, over cloning AAV insertion plasmids, to the production of the virus in required amounts. Especially for a personalized strategy, timely delivery of the vaccine is crucial [130]. As the vaccine production could take several months, the most likely application would be a subsidiary therapy in combination with other strategies, like surgery or radiotherapy, to prevent recurrence and propagation of metastases.

In conclusion, cancer immunotherapy by vaccination is a complex field with many hurdles. The observed reduction in tumor growth by AAVLP vaccination is a first indicator for the potential of this vaccine. Nevertheless, the strategy needs to be further tested and improved to achieve sufficient anti-tumor efficacy.

5.5 Evaluation of AAVLPs as future (cancer) vaccine candidates

A successful vaccine is defined by I) efficacy to induce strong immune responses, II) safety for human administration, III) stability for storage/transport, and IV) a simple production.

I) In general, the AAVLP-based vaccine proved its potential to induce effective CD8⁺ T cell responses in a SIINFEKL and LCMV model system. CD4⁺ T cell epitopes within the AAVLP capsid are of advantage as they provide required help for induction of CD8⁺ T cell responses. Nevertheless, some restrictions were observed, as not all displayed antigens induced T cell responses. The final efficacy of the vaccine for cancer therapy is hard to estimate at the current stage, as further evaluation is required. In addition, restrictions of T cell induction can likely be solved in future experiments by testing alternative strategies for increased immune responses.

II) The safety of AAVLP administration in humans has already been proven in numerous clinical trials. The ultimate proof is the FDA-approval of two AAV formulations as gene therapy vectors [24]. Especially the non-pathogenic character and inability to replicate are compelling safety aspects.

III) AAVLPs are very stable and can be stored for several months at 4 °C or RT without considerably losing integrity [255]. Storage at -20 °C or -80 °C even prolongs the storage time up to several years. In addition, repeated freeze/thaw cycles have little effect on the stability of AAVLPs [255]. These aspects are of high advantage, if the vaccine needs to be transported from the production facility to the patient or if batches need to be stored for future re-immunizations.

IV) The simple and cost-effective production of AAVLPs is currently the greatest obstruction. In general, AAVs can be produced in large-scale at a good manufacturing practices (GMP) grade [256]. Yet, the current experiments showed that several epitope insertions into the capsid prevented formation of AAVLPs. Some insertions could be saved by different linker designs, but other inserts disrupted AAVLP formation entirely. For the 21 amino acid-long neoepitopes, only 30 % of the candidates yielded producible AAVLPs. This was significantly increased to around 80 % by choosing shorter sequences between 8 and 11 amino acids and might be a valid option for future vaccine designs. Another possible solution could be the alternative insertions site within the HI loop, which was not tested in this project. Recent research showed that in contrast to the VR-IV and VR-VIII loops, amino acids in the HI loop develop little interaction with other amino acids in assembled particles, which likely reduces the effect on particle formation [257].

Even if AAVLPs are readily producible, the production costs and turnaround time are factors that need to be considered. Calculations according to Nair et al. [258] for conversion of the currently tested mouse dosage to humans (60 kg) resulted in an approximate dose of 1.0-1.5E+14 capsids per AAVLP. Total costs of such treatments are currently difficult to estimate and depend on multiple factors. In the end, the price should not play a role if cancer patients can be successfully treated with a vaccine. Nevertheless, the costs and benefits should be carefully compared to other technologies, like RNA-based vaccines, which are currently easier and more flexible to produce and might show similar anti-tumor efficacy.

5.6 Outlook

This project tested only a fraction of parameters influencing AAVLP vaccination, and the improvement strategies are nearly endless. With different combinations of adjuvants, injection routes, vaccination regimens and dosages, the vaccine can be fine adjusted to application in mice, while it is questionable whether these also apply to humans. Nevertheless, acquired results provide suggestions for following experiments to improve the AAVLP vaccination strategy on a general level.

A stronger focus should be set on the capsid insertion site. Specifically, insertion into the VR-IV loop (aa453) and the HI loop, which retain a natural tropism, should be considered for thorough testing of vaccine efficacy and mechanistic effects.

Another feature, which should most certainly be evaluated for the vaccine, is inclusion of internal adjuvants. Thus, packaging CpG DNA within AAVLPs has a potential to significantly increase T cell responses.

Finally, alternative serotypes need to be considered for future vaccines. The literature showed clear differences between serotypes concerning the extent of induced immune responses. A promising candidate in this respect is the AAVrh32.33 with no seroprevalence in the human population and an internal T cell activating domain.

Next to modifications of the vaccine platform, potential targets should be revised for general tests. Some antigen targets failed in the current project, due to non-producible AAVLPs after antigen-insertion in the VR-IV or VR-VIII loop. Additional tumor model antigens should be tested for a proof-of-concept, such as common epitopes derived from pMEL17/gp100 [168, 248], heparanase [249], tyrosinase [250] or survivin [251].

CD8+ T cell responses were not induced reliably for all displayed antigens. If this circumstance cannot be resolved by changing previously suggested parameters of the vaccination strategy, a fundamental change of the vaccine might be required to develop a personalized vaccine. Packaging of neoantigen-expressing DNA in AAVLPs as a genetic vaccine could solve the problem of non-producible particles and has the potential to induce strong immune responses [86-106].

6 Conclusion

To conclude this work, the vaccination strategy showed partial efficacy against tumor growth by targeting neoantigens, fulfilling the aim of this project. Although further experiments need to be conducted for validation and improvement of the approach, neoantigen-displaying AAVLPs could be an alternative for current therapies and a potential candidate for future clinical applications.

7 References

1. abm. *Adeno-Associated Virus — An Introduction*. [cited 2021 21.03.2021]; Available from: https://old.abmgood.com/marketing/knowledge_base/Adeno_Associated_Virus_Introduction.php.
2. Jenner, E., *History of the Inoculation of the Cow-Pox: Further Observations on the Variolæ Vaccinæ, or Cow-Pox*. *Med Phys J*, 1799. **1**(4): p. 313-318.
3. Plotkin, S., *History of vaccination*. *Proc Natl Acad Sci U S A*, 2014. **111**(34): p. 12283-7.
4. Mohsen, M.O., et al., *Major findings and recent advances in virus-like particle (VLP)-based vaccines*. *Semin Immunol*, 2017. **34**: p. 123-132.
5. Chackerian, B., *Virus-like particles: flexible platforms for vaccine development*. *Expert Rev Vaccines*, 2007. **6**(3): p. 381-90.
6. Bachmann, M.F. and G.T. Jennings, *Vaccine delivery: a matter of size, geometry, kinetics and molecular patterns*. *Nat Rev Immunol*, 2010. **10**(11): p. 787-96.
7. Zhang, L.F., et al., *HPV6b virus like particles are potent immunogens without adjuvant in man*. *Vaccine*, 2000. **18**(11-12): p. 1051-8.
8. Greenstone, H.L., et al., *Chimeric papillomavirus virus-like particles elicit antitumor immunity against the E7 oncoprotein in an HPV16 tumor model*. *Proc Natl Acad Sci U S A*, 1998. **95**(4): p. 1800-5.
9. Sedlik, C., et al., *Recombinant parvovirus-like particles as an antigen carrier: a novel nonreplicative exogenous antigen to elicit protective antiviral cytotoxic T cells*. *Proc Natl Acad Sci U S A*, 1997. **94**(14): p. 7503-8.
10. Jegerlehner, A., et al., *Regulation of IgG antibody responses by epitope density and CD21-mediated costimulation*. *Eur J Immunol*, 2002. **32**(11): p. 3305-14.
11. Bachmann, M.F., et al., *The influence of antigen organization on B cell responsiveness*. *Science*, 1993. **262**(5138): p. 1448-51.
12. Fehr, T., et al., *T cell-independent type I antibody response against B cell epitopes expressed repetitively on recombinant virus particles*. *Proc Natl Acad Sci U S A*, 1998. **95**(16): p. 9477-81.
13. Oussoren, C., et al., *Lymphatic uptake and biodistribution of liposomes after subcutaneous injection. II. Influence of liposomal size, lipid composition and lipid dose*. *Biochim Biophys Acta*, 1997. **1328**(2): p. 261-72.
14. Supersaxo, A., W.R. Hein, and H. Steffen, *Effect of molecular weight on the lymphatic absorption of water-soluble compounds following subcutaneous administration*. *Pharm Res*, 1990. **7**(2): p. 167-9.
15. Bachmann, M.F., et al., *Dendritic cells process exogenous viral proteins and virus-like particles for class I presentation to CD8+ cytotoxic T lymphocytes*. *Eur J Immunol*, 1996. **26**(11): p. 2595-600.
16. Kovacsics-Bankowski, M., et al., *Efficient major histocompatibility complex class I presentation of exogenous antigen upon phagocytosis by macrophages*. *Proc Natl Acad Sci U S A*, 1993. **90**(11): p. 4942-6.
17. Fifis, T., et al., *Size-dependent immunogenicity: therapeutic and protective properties of nano-vaccines against tumors*. *J Immunol*, 2004. **173**(5): p. 3148-54.
18. Mohsen, M.O., et al., *Delivering adjuvants and antigens in separate nanoparticles eliminates the need of physical linkage for effective vaccination*. *J Control Release*, 2017. **251**: p. 92-100.

19. Daya, S. and K.I. Berns, *Gene therapy using adeno-associated virus vectors*. Clin Microbiol Rev, 2008. **21**(4): p. 583-93.
20. Lugin, M.L., R.T. Lee, and Y.J. Kwon, *Synthetically Engineered Adeno-Associated Virus for Efficient, Safe, and Versatile Gene Therapy Applications*. ACS Nano, 2020. **14**(11): p. 14262-14283.
21. Atchison, R.W., B.C. Casto, and W.M. Hammon, *ADENOVIRUS-ASSOCIATED DEFECTIVE VIRUS PARTICLES*. Science, 1965. **149**(3685): p. 754-6.
22. Hoggan, M.D., N.R. Blacklow, and W.P. Rowe, *Studies of small DNA viruses found in various adenovirus preparations: physical, biological, and immunological characteristics*. Proc Natl Acad Sci U S A, 1966. **55**(6): p. 1467-74.
23. Hermonat, P.L. and N. Muzyczka, *Use of adeno-associated virus as a mammalian DNA cloning vector: transduction of neomycin resistance into mammalian tissue culture cells*. Proc Natl Acad Sci U S A, 1984. **81**(20): p. 6466-70.
24. *Voretigene neparvovec-rzyl (Luxturna) for inherited retinal dystrophy*. Med Lett Drugs Ther, 2018. **60**(1543): p. 53-55.
25. Srivastava, A., E.W. Lusby, and K.I. Berns, *Nucleotide sequence and organization of the adeno-associated virus 2 genome*. J Virol, 1983. **45**(2): p. 555-64.
26. Mendelson, E., J.P. Trempe, and B.J. Carter, *Identification of the trans-acting Rep proteins of adeno-associated virus by antibodies to a synthetic oligopeptide*. J Virol, 1986. **60**(3): p. 823-32.
27. Hölscher, C., J.A. Kleinschmidt, and A. Bürkle, *High-level expression of adeno-associated virus (AAV) Rep78 or Rep68 protein is sufficient for infectious-particle formation by a rep-negative AAV mutant*. J Virol, 1995. **69**(11): p. 6880-5.
28. Chejanovsky, N. and B.J. Carter, *Mutagenesis of an AUG codon in the adeno-associated virus rep gene: effects on viral DNA replication*. Virology, 1989. **173**(1): p. 120-8.
29. Johnson, F.B., H.L. Ozer, and M.D. Hoggan, *Structural proteins of adenovirus-associated virus type 3*. J Virol, 1971. **8**(6): p. 860-63.
30. Janik, J.E., M.M. Huston, and J.A. Rose, *Adeno-associated virus proteins: origin of the capsid components*. J Virol, 1984. **52**(2): p. 591-7.
31. Becerra, S.P., et al., *Synthesis of adeno-associated virus structural proteins requires both alternative mRNA splicing and alternative initiations from a single transcript*. J Virol, 1988. **62**(8): p. 2745-54.
32. Sonntag, F., K. Schmidt, and J.A. Kleinschmidt, *A viral assembly factor promotes AAV2 capsid formation in the nucleolus*. Proc Natl Acad Sci U S A, 2010. **107**(22): p. 10220-5.
33. Xie, Q., et al., *The atomic structure of adeno-associated virus (AAV-2), a vector for human gene therapy*. Proc Natl Acad Sci U S A, 2002. **99**(16): p. 10405-10.
34. Gao, G., et al., *Adeno-associated viruses undergo substantial evolution in primates during natural infections*. Proc Natl Acad Sci U S A, 2003. **100**(10): p. 6081-6.
35. Gao, G., et al., *Clades of Adeno-associated viruses are widely disseminated in human tissues*. J Virol, 2004. **78**(12): p. 6381-8.
36. Summerford, C. and R.J. Samulski, *Membrane-associated heparan sulfate proteoglycan is a receptor for adeno-associated virus type 2 virions*. J Virol, 1998. **72**(2): p. 1438-45.
37. Qing, K., et al., *Human fibroblast growth factor receptor 1 is a co-receptor for infection by adeno-associated virus 2*. Nat Med, 1999. **5**(1): p. 71-7.

38. Summerford, C., J.S. Bartlett, and R.J. Samulski, *AlphaVbeta5 integrin: a co-receptor for adeno-associated virus type 2 infection*. Nat Med, 1999. **5**(1): p. 78-82.
39. Kashiwakura, Y., et al., *Hepatocyte growth factor receptor is a coreceptor for adeno-associated virus type 2 infection*. J Virol, 2005. **79**(1): p. 609-14.
40. Asokan, A., et al., *Adeno-associated virus type 2 contains an integrin alpha5beta1 binding domain essential for viral cell entry*. J Virol, 2006. **80**(18): p. 8961-9.
41. Akache, B., et al., *The 37/67-kilodalton laminin receptor is a receptor for adeno-associated virus serotypes 8, 2, 3, and 9*. J Virol, 2006. **80**(19): p. 9831-6.
42. Kurzeder, C., et al., *CD9 promotes adeno-associated virus type 2 infection of mammary carcinoma cells with low cell surface expression of heparan sulphate proteoglycans*. Int J Mol Med, 2007. **19**(2): p. 325-33.
43. Pillay, S., et al., *An essential receptor for adeno-associated virus infection*. Nature, 2016. **530**(7588): p. 108-12.
44. Duan, D., et al., *Dynamin is required for recombinant adeno-associated virus type 2 infection*. J Virol, 1999. **73**(12): p. 10371-6.
45. Bartlett, J.S., R. Wilcher, and R.J. Samulski, *Infectious entry pathway of adeno-associated virus and adeno-associated virus vectors*. J Virol, 2000. **74**(6): p. 2777-85.
46. Uhrig, S., et al., *Successful target cell transduction of capsid-engineered rAAV vectors requires clathrin-dependent endocytosis*. Gene Ther, 2012. **19**(2): p. 210-8.
47. Sanlioglu, S., et al., *Endocytosis and nuclear trafficking of adeno-associated virus type 2 are controlled by rac1 and phosphatidylinositol-3 kinase activation*. J Virol, 2000. **74**(19): p. 9184-96.
48. Nonnenmacher, M. and T. Weber, *Adeno-associated virus 2 infection requires endocytosis through the CLIC/GEEC pathway*. Cell Host Microbe, 2011. **10**(6): p. 563-76.
49. Douar, A.M., et al., *Intracellular trafficking of adeno-associated virus vectors: routing to the late endosomal compartment and proteasome degradation*. J Virol, 2001. **75**(4): p. 1824-33.
50. Nonnenmacher, M.E., et al., *Syntaxin 5-dependent retrograde transport to the trans-Golgi network is required for adeno-associated virus transduction*. J Virol, 2015. **89**(3): p. 1673-87.
51. Stahnke, S., et al., *Intrinsic phospholipase A2 activity of adeno-associated virus is involved in endosomal escape of incoming particles*. Virology, 2011. **409**(1): p. 77-83.
52. Samulski, R.J., et al., *Cloning of adeno-associated virus into pBR322: rescue of intact virus from the recombinant plasmid in human cells*. Proc Natl Acad Sci U S A, 1982. **79**(6): p. 2077-81.
53. Tratschin, J.D., et al., *A human parvovirus, adeno-associated virus, as a eucaryotic vector: transient expression and encapsidation of the procaryotic gene for chloramphenicol acetyltransferase*. Mol Cell Biol, 1984. **4**(10): p. 2072-81.
54. Xiao, X., J. Li, and R.J. Samulski, *Production of high-titer recombinant adeno-associated virus vectors in the absence of helper adenovirus*. J Virol, 1998. **72**(3): p. 2224-32.
55. Yang, J.C. and D. Perry-Lalley, *The envelope protein of an endogenous murine retrovirus is a tumor-associated T-cell antigen for multiple murine tumors*. J Immunother, 2000. **23**(2): p. 177-83.

56. Warrington, K.H., Jr., et al., *Adeno-associated virus type 2 VP2 capsid protein is nonessential and can tolerate large peptide insertions at its N terminus*. J Virol, 2004. **78**(12): p. 6595-609.
57. Girod, A., et al., *Genetic capsid modifications allow efficient re-targeting of adeno-associated virus type 2*. Nat Med, 1999. **5**(9): p. 1052-6.
58. Naumer, M., et al., *Development and validation of novel AAV2 random libraries displaying peptides of diverse lengths and at diverse capsid positions*. Hum Gene Ther, 2012. **23**(5): p. 492-507.
59. Müller, O.J., et al., *Random peptide libraries displayed on adeno-associated virus to select for targeted gene therapy vectors*. Nat Biotechnol, 2003. **21**(9): p. 1040-6.
60. Shi, X., et al., *Insertional mutagenesis at positions 520 and 584 of adeno-associated virus type 2 (AAV2) capsid gene and generation of AAV2 vectors with eliminated heparin-binding ability and introduced novel tropism*. Hum Gene Ther, 2006. **17**(3): p. 353-61.
61. DiPrimio, N., et al., *Surface loop dynamics in adeno-associated virus capsid assembly*. J Virol, 2008. **82**(11): p. 5178-89.
62. Li, C., et al., *Cytotoxic-T-lymphocyte-mediated elimination of target cells transduced with engineered adeno-associated virus type 2 vector in vivo*. J Virol, 2009. **83**(13): p. 6817-24.
63. Büning, H. and A. Srivastava, *Capsid Modifications for Targeting and Improving the Efficacy of AAV Vectors*. Mol Ther Methods Clin Dev, 2019. **12**: p. 248-265.
64. Perabo, L., et al., *In vitro selection of viral vectors with modified tropism: the adeno-associated virus display*. Mol Ther, 2003. **8**(1): p. 151-7.
65. Zaiss, A.K., et al., *Differential activation of innate immune responses by adenovirus and adeno-associated virus vectors*. J Virol, 2002. **76**(9): p. 4580-90.
66. Kawai, T. and S. Akira, *The role of pattern-recognition receptors in innate immunity: update on Toll-like receptors*. Nat Immunol, 2010. **11**(5): p. 373-84.
67. Hösel, M., et al., *Toll-like receptor 2-mediated innate immune response in human nonparenchymal liver cells toward adeno-associated viral vectors*. Hepatology, 2012. **55**(1): p. 287-97.
68. Zhu, J., X. Huang, and Y. Yang, *The TLR9-MyD88 pathway is critical for adaptive immune responses to adeno-associated virus gene therapy vectors in mice*. J Clin Invest, 2009. **119**(8): p. 2388-98.
69. Martino, A.T., et al., *The genome of self-complementary adeno-associated viral vectors increases Toll-like receptor 9-dependent innate immune responses in the liver*. Blood, 2011. **117**(24): p. 6459-68.
70. Faust, S.M., et al., *CpG-depleted adeno-associated virus vectors evade immune detection*. J Clin Invest, 2013. **123**(7): p. 2994-3001.
71. Zaiss, A.K., et al., *Complement is an essential component of the immune response to adeno-associated virus vectors*. J Virol, 2008. **82**(6): p. 2727-40.
72. Blacklow, N.R., M.D. Hoggan, and W.P. Rowe, *Serologic evidence for human infection with adenovirus-associated viruses*. J Natl Cancer Inst, 1968. **40**(2): p. 319-27.
73. Calcedo, R., et al., *Worldwide epidemiology of neutralizing antibodies to adeno-associated viruses*. J Infect Dis, 2009. **199**(3): p. 381-90.
74. Boutin, S., et al., *Prevalence of serum IgG and neutralizing factors against adeno-associated virus (AAV) types 1, 2, 5, 6, 8, and 9 in the healthy population:*

- implications for gene therapy using AAV vectors.* Hum Gene Ther, 2010. **21**(6): p. 704-12.
75. Siders, W.M., et al., *Cytotoxic T lymphocyte responses to transgene product, not adeno-associated viral capsid protein, limit transgene expression in mice.* Hum Gene Ther, 2009. **20**(1): p. 11-20.
76. Flotte, T.R., et al., *Phase 2 clinical trial of a recombinant adeno-associated viral vector expressing α 1-antitrypsin: interim results.* Hum Gene Ther, 2011. **22**(10): p. 1239-47.
77. Ferreira, V., et al., *Immune responses to intramuscular administration of alipogene tiparvovec (AAV1-LPL(S447X)) in a phase II clinical trial of lipoprotein lipase deficiency gene therapy.* Hum Gene Ther, 2014. **25**(3): p. 180-8.
78. Sabatino, D.E., et al., *Identification of mouse AAV capsid-specific CD8+ T cell epitopes.* Mol Ther, 2005. **12**(6): p. 1023-33.
79. Wang, L., et al., *Cross-presentation of adeno-associated virus serotype 2 capsids activates cytotoxic T cells but does not render hepatocytes effective cytolytic targets.* Hum Gene Ther, 2007. **18**(3): p. 185-94.
80. Li, H., et al., *Pre-existing AAV capsid-specific CD8+ T cells are unable to eliminate AAV-transduced hepatocytes.* Mol Ther, 2007. **15**(4): p. 792-800.
81. Manno, C.S., et al., *Successful transduction of liver in hemophilia by AAV-Factor IX and limitations imposed by the host immune response.* Nat Med, 2006. **12**(3): p. 342-7.
82. Mingozzi, F., et al., *CD8(+) T-cell responses to adeno-associated virus capsid in humans.* Nat Med, 2007. **13**(4): p. 419-22.
83. Pien, G.C., et al., *Capsid antigen presentation flags human hepatocytes for destruction after transduction by adeno-associated viral vectors.* J Clin Invest, 2009. **119**(6): p. 1688-95.
84. Lu, Y. and S. Song, *Distinct immune responses to transgene products from rAAV1 and rAAV8 vectors.* Proc Natl Acad Sci U S A, 2009. **106**(40): p. 17158-62.
85. Vandenberghe, L.H., et al., *Heparin binding directs activation of T cells against adeno-associated virus serotype 2 capsid.* Nat Med, 2006. **12**(8): p. 967-71.
86. Brockstedt, D.G., et al., *Induction of immunity to antigens expressed by recombinant adeno-associated virus depends on the route of administration.* Clin Immunol, 1999. **92**(1): p. 67-75.
87. Pandya, M., et al., *Reprogramming Immune Response With Capsid-Optimized AAV6 Vectors for Immunotherapy of Cancer.* J Immunother, 2015. **38**(7): p. 292-8.
88. Perrin, G.Q., et al., *Dynamics of antigen presentation to transgene product-specific CD4(+) T cells and of Treg induction upon hepatic AAV gene transfer.* Mol Ther Methods Clin Dev, 2016. **3**: p. 16083.
89. Krotova, K., A. Day, and G. Aslanidi, *An Engineered AAV6-Based Vaccine Induces High Cytolytic Anti-Tumor Activity by Directly Targeting DCs and Improves Ag Presentation.* Mol Ther Oncolytics, 2019. **15**: p. 166-177.
90. Liu, D.W., et al., *Co-vaccination with adeno-associated virus vectors encoding human papillomavirus 16 L1 proteins and adenovirus encoding murine GM-CSF can elicit strong and prolonged neutralizing antibody.* Int J Cancer, 2005. **113**(1): p. 93-100.
91. Kuck, D., et al., *Intranasal vaccination with recombinant adeno-associated virus type 5 against human papillomavirus type 16 L1.* J Virol, 2006. **80**(6): p. 2621-30.

92. Nieto, K., et al., *Combined prophylactic and therapeutic intranasal vaccination against human papillomavirus type-16 using different adeno-associated virus serotype vectors*. *Antivir Ther*, 2009. **14**(8): p. 1125-37.
93. Xin, K.Q., et al., *Induction of robust immune responses against human immunodeficiency virus is supported by the inherent tropism of adeno-associated virus type 5 for dendritic cells*. *J Virol*, 2006. **80**(24): p. 11899-910.
94. Lin, J., et al., *Vaccines based on novel adeno-associated virus vectors elicit aberrant CD8+ T-cell responses in mice*. *J Virol*, 2007. **81**(21): p. 11840-9.
95. Lin, S.W., et al., *Recombinant adeno-associated virus vectors induce functionally impaired transgene product-specific CD8+ T cells in mice*. *J Clin Invest*, 2007. **117**(12): p. 3958-70.
96. Manning, W.C., et al., *Genetic immunization with adeno-associated virus vectors expressing herpes simplex virus type 2 glycoproteins B and D*. *J Virol*, 1997. **71**(10): p. 7960-2.
97. Mekonnen, Z.A., et al., *Single-Dose Vaccination with a Hepatotropic Adeno-associated Virus Efficiently Localizes T Cell Immunity in the Liver with the Potential To Confer Rapid Protection against Hepatitis C Virus*. *J Virol*, 2019. **93**(19).
98. Sipo, I., et al., *Vaccine protection against lethal homologous and heterologous challenge using recombinant AAV vectors expressing codon-optimized genes from pandemic swine origin influenza virus (SOIV)*. *Vaccine*, 2011. **29**(8): p. 1690-9.
99. Du, L., et al., *Priming with rAAV encoding RBD of SARS-CoV S protein and boosting with RBD-specific peptides for T cell epitopes elevated humoral and cellular immune responses against SARS-CoV infection*. *Vaccine*, 2008. **26**(13): p. 1644-51.
100. Slon-Campos, J.L., et al., *Use of Adeno-associated viral vectors to improve delivery of a DNA vaccine against dengue virus*. *J Gen Virol*, 2020. **101**(1): p. 73-78.
101. Lin, J., et al., *A new genetic vaccine platform based on an adeno-associated virus isolated from a rhesus macaque*. *J Virol*, 2009. **83**(24): p. 12738-50.
102. Yusuf, Y., et al., *Adeno-Associated Virus as an Effective Malaria Booster Vaccine Following Adenovirus Priming*. *Front Immunol*, 2019. **10**: p. 730.
103. Hensel, J.A., et al., *Recombinant AAV-CEA Tumor Vaccine in Combination with an Immune Adjuvant Breaks Tolerance and Provides Protective Immunity*. *Mol Ther Oncolytics*, 2019. **12**: p. 41-48.
104. Johnson, P.R., et al., *Novel adeno-associated virus vector vaccine restricts replication of simian immunodeficiency virus in macaques*. *J Virol*, 2005. **79**(2): p. 955-65.
105. Priddy, F.H., et al., *Adeno-associated virus vectored immunoprophylaxis to prevent HIV in healthy adults: a phase 1 randomised controlled trial*. *Lancet HIV*, 2019. **6**(4): p. e230-e239.
106. Vardas, E., et al., *A phase 2 study to evaluate the safety and immunogenicity of a recombinant HIV type 1 vaccine based on adeno-associated virus*. *AIDS Res Hum Retroviruses*, 2010. **26**(8): p. 933-42.
107. Manzano-Szalai, K., et al., *Adeno-associated virus-like particles as new carriers for B-cell vaccines: testing immunogenicity and safety in BALB/c mice*. *Viral Immunol*, 2014. **27**(9): p. 438-48.
108. Nieto, K., et al., *Intranasal vaccination with AAV5 and 9 vectors against human papillomavirus type 16 in rhesus macaques*. *Hum Gene Ther*, 2012. **23**(7): p. 733-41.
109. Nieto, K., et al., *Development of AAVLP(HPV16/31L2) particles as broadly protective HPV vaccine candidate*. *PLoS One*, 2012. **7**(6): p. e39741.

110. Rybniker, J., et al., *Incorporation of antigens into viral capsids augments immunogenicity of adeno-associated virus vector-based vaccines*. J Virol, 2012. **86**(24): p. 13800-4.
111. Singer, J., et al., *Proof of concept study with an HER-2 mimotope anticancer vaccine deduced from a novel AAV-mimotope library platform*. Oncoimmunology, 2016. **5**(7): p. e1171446.
112. Li, H., et al., *Adeno-associated virus vectors serotype 2 induce prolonged proliferation of capsid-specific CD8+ T cells in mice*. Mol Ther, 2011. **19**(3): p. 536-46.
113. Xiang, Z., et al., *The Effect of CpG Sequences on Capsid-Specific CD8(+) T Cell Responses to AAV Vector Gene Transfer*. Mol Ther, 2020. **28**(3): p. 771-783.
114. Li, C., et al., *Adeno-associated virus capsid antigen presentation is dependent on endosomal escape*. J Clin Invest, 2013. **123**(3): p. 1390-401.
115. He, Y., et al., *Kinetics of adeno-associated virus serotype 2 (AAV2) and AAV8 capsid antigen presentation in vivo are identical*. Hum Gene Ther, 2013. **24**(5): p. 545-53.
116. Pei, X., et al., *Efficient Capsid Antigen Presentation From Adeno-Associated Virus Empty Virions In Vivo*. Front Immunol, 2018. **9**: p. 844.
117. Coley, W.B., *The treatment of malignant tumors by repeated inoculations of erysipelas. With a report of ten original cases. 1893*. Clin Orthop Relat Res, 1991(262): p. 3-11.
118. Oiseth, S.J. and M.S. Aziz, *Cancer immunotherapy: a brief review of the history, possibilities, and challenges ahead*. J Cancer Metastasis Treat, 2017(3): p. 250-261.
119. Conlon, K.C., M.D. Miljkovic, and T.A. Waldmann, *Cytokines in the Treatment of Cancer*. J Interferon Cytokine Res, 2019. **39**(1): p. 6-21.
120. Sharma, P., et al., *Primary, Adaptive, and Acquired Resistance to Cancer Immunotherapy*. Cell, 2017. **168**(4): p. 707-723.
121. Robert, C., *A decade of immune-checkpoint inhibitors in cancer therapy*. Nat Commun, 2020. **11**(1): p. 3801.
122. Hudis, C.A., *Trastuzumab--mechanism of action and use in clinical practice*. N Engl J Med, 2007. **357**(1): p. 39-51.
123. Salles, G., et al., *Rituximab in B-Cell Hematologic Malignancies: A Review of 20 Years of Clinical Experience*. Adv Ther, 2017. **34**(10): p. 2232-2273.
124. Waldman, A.D., J.M. Fritz, and M.J. Lenardo, *A guide to cancer immunotherapy: from T cell basic science to clinical practice*. Nat Rev Immunol, 2020. **20**(11): p. 651-668.
125. Ehrlich, P., *Über den jetzigen Stand der Karzinomforschung*. Beiträge zur experimentellen Pathologie und Chemotherapie, 1909: p. 117-164.
126. DeMaria, P.J. and M. Bilusic, *Cancer Vaccines*. Hematol Oncol Clin North Am, 2019. **33**(2): p. 199-214.
127. van der Bruggen, P., et al., *A gene encoding an antigen recognized by cytolytic T lymphocytes on a human melanoma*. Science, 1991. **254**(5038): p. 1643-7.
128. Haen, S.P., et al., *Towards new horizons: characterization, classification and implications of the tumour antigenic repertoire*. Nat Rev Clin Oncol, 2020. **17**(10): p. 595-610.
129. Martincorena, I. and P.J. Campbell, *Somatic mutation in cancer and normal cells*. Science, 2015. **349**(6255): p. 1483-9.
130. Sahin, U. and Ö. Türeci, *Personalized vaccines for cancer immunotherapy*. Science, 2018. **359**(6382): p. 1355-1360.

131. Castle, J.C., et al., *Exploiting the mutanome for tumor vaccination*. *Cancer Res*, 2012. **72**(5): p. 1081-91.
132. Kreiter, S., et al., *Mutant MHC class II epitopes drive therapeutic immune responses to cancer*. *Nature*, 2015. **520**(7549): p. 692-6.
133. Carreno, B.M., et al., *Cancer immunotherapy. A dendritic cell vaccine increases the breadth and diversity of melanoma neoantigen-specific T cells*. *Science*, 2015. **348**(6236): p. 803-8.
134. Bassani-Sternberg, M., et al., *A Phase Ib Study of the Combination of Personalized Autologous Dendritic Cell Vaccine, Aspirin, and Standard of Care Adjuvant Chemotherapy Followed by Nivolumab for Resected Pancreatic Adenocarcinoma-A Proof of Antigen Discovery Feasibility in Three Patients*. *Front Immunol*, 2019. **10**: p. 1832.
135. Ott, P.A., et al., *An immunogenic personal neoantigen vaccine for patients with melanoma*. *Nature*, 2017. **547**(7662): p. 217-221.
136. Keskin, D.B., et al., *Neoantigen vaccine generates intratumoral T cell responses in phase Ib glioblastoma trial*. *Nature*, 2019. **565**(7738): p. 234-239.
137. Sahin, U., et al., *Personalized RNA mutanome vaccines mobilize poly-specific therapeutic immunity against cancer*. *Nature*, 2017. **547**(7662): p. 222-226.
138. Cafri, G., et al., *mRNA vaccine-induced neoantigen-specific T cell immunity in patients with gastrointestinal cancer*. *J Clin Invest*, 2020. **130**(11): p. 5976-5988.
139. Graham, F.L., et al., *Characteristics of a human cell line transformed by DNA from human adenovirus type 5*. *J Gen Virol*, 1977. **36**(1): p. 59-74.
140. Rio, D.C., S.G. Clark, and R. Tjian, *A mammalian host-vector system that regulates expression and amplification of transfected genes by temperature induction*. *Science*, 1985. **227**(4682): p. 23-8.
141. DuBridge, R.B., et al., *Analysis of mutation in human cells by using an Epstein-Barr virus shuttle system*. *Mol Cell Biol*, 1987. **7**(1): p. 379-87.
142. Shen, Z., et al., *Cloned dendritic cells can present exogenous antigens on both MHC class I and class II molecules*. *J Immunol*, 1997. **158**(6): p. 2723-30.
143. Fidler, I.J. and G.L. Nicolson, *Organ selectivity for implantation survival and growth of B16 melanoma variant tumor lines*. *J Natl Cancer Inst*, 1976. **57**(5): p. 1199-202.
144. Dubielzig, R., et al., *Adeno-associated virus type 2 protein interactions: formation of pre-encapsidation complexes*. *J Virol*, 1999. **73**(11): p. 8989-98.
145. Wang, Z., et al., *Rapid and highly efficient transduction by double-stranded adeno-associated virus vectors in vitro and in vivo*. *Gene Ther*, 2003. **10**(26): p. 2105-11.
146. Wright, J.F., et al., *Identification of factors that contribute to recombinant AAV2 particle aggregation and methods to prevent its occurrence during vector purification and formulation*. *Mol Ther*, 2005. **12**(1): p. 171-8.
147. Jensen, K.K., et al., *Improved methods for predicting peptide binding affinity to MHC class II molecules*. *Immunology*, 2018. **154**(3): p. 394-406.
148. Reynisson, B., et al., *Improved Prediction of MHC II Antigen Presentation through Integration and Motif Deconvolution of Mass Spectrometry MHC Eluted Ligand Data*. *J Proteome Res*, 2020. **19**(6): p. 2304-2315.
149. Nielsen, M., et al., *Reliable prediction of T-cell epitopes using neural networks with novel sequence representations*. *Protein Sci*, 2003. **12**(5): p. 1007-17.
150. Andreatta, M. and M. Nielsen, *Gapped sequence alignment using artificial neural networks: application to the MHC class I system*. *Bioinformatics*, 2016. **32**(4): p. 511-7.

151. Kamala, T., *Hock immunization: a humane alternative to mouse footpad injections*. J Immunol Methods, 2007. **328**(1-2): p. 204-14.
152. Janik, P., P. Briand, and N.R. Hartmann, *The effect of estrone-progesterone treatment on cell proliferation kinetics of hormone-dependent GR mouse mammary tumors*. Cancer Res, 1975. **35**(12): p. 3698-704.
153. Lissina, A., et al., *Protein kinase inhibitors substantially improve the physical detection of T-cells with peptide-MHC tetramers*. J Immunol Methods, 2009. **340**(1): p. 11-24.
154. Röttschke, O., et al., *Exact prediction of a natural T cell epitope*. Eur J Immunol, 1991. **21**(11): p. 2891-4.
155. Robertson, J.M., P.E. Jensen, and B.D. Evavold, *DO11.10 and OT-II T cells recognize a C-terminal ovalbumin 323-339 epitope*. J Immunol, 2000. **164**(9): p. 4706-12.
156. Kotturi, M.F., et al., *The CD8+ T-cell response to lymphocytic choriomeningitis virus involves the L antigen: uncovering new tricks for an old virus*. J Virol, 2007. **81**(10): p. 4928-40.
157. Peng, S., et al., *Development of a DNA vaccine targeting human papillomavirus type 16 oncoprotein E6*. J Virol, 2004. **78**(16): p. 8468-76.
158. Beckett, D., E. Kovaleva, and P.J. Schatz, *A minimal peptide substrate in biotin holoenzyme synthetase-catalyzed biotinylation*. Protein Sci, 1999. **8**(4): p. 921-9.
159. Cull, M.G. and P.J. Schatz, *Biotinylation of proteins in vivo and in vitro using small peptide tags*. Methods Enzymol, 2000. **326**: p. 430-40.
160. Rosenthal, K.S., P. Taylor, and D.H. Zimmerman, *J-LEAPS peptide and LEAPS dendritic cell vaccines*. Microb Biotechnol, 2012. **5**(2): p. 203-13.
161. Vigna, S.R., et al., *Characterization of antibodies to the rat substance P (NK-1) receptor and to a chimeric substance P receptor expressed in mammalian cells*. J Neurosci, 1994. **14**(2): p. 834-45.
162. Makinen, S.R., et al., *CpG-mediated augmentation of CD8+ T-cell responses in mice is attenuated by a water-in-oil emulsion (Montanide ISA-51) but enhanced by an oil-in-water emulsion (IDRI SE)*. Int Immunol, 2016. **28**(9): p. 453-61.
163. Bonhoure, F. and J. Gaucheron, *Montanide ISA 51 VG as Adjuvant for Human Vaccines*. Journal of Immunotherapy, 2006. **29**(6): p. 647-648.
164. Volckmar, J., et al., *The STING activator c-di-AMP exerts superior adjuvant properties than the formulation poly(I:C)/CpG after subcutaneous vaccination with soluble protein antigen or DEC-205-mediated antigen targeting to dendritic cells*. Vaccine, 2019. **37**(35): p. 4963-4974.
165. Knudsen, M.L., et al., *Kinetic and phenotypic analysis of CD8+ T cell responses after priming with alphavirus replicons and homologous or heterologous booster immunizations*. J Virol, 2014. **88**(21): p. 12438-51.
166. Estcourt, M.J., et al., *Prime-boost immunization generates a high frequency, high-avidity CD8(+) cytotoxic T lymphocyte population*. Int Immunol, 2002. **14**(1): p. 31-7.
167. Gross, B.P., et al., *Biotinylated Streptavidin Surface Coating Improves the Efficacy of a PLGA Microparticle-Based Cancer Vaccine*. Bioconjug Chem, 2020. **31**(9): p. 2147-2157.
168. Hailemichael, Y., et al., *Cancer vaccine formulation dictates synergy with CTLA-4 and PD-L1 checkpoint blockade therapy*. J Clin Invest, 2018. **128**(4): p. 1338-1354.
169. Jordan, K.A., et al., *Kinetics and phenotype of vaccine-induced CD8+ T-cell responses to Toxoplasma gondii*. Infect Immun, 2009. **77**(9): p. 3894-901.

170. French, R.R., et al., *CD40 antibody evokes a cytotoxic T-cell response that eradicates lymphoma and bypasses T-cell help*. *Nat Med*, 1999. **5**(5): p. 548-53.
171. Hunter, T.B., et al., *An agonist antibody specific for CD40 induces dendritic cell maturation and promotes autologous anti-tumour T-cell responses in an in vitro mixed autologous tumour cell/lymph node cell model*. *Scand J Immunol*, 2007. **65**(5): p. 479-86.
172. Taylor, P.R., et al., *J-LEAPS vaccines initiate murine Th1 responses by activating dendritic cells*. *Vaccine*, 2010. **28**(34): p. 5533-42.
173. Taylor, P.R., et al., *Maturation of dendritic cell precursors into IL12-producing DCs by J-LEAPS immunogens*. *Cell Immunol*, 2010. **262**(1): p. 1-5.
174. Malarkannan, S., et al., *The mouse mammary tumor virus env gene is the source of a CD8+ T-cell-stimulating peptide presented by a major histocompatibility complex class I molecule in a murine thymoma*. *Proc Natl Acad Sci U S A*, 1996. **93**(24): p. 13991-6.
175. Chen, W., et al., *Identification of a gag-encoded cytotoxic T-lymphocyte epitope from FBL-3 leukemia shared by Friend, Moloney, and Rauscher murine leukemia virus-induced tumors*. *J Virol*, 1996. **70**(11): p. 7773-82.
176. White, H.D., D.A. Roeder, and W.R. Green, *An immunodominant Kb-restricted peptide from the p15E transmembrane protein of endogenous ecotropic murine leukemia virus (MuLV) AKR623 that restores susceptibility of a tumor line to anti-AKR/Gross MuLV cytotoxic T lymphocytes*. *J Virol*, 1994. **68**(2): p. 897-904.
177. Zwaveling, S., et al., *Established human papillomavirus type 16-expressing tumors are effectively eradicated following vaccination with long peptides*. *J Immunol*, 2002. **169**(1): p. 350-8.
178. Provine, N.M., et al., *Immediate Dysfunction of Vaccine-Elicited CD8+ T Cells Primed in the Absence of CD4+ T Cells*. *J Immunol*, 2016. **197**(5): p. 1809-22.
179. Pennock, N.D., et al., *T cell responses: naive to memory and everything in between*. *Adv Physiol Educ*, 2013. **37**(4): p. 273-83.
180. Shirley, J.L., et al., *Type I IFN Sensing by cDCs and CD4(+) T Cell Help Are Both Requisite for Cross-Priming of AAV Capsid-Specific CD8(+) T Cells*. *Mol Ther*, 2020. **28**(3): p. 758-770.
181. Wu, T.L., et al., *CD8+ T cell recognition of epitopes within the capsid of adeno-associated virus 8-based gene transfer vectors depends on vectors' genome*. *Mol Ther*, 2014. **22**(1): p. 42-51.
182. Gallimore, A., et al., *Induction and exhaustion of lymphocytic choriomeningitis virus-specific cytotoxic T lymphocytes visualized using soluble tetrameric major histocompatibility complex class I-peptide complexes*. *J Exp Med*, 1998. **187**(9): p. 1383-93.
183. Hailemichael, Y., et al., *Persistent antigen at vaccination sites induces tumor-specific CD8+ T cell sequestration, dysfunction and deletion*. *Nat Med*, 2013. **19**(4): p. 465-72.
184. Schumacher, T., et al., *A vaccine targeting mutant IDH1 induces antitumour immunity*. *Nature*, 2014. **512**(7514): p. 324-7.
185. Tran, E., et al., *Cancer immunotherapy based on mutation-specific CD4+ T cells in a patient with epithelial cancer*. *Science*, 2014. **344**(6184): p. 641-5.
186. Quezada, S.A., et al., *Tumor-reactive CD4(+) T cells develop cytotoxic activity and eradicate large established melanoma after transfer into lymphopenic hosts*. *J Exp Med*, 2010. **207**(3): p. 637-50.

187. Xie, Y., et al., *Naive tumor-specific CD4(+) T cells differentiated in vivo eradicate established melanoma*. J Exp Med, 2010. **207**(3): p. 651-67.
188. Tay, R.E., E.K. Richardson, and H.C. Toh, *Revisiting the role of CD4(+) T cells in cancer immunotherapy-new insights into old paradigms*. Cancer Gene Ther, 2021. **28**(1-2): p. 5-17.
189. Mallet-Designe, V.I., et al., *Detection of low-avidity CD4+ T cells using recombinant artificial APC: following the antiovalbumin immune response*. J Immunol, 2003. **170**(1): p. 123-31.
190. Weaver, J.M., et al., *Immunodominance of CD4 T cells to foreign antigens is peptide intrinsic and independent of molecular context: implications for vaccine design*. J Immunol, 2008. **181**(5): p. 3039-48.
191. Lamb, C.A., et al., *Invariant chain targets HLA class II molecules to acidic endosomes containing internalized influenza virus*. Proc Natl Acad Sci U S A, 1991. **88**(14): p. 5998-6002.
192. Chang, A.Y., et al., *Opportunities and challenges for TCR mimic antibodies in cancer therapy*. Expert Opin Biol Ther, 2016. **16**(8): p. 979-87.
193. Chang, A.Y., et al., *A therapeutic T cell receptor mimic antibody targets tumor-associated PRAME peptide/HLA-I antigens*. J Clin Invest, 2017. **127**(7): p. 2705-2718.
194. Xu, Y., et al., *T-cell receptor mimic (TCRm) antibody therapeutics against intracellular proteins*. Antibody Therapeutics, 2019. **2**(1): p. 22-32.
195. Schellenberger, V., et al., *A recombinant polypeptide extends the in vivo half-life of peptides and proteins in a tunable manner*. Nat Biotechnol, 2009. **27**(12): p. 1186-90.
196. Kourtis, I.C., et al., *Peripherally administered nanoparticles target monocytic myeloid cells, secondary lymphoid organs and tumors in mice*. PLoS One, 2013. **8**(4): p. e61646.
197. Ols, S., et al., *Route of Vaccine Administration Alters Antigen Trafficking but Not Innate or Adaptive Immunity*. Cell Rep, 2020. **30**(12): p. 3964-3971.e7.
198. Sykulev, Y., et al., *Evidence that a single peptide-MHC complex on a target cell can elicit a cytolytic T cell response*. Immunity, 1996. **4**(6): p. 565-71.
199. Korb, L.C., et al., *Induction of T cell anergy by low numbers of agonist ligands*. J Immunol, 1999. **162**(11): p. 6401-9.
200. Awate, S., L.A. Babiuk, and G. Mutwiri, *Mechanisms of action of adjuvants*. Front Immunol, 2013. **4**: p. 114.
201. Rhee, E.G., et al., *Multiple innate immune pathways contribute to the immunogenicity of recombinant adenovirus vaccine vectors*. J Virol, 2011. **85**(1): p. 315-23.
202. Rogers, G.L., et al., *Plasmacytoid and conventional dendritic cells cooperate in crosspriming AAV capsid-specific CD8(+) T cells*. Blood, 2017. **129**(24): p. 3184-3195.
203. Blair, D.A., et al., *Duration of antigen availability influences the expansion and memory differentiation of T cells*. J Immunol, 2011. **187**(5): p. 2310-21.
204. Kuball, J., et al., *Pitfalls of vaccinations with WT1-, Proteinase3- and MUC1-derived peptides in combination with MontanideISA51 and CpG7909*. Cancer Immunol Immunother, 2011. **60**(2): p. 161-71.
205. Schijns, V., et al., *Modulation of immune responses using adjuvants to facilitate therapeutic vaccination*. Immunological Reviews, 2020. **296**(1): p. 169-190.

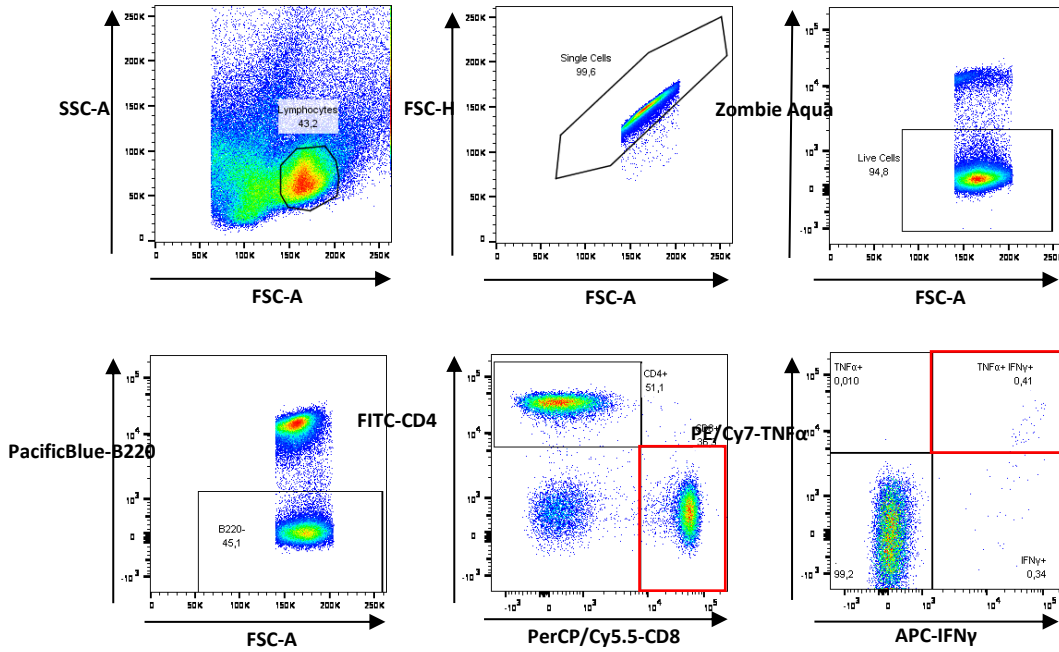
206. Kronenberg, S., et al., *A conformational change in the adeno-associated virus type 2 capsid leads to the exposure of hidden VP1 N termini*. J Virol, 2005. **79**(9): p. 5296-303.
207. Bleker, S., F. Sonntag, and J.A. Kleinschmidt, *Mutational analysis of narrow pores at the fivefold symmetry axes of adeno-associated virus type 2 capsids reveals a dual role in genome packaging and activation of phospholipase A2 activity*. J Virol, 2005. **79**(4): p. 2528-40.
208. Zhang, Y.N., et al., *Nanoparticle Size Influences Antigen Retention and Presentation in Lymph Node Follicles for Humoral Immunity*. Nano Lett, 2019. **19**(10): p. 7226-7235.
209. Ruedl, C., et al., *Virus-like particles as carriers for T-cell epitopes: limited inhibition of T-cell priming by carrier-specific antibodies*. J Virol, 2005. **79**(2): p. 717-24.
210. Schwarz, K., et al., *Efficient homologous prime-boost strategies for T cell vaccination based on virus-like particles*. Eur J Immunol, 2005. **35**(3): p. 816-21.
211. Lu, S., *Heterologous prime-boost vaccination*. Curr Opin Immunol, 2009. **21**(3): p. 346-51.
212. Kamen, L., et al., *A novel method for determining antibody-dependent cellular phagocytosis*. J Immunol Methods, 2019. **468**: p. 55-60.
213. Mays, L.E., et al., *Mapping the structural determinants responsible for enhanced T cell activation to the immunogenic adeno-associated virus capsid from isolate rhesus 32.33*. J Virol, 2013. **87**(17): p. 9473-85.
214. Mays, L.E., et al., *Adeno-associated virus capsid structure drives CD4-dependent CD8+ T cell response to vector encoded proteins*. J Immunol, 2009. **182**(10): p. 6051-60.
215. Clawson, C., et al., *Delivery of a peptide via poly(D,L-lactic-co-glycolic) acid nanoparticles enhances its dendritic cell-stimulatory capacity*. Nanomedicine, 2010. **6**(5): p. 651-61.
216. Saenz, R., et al., *HMGB1-derived peptide acts as adjuvant inducing immune responses to peptide and protein antigen*. Vaccine, 2010. **28**(47): p. 7556-62.
217. Ying, Q., et al., *Construction and immunological characterization of CD40L or GM-CSF incorporated Hantaan virus like particle*. Oncotarget, 2016. **7**(39): p. 63488-63503.
218. Muralidharan, A., et al., *Targeting CD40 enhances antibody- and CD8-mediated protection against respiratory syncytial virus infection*. Sci Rep, 2018. **8**(1): p. 16648.
219. Gogesch, P., et al., *Modular MLV-VLPs co-displaying ovalbumin peptides and GM-CSF effectively induce expansion of CD11b(+) APC and antigen-specific T cell responses in vitro*. Mol Immunol, 2018. **101**: p. 19-28.
220. Thrane, S., et al., *Bacterial superglue enables easy development of efficient virus-like particle based vaccines*. J Nanobiotechnology, 2016. **14**: p. 30.
221. Zakeri, B., et al., *Peptide tag forming a rapid covalent bond to a protein, through engineering a bacterial adhesin*. Proc Natl Acad Sci U S A, 2012. **109**(12): p. E690-7.
222. Aslanidi, G.V., et al., *High-efficiency transduction of human monocyte-derived dendritic cells by capsid-modified recombinant AAV2 vectors*. Vaccine, 2012. **30**(26): p. 3908-17.
223. Bedoui, S., W.R. Heath, and S.N. Mueller, *CD4(+) T-cell help amplifies innate signals for primary CD8(+) T-cell immunity*. Immunol Rev, 2016. **272**(1): p. 52-64.
224. Bennett, S.R., et al., *Help for cytotoxic-T-cell responses is mediated by CD40 signalling*. Nature, 1998. **393**(6684): p. 478-80.

-
225. Ridge, J.P., F. Di Rosa, and P. Matzinger, *A conditioned dendritic cell can be a temporal bridge between a CD4+ T-helper and a T-killer cell*. *Nature*, 1998. **393**(6684): p. 474-8.
226. Godot, V., et al., *TLR-9 agonist and CD40-targeting vaccination induces HIV-1 envelope-specific B cells with a diversified immunoglobulin repertoire in humanized mice*. *PLoS Pathog*, 2020. **16**(11): p. e1009025.
227. Rosalia, R.A., et al., *CD40-targeted dendritic cell delivery of PLGA-nanoparticle vaccines induce potent anti-tumor responses*. *Biomaterials*, 2015. **40**: p. 88-97.
228. Kung, J.T., C.G. Mackenzie, and D.W. Talmage, *The requirement for biotin and fatty acids in the cytotoxic T-cell response*. *Cell Immunol*, 1979. **48**(1): p. 100-10.
229. Báez-Saldaña, A., et al., *Biotin deficiency induces changes in subpopulations of spleen lymphocytes in mice*. *Am J Clin Nutr*, 1998. **67**(3): p. 431-7.
230. Rosenthal, K.S., et al., *Immunization with a LEAPS heteroconjugate containing a CTL epitope and a peptide from beta-2-microglobulin elicits a protective and DTH response to herpes simplex virus type 1*. *Vaccine*, 1999. **17**(6): p. 535-42.
231. Zimmerman, D.H., et al., *A new approach to T-cell activation: Natural and synthetic conjugates capable of activating T cells*. *Vaccine Research*, 1996. **5**(2): p. 91-102.
232. Boonnak, K., et al., *Antigen-activated dendritic cells ameliorate influenza A infections*. *J Clin Invest*, 2013. **123**(7): p. 2850-61.
233. Goel, N., et al., *A L.E.A.P.S. heteroconjugate vaccine containing a T cell epitope from HSV-1 glycoprotein D elicits Th1 responses and protection*. *Vaccine*, 2003. **21**(27-30): p. 4410-20.
234. Rosenthal, K.S., et al., *LEAPS Vaccine Incorporating HER-2/neu Epitope Elicits Protection That Prevents and Limits Tumor Growth and Spread of Breast Cancer in a Mouse Model*. *J Immunol Res*, 2017. **2017**: p. 3613505.
235. Zimmerman, D.H., et al., *Immunization with peptide heteroconjugates primes a T helper cell type 1-associated antibody (IgG2a) response that recognizes the native epitope on the 38-kDa protein of Mycobacterium tuberculosis*. *Vaccine Research*, 1996. **5**(2): p. 103-118.
236. den Haan, J.M., S.M. Lehar, and M.J. Bevan, *CD8(+) but not CD8(-) dendritic cells cross-prime cytotoxic T cells in vivo*. *J Exp Med*, 2000. **192**(12): p. 1685-96.
237. Shedlock, D.J. and H. Shen, *Requirement for CD4 T cell help in generating functional CD8 T cell memory*. *Science*, 2003. **300**(5617): p. 337-9.
238. Sun, J.C. and M.J. Bevan, *Defective CD8 T cell memory following acute infection without CD4 T cell help*. *Science*, 2003. **300**(5617): p. 339-42.
239. Laidlaw, B.J., J.E. Craft, and S.M. Kaech, *The multifaceted role of CD4(+) T cells in CD8(+) T cell memory*. *Nat Rev Immunol*, 2016. **16**(2): p. 102-11.
240. Chen, J., et al., *Determination of specific CD4 and CD8 T cell epitopes after AAV2- and AAV8-hF.IX gene therapy*. *Mol Ther*, 2006. **13**(2): p. 260-9.
241. Hong, S., et al., *B Cells Are the Dominant Antigen-Presenting Cells that Activate Naive CD4(+) T Cells upon Immunization with a Virus-Derived Nanoparticle Antigen*. *Immunity*, 2018. **49**(4): p. 695-708.e4.
242. Kalergis, A.M. and J.V. Ravetch, *Inducing tumor immunity through the selective engagement of activating Fcγ receptors on dendritic cells*. *J Exp Med*, 2002. **195**(12): p. 1653-9.
243. Regnault, A., et al., *Fcγ receptor-mediated induction of dendritic cell maturation and major histocompatibility complex class I-restricted antigen*
-

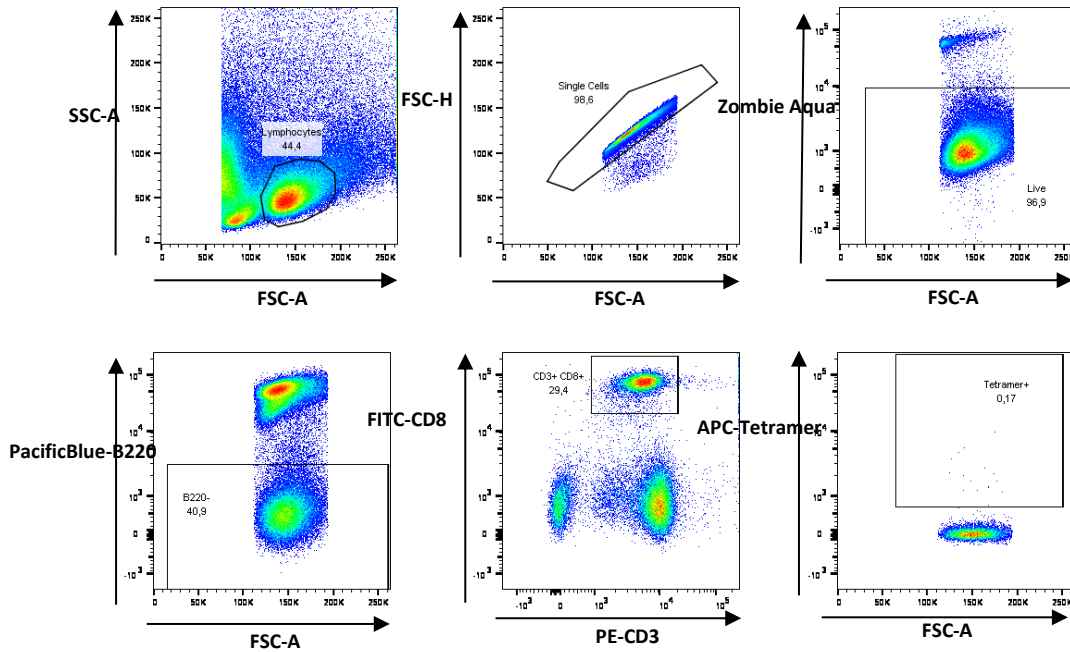
- presentation after immune complex internalization. J Exp Med, 1999. 189(2): p. 371-80.*
244. Da Silva, D.M., et al., *Effect of preexisting neutralizing antibodies on the anti-tumor immune response induced by chimeric human papillomavirus virus-like particle vaccines. Virology, 2001. 290(2): p. 350-60.*
245. Fitzpatrick, Z., et al., *Influence of Pre-existing Anti-capsid Neutralizing and Binding Antibodies on AAV Vector Transduction. Mol Ther Methods Clin Dev, 2018. 9: p. 119-129.*
246. Nurieva, R., J. Wang, and A. Sahoo, *T-cell tolerance in cancer. Immunotherapy, 2013. 5(5): p. 513-531.*
247. Bloom, M.B., et al., *Identification of tyrosinase-related protein 2 as a tumor rejection antigen for the B16 melanoma. J Exp Med, 1997. 185(3): p. 453-9.*
248. Overwijk, W.W., et al., *gp100/pmel 17 is a murine tumor rejection antigen: induction of "self"-reactive, tumoricidal T cells using high-affinity, altered peptide ligand. J Exp Med, 1998. 188(2): p. 277-86.*
249. Tang, X.D., et al., *H-2Kb-restricted CTL epitopes from mouse heparanase elicit an antitumor immune response in vivo. Cancer Res, 2008. 68(5): p. 1529-37.*
250. Colella, T.A., et al., *Self-tolerance to the murine homologue of a tyrosinase-derived melanoma antigen: implications for tumor immunotherapy. J Exp Med, 2000. 191(7): p. 1221-32.*
251. Hofmann, U.B., et al., *Identification and characterization of survivin-derived H-2Kb-restricted CTL epitopes. Eur J Immunol, 2009. 39(5): p. 1419-24.*
252. Catakovic, K., et al., *T cell exhaustion: from pathophysiological basics to tumor immunotherapy. Cell Commun Signal, 2017. 15(1): p. 1.*
253. Tsukahara, T., et al., *Prognostic significance of HLA class I expression in osteosarcoma defined by anti-pan HLA class I monoclonal antibody, EMR8-5. Cancer Sci, 2006. 97(12): p. 1374-80.*
254. Tormoen, G.W., M.R. Crittenden, and M.J. Gough, *Role of the immunosuppressive microenvironment in immunotherapy. Adv Radiat Oncol, 2018. 3(4): p. 520-526.*
255. Gruntman, A.M., et al., *Stability and compatibility of recombinant adeno-associated virus under conditions commonly encountered in human gene therapy trials. Hum Gene Ther Methods, 2015. 26(2): p. 71-6.*
256. Clément, N. and J.C. Grieger, *Manufacturing of recombinant adeno-associated viral vectors for clinical trials. Mol Ther Methods Clin Dev, 2016. 3: p. 16002.*
257. Thadani, N.N., et al., *Frustration and Direct-Coupling Analyses to Predict Formation and Function of Adeno-Associated Virus. Biophys J, 2021. 120(3): p. 489-503.*
258. Nair, A.B. and S. Jacob, *A simple practice guide for dose conversion between animals and human. J Basic Clin Pharm, 2016. 7(2): p. 27-31.*

8 Appendices

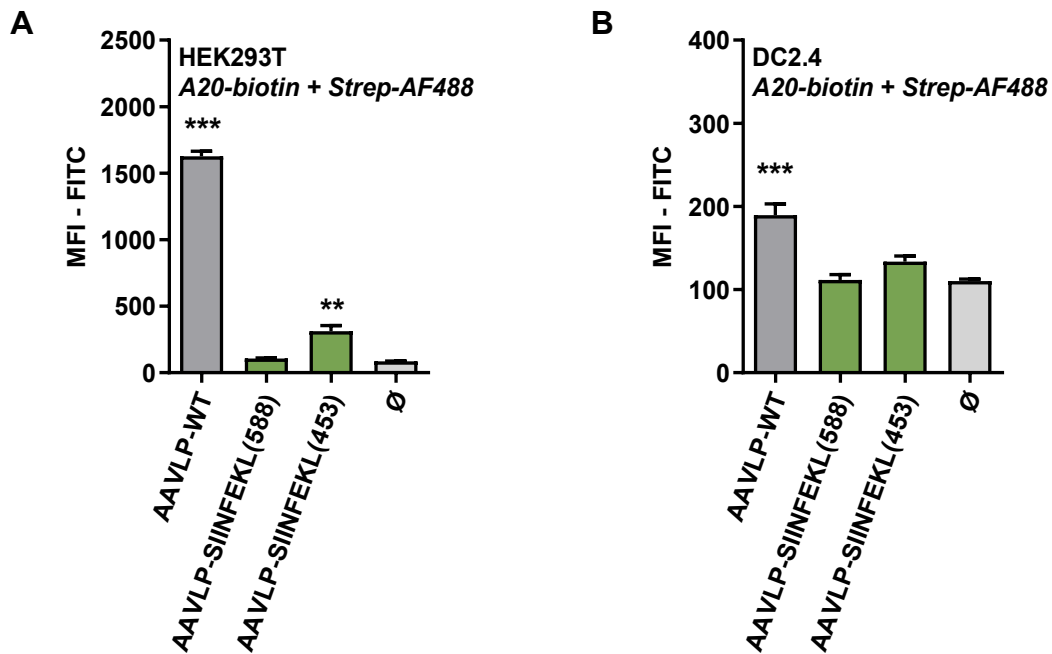
8.1 Additional data



Appendix 1: Flow cytometry gating of intracellular staining.

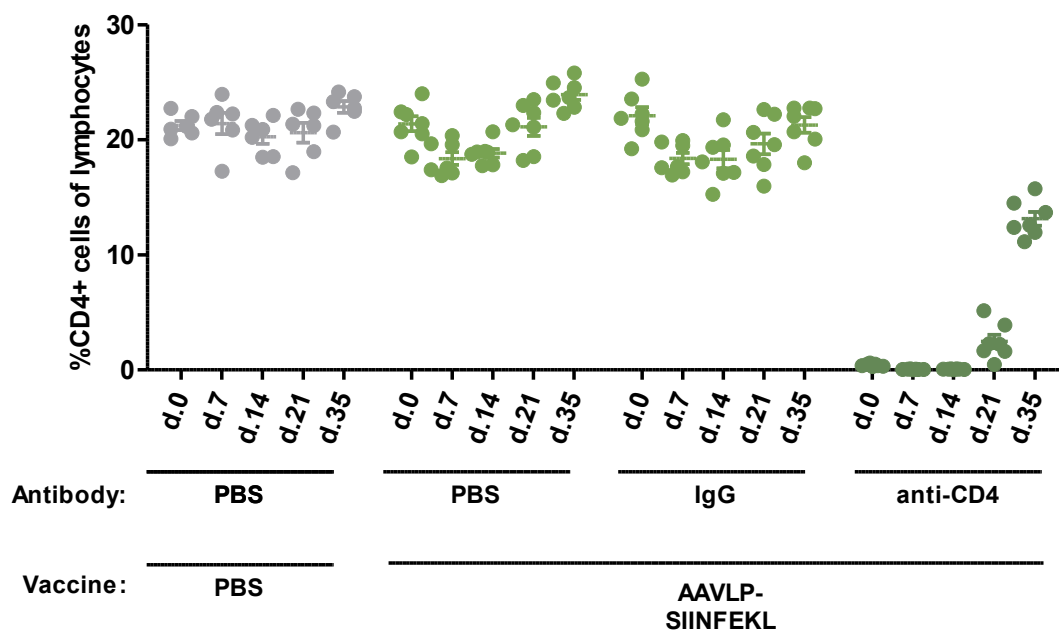


Appendix 2: Flow cytometry strategy of tetramer staining.



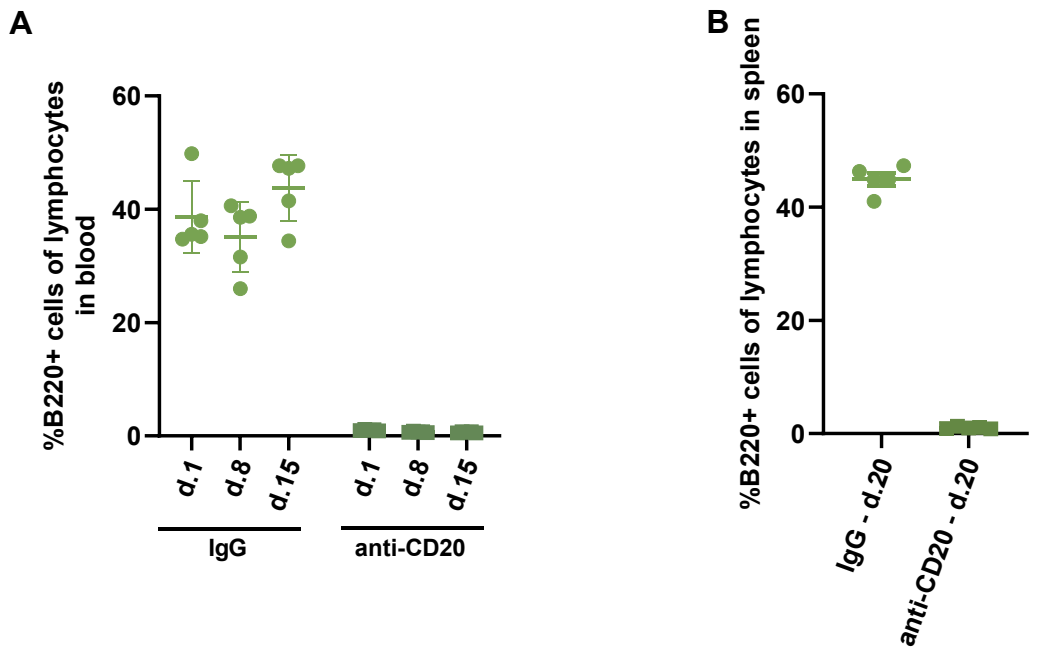
Appendix 3: AAVLP-SIINFEKL binds APCs more efficiently and induces stronger immune responses when the antigen is inserted at aa453 instead of aa588.

Two AAVLP-SIINFEKL variants were compared, incorporating SIINFEKL in the VR-VIII loop (aa588) (AAVLP-SIINFEKL(588)) or the VR-IV loop (aa453) (AAVLP-SIINFEKL(453)) of the capsid protein VP1. **A+B** In order to analyze potential binding of AAVLPs to APCs, HEK293T (A) and DC2.4 cells (B) were incubated with either variant of AAVLP-SIINFEKL or AAVLP-WT. Cells without AAVLPs served as negative controls (Ø). Cells were detached using EDTA and incubated for 1 h at 4 °C with 2.0E+05 capsids per cell. Cell-bound AAVLPs were detected with biotin-coupled A20 antibody (A20-biotin) and streptavidin-coupled Alexa Fluor 488 (Strep-AF488). The graph shows the mean fluorescence intensity (MFI) of FITC (Alexa Fluor 488) in each sample, measured by flow cytometry. Each bar represents the mean of three independent experiments including SEM. Significant differences to the negative control were determined using a One-way ANOVA with a Dunnett's multiple comparison test. Asterisks indicate significant difference with ** ($P \leq 0.01$); *** ($P \leq 0.001$). Although AAVLP-SIINFEKL(453) did not bind as efficiently as AAVLP-WT, a significantly increased binding compared to AAVLP-SIINFEKL(588) was observed.



Appendix 4: Confirmation of CD4+ T cell depletion by anti-CD4.

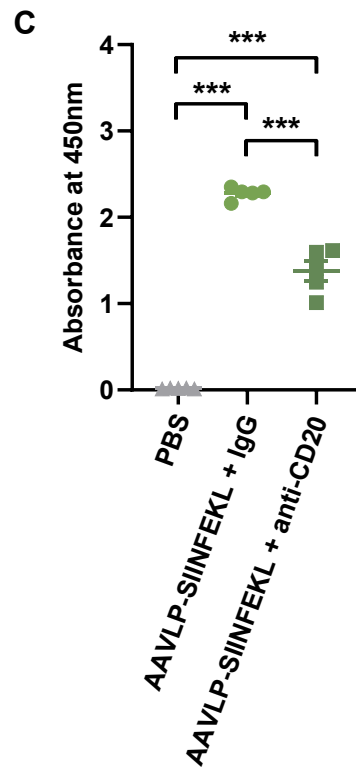
Anti-CD4 (GK1.5) was injected i.p. into mice two days before vaccination (d.1) as well as one and four days after. Successful depletion of CD4+ T cells was confirmed every week by staining blood lymphocytes with PE-labeled anti-CD4 (RM4-4). Mice injected with PBS or IgG isotype control, showed normal levels of CD4+ T cells around 20 % of all lymphocytes. Injection of anti-CD4 depleted all CD4+ T cells to a level of 0 %. The CD4+ T cell population re-emerged around 3 weeks after antibody injection.

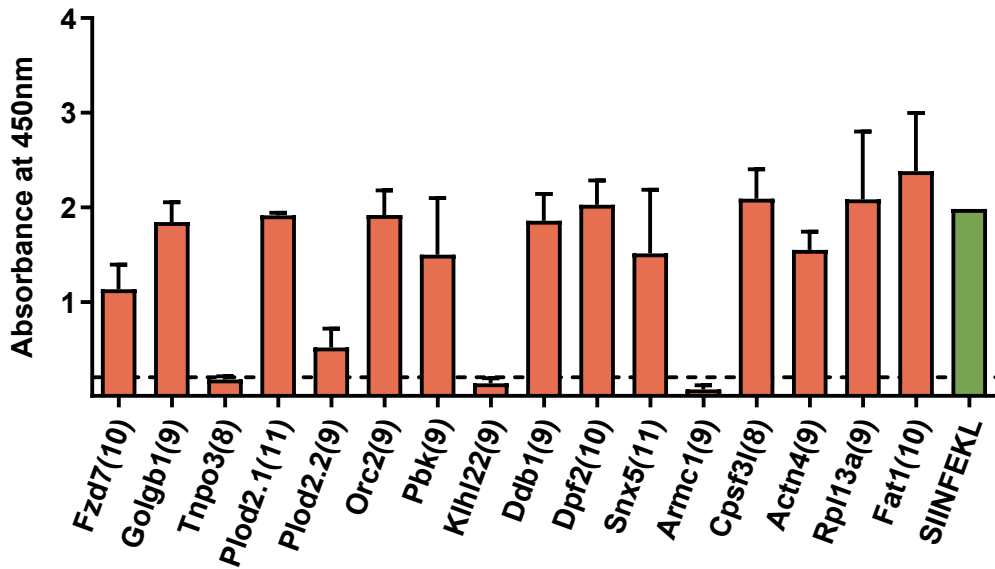


Appendix 5: Confirmation of B cell depletion by anti-CD20.

Anti-CD20 (SA271G2) was injected i.v. into mice two days before vaccination (d.1). **A**) Successful depletion of B cells was confirmed every week by staining blood lymphocytes with PacificBlue-labeled anti-B220 (RA3-6B2). Mice injected with IgG isotype control, showed normal levels of B cells around 40 % of all lymphocytes. Injection of anti-CD20 depleted all B cells to a level of 0.5 % to 1.0 %. **B**) Depletion test in the spleen at the end of the experiment (d.20). Splenocytes were stained with anti-B220, and showed the same B cell levels as in the blood.

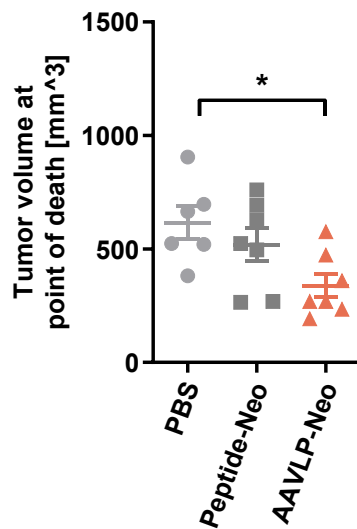
C) The serum antibody level in the blood of AAVLP-SIINFELK vaccinated mice was compared between B cell-intact (AAVLP-SIINFELK + IgG) and B cell-depleted (AAVLP-SIINFELK + anti-CD20) mice. AAVLP-binding antibodies were analyzed by coating AAVLPs on ELISA plates and incubating with blood serum of vaccinated mice (diluted 1:1000). PBS-injected mice served as negative controls. Bound antibodies were detected with HRP-coupled anti-mouse IgG antibodies as in 3.8.8. No AAVLP-specific antibodies were detected in PBS-injected mice. The level of AAVLP antibodies was reduced upon depletion of B cells but still considerable. However, the scope of antibody reduction compared to B cell-intact mice cannot be determined with certainty, as samples were oversaturated. Horizontal bars indicate the mean of each group with SEM. Significant differences between groups were determined using a One-way ANOVA with a Tukey's multiple comparison test. Asterisks indicate significant difference to all other groups with *** ($P \leq 0.001$).





Appendix 6: Ability to produce intact AAVLPs after insertion of short neoantigen sequences into the capsid sequence.

Several neoantigen sequences with a length of 8-11 amino acids were cloned into the AAV capsid sequence at amino acid 588. After production of AAVLPs in a 6-well scale, the preparations were analyzed for intact particles by A20 sandwich ELISA. AAVLP-SIINFEKL (SIINFEKL) served as a positive control. The dashed line shows the threshold of three times the background value.



Appendix 7: AAVLP-Neo vaccination caused reduced tumor volume at point of death due to necrosis.

C57BL/6 mice vaccinated with AAVLP-Neo or Peptide-Neo were challenged s.c. with B16F10 cells. PBS-injected mice served as negative-controls. As most mice had to be euthanized due to development of necrotic wounds, the tumor volume at the point of death was different for each mouse, as shown in the graph. Horizontal bars indicate the mean of each group with SEM. Significant differences between groups were determined using a One-way ANOVA with a Tukey's multiple comparison test. Asterisks indicate significant difference with * ($P \leq 0.05$). Final tumor volumes in mice vaccinated with AAVLP-Neo were significantly smaller compared to the other groups.

8.2 List of figures

Figure 1.1: Structure of the AAV genome and capsid.....	9
Figure 1.2: Production of recombinant AAVs/AAVLPs.	11
Figure 1.3: Current vaccination strategies using AAVs.	14
Figure 1.4: Vaccination strategy.	18
Figure 3.1: Design of peptide insertion site in the AAVLP capsid.	37
Figure 4.1: Design of AAVLPs.	60
Figure 4.2: Vaccination with AAVLP-SIINFEKL induces antigen-specific CD8+ T cells.	63
Figure 4.3: Tetramer staining reveals antigen-specific CD8+ T cells in the spleen and blood of AAVLP-SIINFEKL vaccinated mice.	64
Figure 4.4: CD8+ T cell responses after AAVLP-SIINFEKL vaccination are long-lasting and peak around 3 weeks.	66
Figure 4.5: CD8+ T cell responses are generated after s.c. but not i.m. injection of AAVLP-SIINFEKL.	67
Figure 4.6: A high local concentration of AAVLP-SIINFEKL increases CD8+ T cell responses.	68
Figure 4.7: CD8+ T cell responses are only generated when AAVLP-SIINFEKL is adjuvanted with Montanide ISA 51.	69
Figure 4.8: Higher CD8+ T cell responses are achieved when AAVLP-SIINFEKL particles contain genomic DNA.	70
Figure 4.9: AAVLP-SIINFEKL enters APCs more efficiently when the antigen is inserted into the VR-IV loop instead of the VR-VIII loop.....	71
Figure 4.10: Antigen-insertion in the VR-VIII loop of AAVLPs disrupts liver tropism but sustains localization to the spleen.....	72
Figure 4.11: AAVLP-SIINFEKL induces stronger immune responses when the antigen is inserted in the VR-IV loop instead of the VR-VIII loop.....	73
Figure 4.12: Pre-existing immune responses against AAV particles reduce the effect of the vaccine, and a heterologous prime-boost vaccination does not improve CD8+ T cell responses.....	74
Figure 4.13: Vaccination with AAVLP-SIINFEKL protects mice from tumor growth after s.c. B16F10-OVA challenge.	76
Figure 4.14: Generation of AAVLPs with bound anti-CD40.	77
Figure 4.15: Generation of anti-CD40 coupled AAVLPs.....	79
Figure 4.16: Coupling of anti-CD40 to AAVLPs increases the ability to target CD40-expressing cells.....	80
Figure 4.17: Binding of anti-CD40 to AAVLPs does not improve immune responses but biotinylation has an advantageous effect.....	82
Figure 4.18: Displaying a β -2-microglobulin peptide on AAVLP-SIINFEKL increases CD8+ T cell responses.....	83
Figure 4.19: Depletion of B cells improves CD8+ T cell responses induced by AAVLP-SIINFEKL.	84
Figure 4.20: Tumor protection and induction of CD8+ T cell responses after AAVLP-SIINFEKL vaccination depend on presence of CD4+ T cells.	86

Figure 4.21: Identification of potential T helper epitopes in AAVLPs.	89
Figure 4.22: Vaccination with AAVLP-OVAII induces high serum titers of OVAII-specific antibodies.	90
Figure 4.23: Vaccination with AAVLP-OVAII does not induce antigen-specific CD4+ T cell responses.	91
Figure 4.24: Presentation of an ovalbumin MHC class II epitope on AAVLP-OVAII does not protect mice after B16F10-OVA challenge.....	92
Figure 4.25: Vaccination with AAVLPs displaying an LCMV epitope induces antigen-specific CD8+ T cell responses.	94
Figure 4.26: Selection of neoantigens for AAVLP-Neo.	97
Figure 4.27: AAVLP-Neo does not induce detectable neoantigen-specific CD8+ T cell responses.	98
Figure 4.28: Vaccination with AAVLP-Neo induces antibody responses against neoantigens.....	99
Figure 4.29: Vaccination with AAVLP-Neo reduces tumor growth rate after s.c. B16F10 challenge.	101
Figure 4.30: Tendency of increased immune cell infiltration into tumor tissue of AAVLP-Neo vaccinated mice.....	102
Figure 4.31: Negative correlation between tumor volume and rate of immune cell infiltration.	103
Figure 5.1: Model of AAVLP induced immune responses.	120
Appendix 1: Flow cytometry gating of intracellular staining.....	144
Appendix 2: Flow cytometry strategy of tetramer staining.	144
Appendix 3: AAVLP-SIINFELK binds APCs more efficiently and induces stronger immune responses when the antigen is inserted at aa453 instead of aa588.	145
Appendix 4: Confirmation of CD4+ T cell depletion by anti-CD4.	146
Appendix 5: Confirmation of B cell depletion by anti-CD20.....	147
Appendix 6: Ability to produce intact AAVLPs after insertion of short neoantigen sequences into the capsid sequence.	148
Appendix 7: AAVLP-Neo vaccination caused reduced tumor volume at point of death due to necrosis.	148

8.3 List of tables

Table 3.1: TAE buffer.....	34
Table 3.2: LB medium	35
Table 3.3: Phosphorylation of DNA oligonucleotides	38
Table 3.4: Annealing of DNA oligonucleotides.....	38
Table 3.5: Linearization of vector DNA	38
Table 3.6: Ligation of dsDNA oligonucleotides into linearized vector DNA	38
Table 3.7: PCR mix for SDM	39
Table 3.8: PCR cycles for SDM.....	39
Table 3.9: PCR mix for cloning of BirA.....	40
Table 3.10: PCR cycles for cloning of BirA.....	40

Table 3.11: Restriction digest of PCR product for cloning of BirA	40
Table 3.12: Restriction digest of target vector for insertion of BirA	41
Table 3.13: Reaction mix for generation of cDNA from DC2.4	41
Table 3.14: Selection of potential mutations in the B16F10 genome	42
Table 3.15: PCR mix for neoantigen confirmation	43
Table 3.16: PCR cycles for neoantigen confirmation	43
Table 3.17: Transfection mix for AAVLP small-scale production in 6-well cell culture plate	44
Table 3.18: Transfection mix for AAVLP large-scale production in 15 cm cell culture dish	45
Table 3.19: PEG solution for AAVLP precipitation	47
Table 3.20: AAVLP lysis buffer	47
Table 3.21: Iodixanol solutions for AAVLP purification	47
Table 3.22: AAVLP concentration buffer	47
Table 3.23: Pipetting scheme for qPCR AAVLP titration	49
Table 3.24: qPCR cycling program	49
Table 3.25: Transfection mix for biotinylated AAVLP large-scale production in 15 cm cell culture dish	50
Table 3.26: Non-reducing Tris-Acetate gel	51
Table 3.27: Sample buffer (4x) for polyacrylamide gel electrophoresis	51
Table 3.28: Running buffer (1x) for polyacrylamide gel electrophoresis	51
Table 3.29: Transfer buffer (1x) for wet electroblotting	52
Table 3.30: RBC lysis buffer	57
Table 3.31: Carbonate buffer	58
Table 4.1: List of AAVLPs tested during the project.	61
Table 4.2: <i>In silico</i> predicted helper epitopes in the AAVLP capsid sequence.	87
Table 4.3: Neoantigen selection	95

8.4 Abbreviations

aa	amino acid
AAP	assembly-activating protein
AAV	adeno-associated virus
AAVLP	adeno-associated virus-like particles
AAVLP2/5	AAVLP serotype 2/5
AF488	Alexa Fluor 488
APC	antigen-presenting cell
APC	allophycocyanin
AxLN	axillary lymph node
BAP	biotin acceptor peptide
BirA	<i>E. coli</i> biotin ligase
CAR	chimeric antigen receptor
CD	cluster of differentiation
cDC	conventional DC
c-di-AMP	bis-(3'-5')-cyclic dimeric adenosine monophosphate
CIP	Calf Intestinal Alkaline Phosphatase
CLIC	clathrin-independent carrier
cm	centimeter
CMV	<i>Cytomegalovirus</i>
CpG ODN	CpG oligodeoxynucleotides
CTL	cytotoxic T lymphocyte
CTLA4	cytotoxic T-lymphocyte-associated protein 4
Cy5.5	cyanine 5.5
Cy7	cyanine 7
DAPI	4',6-diamidino-2-phenylindole
DC	dendritic cell
dNTP	deoxyribonucleotide triphosphate
DMEM	Dulbecco's Modified Eagle's Medium
DMSO	dimethyl sulfoxide
DNA	deoxyribonucleic acid
dsDNA	double-stranded DNA

<i>E. coli</i>	<i>Escherichia coli</i>
ELISA	enzyme-linked immunosorbent assay
FACS	fluorescence-activated cell sorting
FCS	fetal calf serum
FDA	U.S. Food and Drug Administration
FITC	fluorescein
fwd	forward
<i>g</i>	gravitational force
GEEC	GPI-enriched endocytic compartment
GFP	green fluorescent protein
GM-CSF	granulocyte-macrophage colony-stimulating factor
GMP	good manufacturing practices
h	hour
HBV	<i>hepatitis B virus</i>
HEK	human embryonic kidney
HEPES	4-(2-hydroxyethyl)-1-piperazineethanesulfonic acid
HER-2	human epidermal growth factor receptor 2
HIV	<i>human immunodeficiency virus</i>
HPV	<i>human papillomavirus</i>
HSPG	heparin sulfate proteoglycan
IFN	interferon
ICBL	immune cell binding ligand
ICS	intracellular staining
IgG	immunoglobulin G
IL	interleukin
i.m.	intramuscular
InLN	inguinal lymph node
i.p.	intraperitoneal
ITR	inverted terminal repeat
i.v.	intravenous
LB medium	lysogeny broth medium
LCMV	<i>lymphocytic choriomeningitis mammarenavirus</i>

LEAPS	ligand epitope antigen presentation system
MAGE	melanoma antigen-encoded gene
MFI	mean fluorescence intensity
min	minute
mg	milligram
MHC	major histocompatibility complex
mL	milliliter
mm	millimeter
MMTV	<i>mouse mammary tumor virus</i>
MS/MS	tandem mass spectrometry
MuLV	<i>murine leukemia virus</i>
MyD88	myeloid differentiation factor 88
NABs	neutralizing antibodies
NEAA	non-essential amino acids
NF- κ B	nuclear factor kappa-light-chain-enhancer of activated B cells
nm	nanometer
Ova	ovalbumin
OVAII	MHC class II epitope of Ova
PAMP	pathogen-associated molecular pattern
PBS	phosphate-buffered saline
PBS-T	PBS with Tween20
PCR	polymerase chain reaction
PD1	programmed cell death protein 1
pDC	plasmacytoid DC
PDL1	programmed death-ligand 1
PE	phycoerythrin
PEG	polyethylene glycol
PEI	polyethylenimine
Pen/Strep	penicillin + streptavidin
PerCP	peridinin-chlorophyll-protein
PFA	paraformaldehyde
PLA2	phospholipase A2

PRR	pattern recognition receptor
PVDF	polyvinylidene difluoride
RBC	red blood cell
rev	reverse
RNA	ribonucleic acid
RPMI	Gibco Roswell Park Memorial Institute 1640 Medium
RT	room temperature
scDNA	self-complementary DNA
s.c.	subcutaneous
SDM	site-directed mutagenesis
SEM	standard error of mean
SIV	<i>simian immunodeficiency virus</i>
ssDNA	single stranded DNA
STING	stimulator of interferon genes
SV40	simian virus 40
T4 PNK	T4 Polynucleotide Kinase
TAA	tumor-associated antigens
TAE	Tris-acetate EDTA
TCR	T cell receptor
Th1	T helper 1
TIL	tumor infiltrating lymphocytes
TLR	Toll-like receptor
TMB	3,3',5,5'-Tetramethylbenzidine
TNF α	tumor necrosis factor alpha
TSA	tumor-specific antigens
U	enzyme unit
V	volt
VG	viral genomes
VLP	virus-like particle
VP	viral protein
VR	variable region
wt	wild type

w/v	weight/volume
μg	microgram
μL	microliter
μM	micromolar
μm	micrometer
∅	negative control

Acknowledgements

First of all, I would like to thank Prof. Dr. Dirk Jäger, who gave me the opportunity to work on this project, and who supported this work with his scientific advice.

I want to thank my academic supervisor apl. Prof. Martin Müller for promoting this project with new ideas during the TAC meetings.

I am grateful to Prof. Dr. Dirk Jäger, apl. Prof. Martin Müller, apl. Prof. Suat Özbek and Prof. Dr. Nina Papavasiliou for reviewing this work and examining the disputation.

Special thanks goes to my project supervisor Dr. Silke Uhrig-Schmidt, who did not only provide good advices and new ideas for the project, but also always gave motivational support.

Further scientific advice was offered by Dr. Inka Zörnig and Dr. Patrick Schmidt, for which I am deeply grateful.

I appreciate the supply of materials and cell lines by Prof. Dr. Oliver Müller, apl. Prof. Dr. Martin Müller, Prof. Dr. Stefan Eichmüller and Dr. Kenneth L. Rock.

I would like to express my gratitude to the members of the AG Jäger for supporting me not only on a work basis but especially on a personal level. Claudia, Alex, Sarah, Aileen, Clemens and everybody else from the lab achieved that almost every day at work was special and that I can look back on a great time as a PhD student.

I am endlessly grateful to my parents Matthias and Karin, my brother Sven and sister Anika, who supported me on every step of the way and always provided a space that I could call home.

The same applies to my friends Katharina, Tim, Maximilian, Aylina, Lasse, Maike, Max, Merrit, Lennart, Anna and Momme, who are responsible for many special moments in the past years.